TEMPERATURE-DRIVEN STRUCTURAL IDENTIFICATION FOR BRIDGE PERFORMANCE EVALUATION

A Dissertation

by

BRITTANY RENE MURPHY

Submitted to the Office of Graduate and Professional Studies of
Texas A&M University
in partial fulfillment of the requirements for the degree of

DOCTOR OF PHILOSOPHY

Chair of Committee,	Matthew Yarnold
Committee Members,	Stefan Hurlebaus
	John Mander
	H. David Jeong
Head of Department,	Robin Autenrieth

May 2019

Major Subject: Civil Engineering

ABSTRACT

Bridges serve as integral components of infrastructure all around the world. Their direct impact to society is substantial, and their reliability is paramount. As such, confidence in the integrity of these structures is important not only for individuals who utilize these structures but also for the bridge owners and engineers who operate and maintain them. In order to develop a comprehensive understanding of the structural behavior, evaluations are conducted to assess the structure's performance. By utilizing input-output relationships between loads and responses, structural performance evaluations provide an opportunity to assess unique bridge behavior such as complex mechanisms or deterioration.

The research presented herein investigates a novel, temperature-driven concept for bridge performance evaluation wherein thermal behavior in response to environmental temperature changes is used to assess the structure. Within this research, two bridges are evaluated using a probabilistic approach of single and multiple model updating within the temperature-driven structural identification process. This technique utilizes Latin Hypercube Sampling as well as Bayesian calibration to identify unknown bridge parameters and evaluate the structural performance. Then, these studies are compiled into a synthesis of temperature-driven evaluations from nineteen bridge studies throughout the world to develop a comprehensive framework and to provide guidance for using thermal behavior for performance evaluations. The intellectual merit from each study illuminates various motivations, methods, successes, and challenges of temperature-driven evaluations. Guidance regarding structure details, monitoring criteria, as well as data and analysis is provided to assist bridge owners, engineers, and researchers who utilize this temperature-

driven technique to conduct evaluations. Based on the research presented herein, temperature-driven performance evaluations provide extensive insight, not only to the thermal behavior of the bridge, but the overall structural health.

DEDICATION

I would like to dedicate this work to my family who have been with me through every success and every hurdle along this journey. Your love and support are the reasons I made it to where I am today. You encouraged me to be pursue my dreams, work hard, and always do my best. You taught me to have courage and not be afraid to pursue opportunities that arise. You taught me to look at challenges not as an opportunity to fail but as an opportunity to grow. You believed in me even when I didn't believe in myself, and for that I am deeply grateful. I love you.

ACKNOWLEDGEMENTS

I would like to thank my committee chair and advisor, Dr. Yarnold, for his guidance, support, hard work, and patience throughout my academic career. I have learned so much under your direction, and it truly has been a pleasure to work with you over the years. I would also like to thank my committee members, Dr. Hurlebaus, Dr. Mander, Dr. Jeong, and Dr. Haque for their guidance and support throughout the course of this research.

Thanks also go to my friends and colleagues and the department faculty and staff for making my time at Texas A&M University a great experience. You all have been my family for the past two years, and I am deeply grateful for your friendship.

I would like to express gratitude to my Tennessee Tech family and friends for all of their support and encouragement. I would like to specifically thank Dr. Mohr, Dr. Ramirez, and Dr. Henderson for their advice and guidance while serving as committee members for this research. Also, I would like to thank my fellow research team members and colleagues for their hard work and contributions to this research: Eric James, Stephen Salaman, Justin Alexander, Wyatt Sherry, James Lawrence, Caleb Smith, and Traci Smith.

Thanks also go to the Tennessee Department of Transportation (TDOT) for your contribution and participation in this research.

Thanks also go to Dr. Branko Glisic at Princeton University for your collaboration on this research.

I would like to thank all of the educators and mentors who have helped prepare me for the next steps in my academic career and in life.

Finally, thanks to my family and friends for their love, encouragement, and support.

CONTRIBUTORS AND FUNDING SOURCES

This work was supported by the National Science Foundation (NSF) under Grants No. CMMI-1434373 and CMMI-1434455. Any opinions, findings, and conclusions or recommendations expressed in this material are those of the author and do not necessarily reflect the views of the National Science Foundation.

The data analyzed for this research was performed using Texas A&M University's High Performance Research Computing (HPRC) group.

TABLE OF CONTENTS

Page

LIST OF FIGURES

Page

LIST OF TABLES

Page

1. INTRODUCTION AND MOTIVATION

In the United States, the average bridge is approximately 43 years old with nearly 4 out of every 10 bridges currently 50 years or older (ASCE 2017). Many of these structures are reaching their design lives at the same time. As a result, a significant number of bridges are in need of intervention. Not only is aging infrastructure a concern, but newer structures may also need repair due to structural deficiency. These problems may be due to instances such as overloading, poor maintenance, or inadequate design to name a few. Due to the large volume of bridges in need of repair and limited financial resources, engineering practices have migrated to more rehabilitative approaches rather than complete replacements. This mentality allows engineers to stagger the scheduling of major bridge replacements rather than attempt them simultaneously. With nearly 58,495 bridges in the United States deemed structurally deficient and in need of intervention, prioritization has become necessary to determine the order in which bridges are rehabilitated or replaced (ARTBA 2016). One way of doing this is through structural monitoring. Contractors, engineers, researchers, and bridge inspectors acknowledge structural monitoring is beneficial but needs improving (Figueiredo et al. 2013). The structural monitoring research presented herein intends to advance the knowledge of a novel, temperature-driven approach to structural monitoring and develop a framework to assist engineers/researchers when using this process to evaluate bridge performance.

2. OBJECTIVES

The primary objectives of this research are to advance the knowledge of a temperature-driven structural evaluation technique and create a framework to assist engineers/researchers when using this method to evaluate bridges. Guidelines regarding the applicability and limitations of this method are investigated and developed by utilizing two unique bridge studies conducted by the author and a synthesis of similar studies from various researchers and practicing engineers. These projects encompass a wide variety of parameters that contribute to the knowledge and guidance of using temperature to assess the structural integrity of bridges. In particular, this research aims to address the following objectives with respect to the bridge geometry, bridge composition, movement systems, and monitoring criteria:

- Temperature-Driven Value: Determine if this evaluation technique can provide valuable information pertaining to the structural health or behavior of a bridge. Explore any successes and failures of using the temperature-driven method.
- Temperature-Driven Framework: Investigate how temperature-driven evaluations are performed and the project logistics utilized by each study.

3. BACKGROUND AND LITERATURE REVIEW

Bridge monitoring encompasses a wide range of procedures and methodologies, the most common of which are visual inspections and field testing. As common practice, bridges often undergo visual inspections by appropriately trained personnel. These inspections typically reveal any obvious degradation (e.g. cracks or rust on a steel girder) that may affect the integrity of the structure. Although visual inspections are beneficial, investigations from the Federal Highway Administration (FHWA) have revealed a significant lack of reliability from these field inspections alone (FHWA 2001). A more efficient and comprehensive method of evaluating bridge behavior is possible via field testing (Aktan et al. 1997; Bakht and Jaeger 1990; Catbas and Aktan 2002).

Structural monitoring through field testing is a means of evaluating a structure based on its performance rather than age or appearance. This monitoring technique allows for engineers, consultants, and owners to possess information regarding modal or numerical characteristics to validate a bridge's structural integrity. Field testing has been shown to identify numerical characteristics such as strains, displacements, and rotations as well as modal characteristics such as mode shapes and frequencies (Karbhari and Lee 2009). These characteristics can provide a more comprehensive evaluation when investigating deterioration such as fatigue cracks and condition assessment of bridge decks (Chong et al. 2003). The path from field testing to evaluation of a structure can be an extensive and complex process; therefore, guides for evaluating constructed systems have been developed. Two common processes are known as Structural Health Monitoring (SHM) and Structural Identification (St-Id).

3.1 Structural Health Monitoring (SHM)

SHM is the process of utilizing continuous, global observation and analysis of a structure to extract information about its current state of health (Farrar and Worden 2007). SHM systems vary in robustness according to specific objectives of individual projects. Shown in Figure 1, the basic framework for SHM is typically defined in levels, each encompassing the extent of the level prior and increasing the robustness of the monitoring system (Rytter 1993). SHM systems use sensor technology to track the structural behavior and identify any changes over time. These systems are used to quantify bridge behavior in order to efficiently manage bridges with regard to degradation, obsolescence, maintenance, and security (Alampalli et al. 2005; Alampalli and Ettouney 2008; Del Grosso 2013). Many SHM systems include real-time monitoring with alert notifications to quickly inform engineers and bridge owners of significant changes (Masri et al. 2004; Yarnold et al. 2012b).

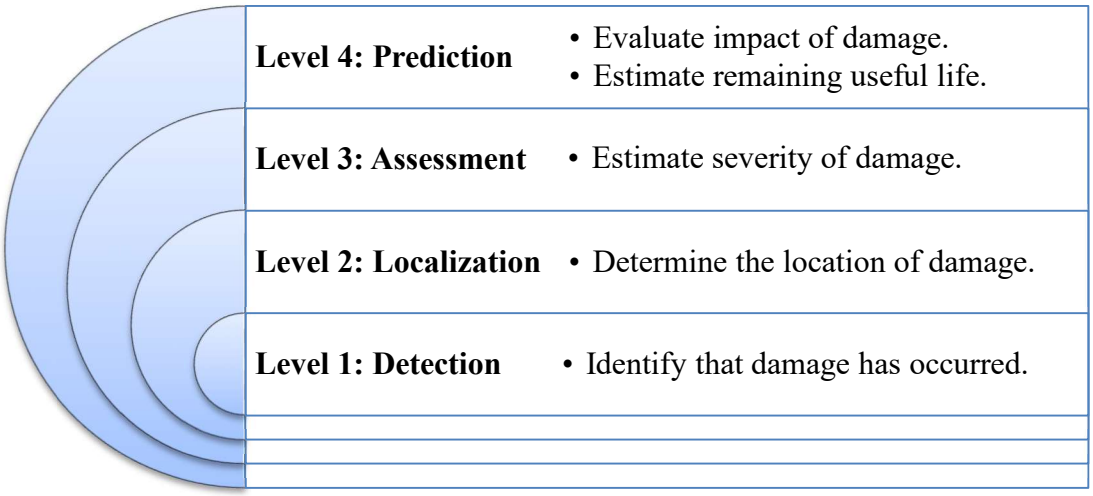

Figure 1: Levels of Structural Health Monitoring (Rytter 1993)

3.2 Structural Identification (St-Id)

St-Id is the process of using sensing technology and structural modeling to assess the performance of a constructed system within a specified time period (Catbas et al. 2013). Liu and Yao originally developed the theory behind St-Id for civil-structural engineering purposes in 1978 (Liu and Yao 1978). The primary goal of St-Id is to identify a structural model or models that accurately represent the behavior of a structure. These models are then used to provide insight regarding the health and performance of the structure. The overall concept of St-Id is shown in Figure 2 below.

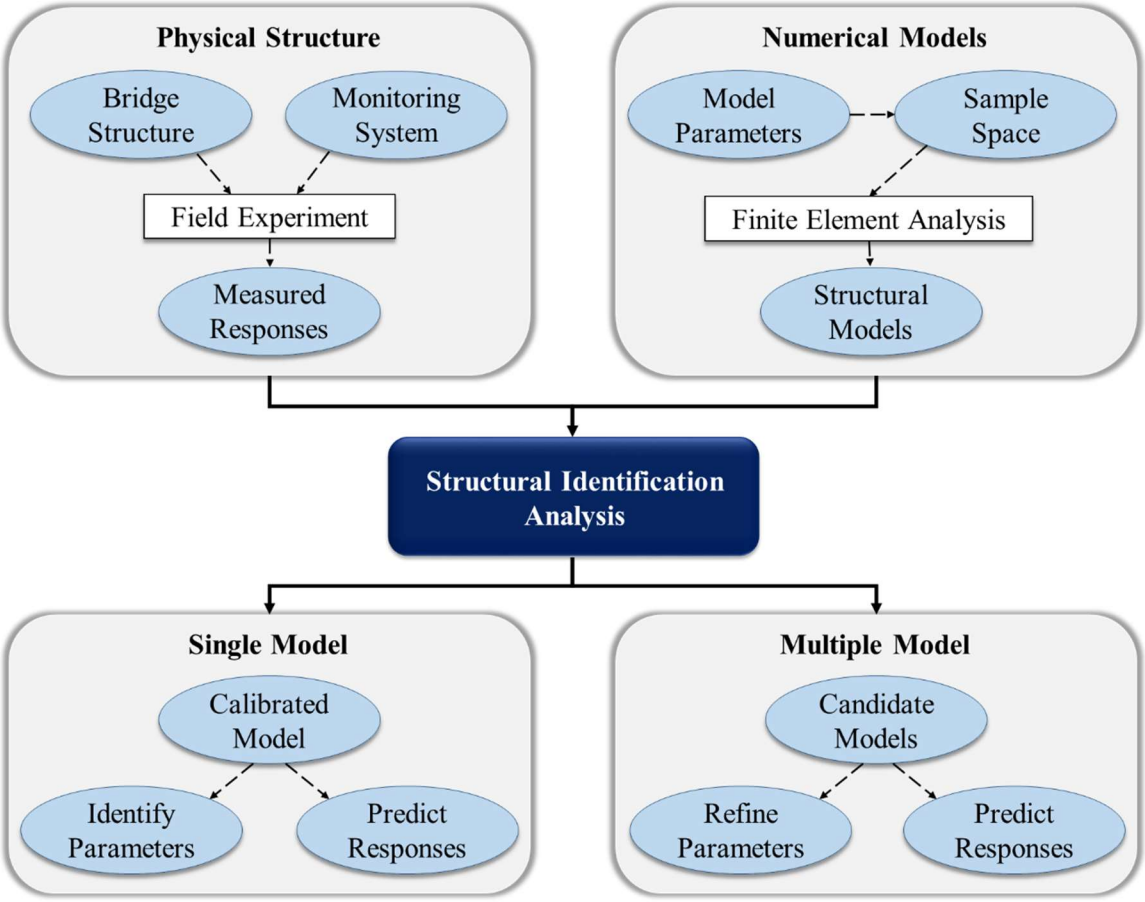

Figure 2: Structural Identification Concept

St-Id utilizes two unique components: the physical structure and numerical models. With regard to the physical structure, measured responses are collected by means of conducting a field experiment. A monitoring system is installed on the structure and records the structure's response as it is subjected to a load. As a result, these measured responses provide a quantitative representation of the structure's behavior. Pertaining to the numerical models, a collection of structural models is usually developed via finite element analyses. Model parameters corresponding to specific conditions of the structure are varied to develop a sample space. The sample space is a collection of parameter combinations that are individually subjected to a finite element analysis and produce structural models that encapsulate many different behaviors of the structure. The measured responses are then compared to corresponding responses of the structural models within the structural identification analysis with either a single model or multiple model approach.

In 2005 Aktan and Moon shaped the structural identification concept into a comprehensive framework for evaluating constructed systems using a single model approach (Aktan and Moon 2005). Moon later evolved the process into a multiple model approach as well (Beck and Katafygiotis 1998; Goulet et al. 2010; Moon 2008; Ravindran et al. 2007; Smith and Saitta 2008). Both approaches are outlined in depth in the following sections.

3.2.1 Single Model Structural Identification (SM St-Id)

The single model (SM) St-Id process shown in Figure 3 was developed by Aktan and Moon and is a six step procedure for evaluating constructed systems. With this technique, only one structural model is identified to represent the behavior of the structure. Each step of the process is thoroughly outlined in Catbas et al. (2013) and condensed in the sections below.

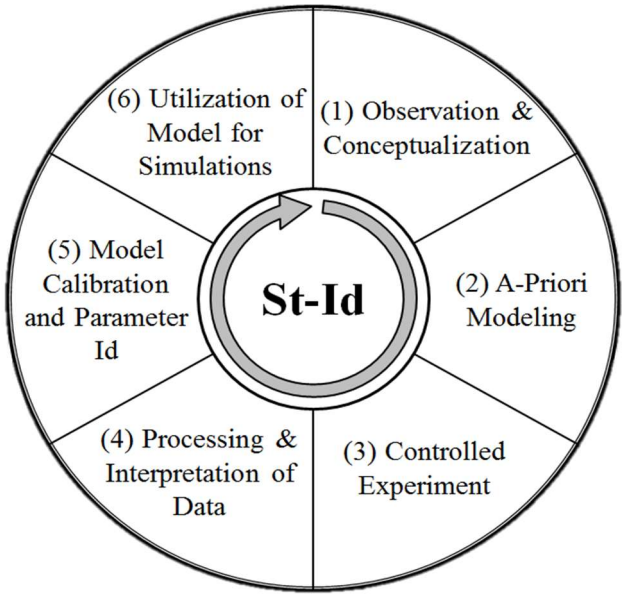

Figure 3: Structural Identification Process (Reprinted from Catbas et al. 2013)

3.2.1.1 Step 1: Observation and Conceptualization

The initial step of SM St-Id is "Observation and Conceptualization" during which an understanding of the structure and motivation of the investigation is developed. In many cases, the presence of damage provokes an inquiry as to why the damage exists or how quickly the damage is progressing. Another common motivation is simply the lack of confidence and information about a structure's integrity. For example, the structural behavior of aged bridges or those with extensive retrofits may be more complex and different than the original design. Thus, an assessment may be necessary to understand the structural behavior of such bridges. During this step, all available pertinent information about the structure and its behavior is gathered. This includes but is not limited to original drawings, rehabilitation drawings, inspection reports, and site visits to name a few. In-depth knowledge of the structure and its components is essential for understanding its behavior

and for proper modeling in Step 2. With all of the structure information available, conceptualization of the project begins by identifying specific objectives as well as potential challenges.

3.2.1.2 Step 2: A-Priori Modeling

With many model types used to evaluate structures, analytical models are generally classified into two categories: non-physics-based and physics-based. Non-physics-based models are primarily data-driven and utilize a variety of numerical techniques such as probabilistic or statistical approaches (Catbas et al. 2013). However, physics-based models most commonly utilize geometric approaches such as finite element or modal models. Physics-based models are specifically designed to address behavior parameters such as equilibrium, movement mechanisms, continuity, and boundary conditions (Catbas et al. 2013). For this reason, St-Id primarily applies to physics-based models. "A-priori Modeling" consists of creating a physics-based model that represents the as-designed or theoretical behavior of the structure. Depending on the structure and the objectives of the assessment, the a-priori model can range from a low resolution phenomenological model to a high resolution finite element model. The purposes of the a-priori model are to establish a baseline of how the structure in question is designed to behave and to determine sensitive areas of the structure that are most beneficial for monitoring. Based on those areas, the monitoring system is designed and implemented during the third step, "Controlled Experiment".

3.2.1.3 Step 3: Controlled Experiment

The next step of the SM St-Id process is "Controlled Experiment", wherein the monitoring system is designed/installed and field testing is conducted. While designing the

controlled experiment, logistics of the bridge itself such as access, closure availability, and project budget are taken into consideration. These restrictions potentially influence the type or robustness of the monitoring system being designed. The monitoring system logistics such as monitoring duration, monitoring/data acquisition equipment, sensor type/resolution, sampling rate, and power requirements are generally dependent on the type of field testing being conducted. Controlled experiment techniques include field testing with respect to static loads, vibrations, and temperature (Figure 4).

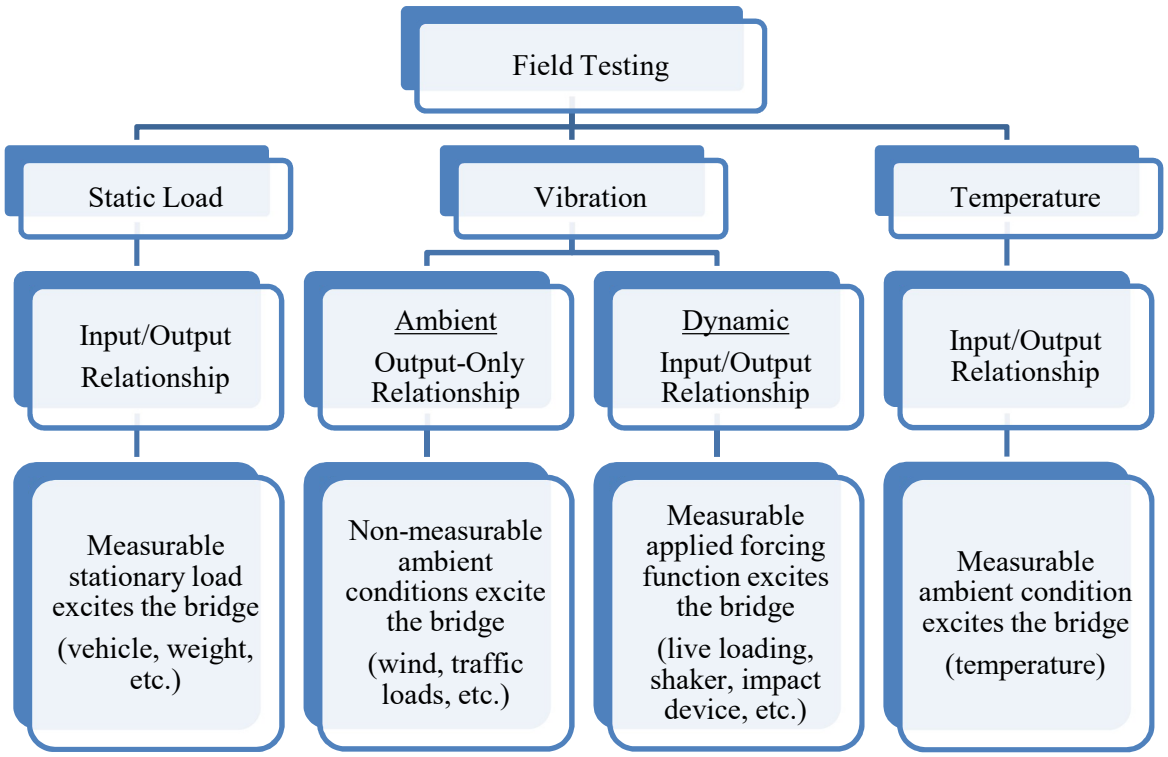

Figure 4: Field Testing Methods for Structural Monitoring

3.2.1.3.1 Static Load Testing

Static load testing is an input-output field testing procedure in which the input is a stationary or low-speed load and the output is the structure's response to the load. Often, static load tests on bridges use inputs like weights or vehicles (trucks or railcars) with known measurements of force applied from each axle. Static load tests in which the load is completely stationary are referred to as park tests. During a park test, a vehicle is driven to a predetermined location on the bridge and parked, remaining completely stationary until measurements are recorded. Once the measurements are recorded, the vehicle moves to another position to record additional measurements. The vehicle is parked at various locations on the bridge until sufficient amounts of data are collected. Live load static testing is the process of using a vehicular load moving at a low-speed to excite a bridge. This method of testing is known as a crawl test. During a crawl test, the load (vehicle) travels along the bridge at a low speed while measurements are recorded. Although the vehicle is non-stationary, the bridge does not experience dynamics effects due to the low-speed travel. Crawl tests are used to divulge various types of information including the composite action of decks and girders, neutral axis location, live load distribution factors, span continuity, load ratings, and load carrying capacity (Bakht and Jaeger 1990; Barr et al. 2001; Bell et al. 2013; Breña et al. 2013; Chajes and Shenton 2006; Eom and Nowak 2001; James 2016; James and Yarnold 2017). Other outputs of static testing include a variety of responses including girder deflections / rotations and flexural strains or even cable forces on a cable-stayed bridge (Bacinskas et al. 2013; Fang et al. 2004).

3.2.1.3.2 Vibration Testing

3.2.1.3.2.1 Ambient

Currently, the most prevailing technique for monitoring long-span bridges is ambient vibration monitoring. This technique monitors a structure under ambient loading conditions such as vehicular or pedestrian traffic, wind, ocean waves, or low-intensity seismic loads (Abdel-Ghaffar and Scalan 1985; Coppolino and Rubin 1980; Farrar et al. 1999; Nakamura and Sakamoto 2000). Using this method, modal parameters such as natural frequencies, mode shapes, and damping can be determined and tracked for a structure (Bolton et al. 2001; Karbhari and Lee 2009; Kim et al. 2005; Mazurek and Dewolf 1990). With this information, the location and extent of damage can be identified and assessed (Bolton et al. 2005; Kim and Stubbs 1995; Park et al. 2002). Although this method has been utilized, ambient vibration monitoring also has challenges associated with it (Catbas et al. 2007; Karbhari and Lee 2009). Ambient vibration monitoring is limited to low frequency excitation (Karbhari and Lee 2009). This method also has difficulty dealing with measurable inputs and environmental effects. These effects can be of the same order of magnitude as damage effects, making identification of damage difficult to achieve (Peeters and De Roeck 2001; Sohn 2007). Although removing temperature effects is possible (Zhu et al. 2016), these effects still pose a significant challenge for this type of testing. The prevailing reason for the limited success of ambient vibration monitoring of long-span bridges is the limited sensitivity to structural damage (Brownjohn et al. 2011).

3.2.1.3.2.2 Dynamic

Live load dynamic testing is the process of using a non-stationary vehicular load with a known weight and appreciable speeds to excite a bridge for evaluation. This type of testing

utilizes a measurable input-output relationship to assess the structural integrity of a bridge. Dynamic displacements and modal properties such as natural frequencies, mode shapes, and damping ratios can be determined (Bacinskas et al. 2013). Live load dynamic testing can also provide insight on load distribution throughout the bridge (Eom and Nowak 2001) as well as composite action between the superstructure and the deck (Alampalli and Kunin 2003). This method is generally the most common technique to assess relatively small structures due to their heightened sensitivity to live loads. However, large-scale structures often have a low sensitivity to live loading. This along with temperature challenges similar to ambient vibration testing can increase the difficulty of identifying effects from live load testing. Structural excitation is also achievable through the use of impact (i.e. dropping a weight or using an impact hammer) or shakers (Farrar et al. 1999).

3.2.1.3.3 Temperature Testing

Temperature effects from daily or seasonal temperature changes are often significant enough to warrant consideration regardless of the type of test being performed (Catbas et al. 2007; Del Grosso and Lanata 2014; De Roeck 2003). Temperature effects are often filtered out of analysis processes or accounted for during field testing procedures. For example, while static load testing a cable-stayed bridge in Taiwan, researchers removed the static load from the bridge every two hours to reinitialize the data and mitigate temperature effects (Fang et al. 2004). However, in recent years, temperature has been used to excite structures for damage detection and performance evaluation (Cao et al. 2010; Glisic et al. 2008; Kulprapha and Warnitchai 2012; Yarnold et al. 2012a; Zhou et al. 2018). Since bridges have a high sensitivity to thermal effects, everyday temperature exposure can excite a response from the structure. The temperature-driven concept utilizes this cause-and-effect

relationship to develop a behavioral signature for the bridge. This process is detailed in Figure 5 below. The temperature variations (input) are quantifiable and can be measured simultaneously with the member strains, displacements, and/or rotations (output) that the bridge experiences in response to the thermal load. This input-output relationship can be used to identify and monitor unknown quantifiable information with regard to the bridge (e.g. boundary conditions, continuity conditions, force distribution, etc.). Once the behavioral signature has been determined, it can be used to update a model and represent the current condition of the structure.

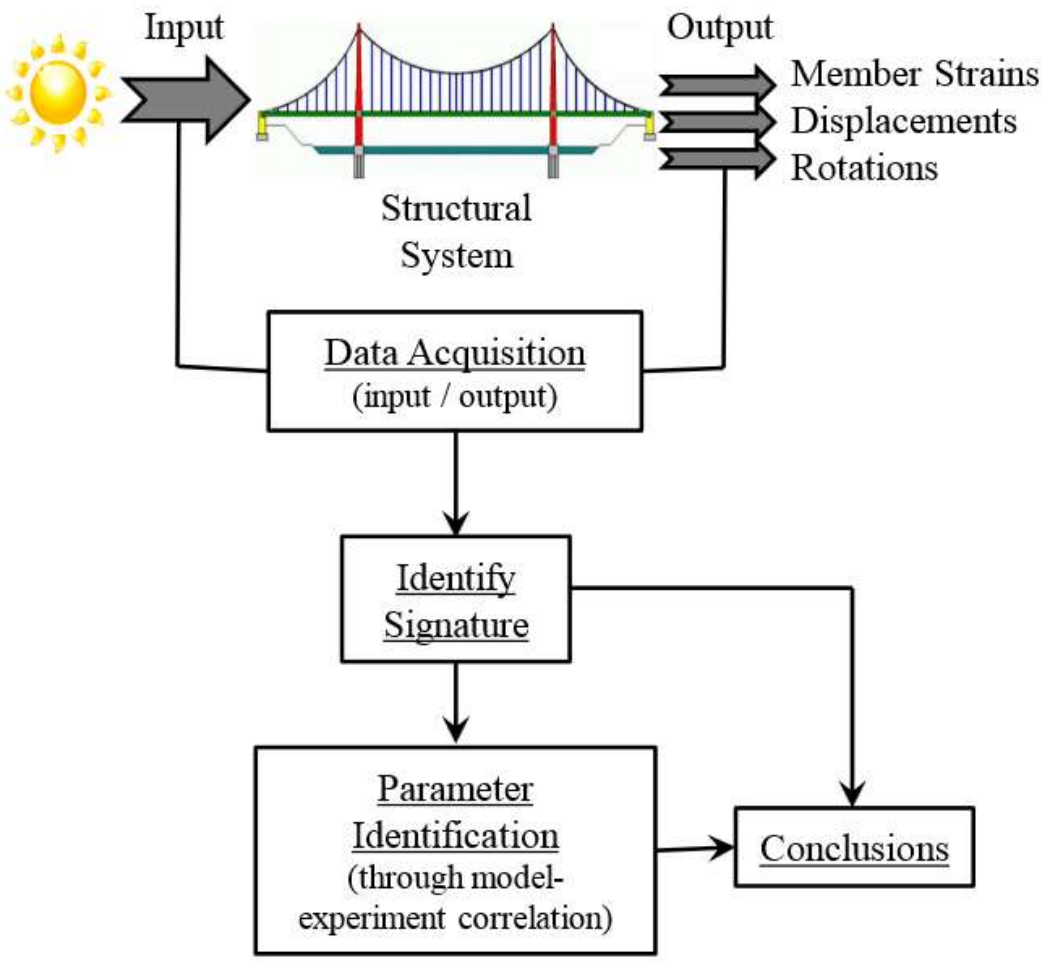

Figure 5: Temperature-Driven Concept (Reprinted from Murphy and Yarnold 2017)

3.2.1.4 Step 4: Processing and Interpretation of Data

Next, in "Processing and Interpretation of Data", data is collected from the monitoring system and quality checked. Any erroneous data (possibly from malfunctioning sensors or electrical interference, for example) is identified and subsequently removed from analysis. Also, investigation of specific information through windowing, filtering, or averaging is possible during this step. If appropriate, direct data interpretation is performed.

Since the data is available, non-physics-based numerical models such as artificial neural networks and auto-regressive models are also used to analyze and process data. Any conclusions based solely on the data are determined.

3.2.1.5 Step 5: Model Calibration and Parameter Identification

In Step 5 "Model Calibration and Parameter Identification", variable parameters such as boundary or continuity conditions are identified for the calibration process. Using optimization algorithms such as objective functions or maximum likelihood estimations (further discussed later in Section 5), the preliminary model developed in Step 2 is calibrated with the measured results from Step 4 to identify a single model that depicts the structure and its behavior in its current condition. Parameters from the calibrated model are used to identify conditions of the structure.

3.2.1.6 Step 6: Utilization of Model for Simulations

Finally, in Step 6 the calibrated model is used for simulations and to acquire more knowledge about the structure in its current state. This model is also used to predict responses of the structure. With the information acquired from the calibrated model, engineers are able to conduct a proper assessment of the structure's behavior and integrity. The calibrated model is intended to assist engineers and owners with decisions regarding maintenance, rehabilitation, or potential retrofit.

3.2.2 Multiple Model Structural Identification (MM St-Id)

The multiple model (MM) St-Id technique described within Moon (2008) is beneficial when many different structural models, each with varying parameter combinations, are capable of reasonably describing the structural behavior (also referred to

as nonuniqueness). The multiple model approach evolves from the single model approach by modifying Steps 5 and 6 to consider more than one calibrated model.

3.2.2.1 Step 5 Modification: Model Calibration and Parameter Identification

Engineering experience, data mining, or calibration techniques reduce the large number of structural models to a predetermined number of most probable scenarios called candidate models. Distributions of the model parameters and predictive responses are used to reduce uncertainty of the behavior and conditions of the structure.

3.2.2.2 Step 6 Modification: Utilization of Models to Identify Trends

Rather than using each of the candidate models individually, the information from all of the candidate models is used collectively to identify trends. Distributions of the responses are used to better understand the behavior of the structure.

Both the single and multiple model approaches have the potential to assist engineers and bridge owners with decisions regarding a structure's health and maintenance; however, in some cases, one method may prove superior over the other. One major benefit of the single model approach is that direct information is provided by utilizing just one model. For instance, if the model was developed within a finite element software, an engineer could open the model file and have all the capabilities and amenities of the finite element software available to analyze the structure. Unfortunately, this commodity does not extend to the multiple model approach. Since a number of models influence the definition of the behavior of the bridge, an engineer cannot simply open and analyze all of the models simultaneously. The multiple modeling approach can, however, provide information about the importance or sensitivity of a parameter to the load scenario. For example, within a set of candidate models one parameter may converge to a discrete value (indicating a heightened sensitivity) whereas

another may vary significantly (indicating a reduced sensitivity). An engineer may then be able to identify which parameters have more influence over the behavior of the structure.

The St-Id process has been successful in laboratory/small scale settings (Jesus et al. 2016, 2017; Mazurek and Dewolf 1990). However, one of the primary disadvantages of St-Id is the difficulty of experimenting on an actual structure (Aktan et al. 1997; Catbas and Aktan 2002). In reality, structures are often complex and difficult to model accurately which is crucial for model-based evaluation (Yuen et al. 2004). In addition, the logistics of conducting an experiment on a large structure are substantial. Researchers are often forced to make assumptions for experiment variables out of their control, introducing more possibility for errors. Often structures must be monitored for long periods of time before a reliable evaluation of the structure can be completed (Sikorsky et al. 2001). For the purpose of this research, a temperature-driven approach to the St-Id process is currently being explored.

3.3 Temperature-Driven Structural Identification (TD St-Id)

The temperature-driven (TD) approach to the St-Id process (Figure 6), where thermal "loads" are treated as the excitation and the corresponding static responses are correlated, shows promise to mitigate many of the shortcomings of ambient vibration monitoring (Kromanis and Kripakaran 2016; Yarnold and Moon 2015). Logistically, TD St-Id can be performed continuously over a period of time with minimal data storage and time synchronization requirements. In addition, the equipment is relatively inexpensive and generally self-sustaining with little need for man-power resources once the system is installed and operational. The results can be recorded throughout the structure's changing environments and can potentially identify structural changes that occur as a result of seismic,

wind, ice, impact, or similar nature. This is primarily due to the fact that a TD baseline is highly sensitive to many changes of structural systems (Laory et al. 2013; Yarnold and Moon 2015). TD monitoring is particularly useful for large structures. Long-span bridges, for example, are more responsive to thermal loads than live loads, making the results easier to identify.

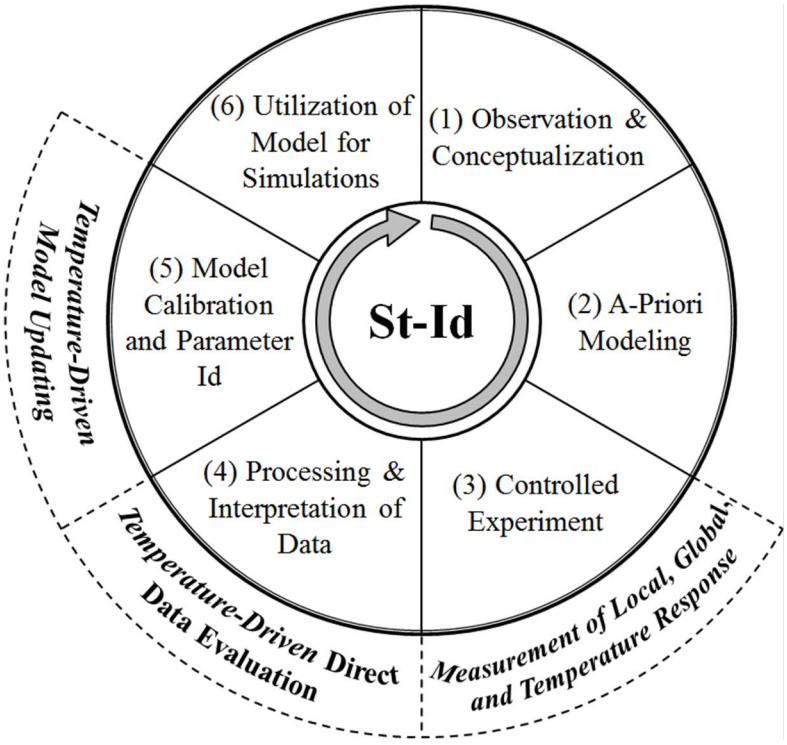

Figure 6: Temperature-Driven Structural Identification Process (Reprinted from Murphy and Yarnold 2017)

4. CONCEPT

4.1 Thermal Behavior

In order to complete a TD structural analysis of a bridge, an extensive knowledge of thermal behavior is required. An insight into some of this knowledge is provided below. Construction material properties, structure geometry, and restraints imparted by boundary conditions heavily influence deflections, stresses, and strains that occur as results of thermal "loads". Like most materials, bridge materials such as steel, concrete, and asphalt expand and contract in response to such loading. The physical make-up of these materials allows for unique rates of heating/cooling (quantified as thermal inertia) as well as expansion/contraction (quantified as coefficient of expansion) for each material. The coefficient of thermal expansion (α) directly relates how much the material expands or contracts, thus it affects the stress or strain in particular members of the bridge. Boundary conditions also affect the strain or stress in those members of the bridge. Boundary conditions can vary in extent of impeded motion; therefore, it is possible to have boundary conditions that are unrestrained, partially restrained, or fully restrained. If the structure is assembled in such a way that prevents movement from thermal effects, stress accumulates within the members.

4.2 Types of Thermal Loading

Another important aspect of thermal behavior is the type of thermal loading that the structure is experiencing. If the structure is subjected to a consistent temperature change throughout, the structure is experiencing uniform thermal loading. However, if the structure is subjected to inconsistent temperature changes where parts of the structure are cooler or

warmer than others, the structure is experiencing thermal gradients. Each of these loading types is discussed further below.

4.2.1 Uniform Thermal Loading

To fully understand uniform thermal loading, Figure 7 provides an illustrative example of a partially restrained W10x54 beam, subjected to a uniform temperature change increase (ΔT). The structure is simply-supported and uses a spring to define the extent of restraint at one end of the member.

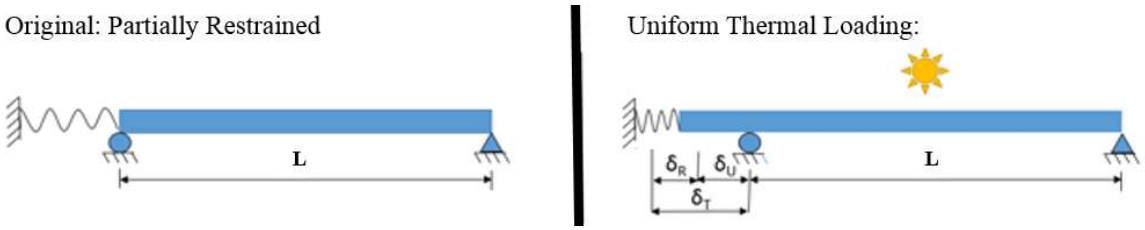

Figure 7: Example of Partially Restrained W10x54 Beam Subjected to Uniform Thermal Loading (Reprinted from Murphy and Yarnold 2018)

A critical aspect of thermal behavior is that the response includes an unrestrained portion and a restrained portion. Furthermore, the total displacement (δ_T) is a combination of the unrestrained displacement (δ_U) and the restrained displacement (δ_R) and is calculated according to Equation 1.

$$\boldsymbol{\delta_T = \delta_U + \delta_R = \alpha\, \Delta T\, L} \quad \textbf{(1)}$$

The restrained displacement (δ_R) is the portion that produces stress in the member (δ_U produces no stress). This restraint occurs as a result of the spring support exerting a longitudinal axial force (P) on the member. Therefore, δ_R can be calculated as shown in

Equation 2, where *A* represents the cross-section area and *E* represents the modulus of elasticity.

$$\boldsymbol{\delta_R = \frac{PL}{AE}} \quad \textbf{(2)}$$

The axial stress in the beam is simply the longitudinal axial force (P) divided by the cross-section area (A). Therefore, δ_R can also be expressed in terms of stress as shown in Equation 3.

$$\boldsymbol{\delta_R = \frac{\sigma L}{E}} \quad \textbf{(3)}$$

The unrestrained displacement (δ_U) can be calculated from the spring force (P) and the stiffness of the spring (K_S) as shown in Equation 4.

$$\boldsymbol{\delta_U = \frac{P}{K_s}} \quad \textbf{(4)}$$

Equations 1 through 4 show the total displacement and the unrestrained and restrained components of displacement due to thermal loading. Thermal strain can be determined in a similar fashion. As with displacement, strain induced from thermal loading is comprised of unrestrained and restrained components that can be calculated as well. This is achieved simply by dividing each of the prior displacement equations by the length (L).

As mentioned previously, the structure can have various levels of restraint. The partially restrained scenario is most prevalent in reality as unintended stiffness from weathering and exposure, for example, can affect the boundary conditions of the structural system. Since conditions may change naturally over time, the unintended stiffness of each boundary condition is generally unknown. Fortunately, the boundary conditions can be

determined using thermal strains and displacements since they are sufficiently sensitive to these parameters. Figure 8 shows how temperature change and boundary stiffness affect strains and displacement in the example described above. If the boundary stiffness was low in magnitude (1 kN/m, for example), a relatively large unrestrained displacement of nearly 30 mm for a 50°C temperature change would be expected (Figure 8(a)). However, if the boundary stiffness was high or rigid, large measurements of nearly 600 microstrain of restrained strain would be expected (Figure 8 (b)). This simple uniform thermal load TD example illustrates how the input (temperature) and outputs (restrained strains and unrestrained displacements) can be used to identify a boundary condition (stiffness).

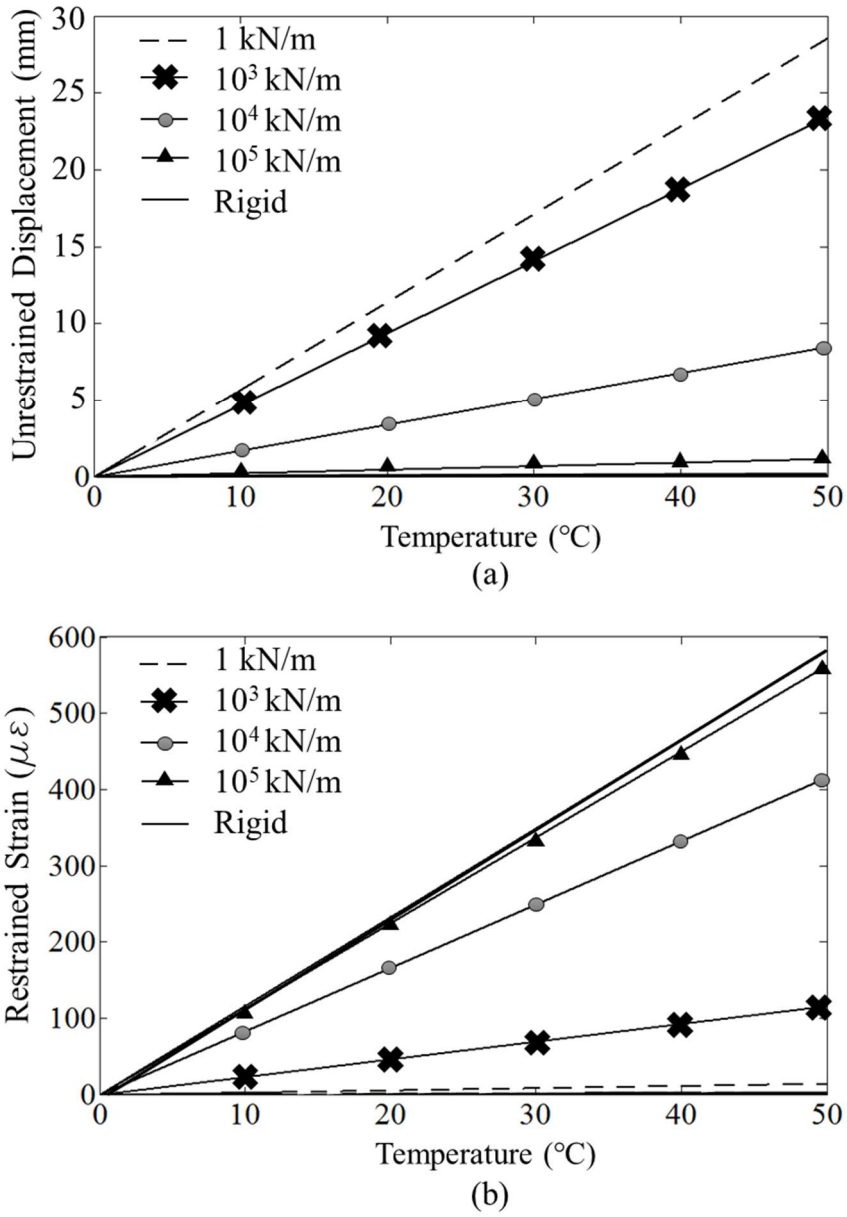

Figure 8: Example Results for Varying Translational Stiffness Values of a W10x54 Steel Member (Modulus of Elasticity = 200 MPa, Coefficient of Thermal Expansion = 11.7x10^{-6} /°C, Cross-sectional Area = 10,200 mm^2, and Length = 50 m): a) Unrestrained Displacement vs. Temperature and b) Restrained Strain vs. Temperature (Reprinted from Murphy and Yarnold 2018)

4.2.2 Thermal Gradients

Structures can also be affected by thermal gradients which occur when the thermal load applied to the structure is not uniform throughout. For example, thermal gradient effects can occur as the result of direct sunlight on a structure as shown in Figure 9. The parts of the bridge that are exposed to direct sunlight experience greater temperatures than those that are shielded from the direct radiation (Figure 9(b)). The structure reacts according to the temperature load experienced and thus can cause the overall structural behavior to be inconsistent. The side of the bridge with direct sunlight wants to expand like the unrestrained deformed shape shown in Figure 9(c). However, the assembly of the structure provides restraint and does not allow for such deformation. As a result, gradient forces occur. The warmer members of the bridge experience a compressive force since they want to expand but are unable. Conversely, the cooler members experience a tensile force since they want to contract but are unable.

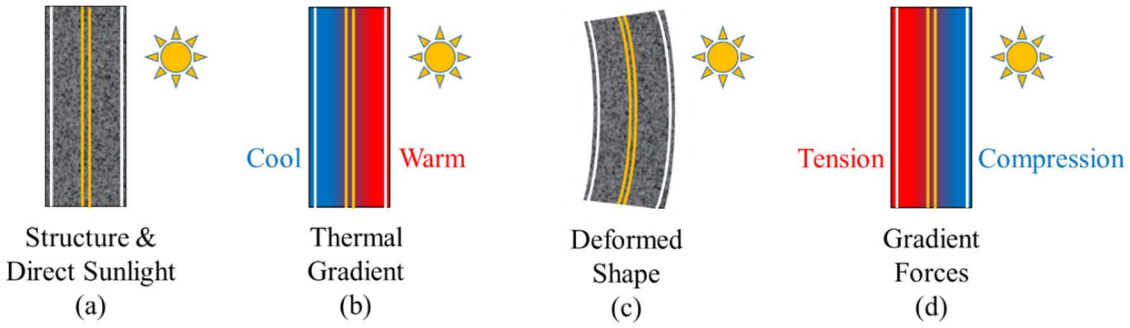

Figure 9: Thermal Gradient Effects from Direct Sunlight: a) Structure, b) Thermal Gradient, c) Deformed Shape, and d) Gradient Forces

Thermal effects can also be present with other environmental conditions such as when precipitation collects on a structure as shown in Figure 10. When this happens, the precipitation causes the deck of the bridge to be cooler than the bridge structure beneath (Figure 10(b)). The deck contracts and the structure wants to bend upward (Figure 10(c)). However, restraint again causes gradient forces to occur. Tension occurs at the cooler surface, whereas compression occurs at the warm members underneath.

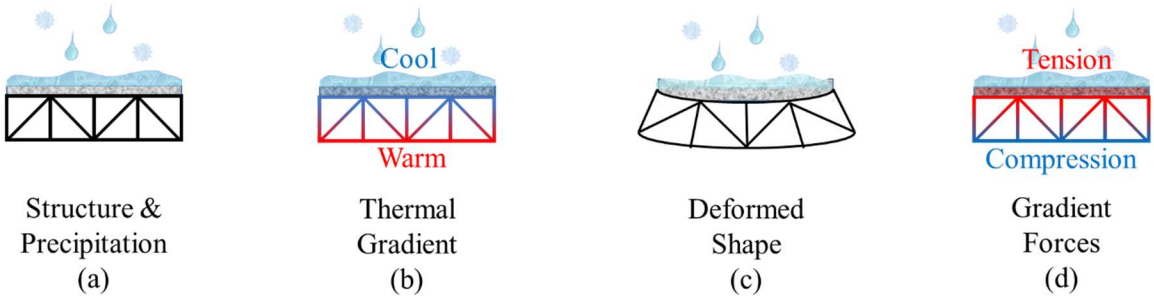

Figure 10: Thermal Gradient Effects from Precipitation: a) Structure, b) Thermal Gradient, c) Deformed Shape, and d) Gradient Forces

Thermal gradients are addressed by analyzing the stress distributions that occur as the temperature changes throughout a structure. The total stress from temperature gradients is comprised of restrained and unrestrained components. The restrained component, $\sigma_{restrained,}$ is calculated by rearranging Equation 1 to solve for the stress. The unrestrained components can be determined by discretizing the structure into elements affected by thermal gradients. The unrestrained components are comprised of the bending and axial behavior caused by the differential temperature along the element. The differential temperature for each element can be determined by Equation 5, where T_{ai} is the temperature at the element centroid, ΔT_i is the temperature difference within each element, d_i is the depth

of the element, y is the distance from the neutral axis, and $\bar{y}_i$ is the distance to the element's elastic centroidal axis from the neutral axis of the structure.

$$\boldsymbol{T(y) = T_{ai} + \frac{\Delta T_i}{d_i}(y - \bar{y}_i)} \quad \textbf{(5)}$$

Then Equations 9 and 13 below can be used to calculate the stresses. To calculate the axial stresses, the axial strain must be determined using Equation 6, where α is the coefficient of thermal expansion of the material and A is the cross-sectional area of the structure.

$$\boldsymbol{\varepsilon = \frac{\alpha}{A}\int T(y)\, dA} \quad \textbf{(6)}$$

Substituting the gradient temperature (T(y)), Equation 6 becomes Equation 7 shown below, where A_i.is the area of the element.

$$\boldsymbol{\varepsilon = \frac{\alpha}{A}\sum T_{ai}\, A_i} \quad \textbf{(7)}$$

The thermal strain is then converted to axial force (N) using Equation 8, where E is the modulus of elasticity of the material.

$$\boldsymbol{N = EA\varepsilon} \quad \textbf{(8)}$$

Then axial stress is determined in Equation 9 by dividing by the cross-sectional area.

$$\boldsymbol{\sigma_{axial} = \frac{N}{A}} \quad \textbf{(9)}$$

To calculate the bending stress, the curvature ψ must first be determined by Equation 10, where *I* is the moment of inertia.

$$\boldsymbol{\psi = \frac{\alpha}{I}\int T(y)\, y\, dA} \quad \textbf{(10)}$$

By substituting the gradient temperature (T(y)), Equation 10 becomes Equation 11, where $\bar{I}_i$ is the moment of inertia of the element.

$$\boldsymbol{\psi = \frac{\alpha}{I}\sum\left[T_{ai}\,\bar{y}_i A_i + \frac{\Delta T_i}{d_i}\bar{I}_i\right]} \quad \textbf{(11)}$$

Then, the curvature is used to calculate the bending moment *M* applied to the structure as shown in Equation 12 below.

$$\boldsymbol{M = EI\psi} \quad \textbf{(12)}$$

The bending stress is calculated for the top and bottom of the structure using Equation 13, where c is the distance from the neutral axis to the outermost top or bottom fiber.

$$\boldsymbol{\sigma_{bending} = \frac{Mc}{I}} \quad \textbf{(13)}$$

Finally, the total stress (σ_{total}) is calculated by adding the stresses of the restrained, bending, and axial distributions.

$$\boldsymbol{\sigma_{total} = \sigma_{restrained} + \sigma_{bending} + \sigma_{axial}} \quad \textbf{(14)}$$

For clarity, an example of stress distributions for an arbitrary structure, in this case a beam, is shown in Figure 11 below.

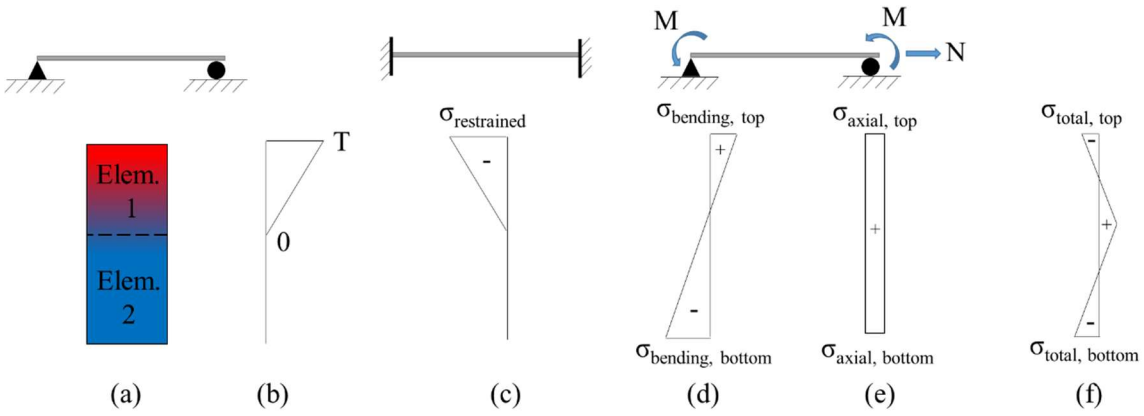

Figure 11: Stress Distributions for Thermal Gradients: a) Structure, b) Temperature Gradient, c) Restrained Stress, d) Bending Stress, e) Axial Stress, and f) Total Stress

Structures in reality are rarely this simple, but the same concept can be applied to more complex systems. For these systems, model calibration through TD St-Id can be used to determine unknown boundary conditions and/or continuity conditions. Once the boundary/continuity conditions have been identified, the structure and its behavior can be analyzed.

5. METHODOLOGY

As mentioned in Section 3, the St-Id method using either the single or multiple model approach can be accomplished with a variety of techniques for modeling, calibration, analysis, etc. This section explains the specific method used for the evaluation of two bridge structures within this study. Finally, an example of the technique is demonstrated on a simple structure exposed to a uniform temperature change.

5.1 Temperature-Driven St-Id using Single and Multiple Model Approach with Bayes Theorem

Overall, the method used in this research for TD St-Id is a probabilistic approach of Latin Hypercube Sampling and Bayes Theorem calibration of finite element structural models. Bayesian techniques have been used for the purpose of structural identification previously (Beck and Katafygiotis 1998; Ravindran et al. 2007). To adequately understand this method, the following sections present the overall process with additional explanation of how the structural evaluation was performed. For completeness, all aspects of the evaluation method are addressed; however, this section primarily focuses on the numerical models and analysis.

5.1.1 Field Experiment

The field experiments conducted for this research were completed according to Steps 1-4 of the SM St-Id process. The specific details of each experiment are discussed in detail later in their respective sections.

5.1.2 Numerical Models

5.1.2.1 Model Parameters

The TD structural evaluation process requires a population of structural models with various defining characteristics. The model parameters are chosen based on their potential influence of the behavior of the structure with respect to the load scenario being applied (in this case, thermal loading). As evident from Equations 1-4, changes in many structural characteristics (such as cross-sectional area of bridge member or the properties of the construction materials, to name a few) have the potential to drastically alter the thermal responses of displacement and strain. As a result, these characteristics can be used as model parameters that define the various structural models. Each model parameter is associated with its own set of values (what these values actually are will be discussed later). These values make up what is called the sample space for that parameter.

5.1.2.2 Development of Sample Space

For a multi-parameter study, the sample space for the structure becomes an n-th dimensional space, where n is the number of parameters. Imagining an n-th dimensional sample space can be difficult, so plots like the ones shown in Figure 12 through Figure 14 are used as visual aids to understand the sample space more clearly. Plots along the diagonal are histograms of the values of each respective parameter. The remaining plots show a two-dimensional slice of the sample space according to the parameters to the left of each row (y-axis) and below each column (x-axis). Sample spaces for a structure can be developed either deterministically or probabilistically. While each approach has benefits and drawbacks, either can be more efficient depending on the goals and specifics of a particular project. Both approaches are described briefly below.

5.1.2.2.1 Deterministic Approach

The deterministic approach is an iterative, brute force method of sampling the parameters. First, a set of values is assigned to each parameter. Then, the sample space is developed by creating every possible combination of those parameters. An example of this type of sample space can be seen in Figure 12 below. In this figure, each parameter was assigned a set of values ranging from 0 to 100 in increments of 20. The number of samples is determined by the number of parameters and the size of their sets of values. For this scenario with three parameters and six potential values each, the number of combinations (or samples) is equal to 6^3 or 216.

The deterministic approach is incredibly useful if specific combinations need to be investigated. Also, this method is beneficial for developing the sample space for sensitivity studies, in particular, where one parameter is investigated at a time or compared to other parameters individually. The method can also be used to identify trends that do not need all the information in between but only information at particular intervals. The deterministic approach also has some substantial drawbacks. This method is an iterative process and typically requires more samples, and thus, more time to complete. Also, many samples may be nonsensical as some parameter combinations may produce structural behaviors that do not occur realistically. Another downside of this method is the large areas of parameter combinations that are not sampled. In this example, no samples are developed with values between 0 and 20, 20 and 40, and so on. This aspect significantly limits the application of this approach.

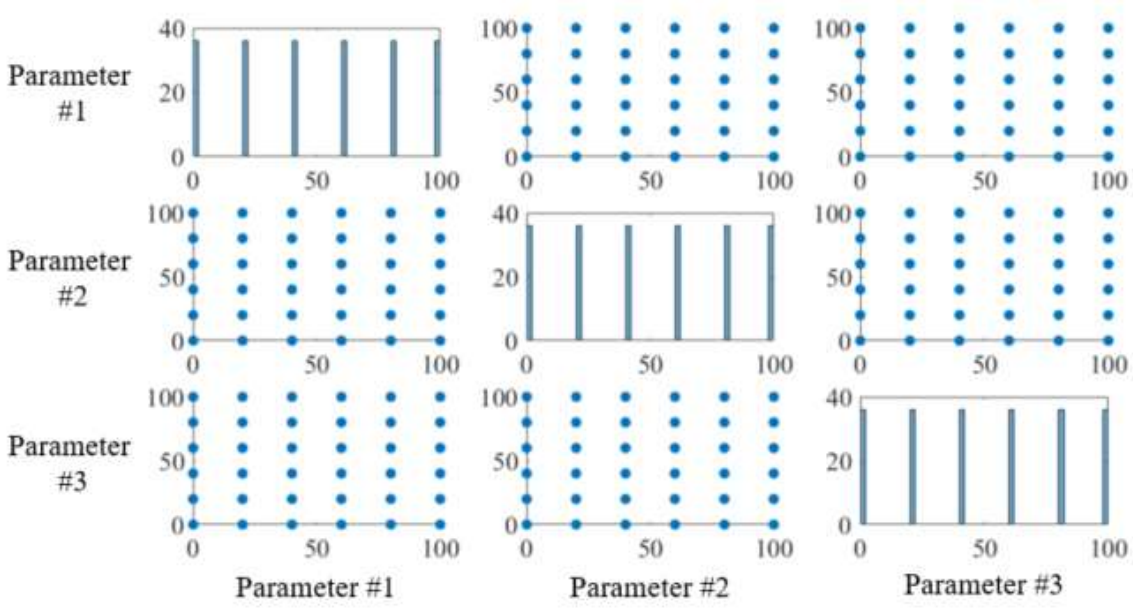

Figure 12: Sample Space of a Deterministic Approach

5.1.2.2.2 Probabilistic Approach

An alternative method of sampling is via a probabilistic approach. Unlike the deterministic method, the probabilistic method is not an iterative process. The number of samples desired is chosen rather than determined from the parameters, and the sample space for the structure is developed based on prior probabilities of each parameter.

5.1.2.2.2.1 Prior Probability Distributions of the Model Parameters

Ideally, structures have minimal uncertainty associated with parameters such as boundary conditions and material properties. In reality, however, these parameters can be difficult to identify with absolute certainty due to the complexity or assembly of the structure as well as the precision of the material manufacturer. In some cases, slight changes in these parameters can drastically alter the model responses. In order to account for these

uncertainties, a probability distribution is applied to each model parameter. For the purpose of better understanding this section, parameter distributions were arbitrarily chosen. Parameters #1 and #2 are normally distributed, and Parameter #3 is uniformly distributed. Once the prior probabilities for each parameter are determined, the sample space is developed by means of Monte Carlo simulations.

5.1.2.2.2.2 Monte Carlo (MC) Simulations

Monte Carlo (MC) simulation is a technique of randomly sampling values within a set domain. Within the probabilistic approach, values are randomly selected based on their respective probability distributions. This selection process determines the parameter combination for each sample before any analysis is conducted. For the parameters mentioned above, Monte Carlo simulations were used to develop the sample space shown in Figure 13 for a total of 500 samples.

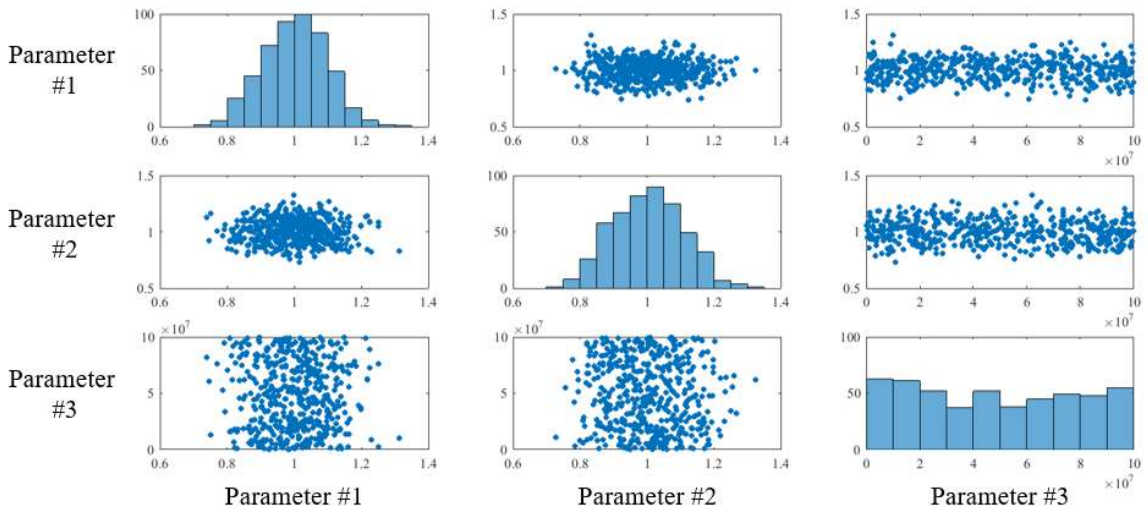

Figure 13: Sample Space of 500 Samples via Monte Carlo (MC) Simulations

Many sampling techniques have been derived from Monte Carlo simulations. One such technique is Markov Chain Monte Carlo (MCMC) simulations. MCMC uses informed decision-making to select the parameters of the sample combinations. In contrast to MC, the sampling and analysis of one sample is completed before the next sample is selected. The information gathered from the analysis of the previous sample is used to determine the parameter combination of the following sample. This process continues until convergence is achieved within all of the parameters. The informed decision-making ability of this technique allows for a smaller sample space thus decreasing computation time. While more efficient than the MC procedure, MCMC is more complicated and computationally involved. Therefore, a simple but efficient MC-derived technique called Latin Hypercube sampling (LHS) is used for this study.

5.1.2.2.2.3 Latin Hypercube Sampling (LHS)

Latin Hypercube Sampling (LHS) is an un-informed sampling technique that retains the defining feature of MC simulations in the fact that the sampling is random; however, LHS methods produce sample spaces that more accurately define the probability distributions of each parameter, as shown in Figure 14. In comparison to Figure 13, notice how the distributions of the LHS sample space in Figure 14 more accurately depict the probability distributions even though both methods use 500 samples. During LHS, the sample space of each parameter is divided into bins and then sampled randomly from within each of those bins. This allows the distributions to be defined more effectively with fewer samples. Furthermore, by implementing this method, a smaller sample space is required, and the time needed for model simulations is reduced. One drawback of the LHS method is that the number of samples needed for a particular project is unknown before conducting the

analysis of the structure. Therefore, a large initial sample size must be chosen at the beginning of the process, and a smaller number of samples required is determined by convergence later. Although not as efficient as the MCMC technique, the LHS technique is a viable option for creating the sample space as it is more efficient than MC and less computationally involved than MCMC. The sample space is then used to develop structural models via finite element analysis.

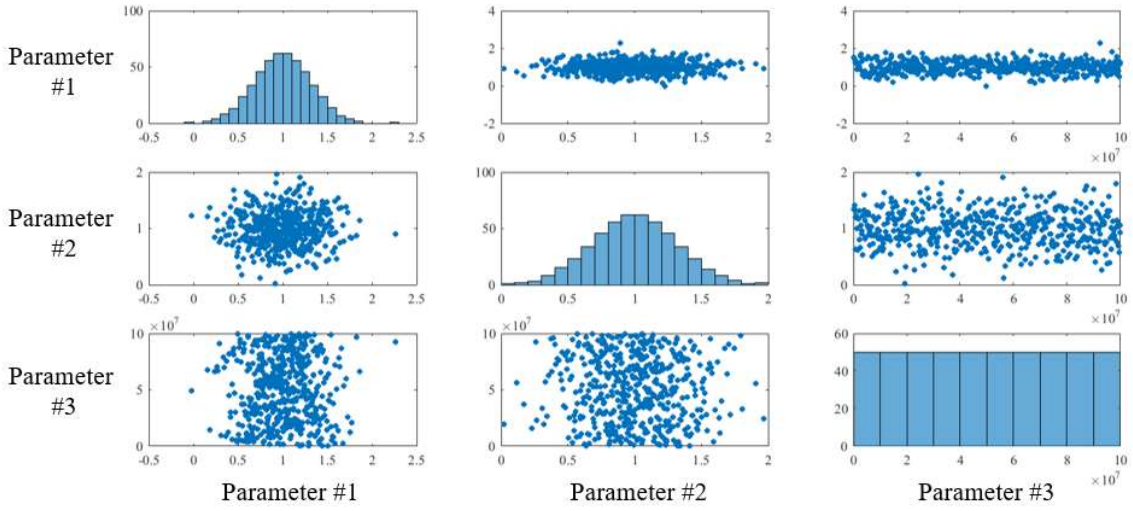

Figure 14: Sample Space for 500 Samples via Latin Hypercube Sampling (LHS)

5.1.2.3 Structural Models via Finite Element Analysis

Once the sample space has been created, the structure must undergo a finite element analysis using the parameter combination from each sample. This task can be a meticulous and time-consuming process, especially if the parameters are addressed manually. However, one way of alleviating these hassles is automation. By using automation, the process has

little need for human intervention, is more efficient, and reduces errors. For this study, the process of automation is made possible by an application programming interface (API) between a programming software (Matlab) and the finite element software (Strand7). The Matlab program sets the model parameters within Strand7 as the parameter combination of the first sample of the sample space. Then, a finite element analysis of the structure is performed. In this case, the linear static solver within Strand7 is utilized to perform this task. Finally, desired structural responses are recorded as output in a results file. The Matlab program repeats the process with the parameter combination of the second sample and continues until all of the samples have completed a finite element analysis to form the structural models.

5.1.3 Single Model Analysis using Bayes Theorem

5.1.3.1 Calibrated Model

5.1.3.1.1 Parameter Limits Check

The first task after the results file has been completed is to verify that the measured values are within the ranges of responses from the models. If the measured values are outside of these limits, the model parameters were not chosen properly and need to be adjusted. This result could be indicative of a missing mechanism, meaning an important model parameter was not included in the analysis or the bounds of a parameter were incorrect.

5.1.3.1.2 Posterior Probability for Each Model

Referring back to Figure 2, the ultimate goal of the evaluation process is to identify a structural model or multiple models that behave in a similar manner to a physical structure. For this study, the similarity of the structural models to the physical structure is quantified by their respective posterior probabilities. The posterior probability of each model

essentially equates to a weight on that model. Higher weights indicate that a sample has a higher likelihood of generating results similar to those measured from the actual structure. The posterior probability for each model is determined by Bayes Theorem shown in Equation 15, where *H* is defined as the hypothesis and *e* is defined as the evidence.

$$\boldsymbol{P(H|e) = \frac{P(e|H)\,P(H)}{P(e)}} \quad \textbf{(15)}$$

For the purpose of this research, the evidence is the measured responses and the hypothesis is the structural model. The posterior probability, P(H|e), answers the question "how probable is a structural model given the observed measured responses?" and is comprised of three unique components: prior probability, likelihood, and marginal probability. The prior probability, P(H), answers the question "how probable was a structural model before observing the measured responses?" The likelihood, P(e|H), answers the question "how probable is the measured response given that the structural model is true?" The marginal probability, P(e), answers the question "how probable is a structural model compared to all other structural models?". Bayes Theorem as it applies to this study is shown in Equation 16 and explained in further detail below:

$$\boldsymbol{Post_{model} = \frac{Prior_{model} * MLE_{model}}{Marginal}} \quad \textbf{(16)}$$

5.1.3.1.2.1 Prior Probability of Each Model

The prior probability ($Prior_{model}$) of each model is dependent upon the number of samples and the probability distributions of each parameter that were used for the development of the sample space. Equation 17 below displays how to calculate the prior probability for a model. First, the prior probabilities for each parameter ($Prior_{parameters}$) are

determined from the probability distributions used for the development of the sample space. For each model, the probabilities associated with the parameters within the model are multiplied. Then, this number is normalized with respect to all of the models. This is done by summing the product of the $\text{Prior}_{\text{parameters}}$ of each of the models to create a normalization constant. Finally, the product of the $\text{Prior}_{\text{parameters}}$ for each model is divided by the normalization constant to create the $\text{Prior}_{\text{model}}$ for each model. Note that when the number of samples changes, the prior probabilities of each parameter change thus changing the prior probability of the model.

$$\boldsymbol{Prior_{model}} = \frac{\prod \boldsymbol{Prior_{parameters}}}{\sum(\prod \boldsymbol{Prior_{parameters}})} \tag{17}$$

5.1.3.1.2.2 Likelihood of Each Model

The likelihood of each model considers how accurate the measured responses from the actual structure are to the responses from each model. The likelihood of each model is determined numerically by a maximum likelihood estimator (MLE) shown in Equation 18 below where *i* is the model number, *n* is the number of responses measured, *x* is the value of the measured response, *u* and *σ* are the value of the response and associated error, respectively, from the structural model. Note that each model has only one MLE.

$$\boldsymbol{MLE_i} = \prod_{j=1}^{n} \frac{1}{2\pi\sigma_j^2} * \boldsymbol{e}^{\frac{-(x_j - u_{ij})^2}{2\sigma_j^2}} \tag{18}$$

5.1.3.1.2.3 Marginal Probability

The marginal probability (Marginal) is with respect to all the models and is essentially a normalizing constant of the product of the prior probability and likelihood of each model. The calculation of marginal probability is shown in Equation 19 below.

$$\textbf{Marginal} = \sum(\boldsymbol{MLE_{model}} * \boldsymbol{Prior_{model}}) \quad \textbf{(19)}$$

Finally, the posterior probabilities of each model ($Post_{model}$) are calculated according to Equation 16. These probabilities are used again later to determine the convergence of each parameter.

5.1.3.1.2.4 Models Required for Convergence

As mentioned previously, one of the downsides of using the LHS method is that the number of samples and thus the number of models needed for analysis is not known at the beginning of the analysis process. However, the number of samples required can be determined by investigating the convergence of the expected value and variance of each parameter using Equation 20 and 21, respectively. In these equations, *x* is the parameter value and *f(x)* is the posterior probability for a sample.

$$\boldsymbol{E(X)} = \int_{-\infty}^{\infty} \boldsymbol{x\, f(x) dx} \quad \textbf{(20)}$$

$$\boldsymbol{V(x)} = \int_{-\infty}^{\infty} \boldsymbol{x^2\, f(x)\, dx} - \left(\int_{-\infty}^{\infty} \boldsymbol{x\, f(x)\, dx}\right)^2 \quad \textbf{(21)}$$

Convergence is reached when the expected value and the variance stabilizes and remains within a +/- 5% limit. Mathematically, the expected value and variance stabilize when enough samples exist such that the area under the curve produced by each of the above equations converges to one value. Each parameter will have a required number of samples necessary for convergence. The largest number of samples required from the parameters is

the minimum number of samples to satisfy convergence of all parameters. This number is used as the overall samples required.

Once the sample number is determined, the probability distributions (both prior and posterior) for that sample space are used for analysis. The posterior probabilities are used to weigh each model accordingly. For single model analysis, the model with the largest posterior probability is the calibrated model and is used for determining more information about the structure.

5.1.3.2 Parameter Identification

Once the calibrated model has been identified, the parameters of the model are used to explain the conditions of the bridge. With the value of these parameters now known, insight into conditions defining the thermal behavior of the structure can be obtained.

5.1.3.3 Predictive Responses

The responses of the calibrated model, called predictive responses, are also used to provide information regarding the behavior of the structure. The responses show how well the calibrated model correlates with the measured responses from the physical structure. This is achieved by calculating the error between the response of the calibrated model and the measured response. Another benefit of this process is the ability to inquire additional information about the structure than just what is directly measured. Initially unknown responses such as stresses, strains, or displacements at other locations of the structure can be collected from the calibrated model. To be more efficient, these responses need are identified before generating the structural models so that the responses can be collected simultaneously with the measured responses.

Analysis of the parameters and predictive responses of the calibrated model allows for assessment of the thermal behavior of the structure as well as evaluation of its structural health. Insight regarding thermal behavior is also available from the multiple model approach explained in detail below.

5.1.4 Multiple Model Analysis using Bayes Theorem

5.1.4.1 Candidate Models

5.1.4.1.1 Candidate Model Identification

Once the sample number is determined and the models are weighed according to their respective posterior probabilities, the structural models can be used for a multiple model analysis. The structural models with the largest posterior probabilities are considered candidate models and are used for determining more information about the structure. The number of candidate models is determined by the amount of models required to surpass 95% of the total probability. As illustrated in Figure 15 below, the number of candidate models is significantly less than the required or initial number of models.

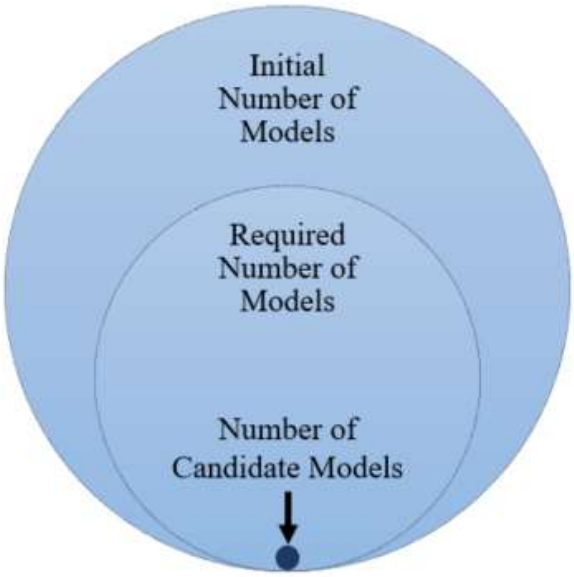

Figure 15: Comparison of Number of Models

5.1.4.2 Predictive Responses

Rather than the responses from just a single model, the responses from all of the candidate models are analyzed to provide more information about the structure. Histograms and plots of the cumulative posterior probabilities are beneficial for comprehending the results. By using these tools, the results are studied to determine if any trends regarding the behavior of the structure exist. Similar to the single model approach, the predictive responses can be used to see how well the candidate models correlate to the measured responses from the physical structure. This is achieved by calculating the error between the measured responses and the mean of the corresponding responses within the candidate models.

5.1.4.3 Refined Parameters

The model parameters from the candidate models are analyzed to provide more information about the structure. By analyzing multiple models, the parameters may be refined by investigating the mean and variance associated with each parameter. The mean provides insight to the value of the parameter where the variance addresses the uncertainty of the parameter. If the variance of the posterior probability is reduced compared to the variance of the prior probability, the uncertainty of that parameter is also reduced.

Furthermore, this information from the multiple model analysis may aid engineers and owners of the structure with decisions regarding rehabilitations or simply provide a better understanding of the overall thermal behavior of the structure. For the purpose of attaining a more comprehensive understanding of the TD structural evaluation method used in this study, an example scenario is provided below.

5.2 Example: Simply Supported Beam Exposed to Uniform Temperature Change

5.2.1 Field Experiment

5.2.1.1 Structure Overview

The structure used this example, shown below in Figure 16, is a simply-supported steel beam that is subjected to a uniform temperature change of +50°C (°F). The beam has a solid, square cross-section with an area of 5800 square-millimeters (9.0 square-inches) and a total length of 76.2 meters (250 feet). The beam is partially restrained longitudinally by a spring, which inhibits the thermal expansion of the structure to an extent.

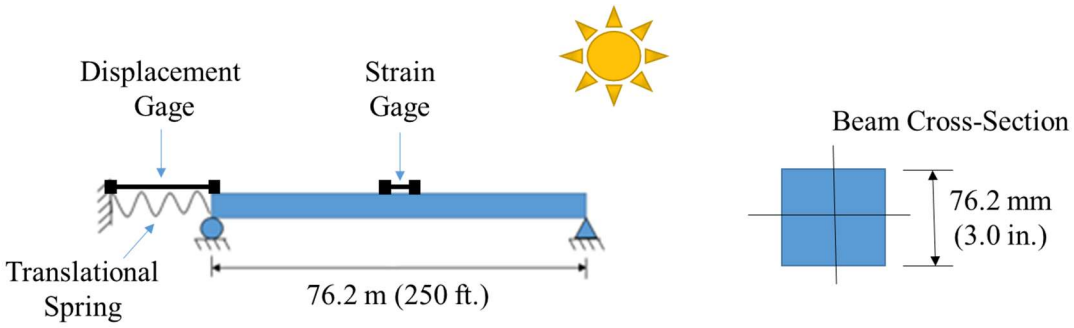

Figure 16: Example Structure Overview

5.2.1.2 Monitoring System

The beam is instrumented with a strain gage at midspan and displacement gage on one end. The displacement gage is located at the expansive (roller) end of the beam in order to identify how much the beam elongates due to the thermal load. Although the total displacement is affected by the partial restrain of the translational spring, the displacement gage only measures the unrestrained displacement. The response measured by the strain gage, however, is attributed to the restrain of the beam by the spring and is the restrained strain.

5.2.1.3 Measured Responses

Since this example is not part of an actual field study, a set of plausible measured responses were chosen. The unrestrained displacement and restrained strain measured for this example are 24.9 millimeters (0.98 inches) and 375 microstrain, respectively. For this example only, the structure conditions that produce these measurements were known and used as theoretical values to test the effectiveness of the method. However, throughout the analysis, these conditions are assumed to be unknown. The measured responses occur when

the translational spring has a stiffness of 1.75×10^4 kN/m (1200 kip/ft) and the coefficient of thermal expansion for the steel is 1.2 times the design value of 11.7×10^{-6} /°C (6.5×10^{-6} /°F). More discussion on the parameter selection is presented below.

5.2.2 Numerical Models

5.2.2.1 Model Parameters

The structure conditions investigated as part of this simple example include a boundary condition as well as a material property. The longitudinal stiffness of the spring (K) and the coefficient of thermal expansion of the steel (CTES) were chosen to have the most uncertainty. Furthermore, these parameters were used to define the structural models.

5.2.2.2 Development of Sample Space

The prior probability distributions assigned to the model parameters were either normal or uniform. A normal distribution was assigned to the CTES parameter since this property is generally quality-controlled in industry and hence less uncertain. The distribution is applied as a multiplier of the true value with a mean of 1.0 and a standard deviation of 0.04. The design value of the coefficient of thermal expansion for steel is 11.7×10^{-6} /°C (6.5×10^{-6} /°F). The mean and standard deviations of the distributions were chosen based on related literature (Dubbs and Moon 2015) as well as the fact that this distribution results in a multiplier between 0 and 2. Parameter multipliers less than or equal to zero are impractical and can produce erroneous results. The stiffness of the spring was considered the most uncertain condition and was assigned a uniform distribution across a range of values. This range was determined in an independent study investigating the degree of fixity of the spring from unrestrained to completely restrained. The stiffness-response relationship is logarithmic with bounds between 0 kN/m to 1.75×10^7 kN/m (12×10^5 kip/ft).

The initial sample size was chosen as 50,000 samples. Using the LHS sampling technique, the prior probability distributions of each parameter produce the sample space shown in Figure 17.

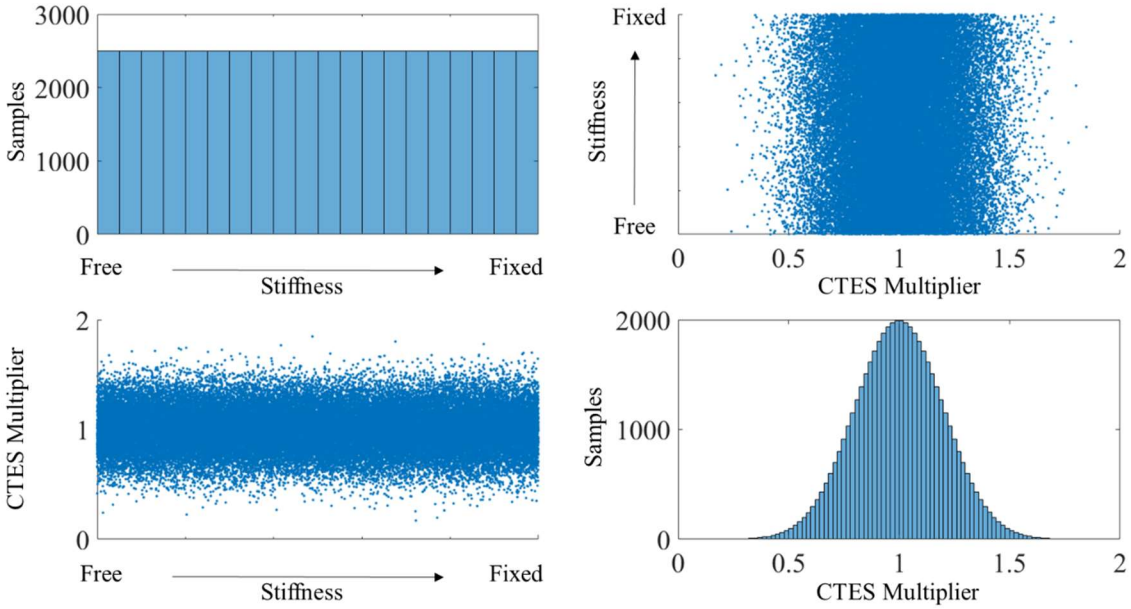

Figure 17: Sample Space for 50,000 Total Samples

5.2.2.3 Structural Models via Finite Element Analysis

Once the sample size was determined and the sample space developed, a structural model was created with each parameter combination of the sample space for a total of 50,000 models.

5.2.3 Single Model Analysis using Bayes Theorem

5.2.3.1 Calibrated Model

In order to identify the calibrated model, the first task was to ensure that response distribution included the value of the measured response. All of the measured responses were within the distribution for their respective responses. The next task was to proceed to calibration with the measured responses using Bayes Theorem. Once Bayes Theorem was completed on the data, the posterior probabilities of each of the samples were analyzed. The required number of models determined by the convergence of the expected value and variance of each parameter was 24,600. The model with the largest posterior probability was identified and used as the calibrated model.

5.2.3.2 Parameter Identification

The model parameters associated with the calibrated model are shown in Figure 18 and quantified below in Table 1. The parameters for the calibrated model were identified as 1.74×10^4 kN/m (1,190 kip/ft) for the spring stiffness and 1.16 for the coefficient of thermal expansion multiplier. Since the theoretical values are known, the accuracy of the method is investigated via the percent difference between the theoretical parameter values and the parameter values from the calibrated model. In this case, the structural evaluation method was able to identify the parameters accurately as the percent differences were <1% and 4% for the K and CTES parameters, respectively. This is due to the logarithmic nature of the stiffness parameter. As mentioned earlier, the parameter value was randomly sampled evenly among the range from free to fixed conditions; however, the logarithmic nature of the stiffness produced more responses closer in value to the measured response. With more

responses similar to the measured, the calibration was more sensitive and able to identify the parameter with less error.

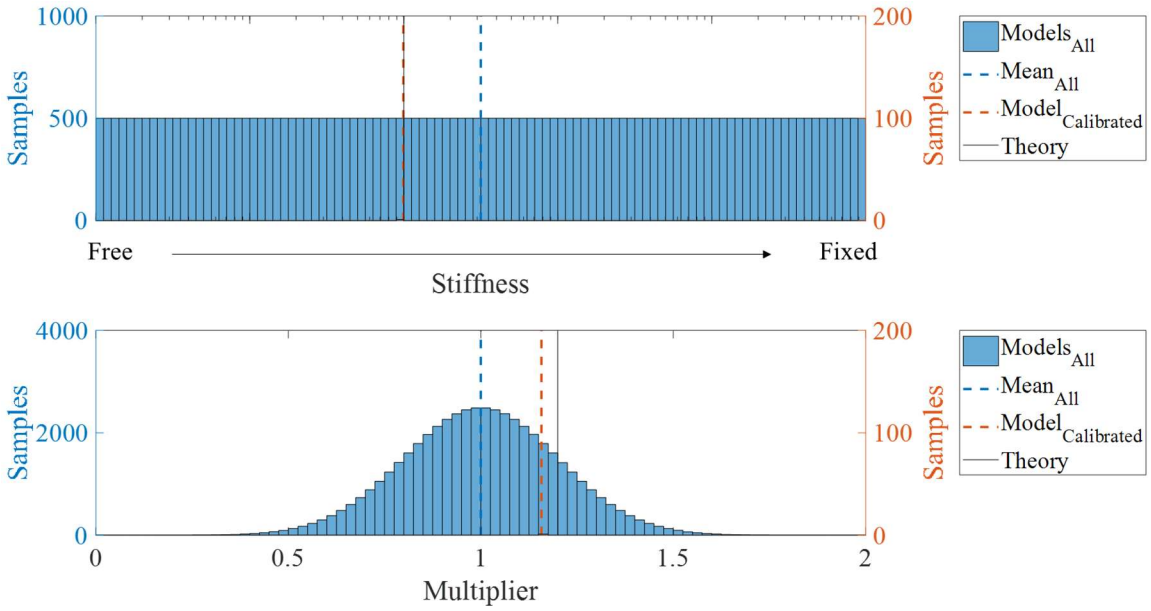

Figure 18: Calibrated Model Parameters of the Spring Stiffness and CTES Multiplier

Table 1: Calibrated Model Percent Difference with Respect to Theoretical Parameter Values

Parameter	Theory	Calibrated	% Diff.
K	1.75e4 kN/m (1,200 kip/ft)	1.74e4 kN/m (1,190 kip/ft)	<1%
CTES	1.20	1.16	4%

5.2.3.3 Predictive Responses

The predictive response are analyzed by comparing the responses from the calibrated model to the measured responses. This shows how similar the calibrated model is to the measured behavior. The responses associated with the calibrated model are shown in Figure 19 and quantified in Table 2. The calibrated model produced a displacement response of 24.1 mm (0.95 in.) compared to the measured response of 24.9 mm (0.98 in.), yielding a 3% difference. Similarly, the strain response of the calibrated model was 361 microstrain compared to the measured 375 microstrain, yielding a 4% difference.

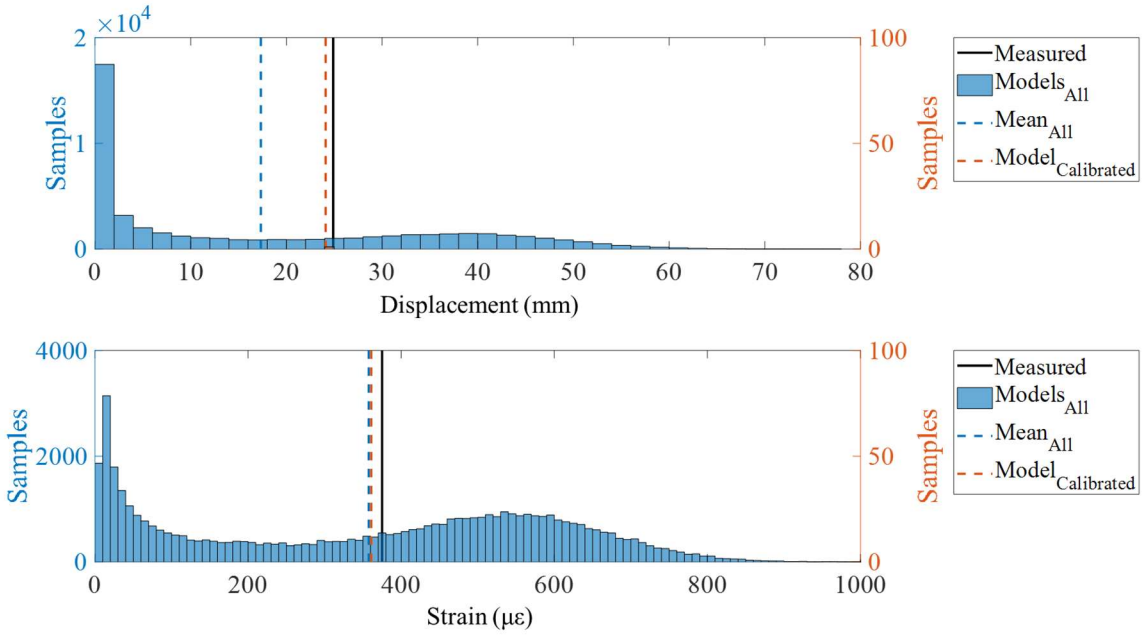

Figure 19: Calibrated Model Response of the Unrestrained Displacement and Restrained Strain

Table 2: Calibrated Model Percent Difference with Respect to Measured Responses

Gage	Measured	Calibrated	% Diff.
Displacement	24.9 mm (0.98 in.)	24.1 mm (0.95 in.)	3%
Strain	375 με	361 με	4%

5.2.4 Multiple Model Analysis using Bayes Theorem

5.2.4.1 Candidate Models

The calibration process using Bayes Theorem described in Section 3 was also used to identify the candidate models. Once Bayes Theorem was completed on the data, the posterior probabilities of each of the samples were analyzed. The candidate models were identified as the samples with the highest probabilities that comprised 95% of the total posterior probability. For this example, the number of samples required to meet or exceed 95% total probability was 484 models. Furthermore, the 484 models that were most probable were used as the candidate models.

5.2.4.2 Predictive Responses

The candidate models were used to analyze the responses of the structure. Figure 20 shows the response distributions from all of the structural models as well as the response distributions from just the candidate models. The values of the measured responses are also shown.

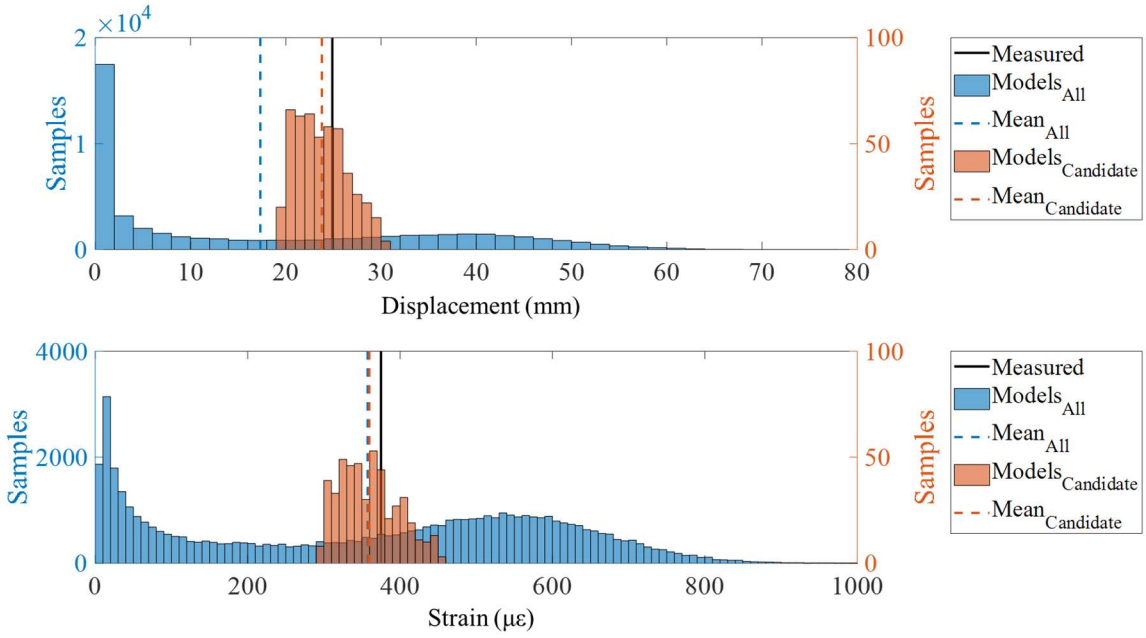

Figure 20: Candidate Model Response of the Unrestrained Displacement and Restrained Strain

The response distributions are given numerically in Table 3. Through the calibration process, the response distributions from the structural models were significantly reduced to the response distributions of the candidate models. The variance of the distributions for the displacement and strain reduced by 85% and 84%, respectively. As expected, the candidate model distributions were also more accurate to the measured responses. The mean of the response distributions were compared to the measured responses. The gages each experienced a relatively low mean percent difference of 4%. This is due to the fact that none of the structural models simulate the measured responses exactly.

Table 3: Candidate Model Response Distributions

Gage	Measured	Prior Distribution		Posterior Distribution		Uncert. Red.	Mean % Diff.
		Mean	Var.	Mean	Var.		
Disp.	24.9 mm (0.98 in.)	17.3 mm (0.68 in.)	18.1 mm (0.71 in.)	23.8 mm (0.94 in.)	2.7 mm (0.11 in.)	85%	4%
Strain	375 με	358 με	243 με	360 με	39 με	84%	4%

5.2.4.3 Refined Parameters

The candidate models were also used to refine the parameters of the models and hence provide insight regarding the boundary conditions of the structure. Figure 21 shows the model parameter distributions from all of the structural models as well as the parameter distributions from just the candidate models. The theoretical parameters are also shown. The parameters from the candidate models were able to significantly reduce the uncertainty of both of the model parameters.

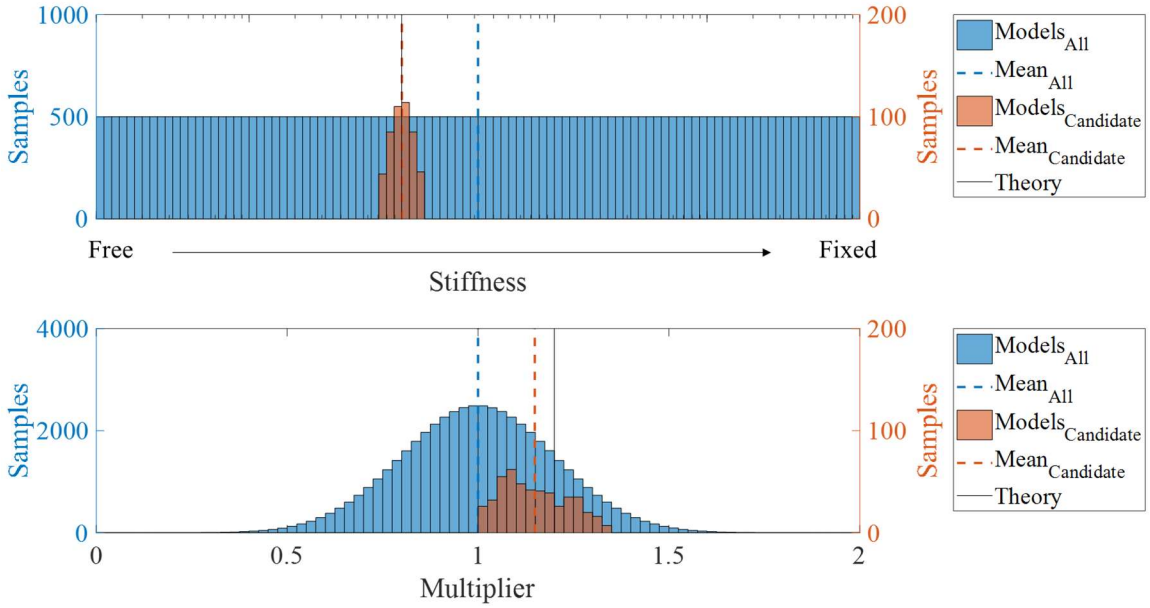

Figure 21: Candidate Model Parameters of the Spring Stiffness and CTES Multiplier

The parameter distributions are given numerically in Table 4 below. The stiffness model parameter experienced the largest reduction of uncertainty by decreasing the variance of the distribution by 95%. The variance of the coefficient of thermal expansion of the steel also experienced a reduction though not to same extent. The K parameter was only reduced by 57%. The theory percent difference compared the mean of the posterior distribution to the theoretical parameters. The evaluation method was able to identify the CTES parameter with a percent difference of 4%. The evaluation method identified the K parameter exceptionally well as indicated with a percent difference of <1%.

Table 4: Candidate Model Parameter Distributions

Parameter	Theory	Prior Distribution		Posterior Distribution		Uncert. Red.	Theory % Diff.
		Mean	Var.	Mean	Var.		
K	1.75e4 kN/m (1,200 kip/ft)	5.54e4 kN/m (3,790 kip/ft)	4,860 kN/m (333 kip/ft)	1.76e4 kN/m (1,200 kip/ft)	206 kN/m (14 kip/ft)	95%	<1%
CTES	1.2	1.00	0.20	1.16	0.08	57%	4%

5.2.5 Conclusions

As demonstrated by this simple example, the evaluation method used in this study has the potential to provide valuable information regarding health conditions of a structure. The single and multiple model approaches provided similar results and are proven valid techniques for this purpose. For both approaches, the boundary condition and material property are identified by each parameter's posterior distribution within a percent difference of 5%. Additionally, the uncertainty of each parameter is reduced compared to initial knowledge of parameter conditions.

6. RESEARCH APPROACH

The approach to this research is a gradual progression from the assessment of a relatively simple structure, then to the analysis of a more complex structure, and finally to the assembly of an extensive synthesis of related studies for comparisons, conclusions, and future recommendations. The objectives of this research are achieved by the successful completion of the four phases listed in Figure 22 below.

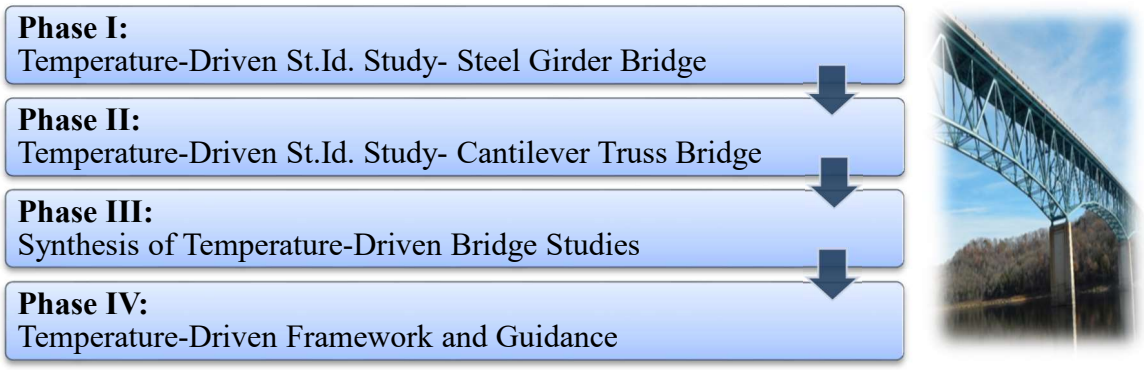

Figure 22: Overview of Research Approach: Phases of Completion

In order to establish a fundamental understanding of a TD evaluation on a physical structure, a steel girder bridge is evaluated as the pilot study in Phase I. The simple movement mechanisms and geometry of this bridge allow for thermal effects to be analyzed and comprehended on an elementary level. The fundamental knowledge and experience acquired in this phase is then directly applied to a more complex structure in Phase II. The supplemental study conducted in Phase II is performed on a long-span cantilever truss bridge. This bridge's complexity is due to its unique, large geometry and increased number

of unknown structural parameters. Both bridge studies from Phases I and II are then compiled into a synthesis with other temperature-related studies in Phase III. These projects comprise a broad spectrum of various approaches, parameters, and objectives utilized for TD evaluation. The purpose of the synthesis is to dissect each study, identify intellectual contributions, and then combine these contributions to provide insight to the overall scope of how and why TD evaluations are being conducted. For example, these contributions are in the form of measured parameters, type of bridge, data analysis method, and model calibration technique to name a few. All of these contributions are then restructured into a framework and set of guidelines for using a TD evaluation in Phase IV. The time of implementation for each of the phases is shown in the research schedule below in Table 5.

Table 5: Research Schedule: Phases of Completion

Research Schedule	Tennessee Tech University							Texas A&M University						
	Fall 2014	Spring 2015	Summer 2015	Fall 2015	Spring 2016	Summer 2016	Fall 2016	Spring 2017	Summer 2017	Fall 2017	Spring 2018	Summer 2018	Fall 2018	Spring 2019
Phase I: TD Study of Steel Girder Bridge														
TD St-Id Step 1														
TD St-Id Step 2														
TD St-Id Step 3														
TD St-Id Step 4														
TD St-Id Step 5														
TD St-Id Step 6														
Phase II: TD Study of Cantilever Truss Bridge														
TD St-Id Step 1														
TD St-Id Step 2														
TD St-Id Step 3														
TD St-Id Step 4														
TD St-Id Step 5														
TD St-Id Step 6														
Phase III: Synthesis of TD Studies														
Phase IV: TD Framework and Guidance														

7. PHASE I: TEMPERATURE-DRIVEN ST-ID STUDY – STEEL GIRDER BRIDGE*

The Tennessee Department of Transportation (TDOT) visually detected recurring structural damage with one of their steel girder bridges in eastern Tennessee, USA. In 2014, TDOT approached the structural research team in Tennessee Technological University's Civil and Environmental Engineering Department to conduct an investigation into the source of the damage on the Anderson County Route 61 Bridge. In the presented study, TD St-Id is employed on the Route 61 Bridge to assess the structural damage and determine potential causes of such deterioration. Preliminary findings of this study were presented and published in Engineering Structures (Murphy and Yarnold 2018).

7.1 Field Experiment

7.1.1 Structure Overview

The Route 61 Bridge shown in Figure 23(a) is a continuous, steel girder bridge located along State Route 61 in Anderson County, Tennessee, United States (Figure 23(b)). The bridge is oriented north to south and overpasses both a CSX railroad as well as Market Place, a downtown street (Figure 23(c)). Originally built in 1987 by TDOT, this structure was designed according to the specifications outlined in the 1977 Edition of American Association of State Highway and Transportation Officials (AASHTO) Standard Specifications for Highway Bridges (AASHTO 1977). The primary design load considered

* Reprinted with permission from "Temperature-Driven Structural Identification of a Steel Girder Bridge with an Integral Abutment" by Murphy, B. and Yarnold, M. 2018. *Engineering Structures*, Vol. 155, pp 209-221, Copyright 2018 Elsevier.

was a live load (HS20-44 with alternate military). Thermal considerations were also accounted for. The climate in Tennessee is classified as "moderate" with a design temperature range between -17.7℃ and 48.9℃ (0°F and 120°F) according to design standards.

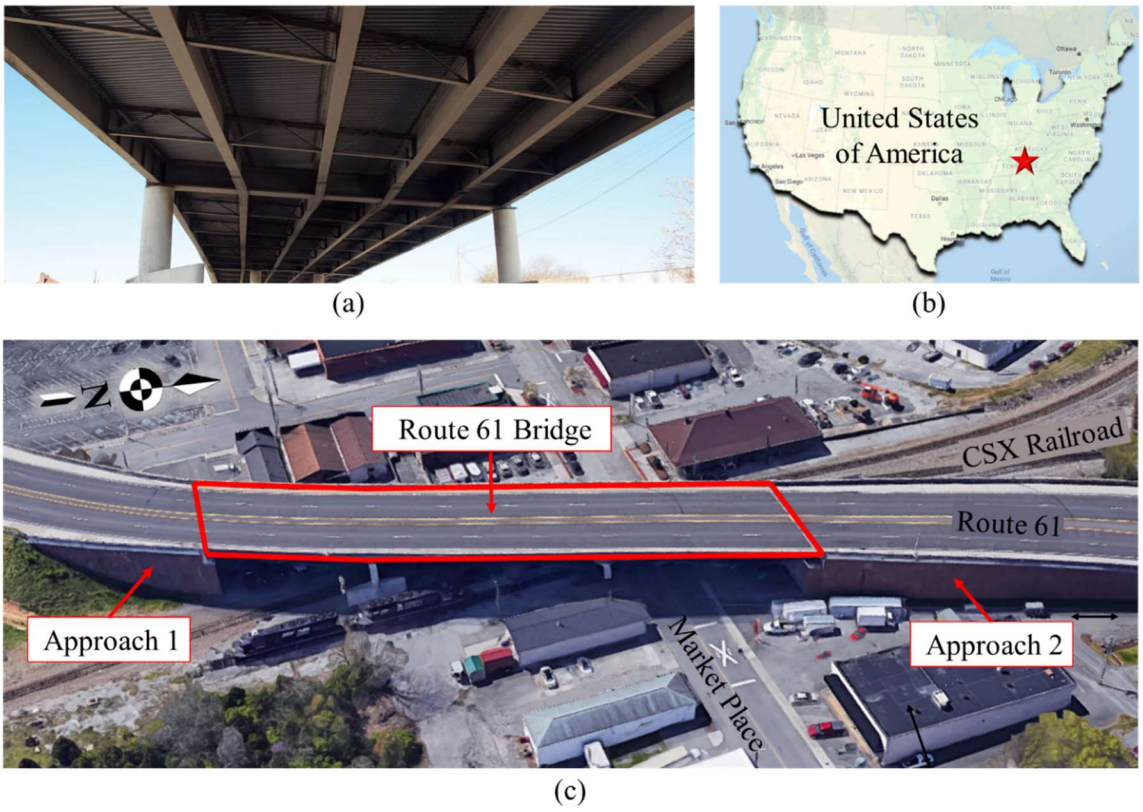

Figure 23: Route 61 Bridge: a) Structure, b) Location, and c) Orientation

The Route 61 Bridge has three spans and is a total length of approximately 108 meters (352 feet). The approaches leading up to the bridge are mechanically stabilized earth (MSE) retaining walls that support the roadway, concrete sidewalks, and barriers. The bridge is supported by an integral abutment on the southern end (Abutment 1) and rests on neoprene

bearings at the piers (Piers 1 and 2) and northern abutment (Abutment 2) as shown in Figure 24. Abutment 2 has an expansion joint with a total range of 8.9 centimeters (3.5 inches) per design specifications to accommodate for thermal expansion and contraction of the bridge. Spans 1 and 3 have a 21-degree skew while Span 2 has a 15-degree skew.

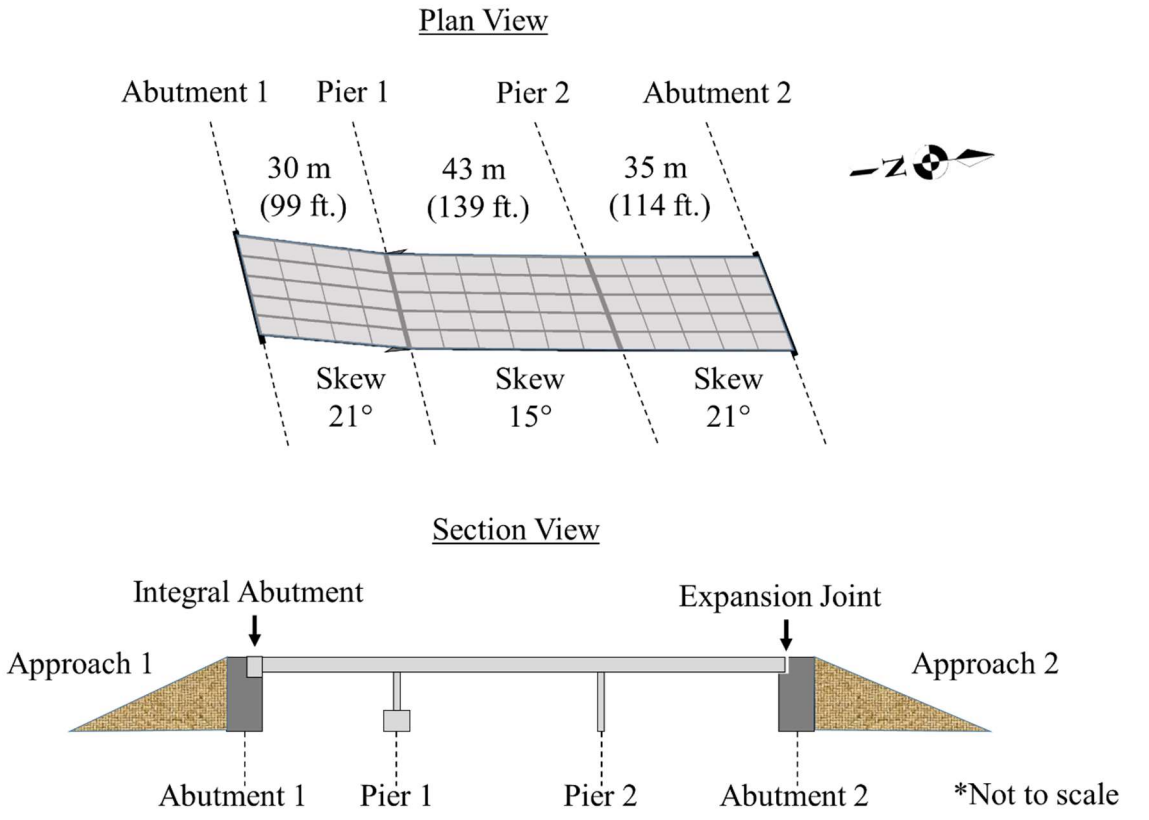

Figure 24: Route 61 Overview (Reprinted from Murphy and Yarnold 2018)

The Route 61 Bridge is composed of two materials: steel and concrete. The structural steel in the superstructure consists of six girders along the length of the bridge. Shown in Figure 25, the girders are built-up sections of ASTM 36 structural steel with a yield stress of 248 MPa (36 ksi). The web and flange dimensions are 1.1 meters (45 inches) and 0.4 meters

(15 inches), respectively, each with a thickness of 12.7 millimeters (0.5 inches). The concrete components of the bridge are specified as Class "A" with a compressive strength of 20.7 MPa (3 ksi). The deck was designed to be 20.7 meters (68 feet) wide and 248 millimeters (9.8 inches) thick with steel reinforcement. The piers of the substructure are also concrete with steel reinforcement.

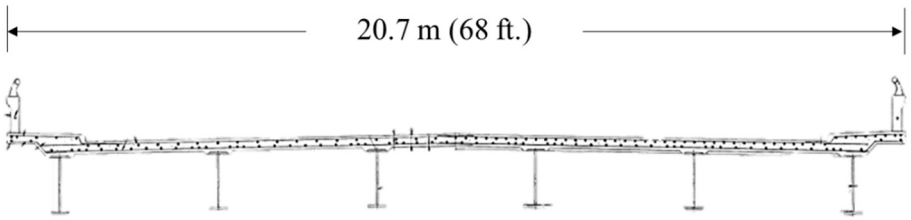

Figure 25: Deck Cross-section

Although a relatively young structure, the Route 61 Bridge had already undergone numerous rehabilitations by 2014. Figure 26 shows indications of deterioration along various components of the structure. Structural degradation including persistent cracking of the concrete sidewalk and abutment at the expansion joint was evident (Figure 26(a) and (b)). Barriers (Figure 26(c) and (d)) and guardrail supports (Figure 26(e)) showed signs of excessive cracking as well as lateral displacement. The neoprene bearings at the northern abutment were constantly in extended positions (Figure 26(f)), and the expansion joint remained closed.

Figure 26: Evidence of Deterioration: a) Cracking along concrete sidewalk, b) Section loss at abutment, c) Spalling on barrier, d) Lateral displacement of barrier, e) Deformed guardrail support, and f) Extended neoprene bearing (Reprinted from Murphy and Yarnold 2018)

7.1.2 Monitoring System

7.1.2.1 Preliminary A-priori Model

A three-dimensional element-level finite element model was created in Strand7 finite element analysis software and is shown in Figure 27. This model was developed according to details from the original plans and rehabilitation drawings. Four-node plate elements defined components such as the abutment caps, deck, and curb. Two-node beam elements defined the remaining components including the girders, diaphragms, piles, and piers. The base of each pile and pier spread footing was modeled as a fixed condition. The deck was modeled compositely with the bridge girders. Continuity conditions between the superstructure and substructure were modeled with two-node connection elements that could

simulate the behavior of the bearings or the integral abutment. Figure 27 depicts an enlarged view of how these conditions were modeled at Abutment 2. Additionally, the approach stiffness was simulated at the mid-height of the deck at both abutments using longitudinal spring elements to account for the potential restraint provided by the approaches. Upon completion, the model was independently checked and screened for errors.

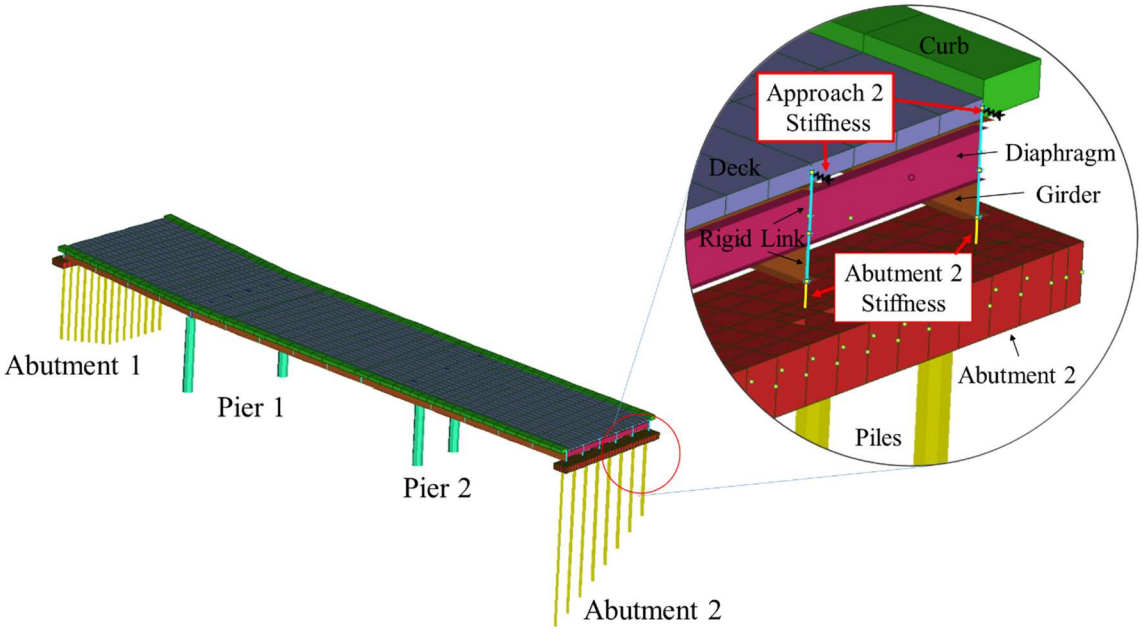

Figure 27: Finite Element Model of the Route 61 Bridge (Reprinted from Murphy and Yarnold 2018)

7.1.2.2 Monitoring System Design and Installation

A sensitivity study was conducted to determine the most effective locations to install monitoring equipment and quantify the thermal behavior of the bridge. The sensitivity study was conducted with a uniform temperature change of 28°C (50°F). Stresses calculated from restrained strain responses were recorded at eight cross-sections of the bridge as shown in

Figure 28 below. Three strain cross sections were located within Span 1 at Abutment 1 (Abut1), Span 1 midspan (Sp1Mid), and near the first pier (Pier1). Two cross sections were located within Span 2, including Span 2 midspan (Sp2Mid) and near the second pier (Pier2). The remaining three cross sections were located in Span 3 near Pier 2 (Sp3Pier), at Span 3 midspan (Sp3Mid), and at Abutment 2 (Abut2). In addition, the relative displacements at Abutment 2 (expansion end) for each of the girders were recorded. The sensitivity study concluded that the most sensitive locations were strain measurements near the abutment cross sections and relative displacement measurements at Abutment 2. Further details of the sensitivity study can be found in Yarnold and Wilson (2015).

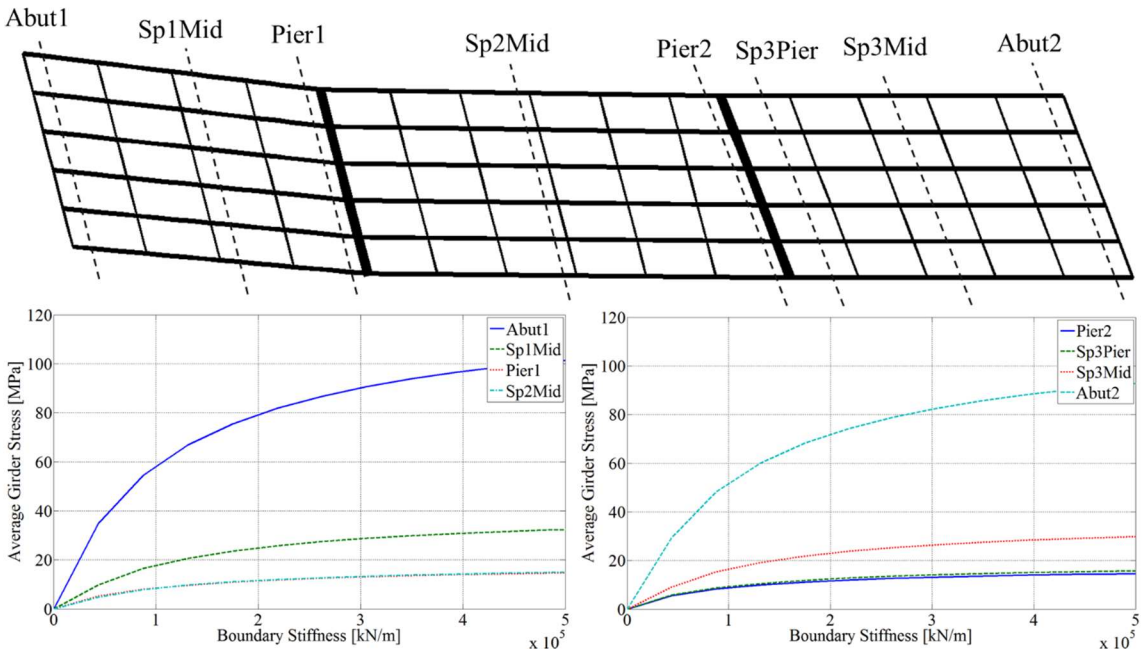

Figure 28: Sensitivity Study (Reprinted from Yarnold and Wilson 2015)

Once the sensitivity study was complete, the instrumentation plan, shown in Figure 29, was designed to utilize the optimum sensor locations. Although the cross section near Abutment 1 showed high sensitivity, the instrumentation plan primarily focused on the bridge behavior from Pier 2 to Abutment 2. This decision was due to project logistics such as limitations in time and resources since the project was an unfunded endeavor.

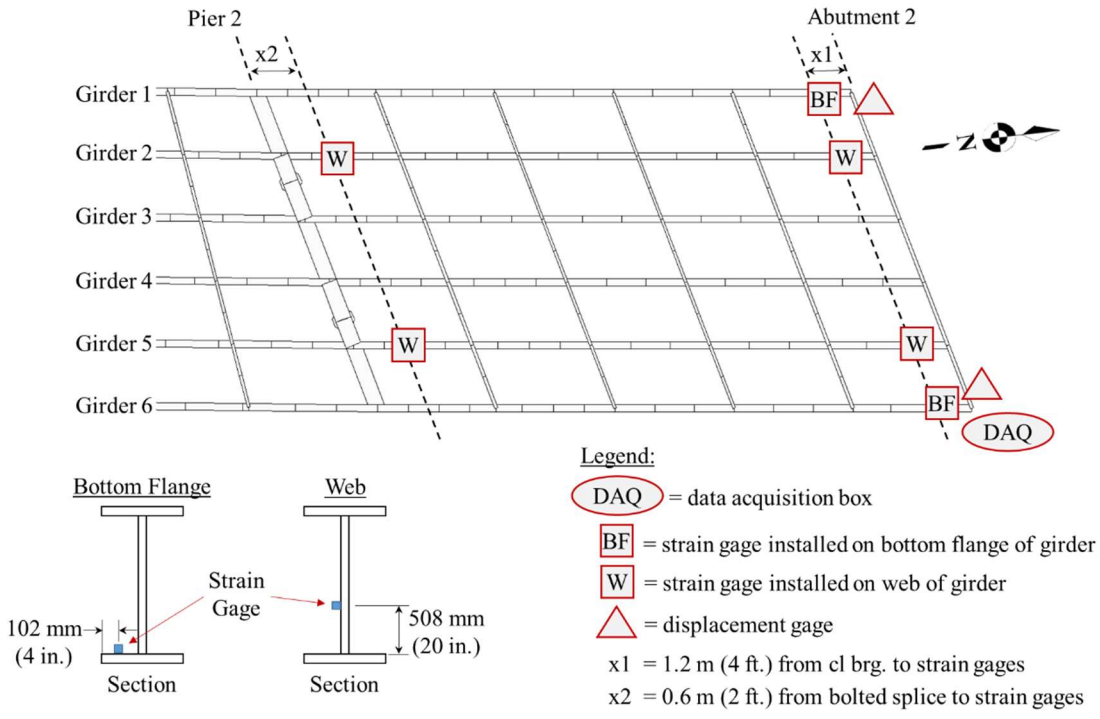

Figure 29: Instrumentation Plan (Reprinted from Murphy and Yarnold 2018)

The sensing equipment used to quantify the behavior of the bridge included six vibrating-wire strain gages and two vibrating wire displacement gages, each equipped with thermistors. Each gage was hardwired into a data acquisition (DAQ) system installed at the

base of Abutment 2. Throughout the experiment, the data from each gage was sent to the DAQ system to be collected and stored until retrieval.

7.1.2.2.1 Sensing Equipment

The strain gages used in this study were 152-millimeter (6-inch) vibrating-wire strain gages from Geokon (Model 4000). Each strain gage had to be bonded directly to the steel of the girder. Since the girders were coated with dirt and rust, the gages locations had to be cleaned using a grinder first. Once the steel was exposed, each strain gage was attached using a high-strength epoxy to bond the gage directly to the bridge girder as shown in Figure 30(a). Afterwards, the gages and exposed steel were painted to prevent corrosion. The strain gages were installed on the inside of the bridge members to mitigate any adverse effects from direct sunlight, which may produce differential temperatures between the sensor and attached area and lead to measurement error. Per the manufacturer's specifications, the strain gages were sampled with a frequency range of 450-1250 Hz.

To quantify the movement at Abutment 2, the displacement gages were mounted on the bridge girder and the abutment seat using clamps and brackets (Figure 30(b)). The displacement gages used in the study were 102-millimeter (4-inch) range vibrating wire displacement gages also from Geokon (Model 4435). The displacement gages were sampled with a frequency range of 1200-2800 Hz.

Figure 30: Sensing Equipment: a) Strain Gage and b) Displacement Gage (Reprinted from Murphy and Yarnold 2018)

7.1.2.2.2 Data Acquisition Equipment

The DAQ system shown in Figure 31 consisted of five pieces of equipment from Campbell Scientific: a CR3000, an AVW, a cellular modem, a battery, and a solar panel. The CR3000 is a datalogger and was essentially the brains of the DAQ system. This piece of equipment executed the code of the monitoring system and initiated when measurements were to be recorded. The CR3000 directly communicated with the AVW, a vibrating-wire analyzer. The AVW was the piece of equipment that actually triggered and recorded the measurement. With vibrating wire technology, measurements are determined by "plucking" and measuring the frequency of a wire within a gage. This "plucking" action is performed by the AVW, and then the data is sent to the CR3000. The CR3000 stored the data until it was retrieved either manually or via the cellular modem. The cell modem allowed the data to be accessed remotely without having the researchers on site. The monitoring system was powered by a 12-volt rechargeable battery. The battery alone could only sustain the

monitoring system for several days; therefore, a 90-watt solar panel (Figure 31) provided additional power and kept the battery charged throughout daytime hours. With the exception of the solar panel, the DAQ system was secured in a weather resistant enclosure to protect the equipment from damage.

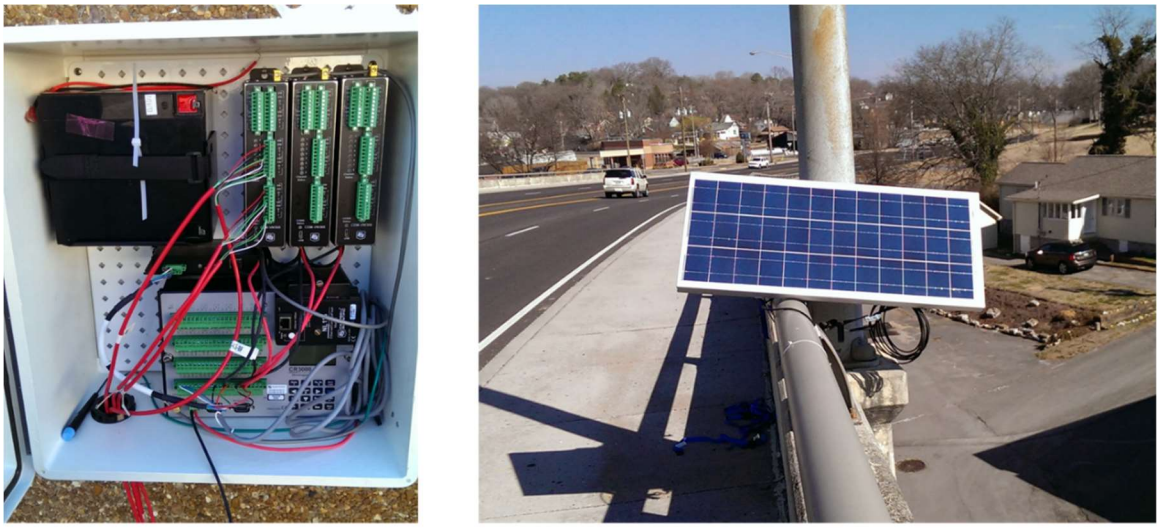

(a) (b)

Figure 31: Data Acquisition Equipment: a) DAQ Setup and b) Solar Panel (Reprinted from Murphy and Yarnold 2018)

7.1.2.3 Monitoring System Installation

Installation of the monitoring system began on March 25, 2014. With a team of three graduate students and a faculty advisor, the installation was completed within four days. Figure 32(a) shows two of the graduate students using a telescopic boom to install a strain gage on one of the interior girders near the pier. Figure 32(b and c) display the installation of strain gages on the inside of the exterior girders.

(a) (b) (c)

Figure 32: Installation Photos: a) Strain Gage on Interior Girder, b) Strain Gage on East Exterior Girder and c) Strain Gage on West Exterior Girder

7.1.3 Measured Responses

The monitoring system recorded data once every minute to maximize the amount of data collected without overconsumption of power. Data collection was initiated on March 25, 2014, and concluded on June 2, 2014, equating to a monitoring duration of approximately 70 days. The temperature of the bridge was measured by the thermistors of each strain or displacement gage throughout the duration of the monitoring period. The average temperature fluctuated from -1°C (30°F) to 32°C (90°F) during this time (

Figure 33).

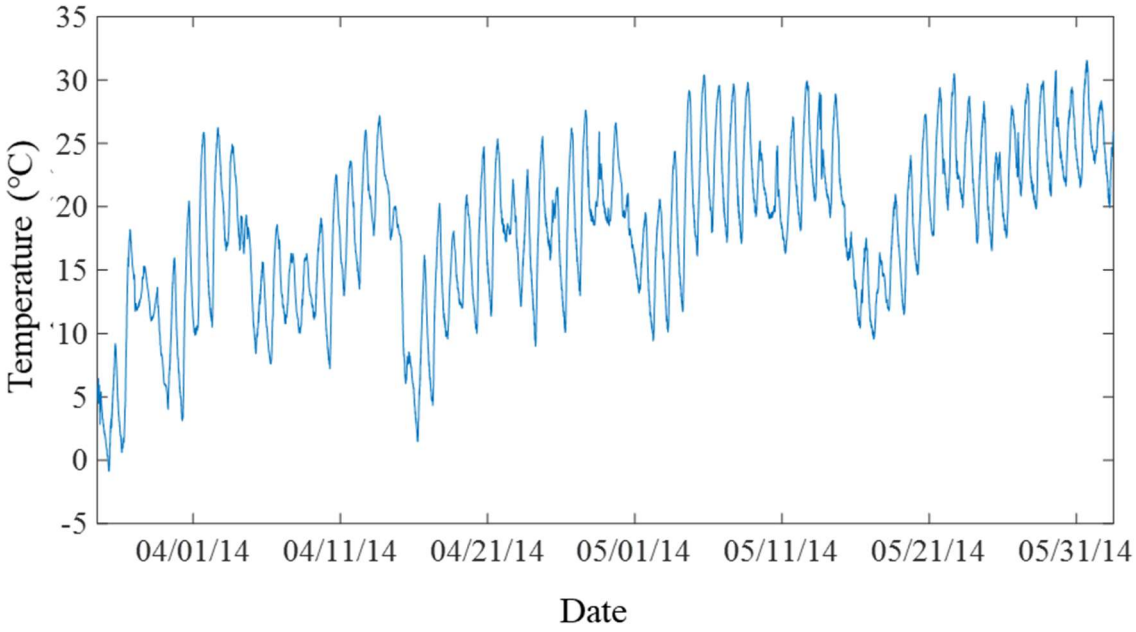

Figure 33: Average Temperature Recorded from All Thermistors

7.1.3.1 Preliminary Data Processing

Data quality checks were performed to ensure reliability of the results. The measured responses of each gage are shown in Figure 34-Figure 41. While each of the gages display daily cyclic behavior as expected, discrepancies during the daytime between gages located on exterior girders versus the interior girders indicated effects from thermal gradients due to direct sunlight may have been present. The thermal effects can be seen in the measurements from the exterior girders in particular (Figure 34 and Figure 37). The data experiences sharp spikes in response during the daylight hours of the majority of the days in the monitoring period.

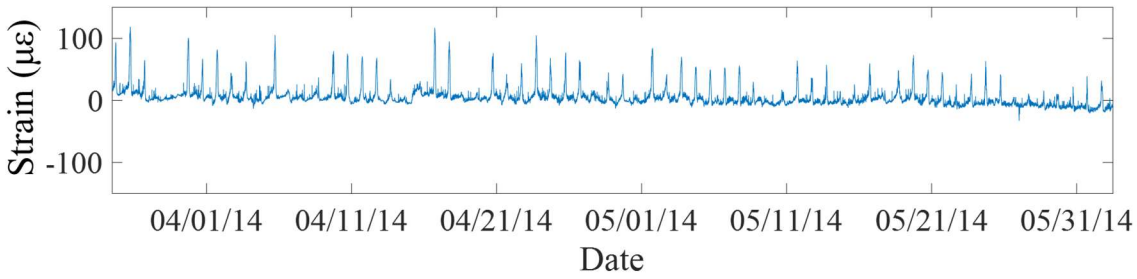

Figure 34: Measured Microstrain for Bottom Flange of Girder 1 at Abutment 2

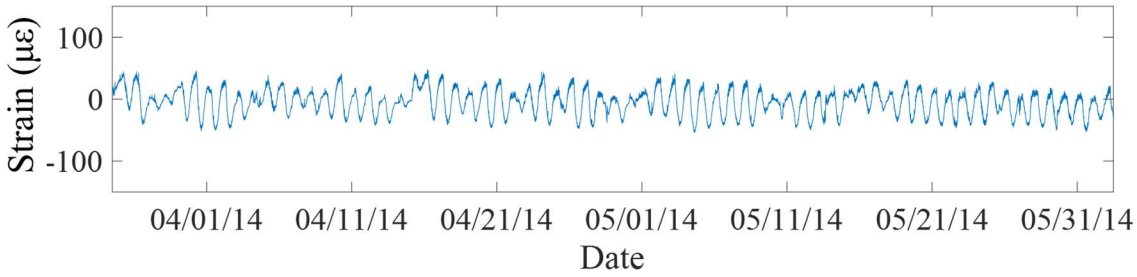

Figure 35: Measured Microstrain for Web of Girder 2 at Abutment 2

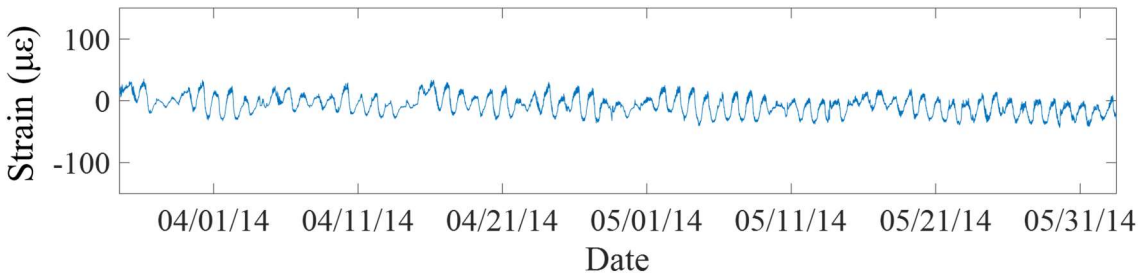

Figure 36: Measured Microstrain for Web of Girder 5 at Abutment 2

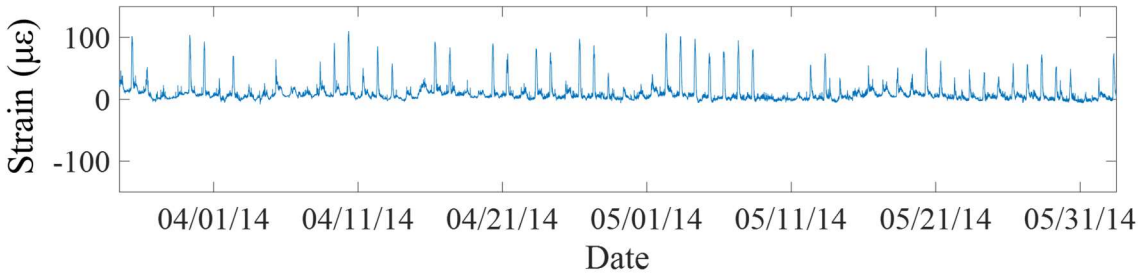

Figure 37: Measured Microstrain for Bottom Flange of Girder 6 at Abutment 2

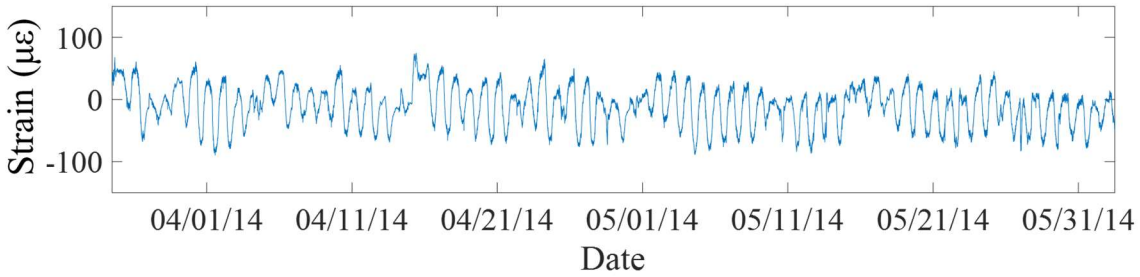

Figure 38: Measured Microstrain for Web of Girder 2 at Pier 2

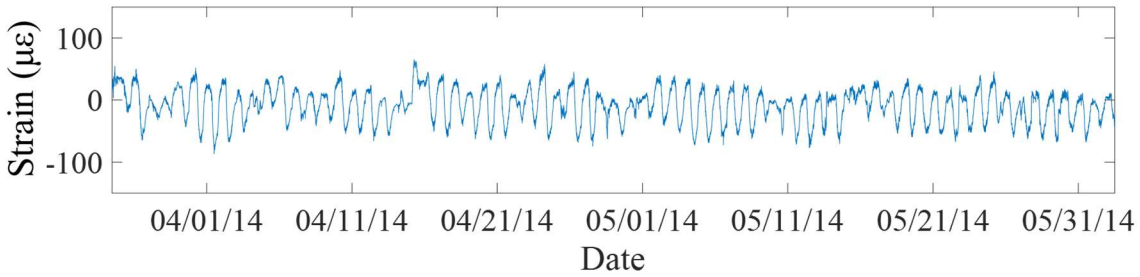

Figure 39: Measured Microstrain for Web of Girder 5 at Pier 2

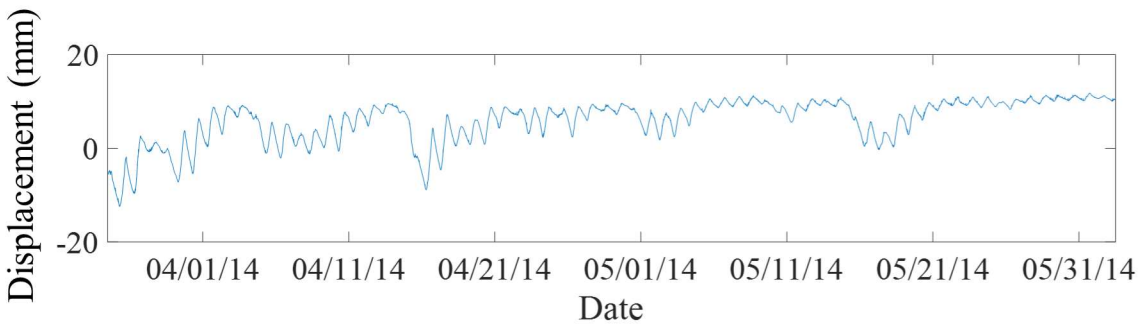

Figure 40: Measured Displacement of Girder 5 at Abutment 2

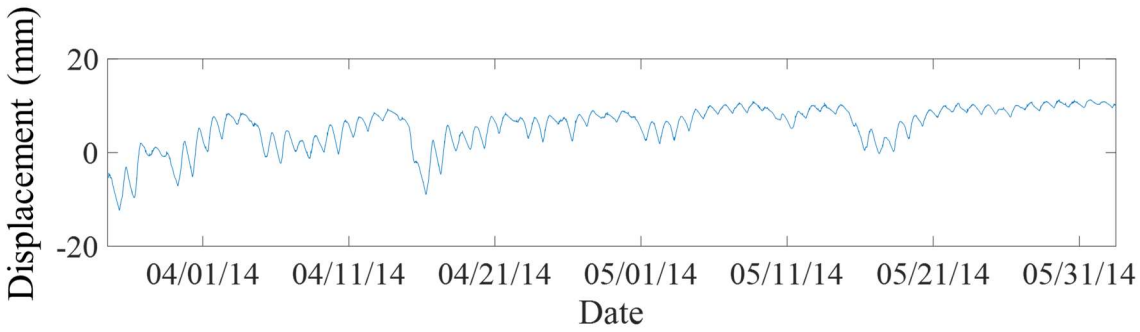

Figure 41: Measured Displacement of Girder 2 at Abutment 2

To investigate the thermal effects further, an inquiry of the sun path in relation to the bridge during the monitoring period was conducted. Figure 42 shows the sunrise and sunset trajectories during the months in which measurements were taken. Since the bridge is oriented north to south and the sun path to some degree east to west, the exterior girders are likely to be influenced by lateral thermal gradients from direct sunlight. Direct sunlight impacts Girder 6 during the sunrise and Girder 1 as the sun sets. Due to the coverage of the deck and the shielding of the exterior girders, the interior girders do not experience lateral thermal effects from direct sunlight but were still subjected to vertical gradients.

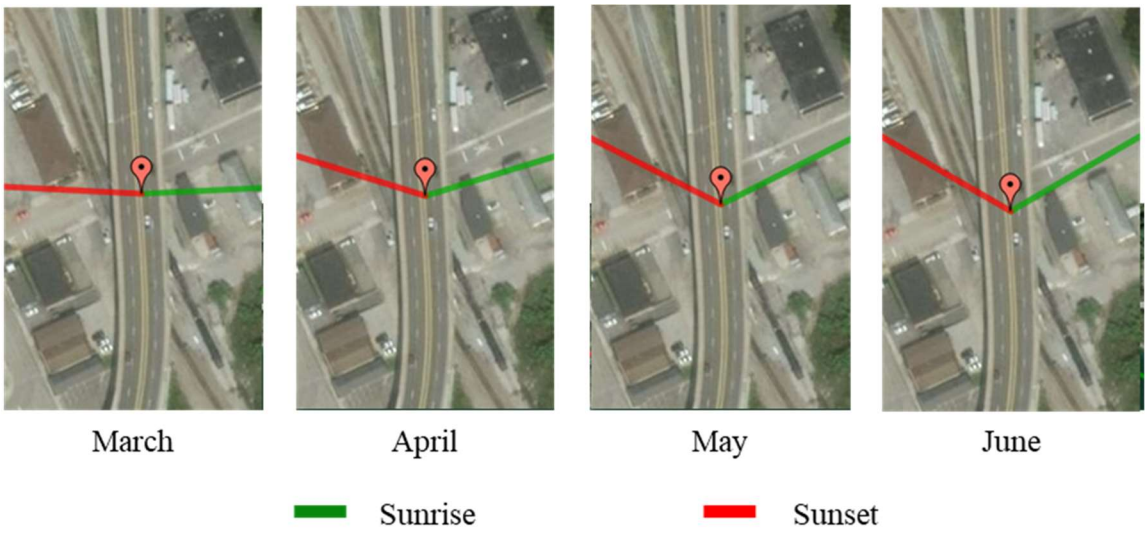

Figure 42: Sunrise and Sunset Paths throughout Monitoring Period

Before any further data processing was conducted, the data was initialized so that only relative responses during the monitoring period were analyzed. The initialization time (time from which the data was zeroed) was chosen such that any influence from unwanted thermal effects could be avoided. For this reason, the initialization time was chosen as March 28, 2014, at which time the sunset and sunrise paths are nearly parallel to one another (Figure 43).

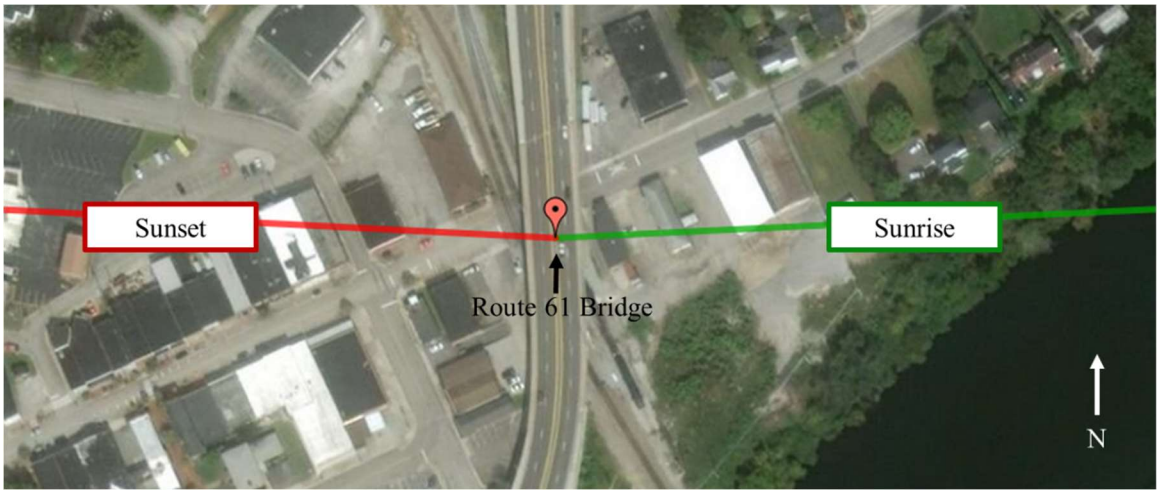

Figure 43: Sunrise and Sunset Paths for Initialization Time on March 28, 2014

7.1.3.2 Short-term Daily Bi-Linear Behavior

Investigation of the short-term thermal behavior of the Route 61 Bridge was conducted by analyzing the data from one daily cycle. A daily cycle from each gage is shown in Figure 44 and Figure 45 below and also in greater detail in Figure 136-Figure 139 in Appendix A. The short-term behavior further confirms the presence of direct sunlight on the exterior gages, specifically Girder 1. The maximum temperature at that gage registers nearly 23°C (73°F) when all other gages record no greater than 17°C (63°F) for that day. Analysis of the thermal behavior of the interior girders shows a clear bi-linear relationship through the course of a day. The longer linear lines occur when the steel and concrete are the same temperature and at a steady-state condition (e.g. heating/cooling in the middle of the day or middle of the night). The second linear relationship occurs when the steel and concrete are not the same temperature (e.g. when the sun sets or rises). Once the sun sets, the bridge is no longer exposed to solar radiation and undergoes a drastic temperature

change. However, the effects of the radiation do not dissipate from the bridge immediately. The steel and concrete heat and cool at different rates, causing temperature gradients to occur along the bridge. Over a period of a few hours, the bridge materials reach ambient temperature and are in steady state again. The sun rises causing the temperature discrepancy between the steel and concrete again until steady-state is reached.

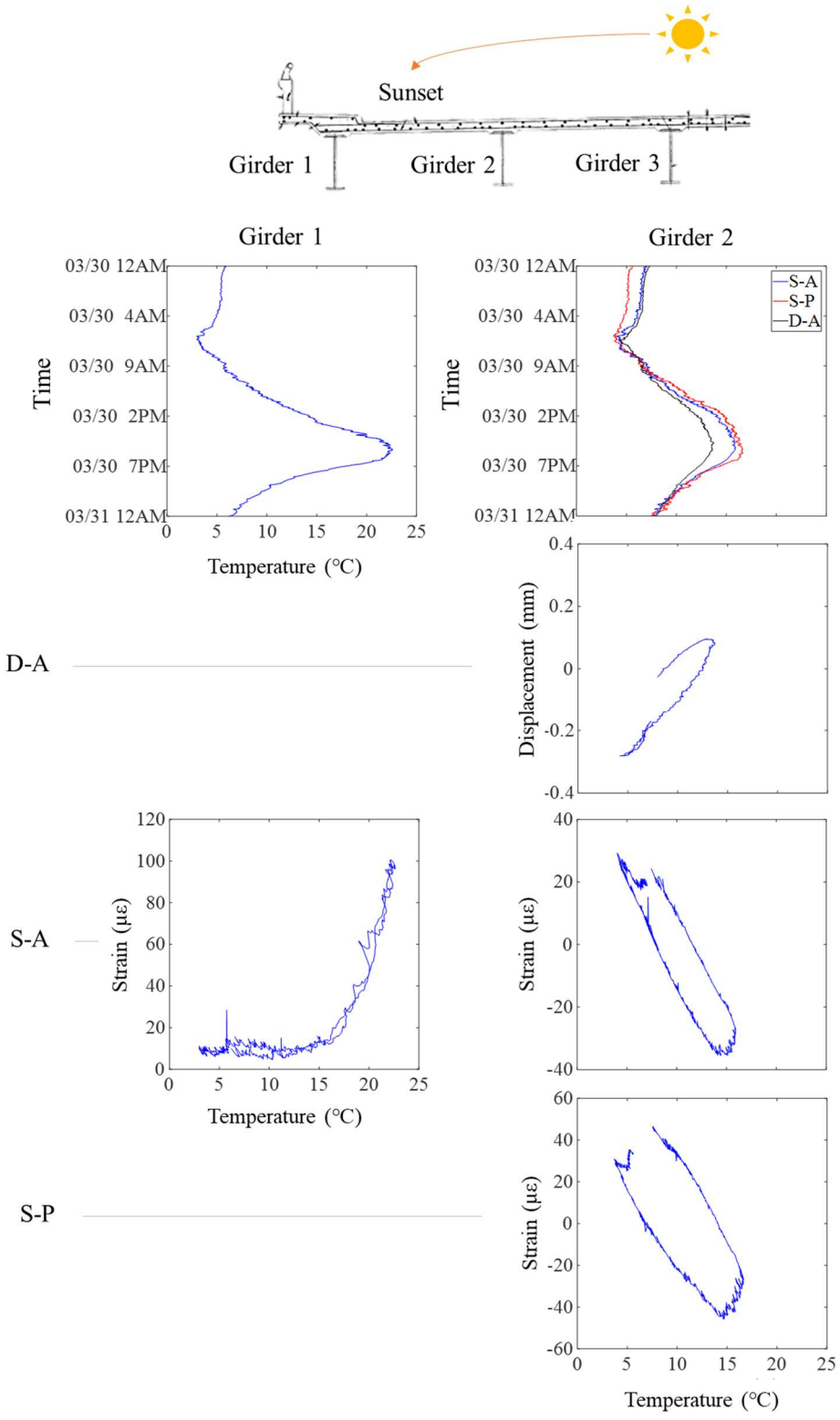

Figure 44: Temperature Time Histories and Measured Responses for West Side of Bridge on March 30, 2014

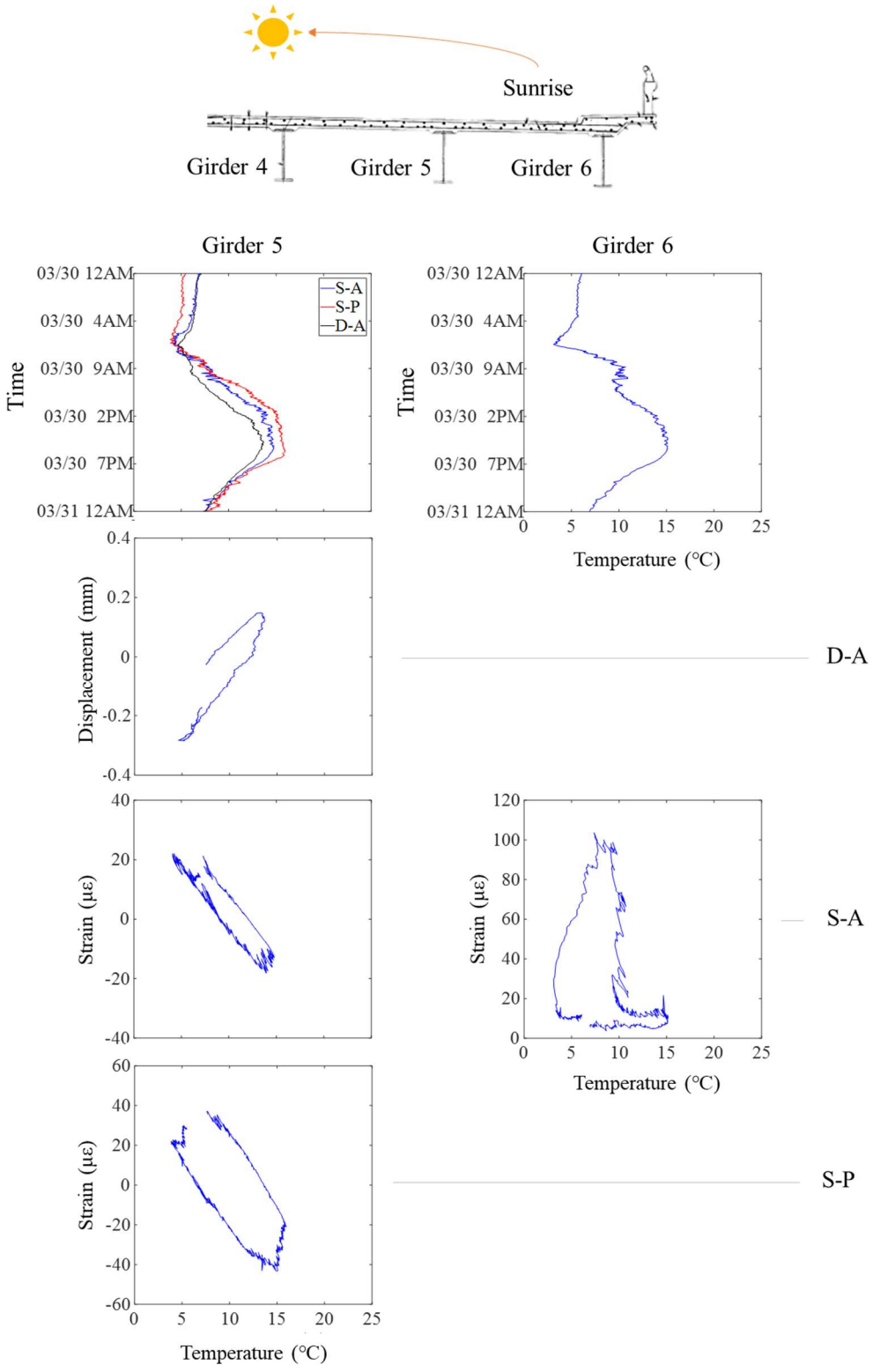

Figure 45: Temperature Time Histories and Measured Responses for East Side of Bridge on March 30, 2014

7.1.3.3 Long-term Linear Behavior

Investigation of the long-term thermal behavior of the Route 61 Bridge was conducted by analyzing the response versus temperature relationship for the entire monitoring period. This relationship is shown for each gage in Figure 46-Figure 49 below. Temperature gradients have proven to be problematic with this data as discussed previously. Therefore, as a means to alleviate errors from thermal gradients, the subset of data used for long-term analysis defined the thermal behavior of the bridge in steady-state conditions at night only. The timeframe for night-only measurements was between midnight and 4:00 AM just before sunrise. The night-only data produced a predominantly linear relationship for all of the gages. The nonlinearity experienced could be due to weathered expansion bearings, frictional restraint, or temperature fluctuations from the moving rail vehicles below. The night-only data was approximated or "smeared" by using a linear best-fit equation to define the measured behavior. Although some degree of nonlinearity was present, linear behavior was used as a means of simplifying the relationship while remaining an accurate representation of the data.

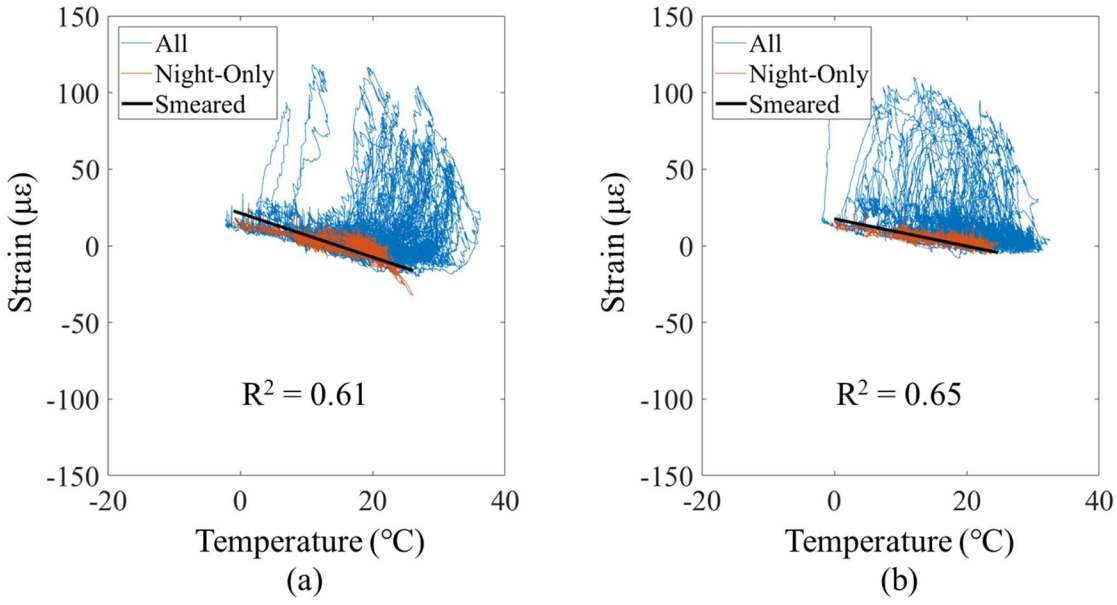

Figure 46: Measured Strain Response of Bottom Flange of Exterior Girders at Abutment 2: a) Girder 1 and b) Girder 6

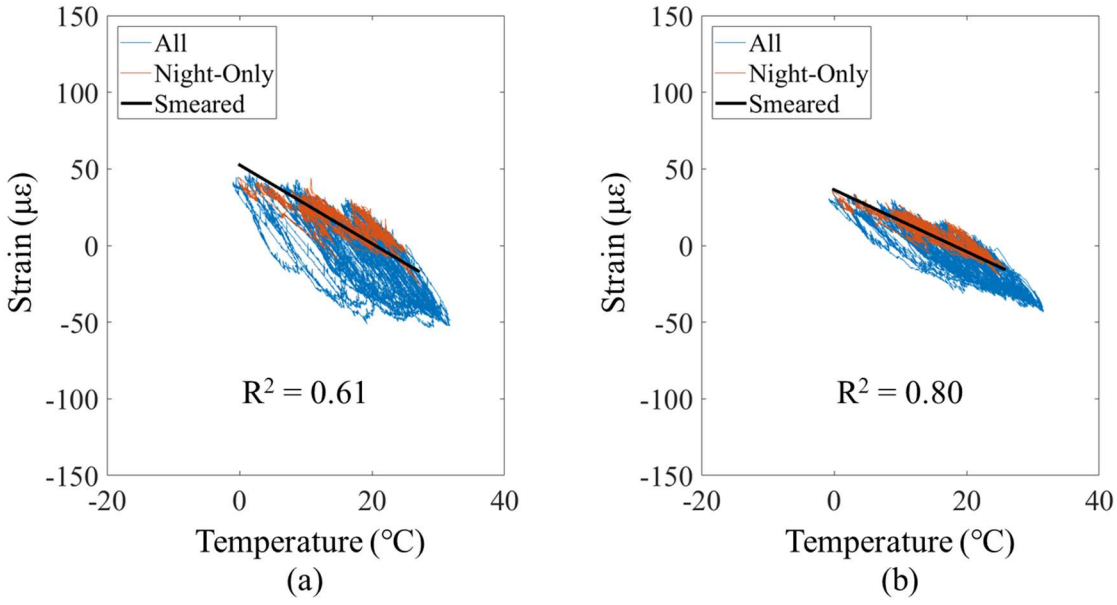

Figure 47: Measured Strain Response of Web of Interior Girders at Abutment 2: a) Girder 2 and b) Girder 5

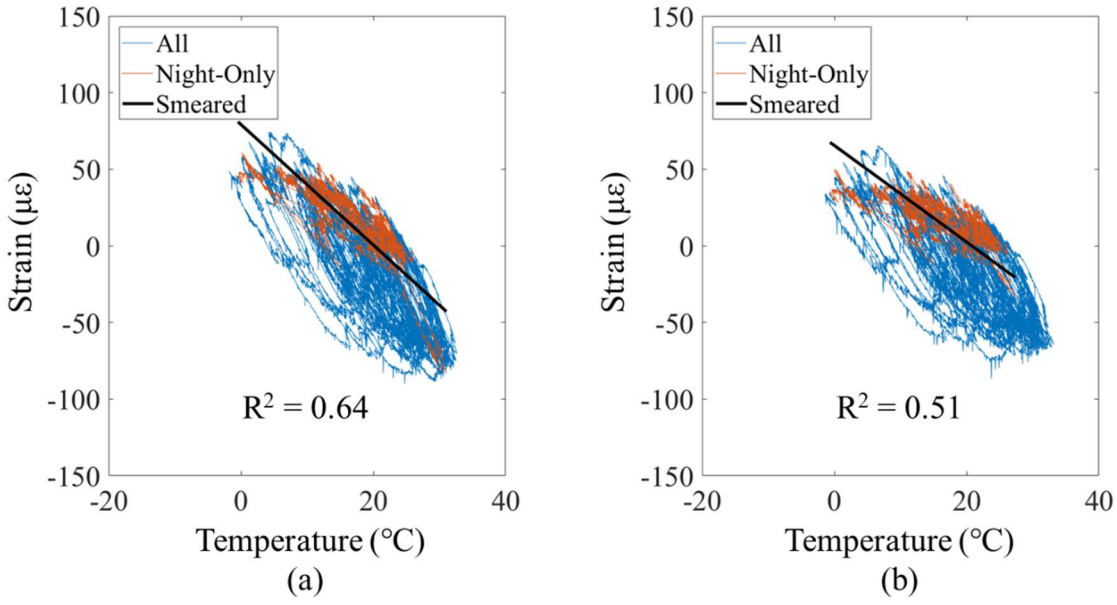

Figure 48: Measured Strain Response of Web of Interior Girders at Pier 2: a) Girder 2 and b) Girder 5

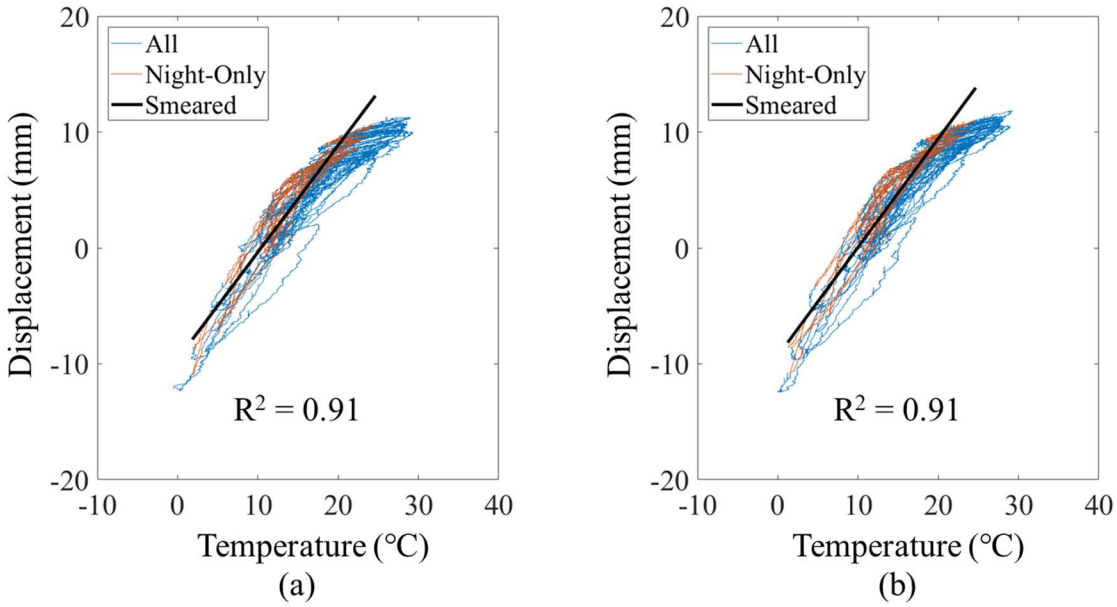

Figure 49: Displacement Response of Interior Girders at Abutment 2: a) Girder 2 and b) Girder 5

7.2 Numerical Models

7.2.1 Model Parameters

Previous studies and experience suggested stiffness was being applied to the structural system by either malfunctioning bearings or encroaching approaches; therefore, the boundary and continuity condition parameters were the primary sources of calibration within the finite element model. Four boundary conditions consisting of the behavior of the approaches and abutments were considered the highest level of uncertainty based on review of the plans and inspection reports. These boundary conditions were modeled by variable stiffness elements that impeded motion at the desired locations as shown in Figure 50 below.

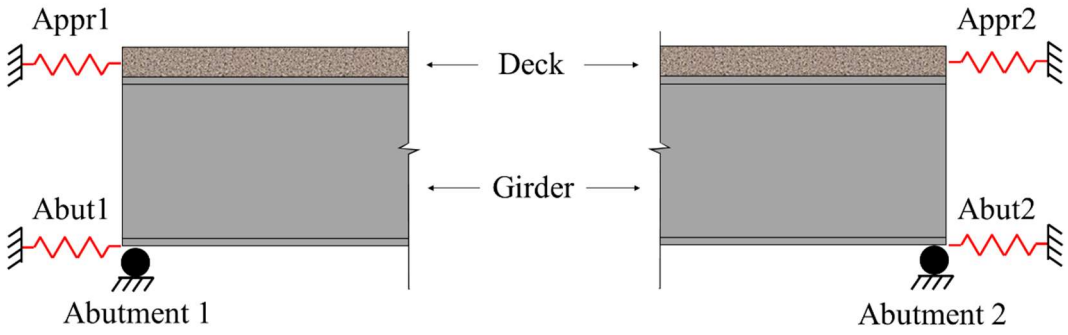

Figure 50: Model Parameters

7.2.1.1 Abutment Stiffness

The stiffness at Abutment 1 (Abut1) defined the longitudinal stiffness of the integral abutment. According to supporting documents, this stiffness should have been rigid; however, the degree of fixity was unknown. If the integral abutment was constructed poorly, the fixity of this boundary condition may be compromised. The stiffness of Abutment 2

(Abut2) defined the longitudinal stiffness of the expansion end of the bridge at the girder level. According to supporting documents, this stiffness should have been relatively small or free conditions. A large stiffness of this parameter may indicate that the girders are expanding enough to meet resistance from another source at the girder level such as the back of the abutment wall or debris between the abutment wall and the girders. Another potential cause for a large Abut2 stiffness is if the bearings were malfunctioning and preventing the bridge from expanding/contracting freely.

7.2.1.2 Approach Stiffness

In contrast to the abutment stiffness being applied at the girder level, the longitudinal stiffness of each approach was applied at deck level. Both approaches leading up to the bridge are relatively lengthy, meaning they have the potential to experience a substantial expansion or contraction in response to temperature as well. The stiffness at Approach 1 (Appr1) is representative of the lack of an expansion joint at Abutment 1. Therefore, this parameter should be a large value. If this parameter is small, the bridge may have expanded, met full resistance at Abutment 2, and pushed back into Abutment 1. The approach restraint at Abutment 2 (Abut2) was potentially resulting from premature closure of the expansion joint.

7.2.2 Development of the Sample Space

The parameters had a large degree of uncertainty regarding their true value due to use, exposure, and deterioration of the bridge. Therefore, the parameters were uniformly distributed between a fully mobile condition (where the structure expands/contracts freely) to a fully fixed condition (were the structure is hindered from expansion/contraction). The stiffness value of the fixed condition was investigated in Murphy and Yarnold (2018). A

preliminary analysis using single model calibration with an objective function algorithm concluded that the stiffness of the fixed condition was approximately 1.75×10^9 kN/m (12×10^7 kip/ft). The preliminary study also found that the relationship between the stiffness and the response was logarithmic. The parameter scale was adjusted accordingly, and the sample space was developed using Latin Hypercube Sampling according to the process described in Section 3. The initial sample size was chosen as 100,000 samples due to previous literature and engineering judgement. Furthermore, the sample space contained 100,000 unique combinations of the model parameters. Figure 51 shows the sample space of the first 5,000 samples in order to display the random sampling and uniform distribution of each parameter.

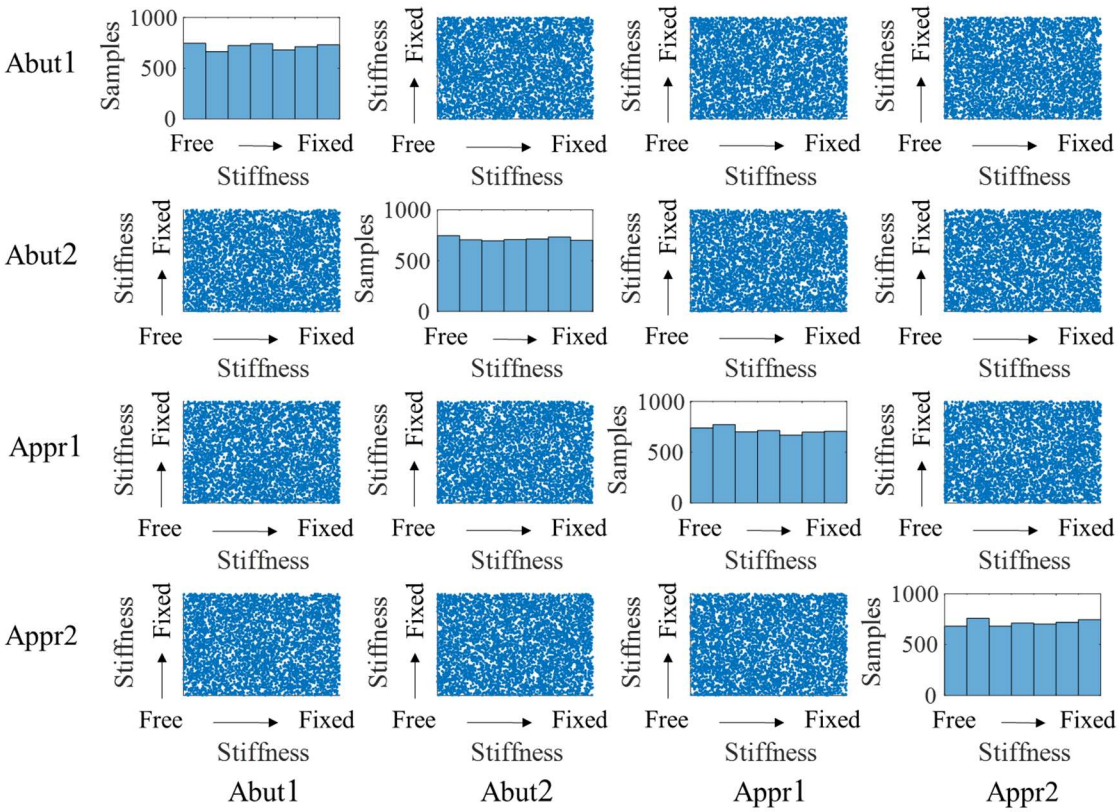

Figure 51: Sample Space for first 5,000 Samples of the 100,000 Total Samples

7.2.3 Structural Models via Finite Element Analysis

Once the sample size was determined and the sample space developed, a structural model was created within Strand7 with each parameter combination of the sample space for a total of 100,000 models.

7.3 Single Model Analysis using Bayes Theorem

7.3.1 Calibrated Model

In order to identify the calibrated model, the first task was to ensure that response distribution included the value of the measured response. All of the measured responses

were within the distribution for their respective responses. The next task was to proceed to calibration with the measured responses using Bayes Theorem as described in Section 5. Once Bayes Theorem was completed on the data, the posterior probabilities of each of the samples were analyzed. The model with the largest posterior probability was identified and used as the calibrated model.

7.3.2 Parameter Identification

The model parameters associated with the calibrated model are shown in Figure 52-Figure 53 and quantified in Table 6 below. The abutment parameters for the calibrated model were identified as 1.95×10^6 kN/m ($12 * 10^{4.05}$ kip/ft) for Abutment 1 (Figure 52(a)) and 189 kN/m ($12 * 10^{0.03}$ kip/ft) for Abutment 2 (Figure 52(b)). Abutment was partially restrained while Abutment 2 essentially experienced free conditions. Each of the approaches experienced partial restraint. The approach parameters for the calibrated model were identified as 1,310 kN/m ($12 * 10^{0.87}$ kip/ft) for Approach 1 (Figure 53(a)) and 7.39×10^4 kN/m ($12 * 10^{2.63}$ kip/ft) for Approach 2 (Figure 53(b)).

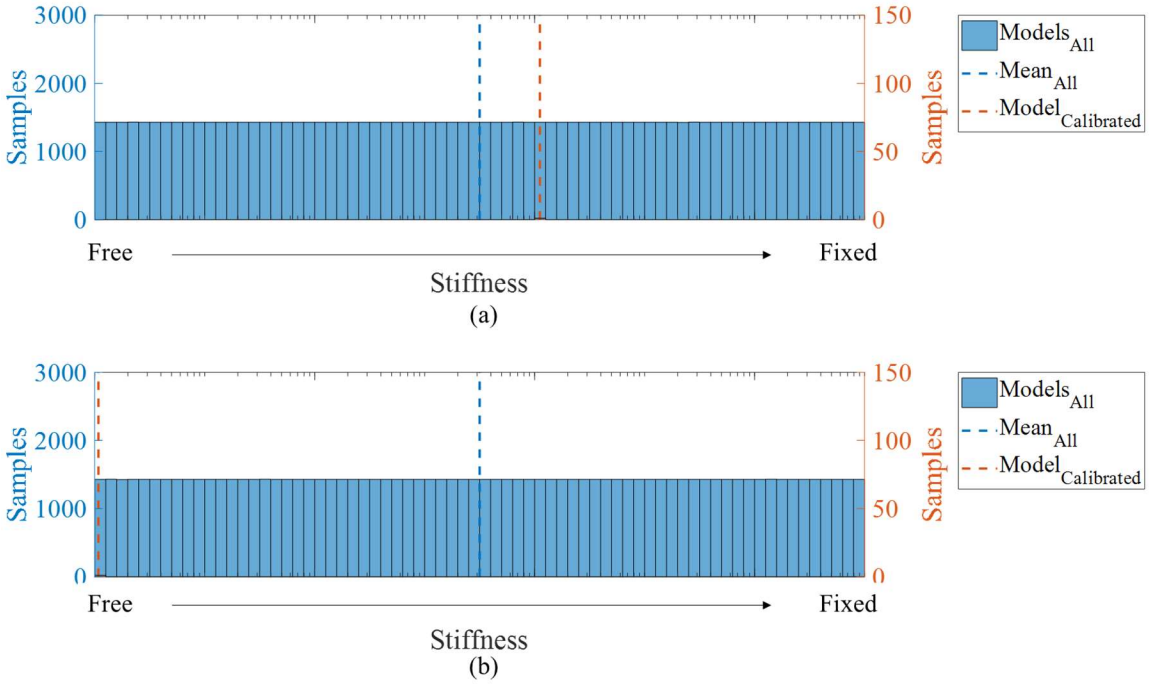

Figure 52: Calibrated Model Parameters of Abutments: a) Abutment 1 and b) Abutment 2

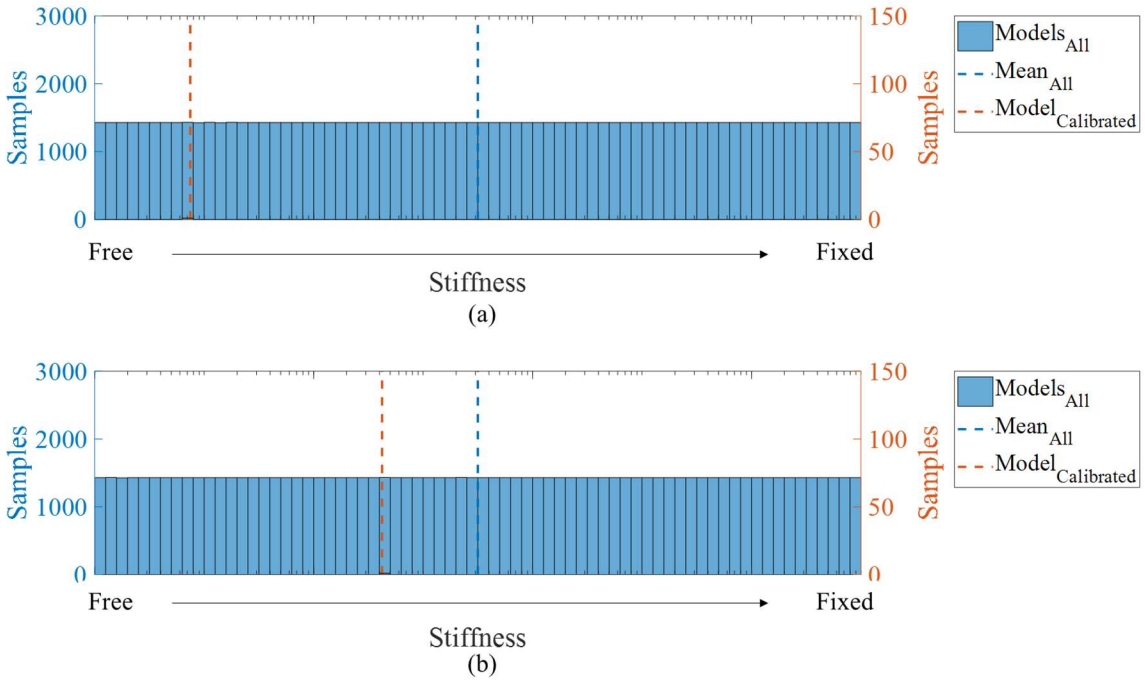

Figure 53: Calibrated Model Parameters of Approaches: a) Approach 1 and b) Approach 2

Table 6: Calibrated Model Parameters

Parameters	Calibrated kN/m (12*10^{x} kip/ft)
Abut1	1.95e6 (4.05)
Abut2	189 (0.03)
Appr1	1,310 (0.87)
Appr2	73,900 (2.63)

7.3.3 Predictive Responses

The predictive response are analyzed by comparing the responses from the calibrated model to the measured responses. The responses associated with the calibrated model are shown in Figure 54-Figure 57 and quantified in Table 7. The exterior girders produced measurements with the highest error (Figure 54). The calibrated model produced a strain response of Girder 1 of 169 microstrain compared to the measured response of 49 microstrain, yielding a percent difference of 245%. The calibrated strain response of Girder 6 was 181 microstrain while the measured response was 31 microstrain, yielding apercent difference of 485%. This could be due to the fact that the data was heavily influenced by direct sunlight and gradient effects. The remaining strains were more accurately simulated as evidenced by lower percent difference values. As shown in Figure 55, the calibrated model produced strains for Girder 2 and Girder 5 at the abutment of 102 microstrain (14% difference) and 98 microstrain (43% difference). As shown in Figure 56, the calibrated model produced a 93 microstrain response for both Girder 2 and Girder 5 at the pier, yielding percent differences of 33% and 14 %, respectively. The calibration of the displacements was the most accurate of all the responses with percent differences of 1% and 7% (Figure 57).

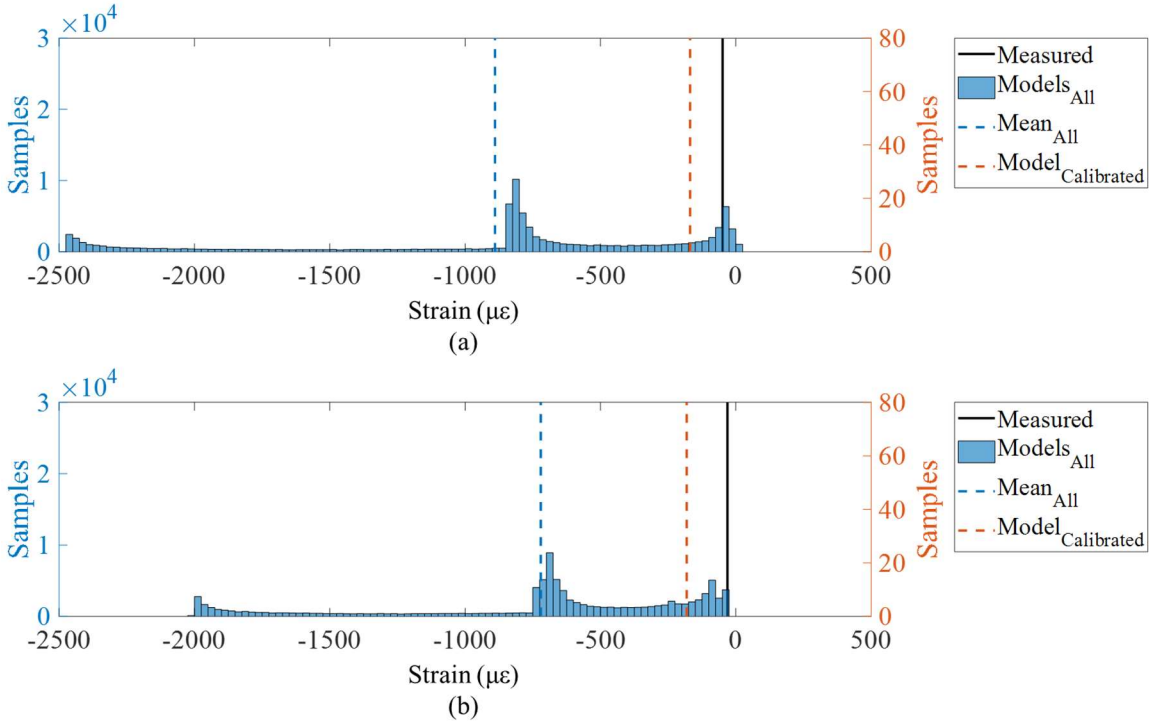

Figure 54: Calibrated Model Strain Response of Bottom Flange of Exterior Girders at Abutment 2: a) Girder 1 and b) Girder 6

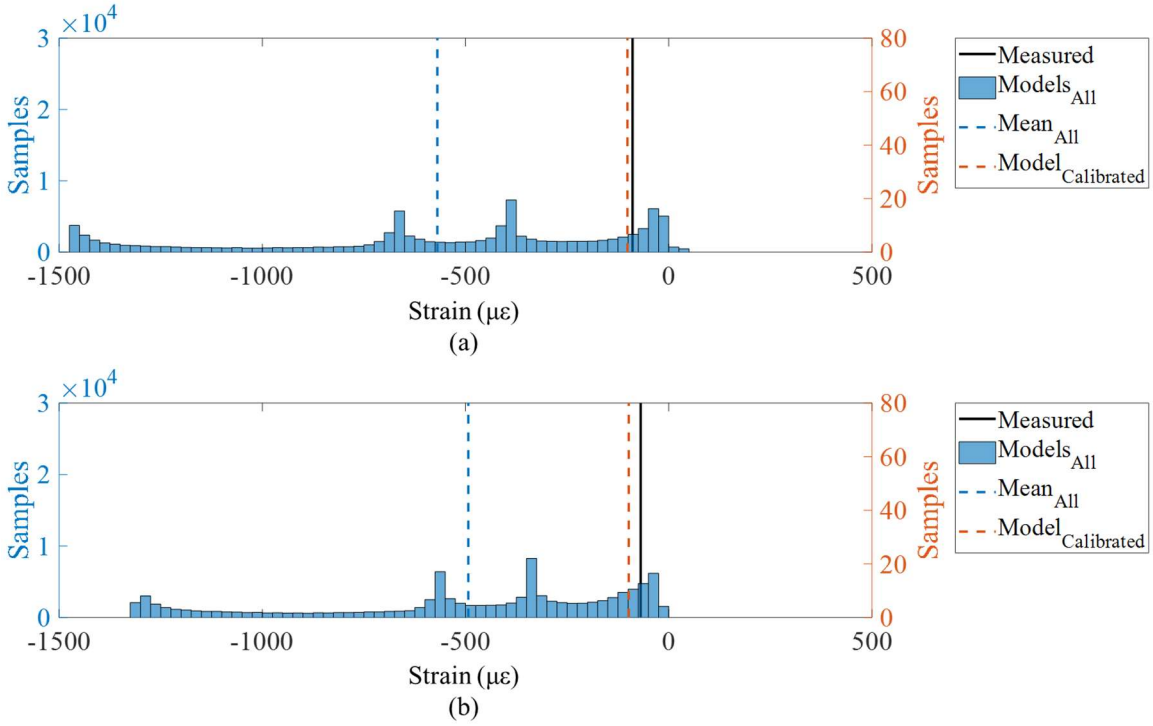

Figure 55: Calibrated Model Strain Response of Web of Interior Girders at Abutment 2: a) Girder 2 and b) Girder 5

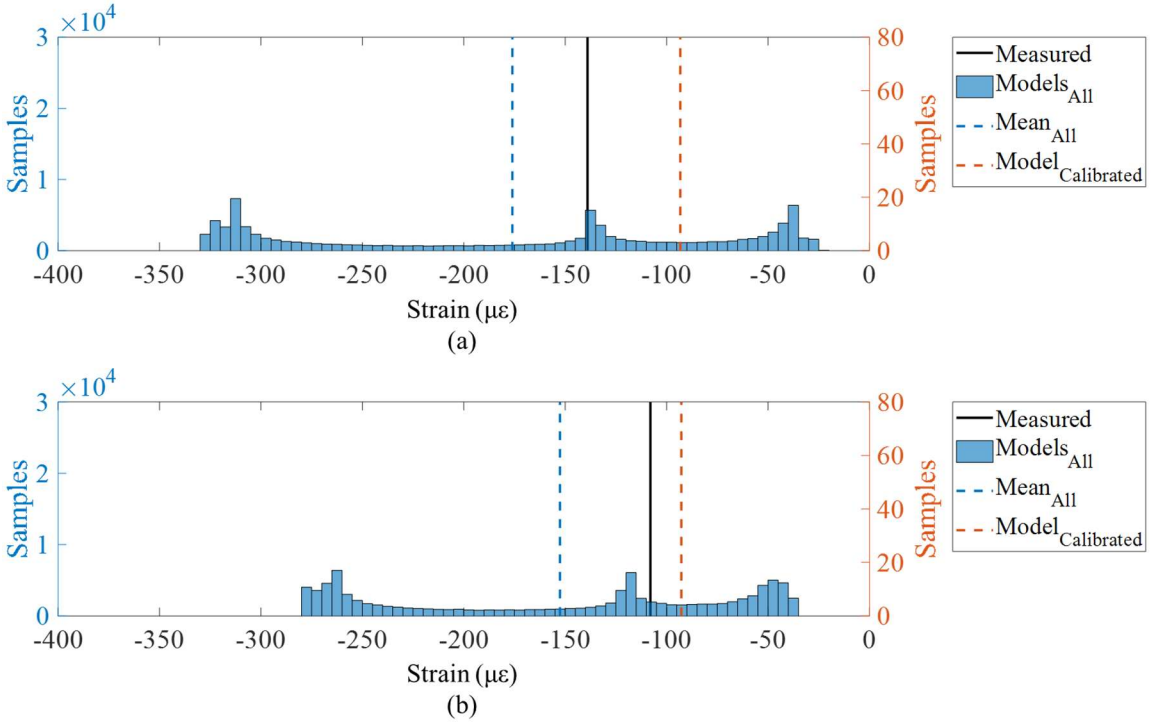

Figure 56: Calibrated Model Strain Response of Web of Interior Girders at Pier 2: a) Girder 2 and b) Girder 5

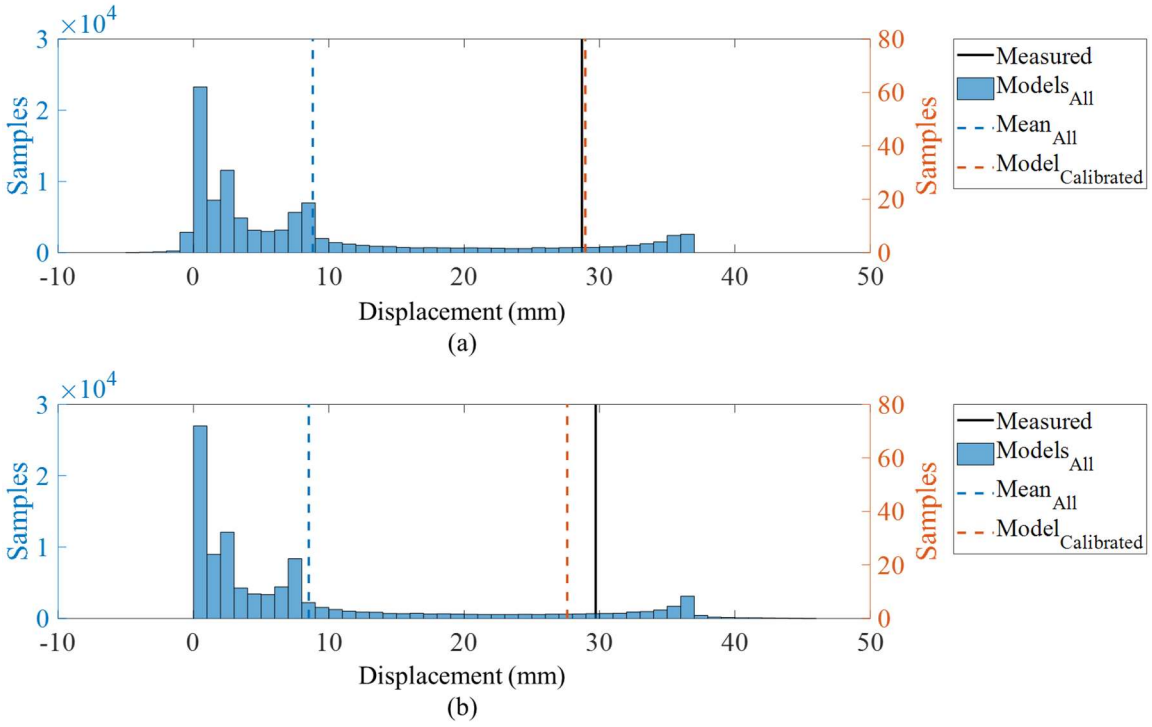

Figure 57: Calibrated Model Displacement Response of Interior Girders at Abutment 2: a) Girder 2 and b) Girder 5

Table 7: Calibrated Model Responses

Gage	Measured	Calibrated	% Diff.
S-A-G1	49 με	169 με	245%
S-A-G2	89 με	102 με	14%
S-A-G5	69 με	98 με	43%
S-A-G6	31 με	181 με	485%
S-P-G2	139 με	93 με	33%
S-P-G5	108 με	93 με	14%
D-G2	28.7 mm (1.1 in.)	29.0 mm (1.1 in.)	1%
D-G5	29.7 mm (1.2 in.)	27.6 mm (1.1 in.)	7%

7.4 Multiple Model Analysis using Bayes Theorem

7.4.1 Candidate Models

The calibration process using Bayes Theorem described in Section 3 was also used to identify the candidate models. Once Bayes Theorem was completed on the data, the posterior probabilities of each of the samples were analyzed. The candidate models were identified as the samples with the highest probabilities that comprised 95% of the total posterior probability. For the Route 61 Bridge, the number of samples required to meet or exceed 95% total probability was 234 models. Furthermore, the 234 models that were most probable were used as the candidate models.

7.4.2 Predictive Responses

The candidate models were used to analyze the responses of the bridge. Figure 58-Figure 61 show the response distributions from all of the structural models as well as the response distributions from just the candidate models. The values of the measured responses are also shown.

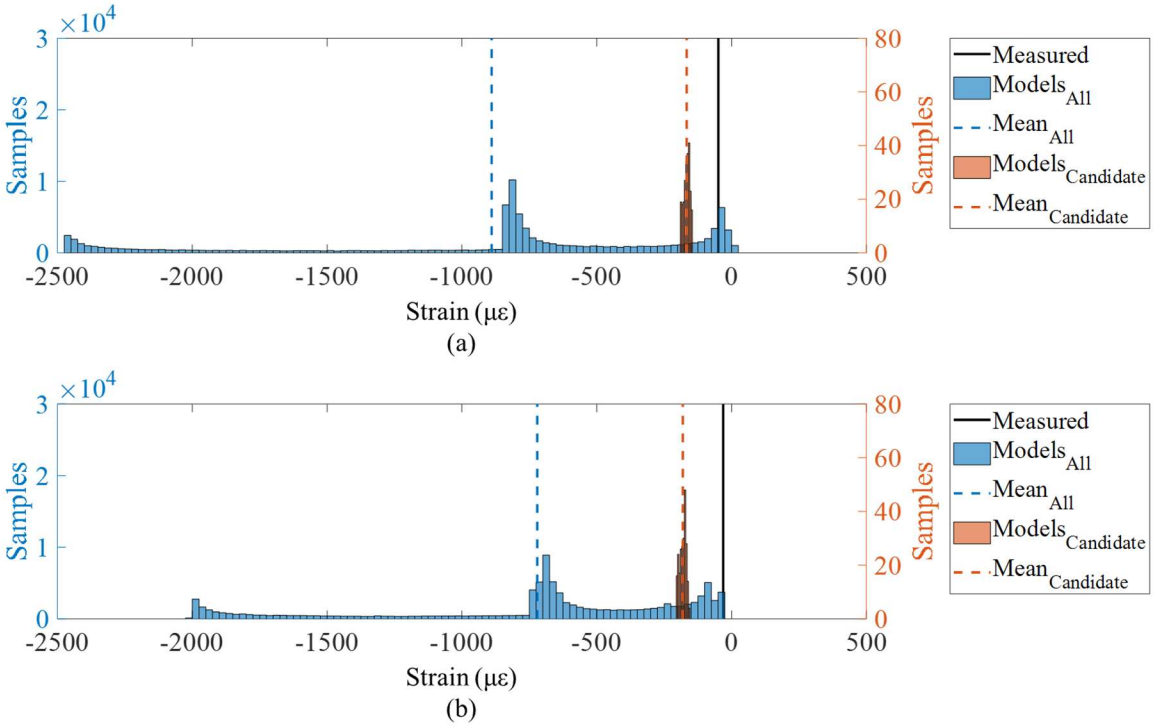

Figure 58: Candidate Model Strain Response of Bottom Flange of Exterior Girders at Abutment 2: a) Girder 1 and b) Girder 6

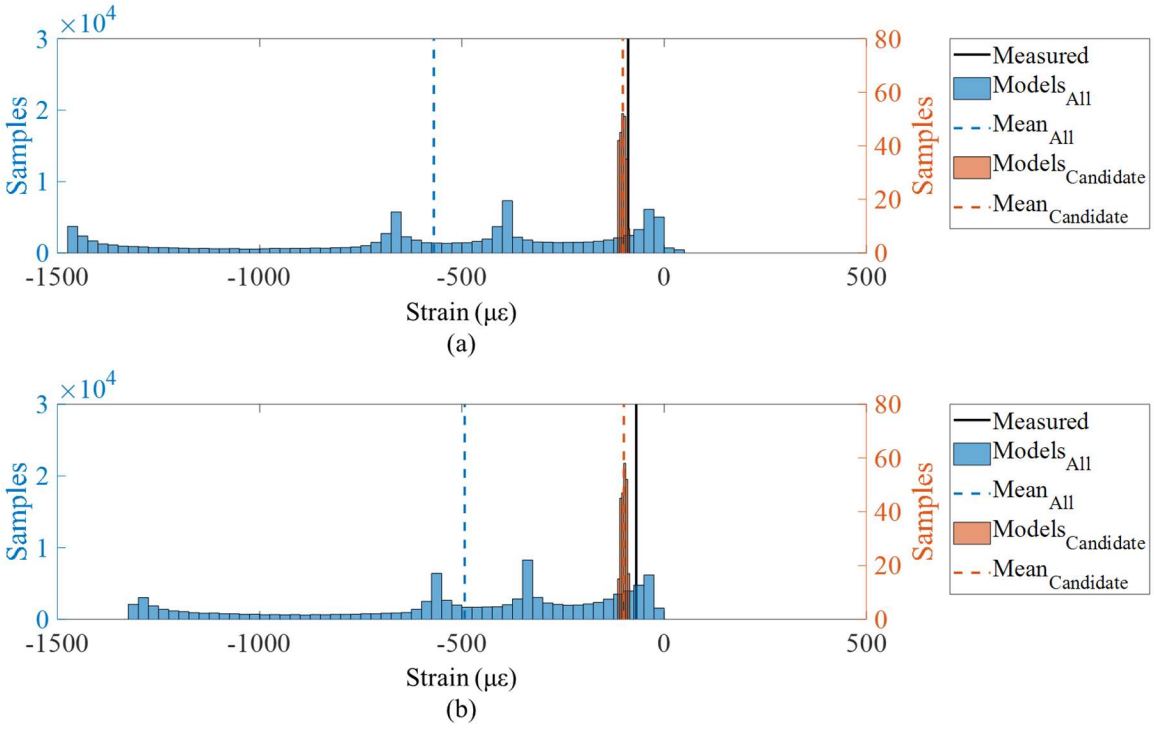

Figure 59: Model Strain Response of Web of Interior Girders at Abutment 2: a) Girder 2 and b) Girder 5

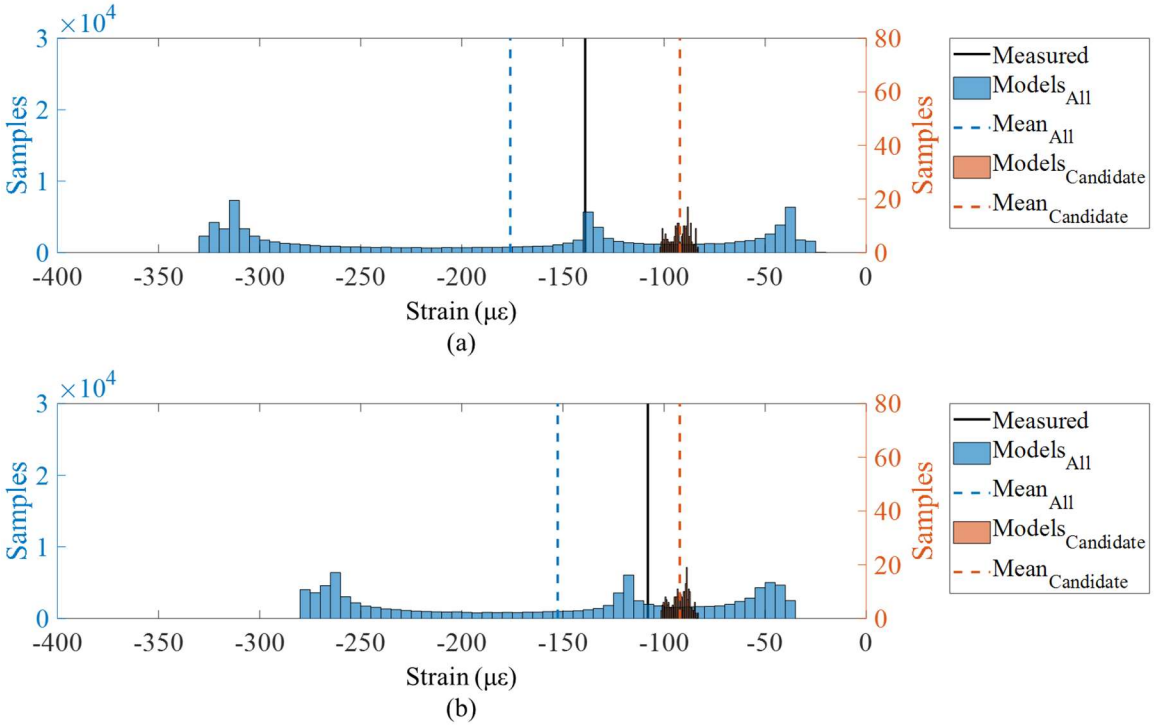

Figure 60: Model Strain Response of Web of Interior Girders at Pier 2: a) Girder 2 and b) Girder 5

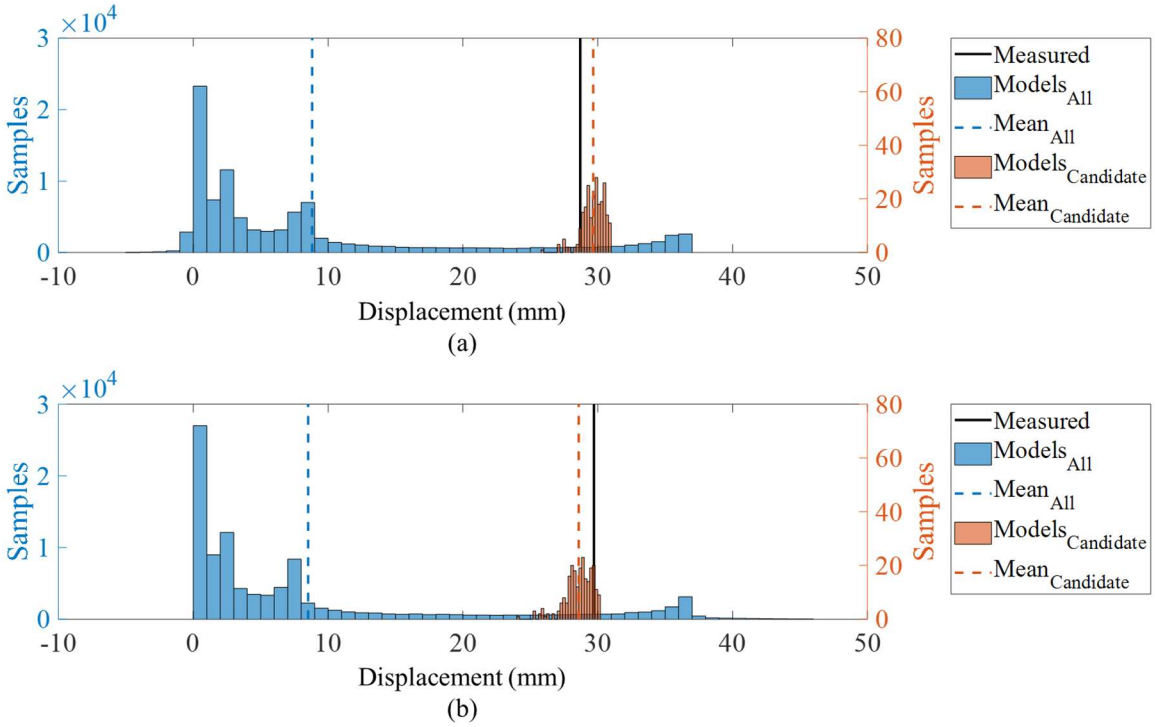

Figure 61: Model Displacement Response of Interior Girders at Abutment 2: a) Girder 2 and b) Girder 5

The response distributions are given numerically in Table 8. Through the calibration process, the response distributions from the structural models were significantly reduced to the response distributions of the candidate models. Each variance of the distribution reduced between 91% and 99%. As expected, the candidate model distributions were also more accurate to the measured responses. The gages with the most percent differences were the exterior girders with errors of 293% and 483% for Girder 1 and Girder 6, respectively. Again, this could be due to the quality of data used for those particular gages since those locations were highly influenced by adverse gradient effects. The remaining gages had percent differences of 44% or less.

Table 8: Candidate Model Response Distributions

Gage	Measured	Prior Distribution		Posterior Distribution		Uncert. Red.	Mean % Diff.
		Mean	Var.	Mean	Var.		
S-A-G1	49 με	-890 με	737 με	-166 με	11 με	99%	293%
S-A-G2	89 με	-569 με	446 με	-102 με	7 με	98%	15%
S-A-G5	69 με	-493 με	385 με	-100 με	7 με	98%	44%
S-A-G6	31 με	-721 με	568 με	-181 με	12 με	98%	483%
S-P-G2	139 με	-176 με	104 με	-92 με	5 με	95%	34%
S-P-G5	108 με	-153 με	87 με	-92 με	5 με	95%	15%
D-G2	28.7 mm (1.1 in.)	8.8 mm (0.3 in.)	11.0 mm (0.4 in.)	29.7 mm (1.2 in.)	0.9 mm (0.03 in.)	92%	3%
D-G5	29.7 mm (1.2 in.)	8.5 mm (0.3 in.)	11.1 mm (0.4 in.)	28.6mm (1.1 in.)	1.1 mm (0.04 in.)	91%	4%

7.4.3 Refined Parameters and Simulation Study

The candidate models were also used to refine the parameters of the models and hence provide insight regarding the boundary conditions of the structure. Figure 62 and Figure 63 show the model parameter distributions from all of the structural models as well as the parameter distributions from just the candidate models. As mentioned previously, the parameters for all of the structural models were uniformly distributed from a free to a fixed

condition. The parameters from the candidate models were able to significantly reduce the uncertainty of two of the model parameters.

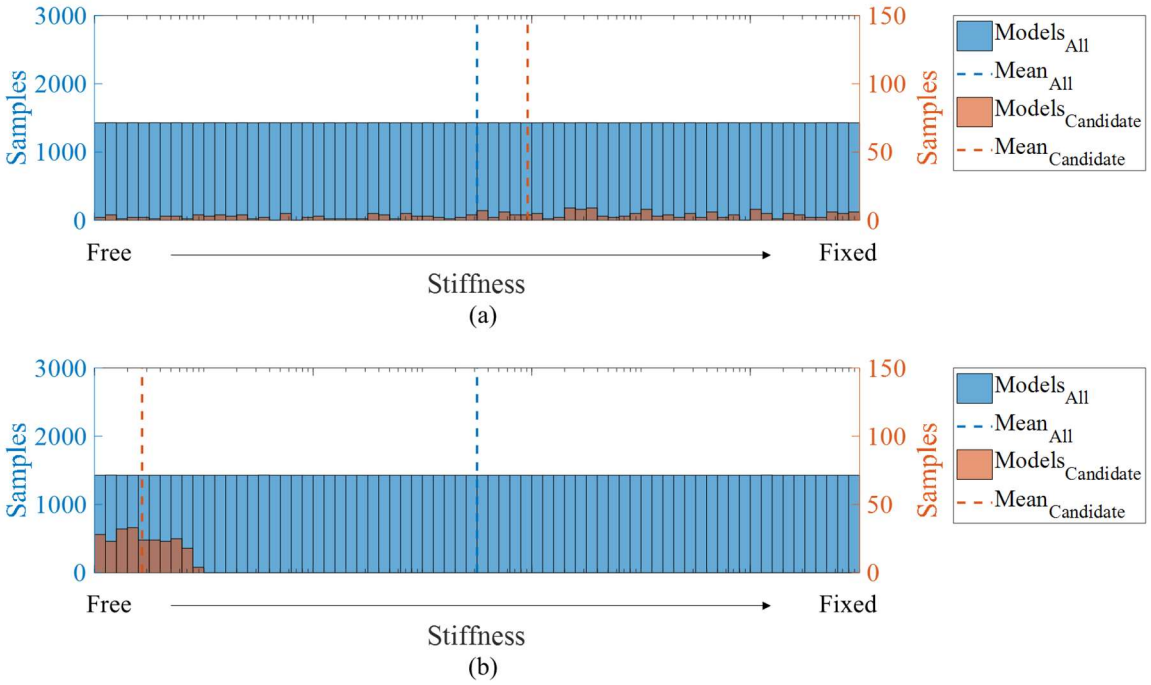

Figure 62: Refined Model Parameters of Abutments: a) Abutment 1 and b) Abutment 2

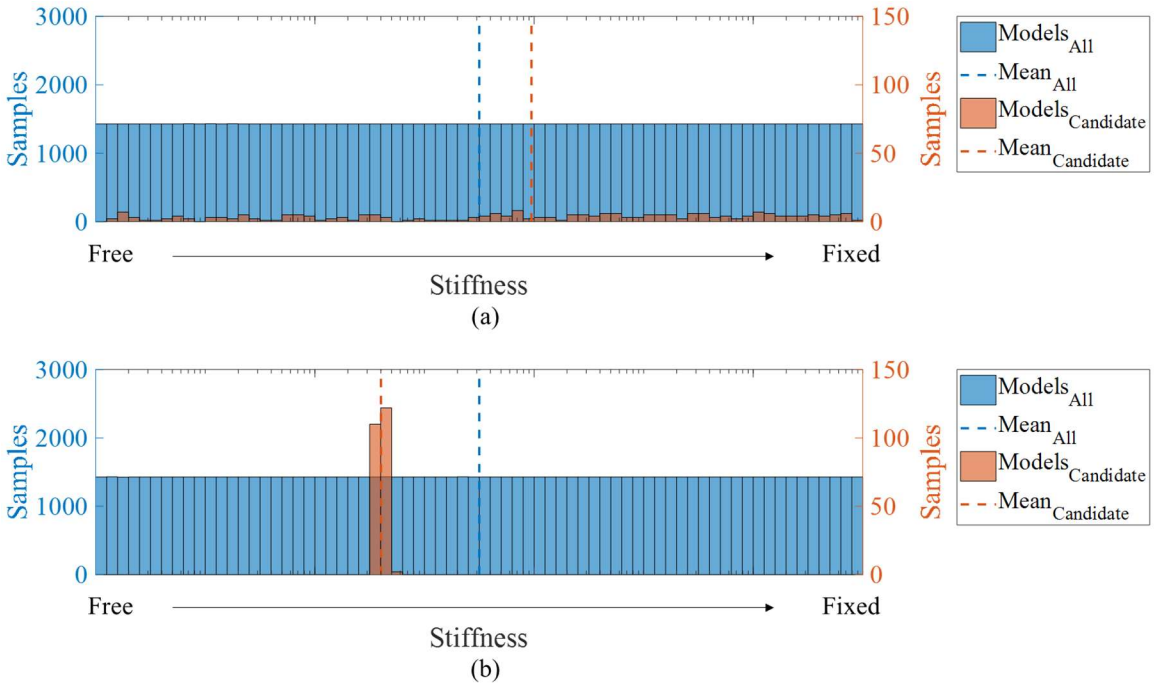

Figure 63: Refined Model Parameters of Approaches: a) Approach 1 and b) Approach 2

The parameter distributions are given numerically in Table 9 below. The model parameters pertaining to the southern end of the bridge (Abut1 and Appr1) did not experience a large reduction of uncertainty. The variance of the distributions reduced only 4% and 2% from all of the models to the candidate models for Abut1 and Appr1, respectively. However, the model parameters pertaining to the northern end of the bridge (Abut2 and Appr2) experienced a significant reduction of uncertainty of 87% and 97%, respectively.

Table 9: Candidate Model Parameter Distributions

Par.	Prior Distribution				Posterior Distribution				Uncert. Red.
	(kN/m)		12*10^x (kip/ft)		(kN/m)		12*10^x (kip/ft)		
	Mean	Var.	Mean	Var.	Mean	Var.	Mean	Var.	
Abut1	5.54e5	1.84e4	3.50	2.02	1.61e6	1.50e4	3.96	1.93	4%
Abut2	5.54e5	1.84e4	3.50	2.02	477	319	0.43	0.26	87%
Appr1	5.54e5	1.84e4	3.50	2.02	1.66e6	1.67e4	3.98	1.98	2%
Appr2	5.54e5	1.84e4	3.50	2.02	7.02e4	195	2.60	0.05	97%

The refined parameters provided insight into the thermal behavior of the bridge and led to a more comprehensive understanding of why deterioration was occurring. The reason for the damage can be illustrated by three scenarios shown in Figure 64.

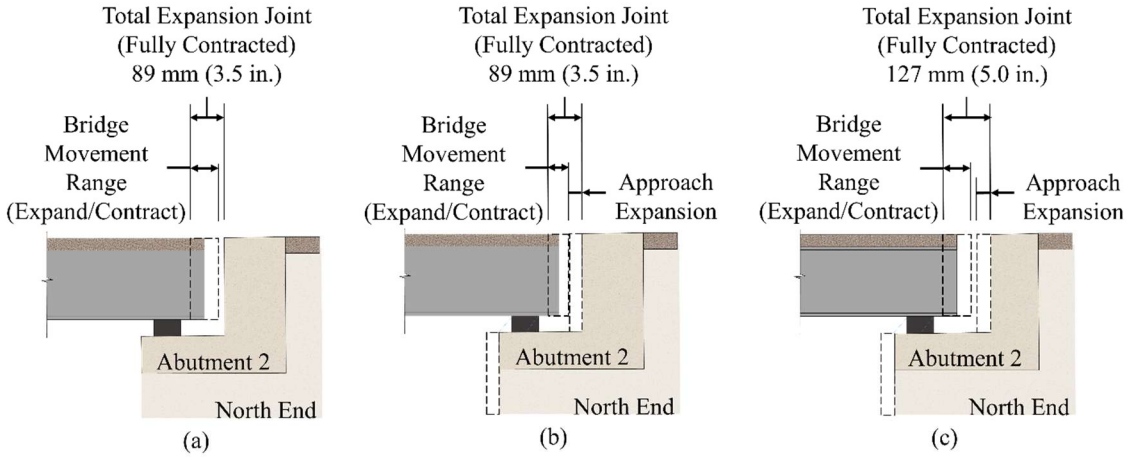

Figure 64: Thermal Evaluation Results: a) Original, b) Current, and c) Recommended (Reprinted from Murphy and Yarnold 2018)

Figure 64(a) shows the "original" scenario, which depicts the behavior of the bridge according to specifications from the original drawings and as the designer intended. In this scenario, the approaches do not experience thermal movement and remain stationary. The bridge expands freely but not enough to contact the wall of the abutment due to a sufficiently sized expansion joint.

Figure 64(b) shows the "current" scenario, which depicts the behavior of the bridge incorporating the refined parameters found during the thermal structural evaluation. The parameters at the north end of the bridge were found to have some degree of stiffness which prevented free thermal movement of the bridge. The results suggest that the expansion joint closed prematurely resulting in crushing of the joint and producing significant boundary stiffness. The premature closure could be due to the lack of consideration of the thermal movement from the large approaches. If the approaches expanded, the expansion joint would lessen but the bridge movement would still occur. The bridge movement was more than the space provided by the joint. As a result, the bridge contacted the abutment and continued to expand, causing damage to occur.

The above scenarios led to two primary findings and recommendations. The first was that the expansion joint at Abutment 2 was too small to accommodate both the bridge and approach or abutment movement. Therefore, enlargement of the expansion joint at Abutment 2 is recommended. The second recommendation was to provide a joint behind the south end of the bridge (behind Abutment 1), removing the restraint provided by the approach during the bridge expansion. Therefore, even if the joint did close at the north end (Abutment 2), the bridge would be able to expand toward Abutment 1 and avoid any stress

build-up. Modifying the fixity of select substructures was considered, but the associated costs were relatively significant and a less desirable alternative.

Finally, the "recommended" scenario shown in Figure 64(c) depicts the behavior of the bridge incorporating recommendations resulting from the thermal evaluation. The enlarged expansion joint is sufficient enough to accommodate both the thermal movement from the bridge as well as from the approaches. As a result, the bridge does not contact the abutment and ceases to contribute further damage to the structure.

7.5 Conclusions

The TD St-ID process described in Section 5 was able to successfully evaluate the structural performance of the Route 61 Bridge. The thermal behavior as a result of daily thermal changes was used to identify the boundary conditions of the structure and provide insight as to why damage was present. Through this study, several conclusions can be made regarding the data analysis of the thermal behavior. This structure was highly susceptible to adverse effects from direct sunlight, which warranted a need for additional data processing. The solar radiation effects were more substantial on the exterior girders as a result of the sun's path during sunrise and sunset. This created transverse gradients on the exterior girders in addition to the vertical gradients experienced by the entire structure. The structure exhibited daily bi-linear behavior consisting of times when the bridge was at steady-state with the ambient air around it and when the bridge and air temperatures were not consistent (during and directly after sunrise and sunset). In an attempt to mitigate adverse effects from thermal gradients, night-only data was used for the analysis. The long-term data showed how thermal gradients skew the results if the entire monitoring period is used. Although not

fully linear, the night-only data could accurately be represented by a smeared linear relationship with high correlation values.

Through the utilization of single and multiple modeling approaches of TD St-ID, the behavior of the boundary conditions was shown to be acting differently than originally designed. The SM St-Id analysis showed that some degree of stiffness was present at each approach and at Abutment 1 while Abutment 2 stiffness experienced a low stiffness value indicating free conditions. The calibration successfully determined a single model to simulate the behavior of the bridge. The displacement measurements were well calibrated with percent differences of 1% and 7%. The interior girders experienced more but still reasonable differences between 14% and 43%. Finally, the exterior girders were not calibrated well as the percent differences were 245% and 485%. Local behavior and out-of-plane bending were concluded as the potential causes of these discrepancies. The MM St-Id provided a more comprehensive understanding of the boundary conditions of the structure. The candidate models showed that the behavior at Abutment 1 and Approach 1 was not unique according to the measured responses. These parameters ranged from free to fixed conditions without having a significant impact on the model responses. Abutment 2 stiffness was confirmed as an essentially free condition. Approach 2 was concentrated at a partially stiff value of 7.02×10^4 kN/m and had an uncertainty of 96.7%. The calibration accuracy of the measurements using the MM approach yielded similar results as the SM approach. The displacements were well calibrated, the strains of the interior girders were reasonably calibrated, and the exterior girders experienced large percent errors due to lack of accuracy.

Overall, the TD St-Id evaluation method provided insight to the thermal behavior of the Route 61 Bridge and alleviated much of the uncertainty regarding its structural performance and health. This method proved to be a viable option for assessing a structure using thermal behavior. This study added to the body of knowledge of thermal behavior of structures as well as increased confidence in using this method as a means of structural evaluation.

8. PHASE II: TEMPERATURE-DRIVEN ST-ID STUDY – CANTILEVER TRUSS BRIDGE[*]

As structures age, exposure to the environment and loads can cause the need for intervention in the form of a bridge rehabilitation. Bridge rehabilitations are common as society has shifted from a total replacement mentality to one of simply extending the life of an existing structure. Often, these rehabilitations are conducted to strengthen a structure or as a means of remedying damage. As such, the structural behavior of the bridge can change after a rehabilitation resulting in much more uncertainty regarding the behavior. This uncertainty can instigate an evaluation of the bridge to further investigate the behavior. Such was the case for the Tennessee Department of Transportation and one of their extensively rehabilitated bridges, the Hurricane Bridge. The structure itself is large and complex with many moving mechanisms. With the additional complexity of the rehabilitation, this bridge serves as an opportune structure to test the TD St-Id process and further develop the knowledge of thermal behavior of bridges. Preliminary findings of this study were presented and published at Structures Congress 2017 (Murphy and Yarnold 2017). Portions of this bridge study are also pending publication within the proceedings of the 9th International Conference on Structural Health Monitoring of Intelligent Infrastructure (ISHMII) (Murphy and Yarnold 2019).

---

[*] Reprinted with permission from "Temperature-Driven Assessment of a Cantilever Truss Bridge" by Murphy, B. and Yarnold, M. 2017. *Structures Congress 2017 Proceedings*, pp 461-473, Copyright 2017 American Society of Civil Engineers.

8.1 Field Experiment

8.1.1 Structure Overview

The Hurricane Bridge shown in Figure 65(a) is a Warren-deck, steel truss bridge located along State Highway 56 in DeKalb County, Tennessee (Figure 65(b)), United States. The structure is orientated west to east and bridges a portion of Center Hill Lake (Figure 65(c)). Originally built in 1949 by the United States Army Corps of Engineers, this structure was designed according to the specifications outlined in the 1944 Edition of AASHTO Standard Specifications for Highway Bridges (AASHTO 1944). The design loads considered were a live load (H15-44), dead load (weight of structure with 0.7 kN/m^2 (15 lb/ft^2) of roadway surface), and a wind load (longitudinal wind of 1.4 kN/m^2 (30 lb/ft^2)). A temperature load was also considered. As with the Route 61 Bridge discussed earlier, Tennessee's moderate climate warranted a design temperature range between -17.8°C and 48.9°C (0°F and 120°F) according to design standards.

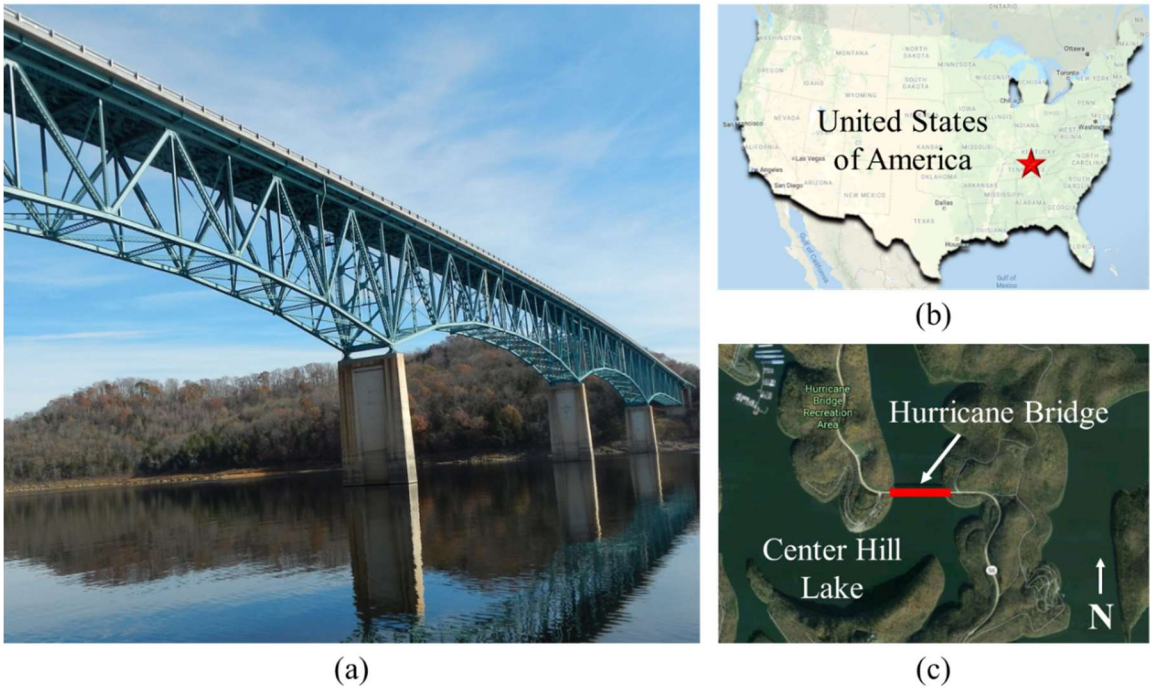

Figure 65: Hurricane Bridge: (a) Structure, (b) Location, and (c) Orientation

The Hurricane Bridge is primarily composed of two materials: steel and concrete. The structural steel in the superstructure is a mix of carbon steel and silicon steel. While some of the truss members are standard Carnegie Steel I-beams, a large majority of the truss members are built-up sections consisting of two channels single-laced or double-laced together to make composite members. The concrete components of the bridge are specified as Class "A" with a compressive strength of 27.6 MPa (4 ksi). The deck was designed to be 8.5 meters (28 feet) wide and 191 millimeters (7.5 inches) thick with steel reinforcement. The substructure is also concrete with steel reinforcement.

The Hurricane Bridge is a relatively large structure with a total length of approximately 545 meters (1,787 feet) and a maximum span length stretching 118 meters

(387 feet) as shown in Figure 66. A pair of approach spans lead up to the bridge from either side. The outer approaches span 19 meters (62 feet) from the abutments to the bents. The inner approaches span approximately 19 meters (61 feet) from the bents to the outermost piers supporting the bridge, Piers 3 and 7.

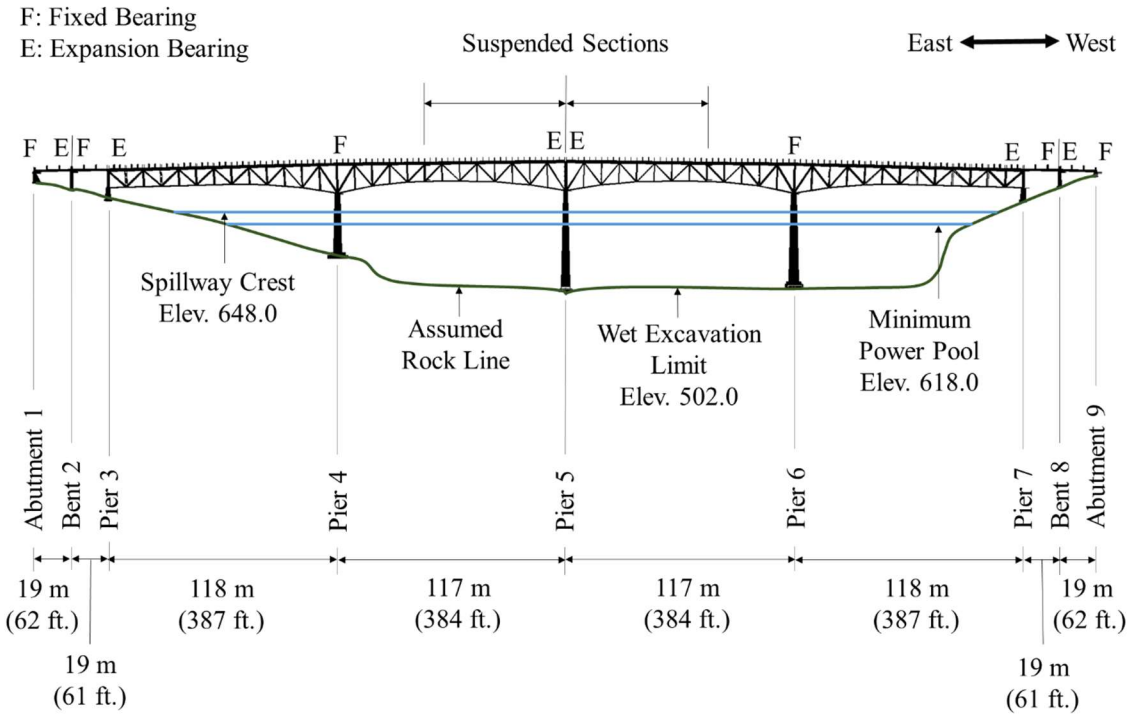

Figure 66: Hurricane Bridge Overview

The superstructure consists of two symmetric, independent truss systems: one from Piers 3 to 5 and the other from Piers 5 to 7. The two middle spans each include a suspended section and a cantilevered section as shown in Figure 67. The cantilevered sections are a total length of approximately 45 meters (148 feet). The suspended sections are a total length

of approximately 72 meters (236 feet). The remaining truss members of these spans are for stability purposes and were designed to have little load transmitted throughout.

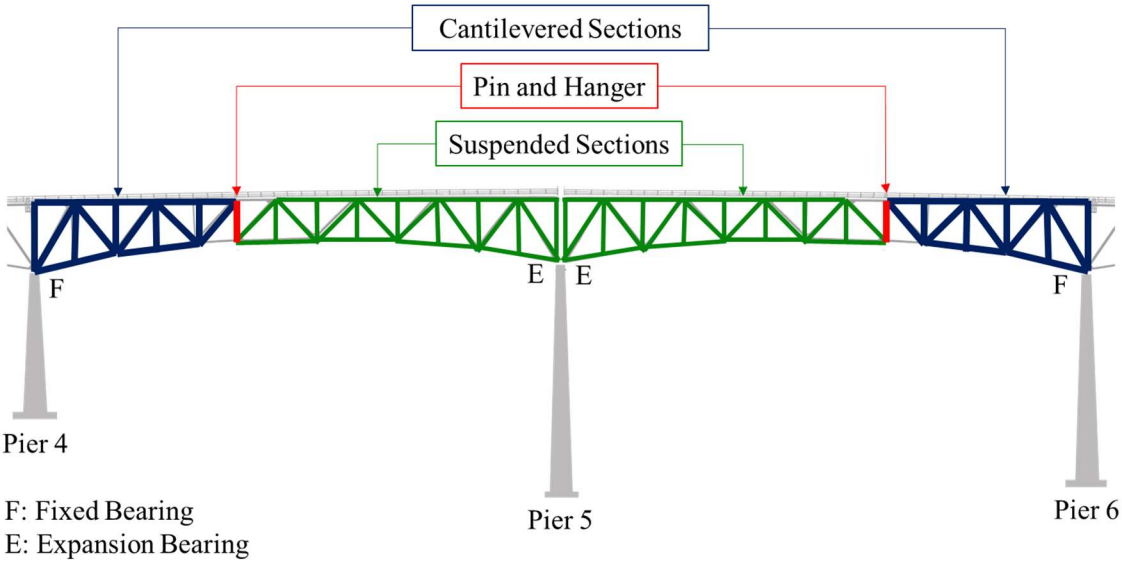

Figure 67: Cantilevered and Suspended Section Configuration

The suspended truss section is attached to the cantilevered section with a "pin and hanger" assembly shown in Figure 68(a) below. A pin holds the sections together at either end of the vertical structural member called the hanger. Slotted connections with the adjacent truss sections (Figure 68(b)) allow appropriate thermal movement throughout the truss section.

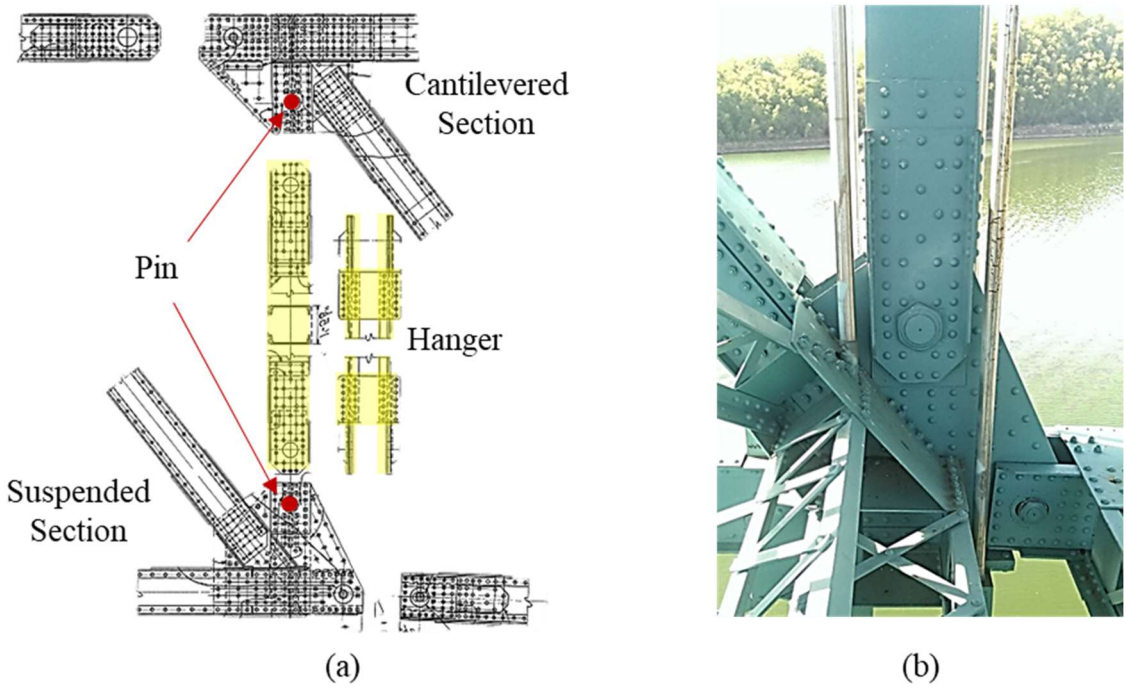

Figure 68: Pin and Hanger Assembly

The superstructure rests on bearings located at the top of each of the five piers of the substructure. As shown in Figure 66 earlier, the bearings at Piers 3,5, and 7 allow for longitudinal expansion while the bearings at Piers 4 and 6 are translationally fixed with pins. The expansion bearings are in the form of rocker bearings (Figure 69(a and c)), and the fixed bearings are pinned like the one shown in Figure 69(b). Access to these bearings is available via ladder access at each pier.

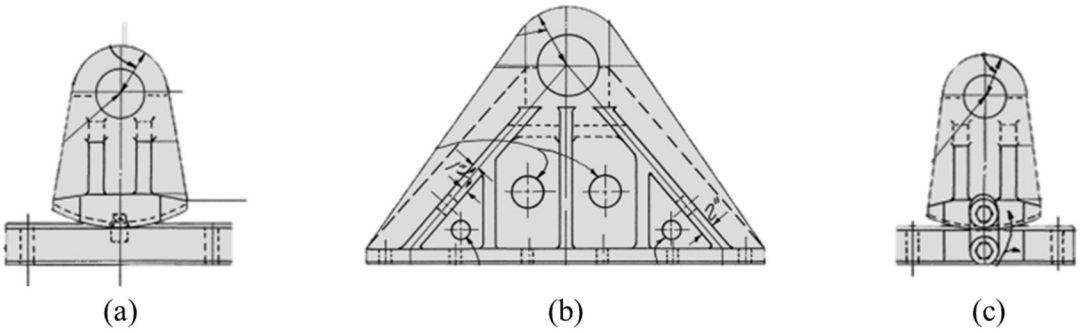

Figure 69: Boundary Conditions: a) Piers 3 and 7, b) Piers 4 and 6, and c) Pier 5

8.1.1.1 2011 Rehabilitation

The Hurricane Bridge underwent a major rehabilitation in 2011. This was due in part to the collapse of a bridge with a similar design, the I-35W Mississippi River Bridge, in 2007. To ensure that the Hurricane Bridge did not experience the same fate as the I-35W Bridge, the rehabilitation focused on two major improvements: installation of an auxiliary support system at the pin and hanger locations for increased redundancy and retrofit of many structural members to add additional strength. The owners also increased the serviceability by capitalizing on the opportunity to widen the deck during the rehabilitation.

8.1.1.1.1 Auxiliary Support System ("Catch System")

The auxiliary support system or "catch system" consists of four stainless steel hanger rods at each pin and hanger location as shown in Figure 70. Each rod has a diameter of 76 millimeters (3 inches) and serves as increased redundancy to secure the suspended sections in the event of a catastrophic failure. If the pin and hanger connection or the member itself fails, the load path will be transferred through the catch system which will act as the vertical hanger until the failure can be remedied.

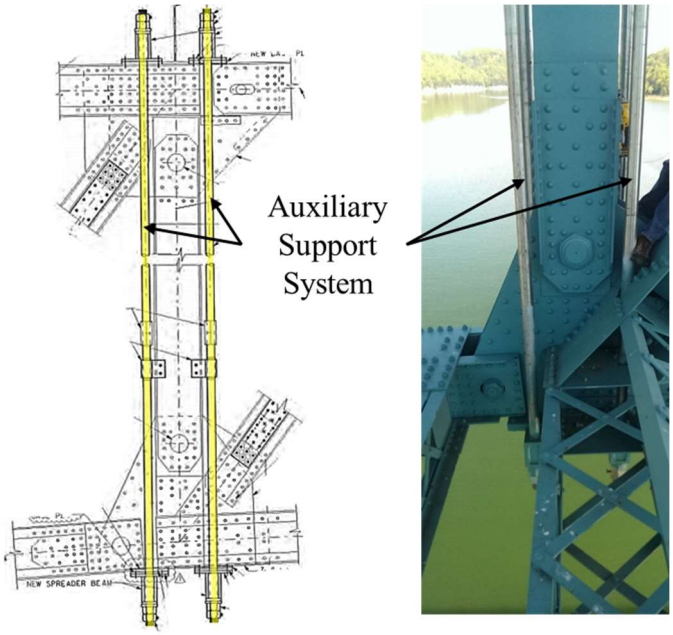

Figure 70: Auxiliary Support System (Catch System)

8.1.1.1.2 Member and Connection Retrofit

Many truss members of the bridge were retrofitted to provide additional strength to the structure. This process was completed by adding additional plates to the existing built-up sections highlighted in Figure 71 below. The same process was also completed with various connection gusset plates throughout the structure.

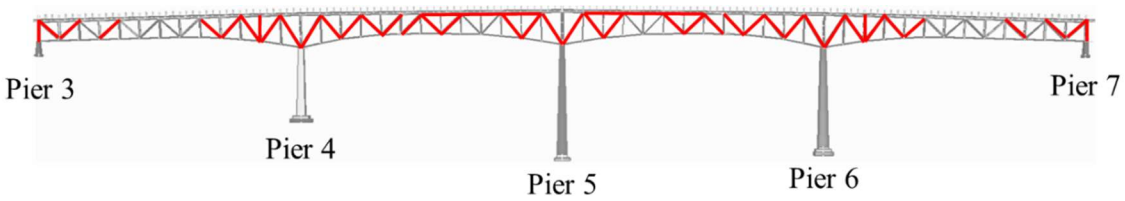

Figure 71: Retrofitted Truss Members

8.1.1.1.3 Widening of Deck

The final objective of the 2011 rehabilitation was to widen the deck. The originally designed width of the bridge was 8.5 meters (28 feet) as shown in Figure 72(a). The deck was widened to a width of 12.1 meters (40 feet) to accommodate growing traffic demand and increase serviceability (Figure 72(b)). The new deck width required an alternate stringer design as well. While the stringer size (W24x76) remained consistent, the original design required only four stringers whereas the rehabilitated design required a total of ten stringers.

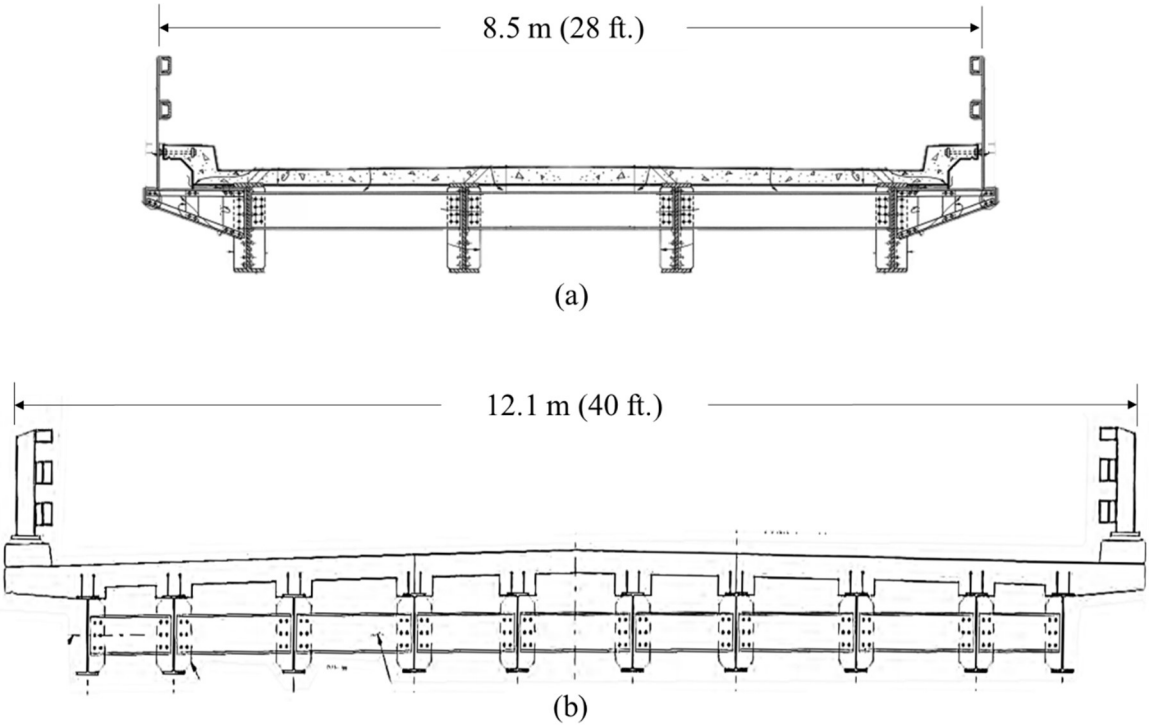

Figure 72: Deck Width Dimensions: a) Original Design and b) Rehabilitated Design

8.1.2 Monitoring System

8.1.2.1 Preliminary A-Priori Model

In order to determine locations along the bridge that would be most beneficial for monitoring, a finite element model was created in Strand7 to investigate the thermal behavior of the bridge. Within this software, structural members were modeled with two-node beam elements. The deck was modeled using four-node plate elements. Continuity conditions between the superstructure and the substructure were modeled with two-node connection elements that could simulate the behavior of the bearings. Upon completion, the model was independently checked and screen for errors. The completed model is shown in Figure 73 below.

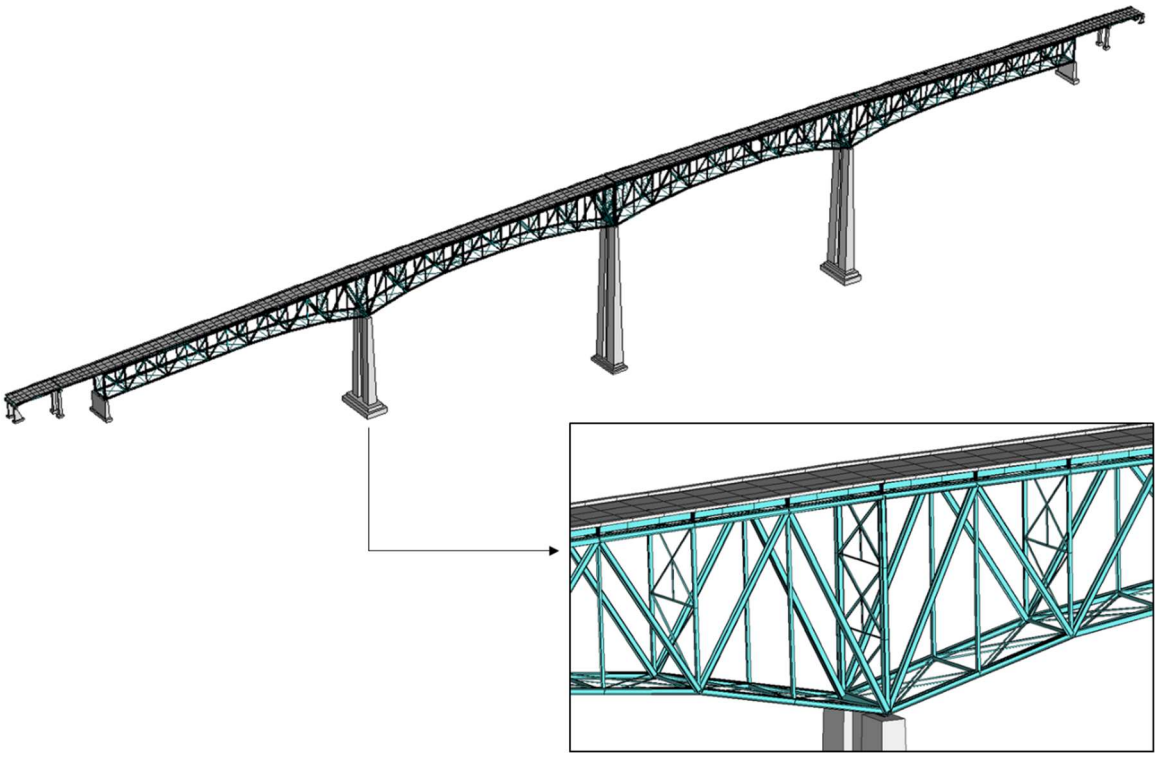

Figure 73: Finite Element Model of the Hurricane Bridge (Reprinted from Murphy and Yarnold 2017)

8.1.2.2 Monitoring System Design and Installation

The Hurricane Bridge has many movement mechanisms that could affect the thermal behavior of the bridge. Therefore, a sensitivity study was performed to assess the movement of these mechanisms. Due to the symmetry of the truss system between Piers 3 to 5 and Piers 5 to 7, only half of the bridge was chosen for monitoring system instrumentation. Convenient ground access to Pier 7 lead to the decision of focusing on the truss system between Piers 5 and 7. For the purpose of the preliminary sensitivity study, the rotational movement at the pin and hanger location as well as the longitudinal bearing movement at the expansion piers (Piers 5 and 7) were analyzed. The extent of mobility of these conditions was varied, and sensitivity studies were performed to identify locations of interest throughout the truss system. Figure 74 shows one of the sensitivity studies conducted. Within the sensitivity study, the model was subjected to a uniform temperature change of 27.8℃ (50℉). Then, thermal responses were collected from various locations along the bridge to identify the magnitude of thermal response at each location. In the figure below, strains along members of the bottom chord of the bridge are presented for three condition scenarios: as drawn conditions, Pier 7 bearings seized, and pin and hanger seized. "As Drawn Conditions" depicts the structure's behavior in ideal conditions according to the original and rehabilitation plans. The remaining scenarios depict the behavior of the bridge when one of the movement mechanisms behaves differently than designed. In this case, a high magnitude thermal response is shown near Pier 6 for the seized pin and hanger scenario. This indicated that the strains of those members are highly sensitive to temperature if the pin and hanger is seized. Therefore, the condition of the pin and hanger can be distinguished by

conducting a thermal evaluation. Several other sensitivity studies were conducted for strains along the diagonal, vertical, and top chord as well as displacements at the deck and bearing levels at Piers 5 and 7.

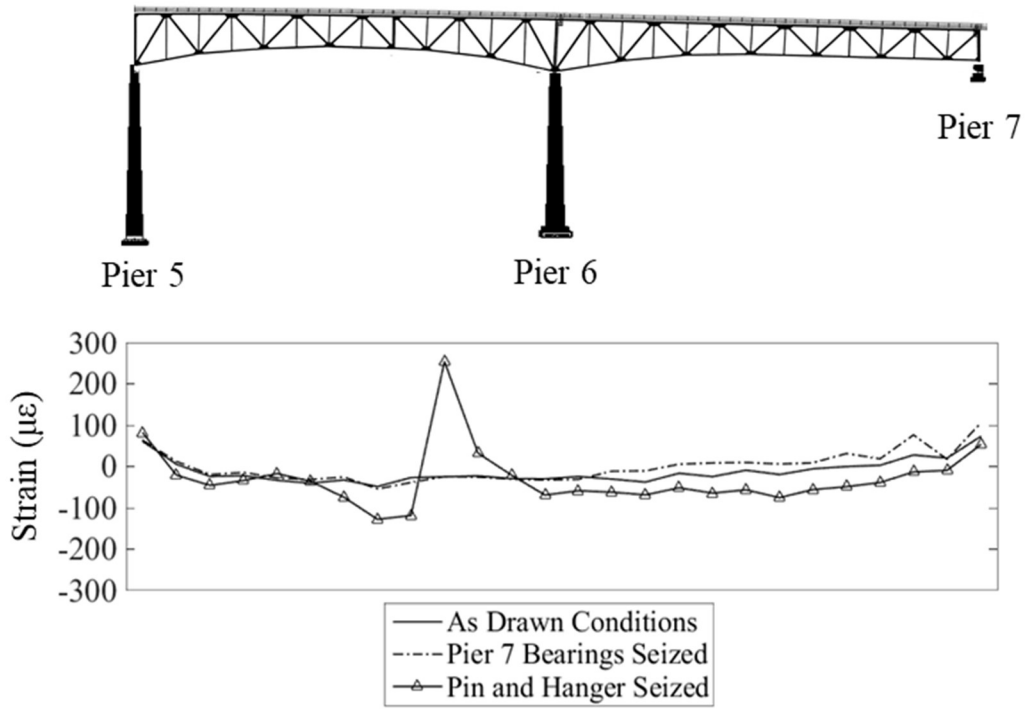

Figure 74: Sensitivity Study of Bottom Chord Strain (Reprinted from Murphy and Yarnold 2017)

The sensitivity studies illuminated key locations necessary for the representation of the bridge's behavior using strain and displacement measurements (Figure 75). The strain measurements included four cross sections, the pin and hanger, and the catch system. The displacement measurements were directed at the movement at the expansive ends of the truss system.

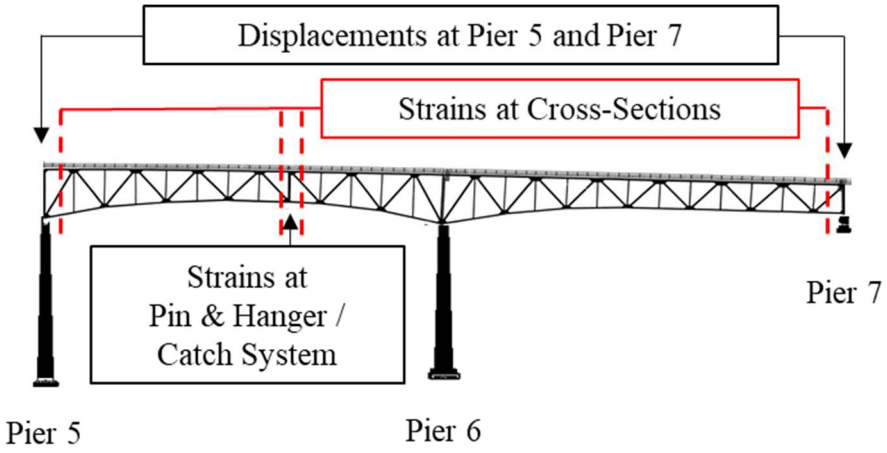

Figure 75: Instrumentation Locations Resulting from the Sensitivity Study (Reprinted from Murphy and Yarnold 2017)

With the results from the sensitivity study in mind, the gage arrangement was designed with a total of fifty-six vibrating-wire strain gages and eight vibrating wire displacement gages. Each gage was also equipped with a thermistor to record the local ambient temperature at the gage location. The gages were arranged according to the final instrumentation shown in Figure 76. The initial design of the Hurricane Bridge monitoring system considered a fully wireless configuration with gages communicating remotely with an onsite DAQ system. However, this idea was abandoned due to the additional expense of a wireless system and some communication interference experienced at the bridge site. Alternatively, a monitoring system featuring both hardwired and wireless aspects was designed and implemented on the bridge. The gages were hardwired into three DAQ boxes located on the bridge. Each DAQ box retrieved the data from the sensors and then wirelessly sent the data to the ground station for storage and retrieval.

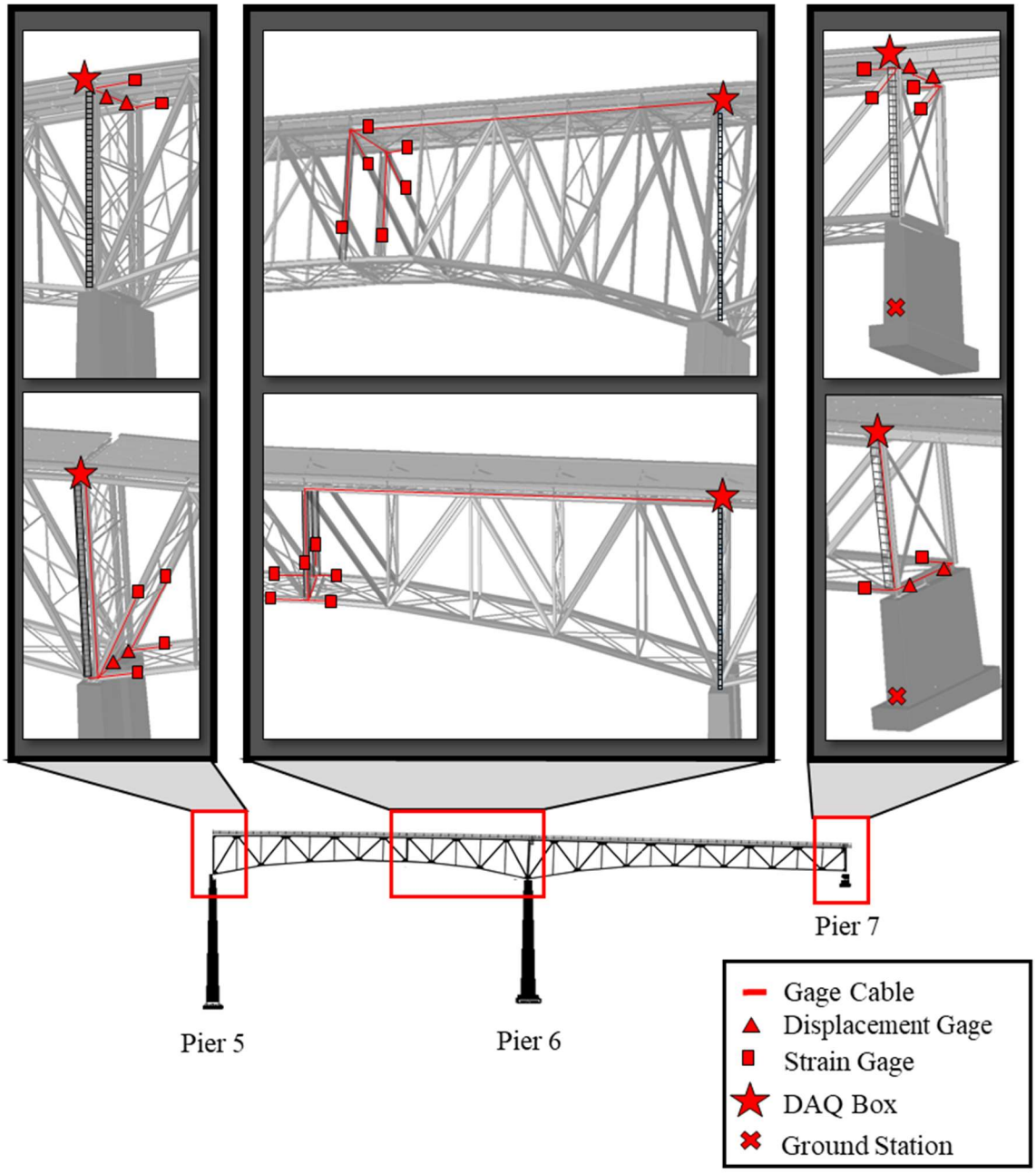

Figure 76: Final Instrumentation Plan (Reprinted from Murphy and Yarnold 2017)

8.1.2.2.1 Sensing Equipment

Two types of strain gages were used in this study. Eight 51-millimeter (2-inch) vibrating-wire strain gages (Geokon Model 4100) were spot welded to the stainless steel rods of the catch system. These gages have a range of 3000 microstrain and are specifically designed for installation on bars or curved surfaces. Per the manufacturer's specifications, these gages sampled with a frequency range of 1400-3500 Hz. The remaining forty-eight strain gages were 152-millimeter (6-inch) vibrating-wire strain gages (Geokon Model 4000) also with a range of 3000 microstrain. Shown in Figure 77(a), two of these strain gages were installed at each structural member location in a similar fashion as the Route 61 Bridge. Two strain gages per member increased the redundancy of the monitoring system and provided the ability to identify any out-of-plane bending. The gages were oriented parallel to the member and attached at the member's centroid to ensure axial responses were measured. Per the manufacturer's specifications, these gages sampled with a frequency range of 450-1250 Hz.

To quantify the longitudinal movement at Piers 5 and 7, two displacement gages were installed at the bearing and deck levels of Piers 5 and 7. Shown in Figure 77(b), the displacement gages used in this study were 102-millimeter (4-inch) range vibrating wire displacement gages (Geokon 4435). The displacement gages sampled with a frequency range of 1200-2800 Hz.

(a) (b)

Figure 77: Gages: a) 152-Millimeter (6-Inch) Strain Gage and b) Displacement Gage

8.1.2.2.2 Data Acquisition Equipment

This monitoring system included three DAQ boxes installed on the ladder access platforms at Piers 5-7 and one ground station located at the base of Pier 7. Each DAQ box contained data acquisition equipment from Campbell Scientific. An AVW200 located in each DAQ box was used to initiate and record the measurements Figure 78(b). Multiplexers were used to increase the sensor capacity of each DAQ box to a maximum of either 16 or 32. A total of four 12-volt batteries were recharged with 10-watt solar panels (Figure 78(a)) and powered each DAQ box and the ground station. The primary DAQ component was the CR1000 located in the ground station box (Figure 78(c)). This piece of equipment communicated with and collected the data from each of the DAQ boxes on the bridge and

stored the information until it could be retrieved. Manual data retrieval was necessary as remote access to the data was unavailable due to insufficient cellular service.

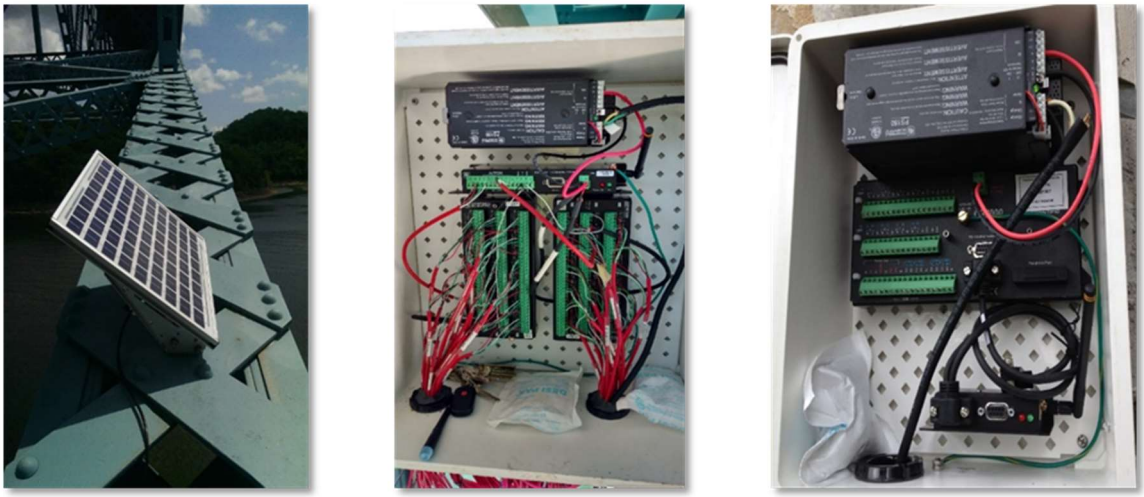

(a) (b) (c)

Figure 78: Data Acquisition Equipment: a) Solar Panel, b) DAQ Box, and c) Ground Station Box (Reprinted from Murphy and Yarnold 2017)

8.1.2.3 Monitoring System Installation

Installation of the monitoring system began on April 18, 2016. With a team of seven graduate students, a faculty advisor, and five employees of TDOT, the installation was completed within one week. Figure 79 displays some of the tasks performed throughout the installation. The installation team was subdivided into small teams to expedite the installation. Figure 79(a) shows two of the teams working simultaneously near the pin and hanger location. One team was within the bucket of a snooper truck and installed gages in the locations that were difficult to access as well as secured the gage cables for the DAQ box at Pier 6. Another team installed gages on the lower chord and verticals which were

accessible via ladder access. Figure 79(b) shows the installation of the small strain gages on the catch system. During the first day of installation, another team shown in Figure 79(c) remained on the bridge and provided assistance when securing the gage cables for the DAQ at Pier 6. Figure 79(d) shows the upper chord at Pier 5 where a displacement is about to be installed.

Figure 79: Installation Photos: a) Gage Cable Securement and Installation of Strain Gage on Vertical Member, b) Strain Gage Installation on Catch System, c) Cable Assistance from Bridge Deck, and d) Displacement Gage Installation

8.1.3 Measured Responses

The Hurricane Bridge was monitored continuously for over a year with a sampling rate of every 5 minutes. Monitoring began on April 26, 2016, and continued until June 14,

2017. Ambient air temperature was measured by the thermistor of each gage throughout the duration of the monitoring period. The ambient temperature fluctuated from -10.7°C (12.7°F) to 33.4°C (92.2°F) during this time (Figure 80).

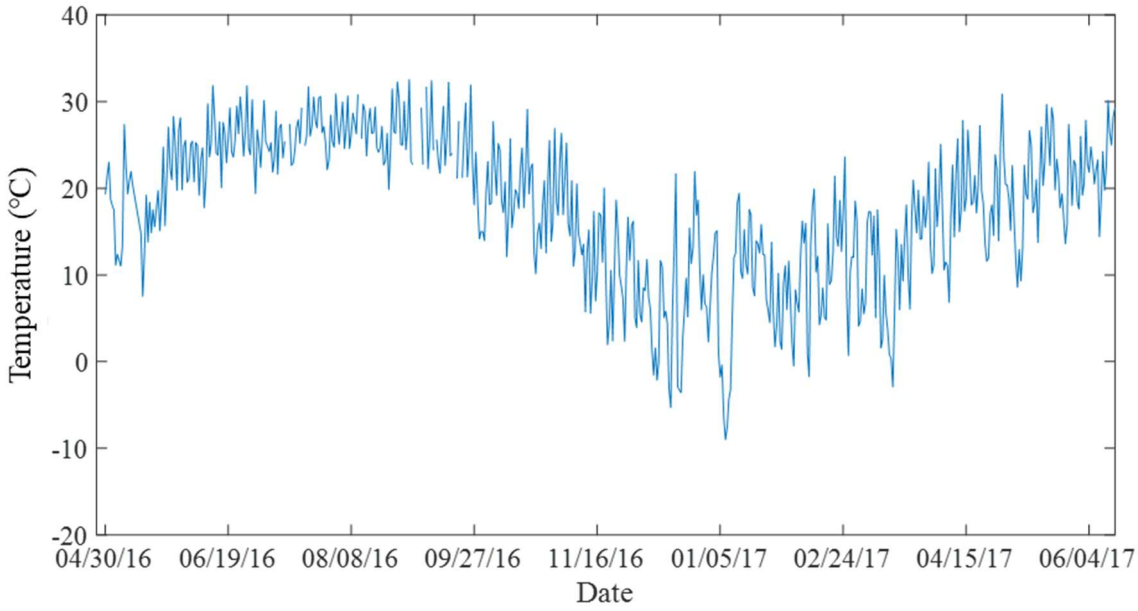

Figure 80: Average Ambient Temperature Measured from Displacement Gages

8.1.3.1 Preliminary Data Processing

Data quality checks were performed to ensure reliability of the results. The measured responses of each displacement gage are shown in Figure 81 and Figure 82. Each of the gages display daily cyclic behavior. Also, the North and South gages at each location are consistent. Obvious indications of direct sunlight effects were not present; however, the sun angle was investigated to further understand the behavior of the structure.

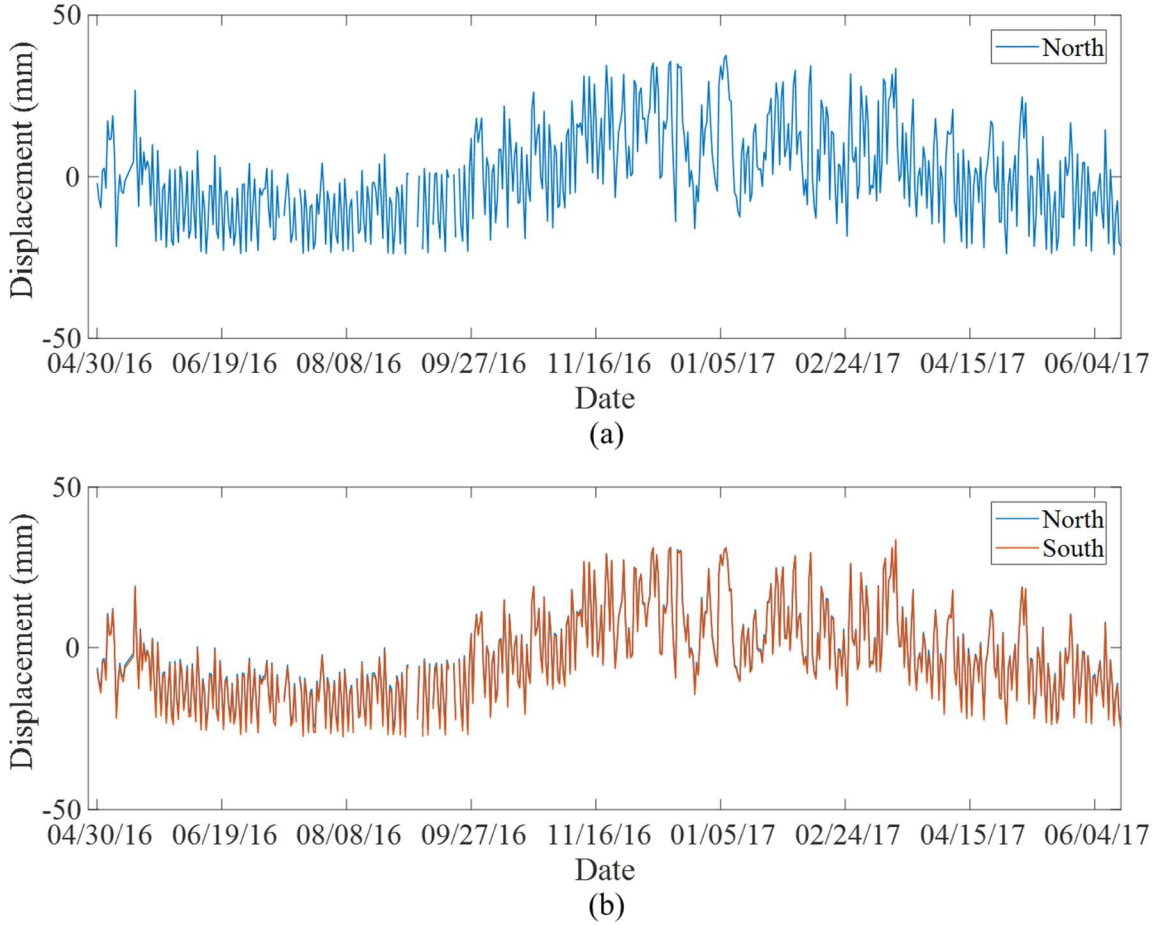

Figure 81: Measured Displacement for Pier 5: a) Deck Level and b) Bearing Level

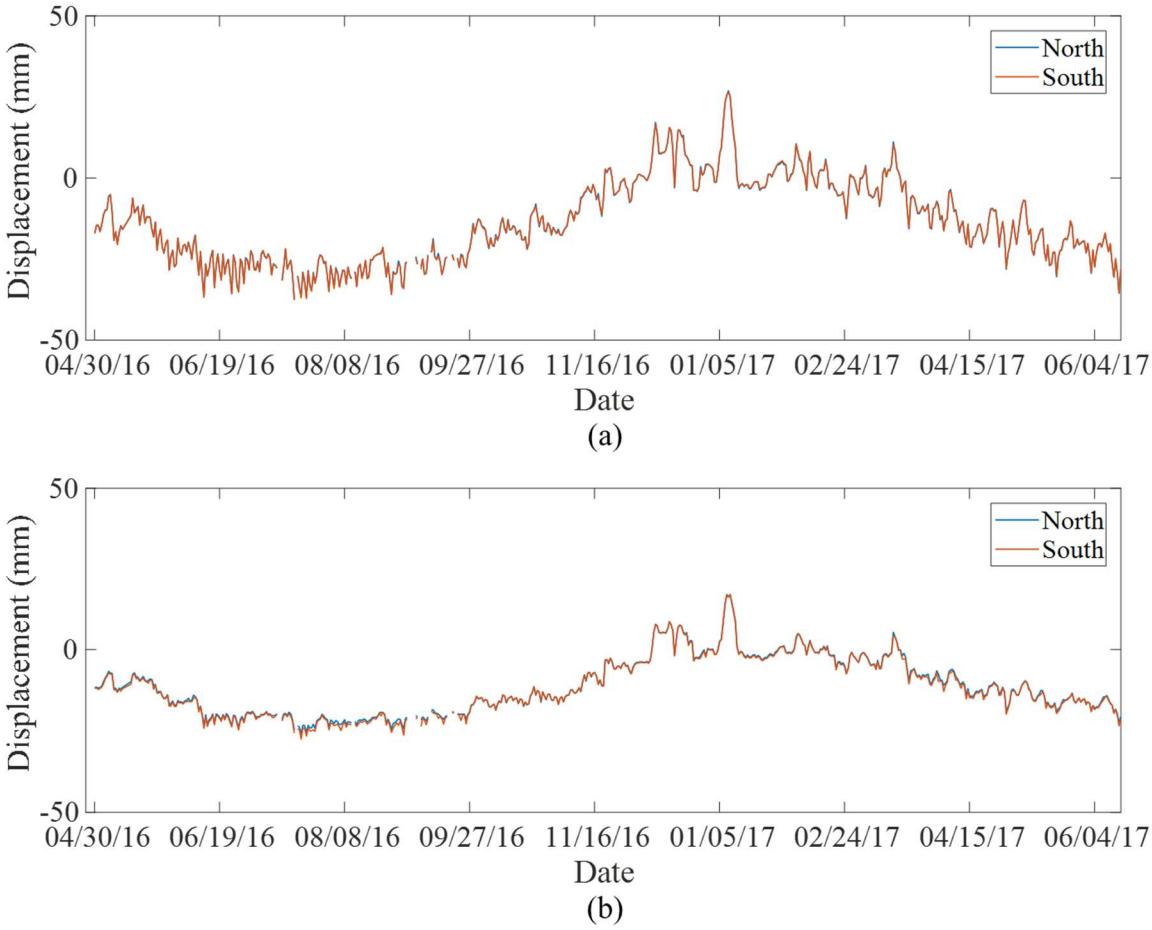

Figure 82: Measured Displacement for Pier 7: a) Deck Level and b) Bearing Level

Due to the location and orientation of the bridge, adverse effects from direct sunlight as the angle of the sun changed throughout the year were anticipated. Using the solar calculator from the NOAA, investigation of the sun angle on the Hurricane Bridge produced the paths shown in Figure 83 during one year. Since the bridge is oriented east to west, the sun angle heavily influences the northern or southern side of the bridge depending on the time of year. The northern side of the bridge is subjected to direct sunlight throughout the

warmer months from mid-April to mid-September, whereas the southern side experiences direct sunlight during the cooler months.

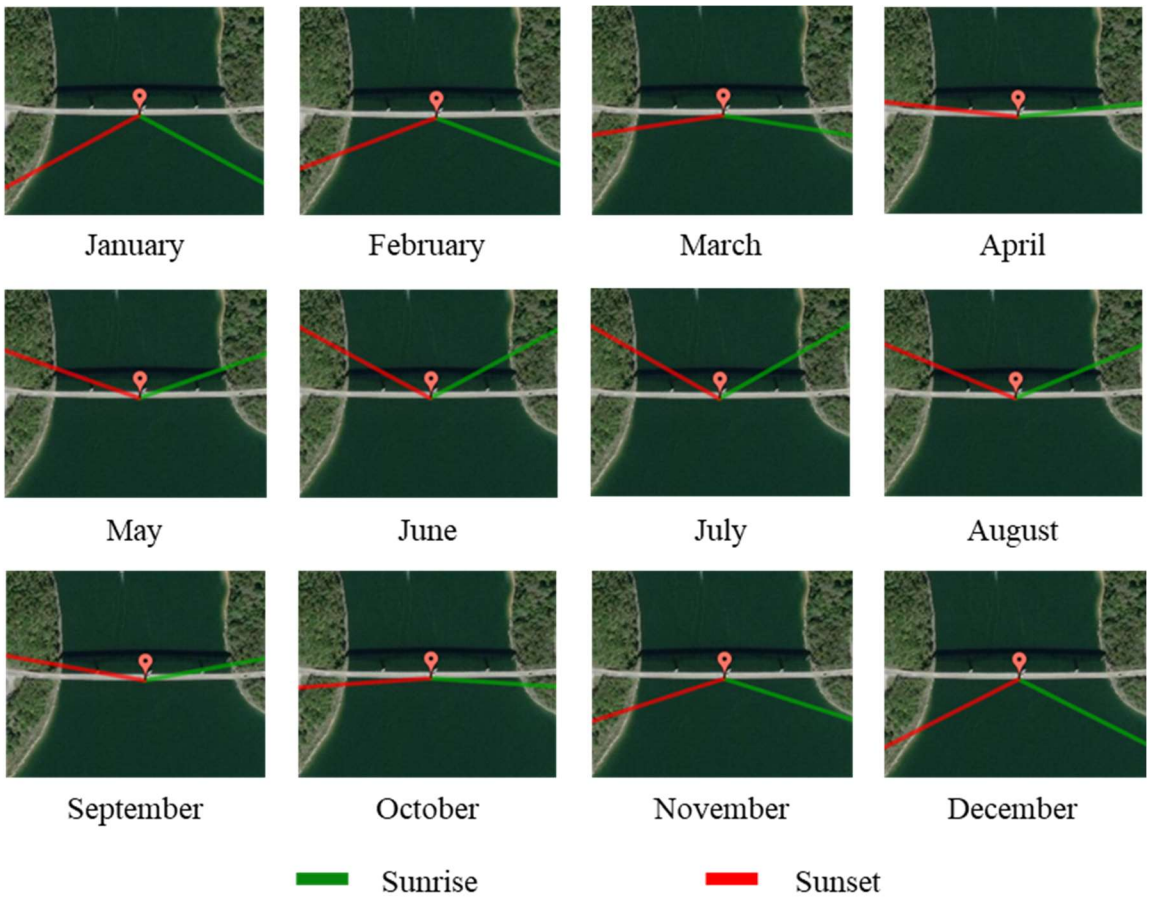

Figure 83: Sunrise and Sunset Paths throughout Year

Before the data could be analyzed, some preliminary data processing was necessary. The data was initialized from a single point in time in order to identify relative thermal behavior from that time. In order to minimize adverse bending effects due to sun angle, the data was initialized during a period in which the path of the sun was directly parallel with

the bridge. This prevented the northern side of the bridge from being exposed to the sun more than the southern side and vice versa. Also, with the sun directly parallel with the bridge, individual truss members were less likely to be exposed and thus minimized local out-of-plane bending within the truss members. The time chosen to be the initialization point was March 18, 2017. As shown in Figure 84, the sun path on this date is nearly perfectly parallel to the bridge.

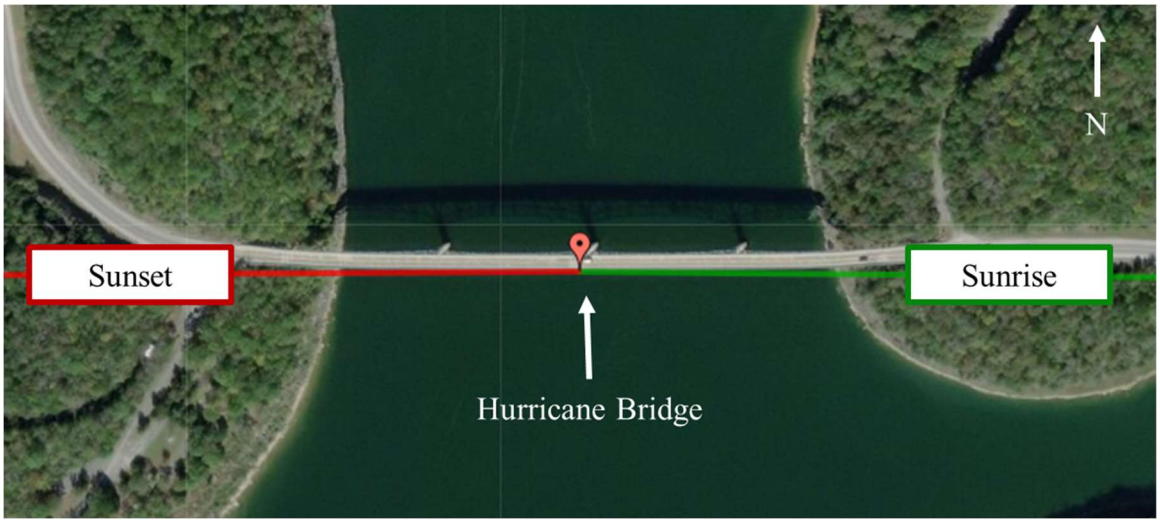

Figure 84: Sunrise and Sunset Paths for Initializing Data Point on March 18, 2017

8.1.3.2 Short-term Daily Bi-Linear Behavior

Investigation of the linearity of the bridge behavior was conducted. Thorough analysis of the data revealed that the daily responses displayed bi-linear behavior. An example of this behavior is shown in Figure 85 below as well as in greater detail in Figure 140 in Appendix B. The thermal behavior at each pier is fairly consistent with respect to the movement at the deck and bearing levels. The truss displaces approximately the same

amount at the bearing level as it does at the deck level. However, the daily thermal behavior contrasts significantly when analyzing the individual piers. Pier 5 experiences much more movement within the day by displacing approximately 35 millimeters (1.4 inches), whereas the truss only displaces approximately 10 millimeters (0.4 inches) at Pier 7.

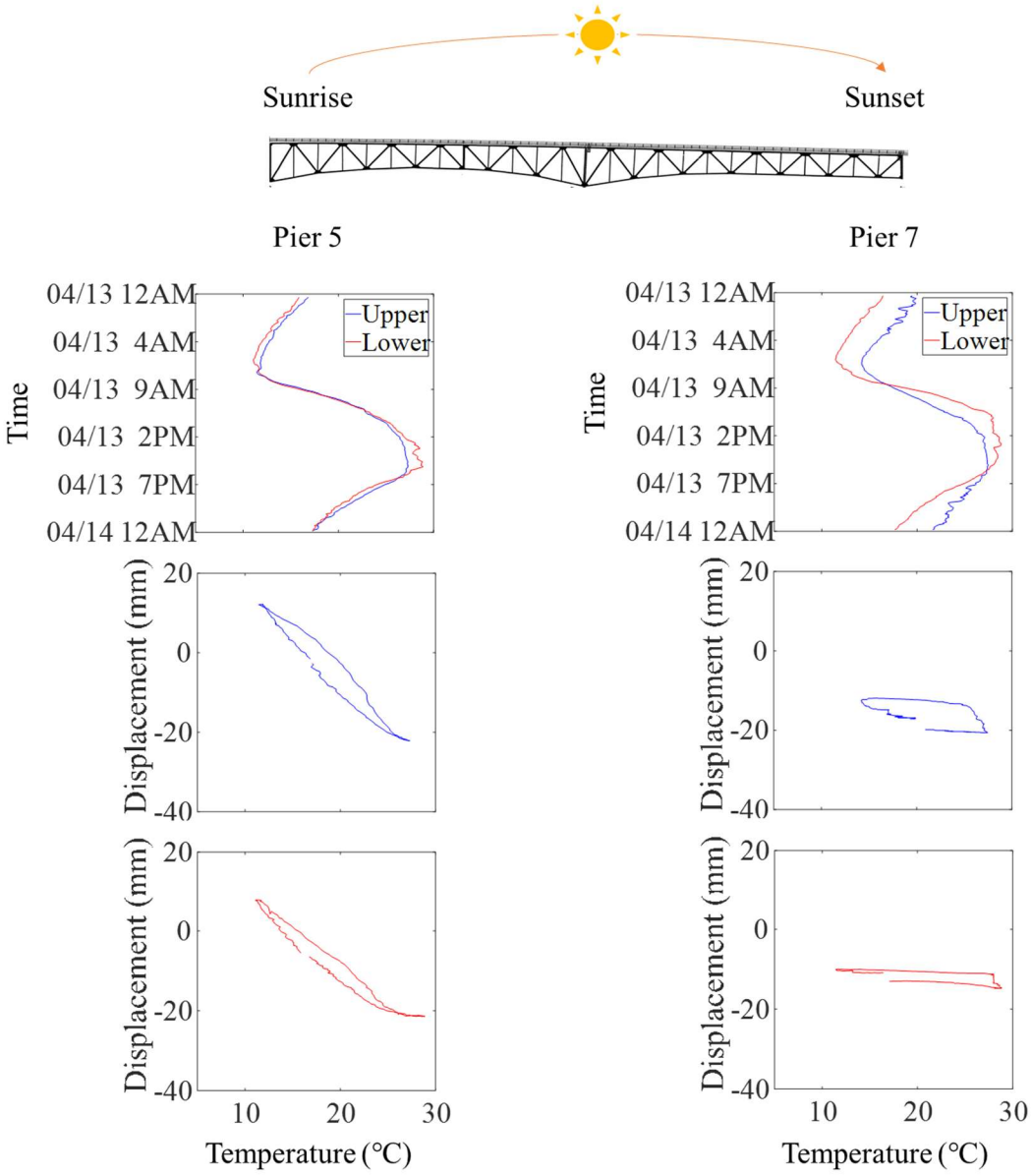

Figure 85: Temperature Time History and Measured Displacement Response on April 13, 2017

8.1.3.3 Long-term Linearity of Displacement Measurements

Investigation of the long-term thermal behavior of the Hurricane Bridge was conducted by analyzing the response versus temperature relationship for the entire

monitoring period. This relationship is shown for each displacement gage in Figure 86 below. In order to investigate the presence of thermal gradients, all of the data from the monitoring period as well as just the night-only data are shown below. The night-only data overlays the data from entire monitoring period with little deviation from the smeared line. This provides sufficient evidence that thermal gradients did not significantly influence the data. Therefore, the smeared data used to define the thermal behavior of the bridge was computed from all the data in the monitoring period rather than just the night-only.

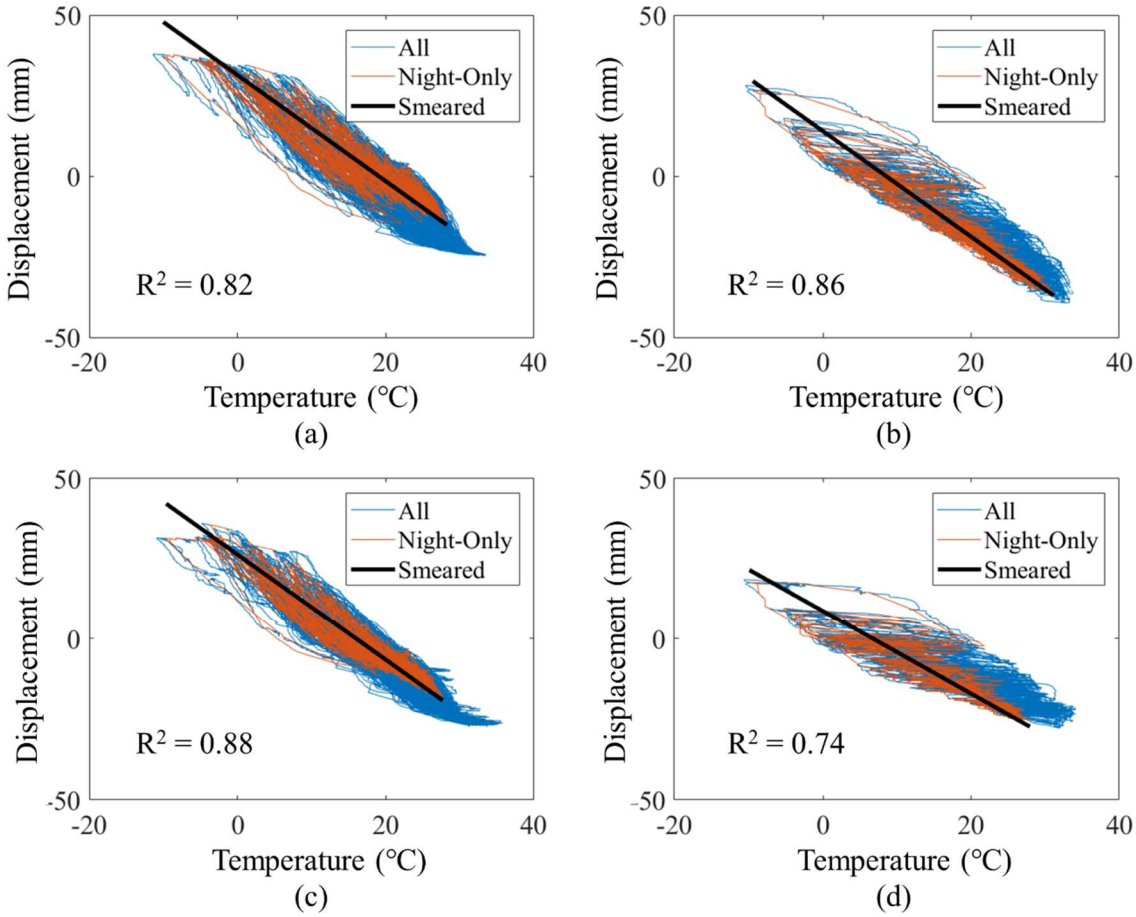

Figure 86: Measured Displacement Response: a) Pier 5 Deck Level, b) Pier 7 Deck Level, c) Pier 5 Bearing Level, and d) Pier 7 Bearing Level

8.1.3.4 Out-of-Plane Bending Effects

The data showed indications of seasonal out-of-plane bending both locally and globally (Figure 87). Local out-of-plane bending occurred when the gages from a single truss member were inconsistent. The response is similar for both the north and the south sides, but the inside gages experience more strain than the outside gages. Global out-of-plane bending occurred when the north and south sides of the bridge were inconsistent. This

occurs in Figure 87 when the strains from both southern gages are larger than both northern gages. These effects add to the complexity of analyzing the structure.

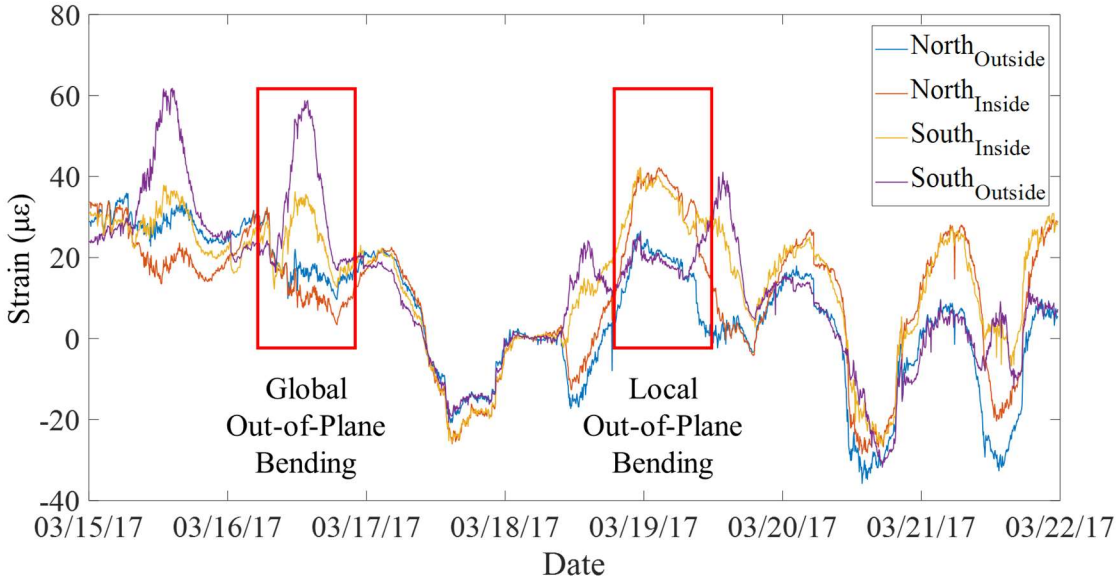

Figure 87: Global and Local Out-of-Plane Bending of Upper Chord Members at Pier 7

8.1.3.5 Long-term Non-Linearity of Strain Measurements

The long-term behavior of the strains proved to be highly non-linear. Throughout the monitoring period, the strains start to drift and no longer exhibit linear behavior. This drift can be observed from a time perspective within the strain time histories. Figure 88 below shows the drift of strain measurements of the diagonal member at Pier 7. Seasonal behavior is observed as the strain behavior is significantly different during the cooler months of November to April as opposed to the warmer months of May to October.

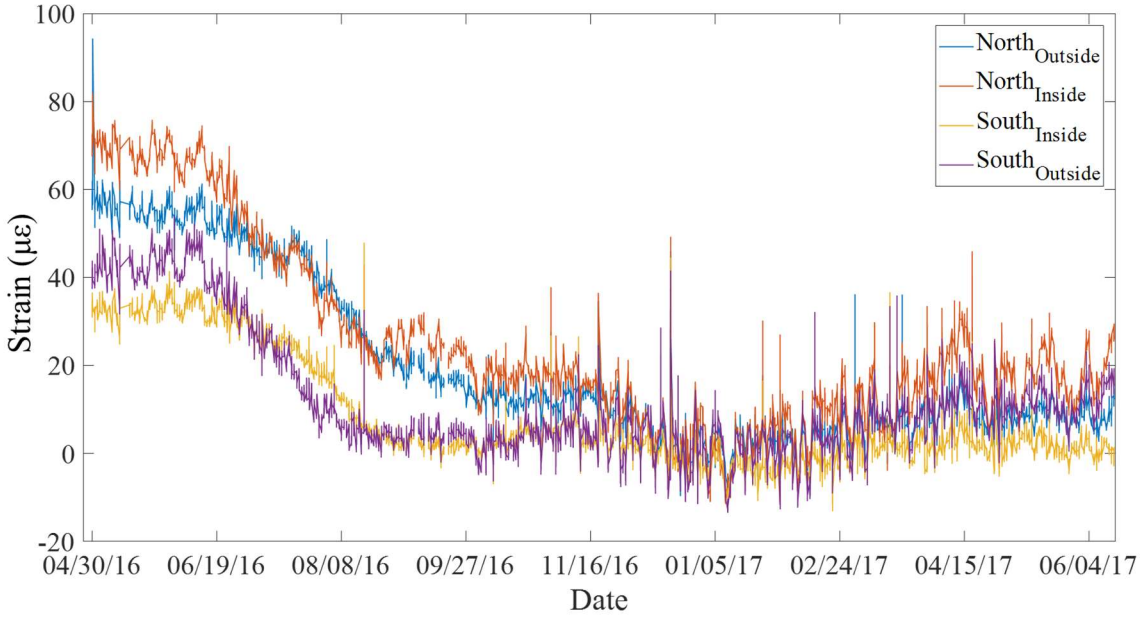

Figure 88: Strains from Diagonal at Pier 7

To further investigate the nonlinear of the strains, the behavior of the strains and displacements with respect to temperature was analyzed at the upper chord and lower chord locations of Piers 5 and 7. The strain-displacement-temperature relationships at each location are shown in Figure 89-Figure 92 below. For the upper chord location at Pier 5, Figure 89(a-c) shows the relationships between each of the responses with respect to temperature and then with respect to each other. Figure 89(c and d) show the plane formed from the three-dimensional relationship from two different angles for clarity. Figure 90-Figure 92 display the relationships for the locations of the lower chord at Pier 5, the upper chord at Pier 7, and the lower chord at Pier 7, respectively. Analysis of these relationships reveals the extent of the non-linearity of the strains. The nonlinearity of the strains is potentially the result of measuring local behavior rather than global behavior of the bridge.

If local behavior is measured, a substantial number of internal mechanisms within the structural model (discussed in the following section) are required to adequately simulate that behavior. The monitoring system must also be able to characterize the extent of the local behavior such as if the behavior is concentrated to one girder or side of the bridge, for example. Furthermore, the monitoring system nor the structural models of this study are robust enough to accurately characterize or address the nonlinear behavior of the strains. Therefore, the structural evaluation henceforth utilizes the displacement measurements only.

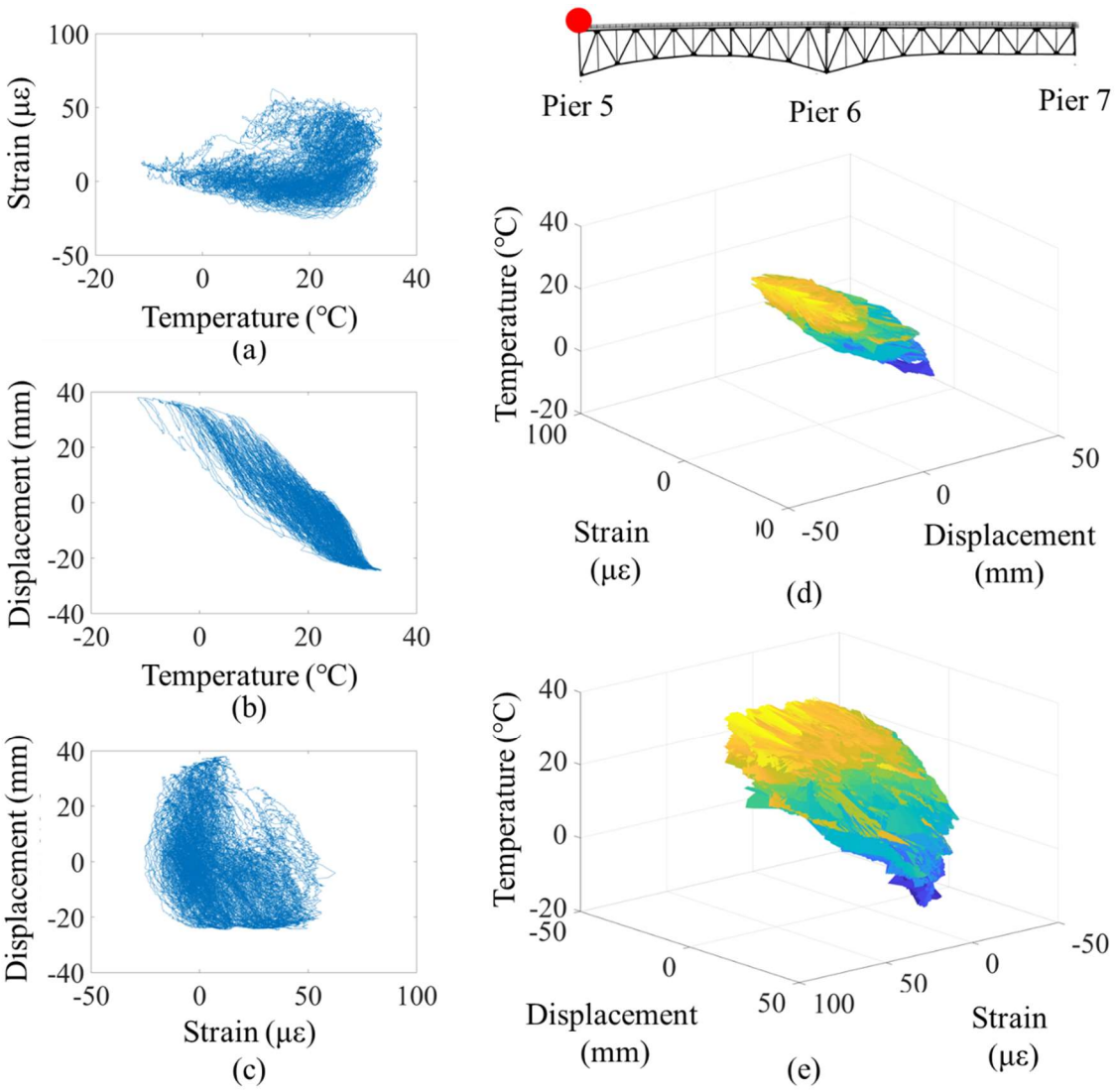

Figure 89: Behavior at Upper Chord of Pier 5: a) Strain vs. Temperature, b) Displacement vs. Temperature, c) Displacement vs. Strain, d) All Responses-View 1, and e) All Responses-View 2

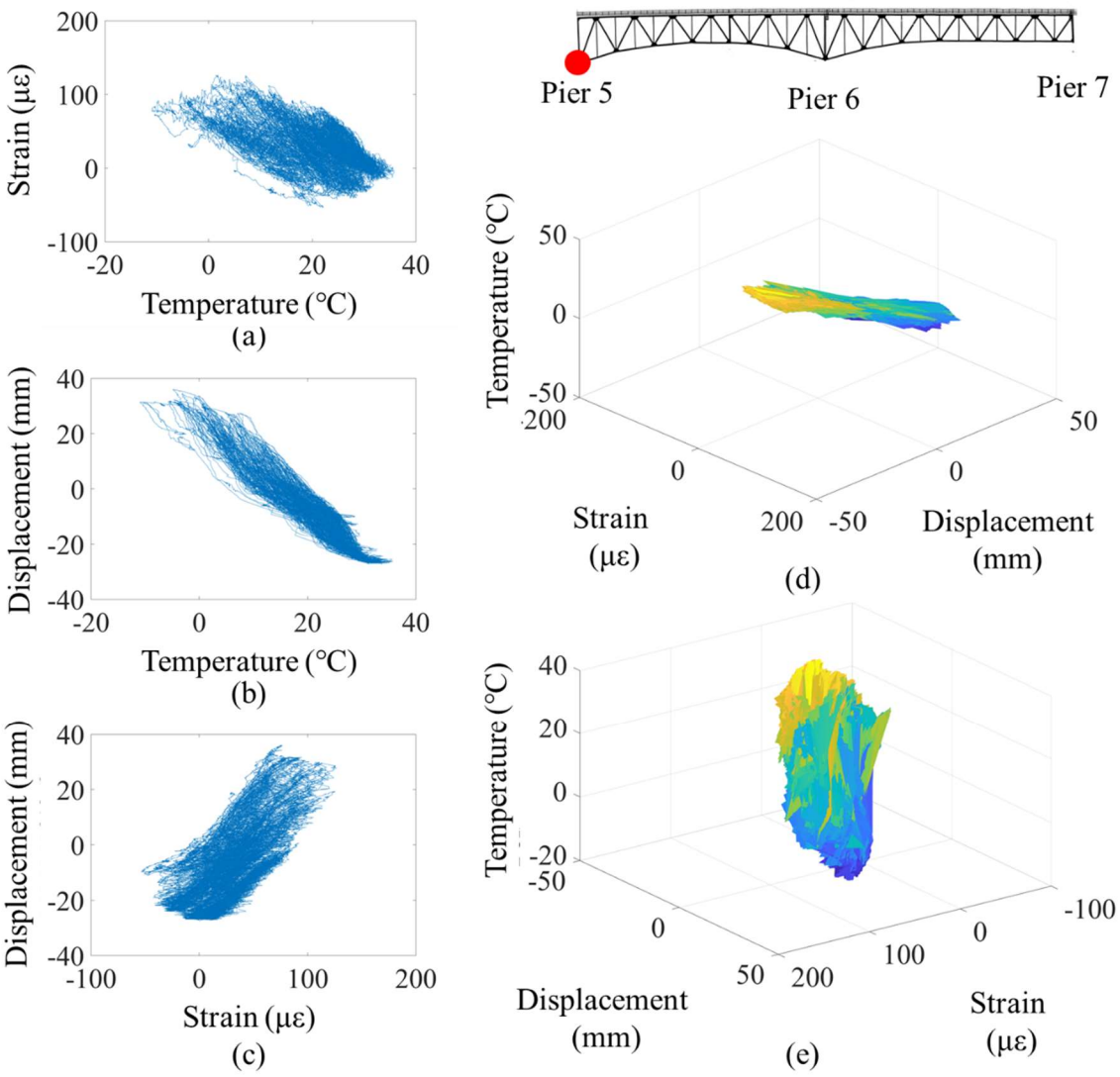

Figure 90: Behavior at Lower Chord of Pier 5: a) Strain vs. Temperature, b) Displacement vs. Temperature, c) Displacement vs. Strain, d) All Responses-View 1, and e) All Responses-View 2

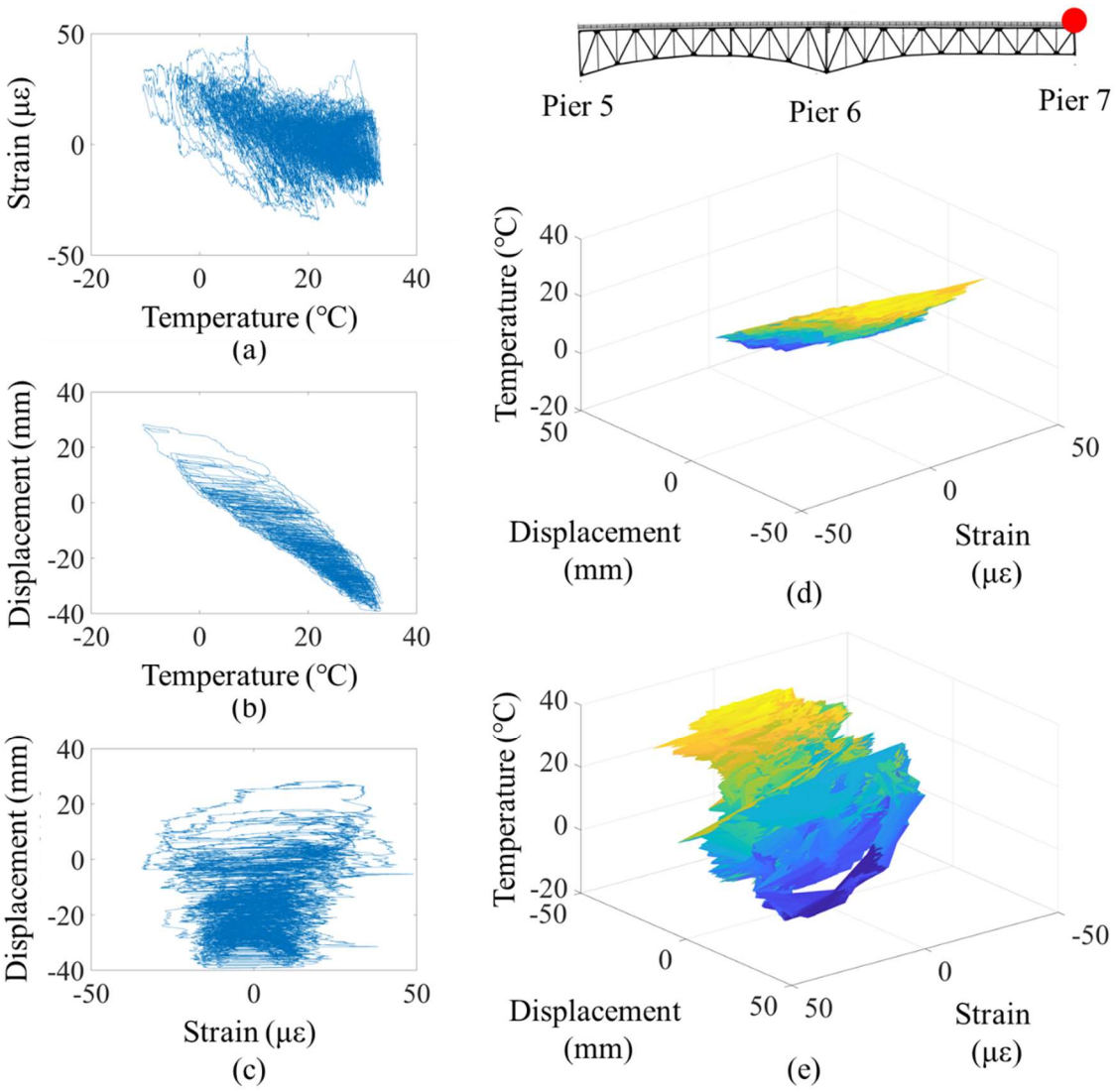

Figure 91: Behavior at Upper Chord of Pier 7: a) Strain vs. Temperature, b) Displacement vs. Temperature, c) Displacement vs. Strain, d) All Responses-View 1, and e) All Responses-View 2

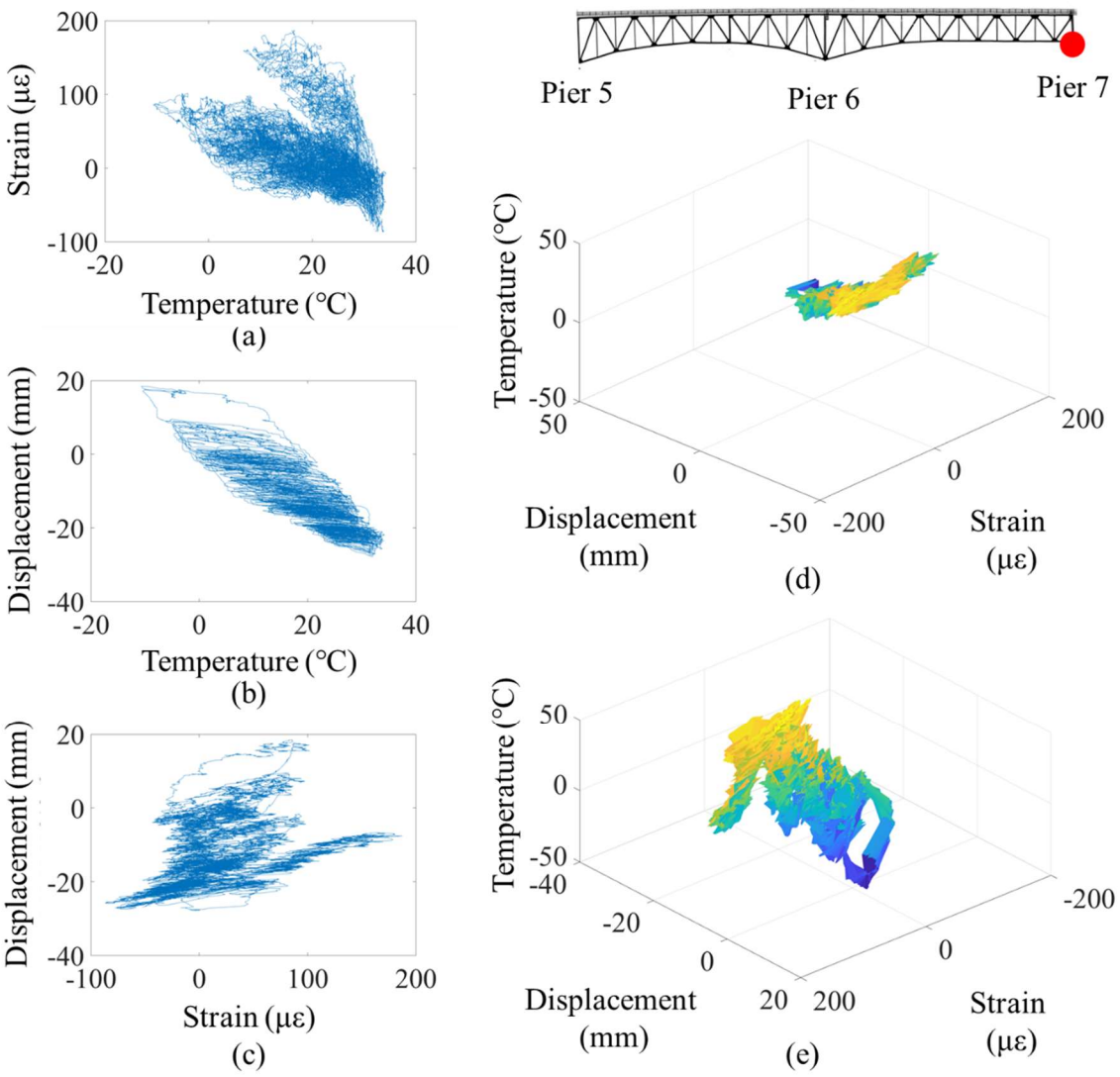

Figure 92: Behavior at Lower Chord of Pier 7: a) Strain vs. Temperature, b) Displacement vs. Temperature, c) Displacement vs. Strain, d) All Responses-View 1, and e) All Responses-View 2

8.2 Numerical Models

8.2.1 Model Parameters

As previously mentioned, the Hurricane Bridge has many boundary and continuity conditions that could affect the thermal behavior of the bridge. The primary conditions are used as model parameters to develop the sample space and is explained in detail below.

8.2.1.1 Boundary/Continuity Parameters

8.2.1.1.1 Longitudinal Bearing Stiffness at Piers 5 and 7

The longitudinal stiffness at the bearing level was defined at Pier 5 (P5B) and Pier 7 (P7B). These parameters emulate the behavior of the bearings. Furthermore, if a bearing is malfunctioning or additional friction is occurring within a bearing, the stiffness of these parameters depict that behavior. Since these parameters are located at the expansive locations of the bridge, the stiffness of these parameters should have been relatively low.

8.2.1.1.2 Longitudinal Expansion Joint Stiffness at Piers 5 and 7

The longitudinal stiffness at the deck level was defined at Pier 5 (P5D) and Pier 7 (P7D). These parameters emulate the behavior of the expansion joints within the deck. If an expansion joint was not sized properly or has filled with debris, the stiffness of these parameters depict that behavior. Similar to the bearing stiffness, these parameters are located at the expansive locations of the bridge and should have a low stiffness.

8.2.1.1.3 Flexural Stiffness of Pier 6

The longitudinal stiffness at the bearing level of Pier 6 (P6B) does not pertain to the stiffness of the connection to the pier but rather the top of the pier's ability to displace. Pier 6 is a tall component of this structure with a height of 61 meters (200 feet). With such a large height, the flexural rigidity of the pier may cause the top of the pier to displace slightly.

This component has the potential to be influenced by direct sunlight effects as well, which would cause the pier to flex and displace at the top. According to supporting documents, the stiffness of this parameter should be very large, indicating little displacement of the top of the pier.

8.2.1.1.4 Rotational Stiffness of Pin and Hanger Connections

The rotational stiffness of the pin and hanger connection at the top (PHT) and bottom (PHB) was highly uncertain. These parameters provide information regarding if the suspended section is rotating or translating. If the stiffness of these parameters was large, the cantilevered section and suspended section would act as one rigidly connected truss. If the stiffness was low (as designed), the hanger is able to rotate and the entire suspended section displaces.

8.2.1.2 Material Property Parameters

8.2.1.2.1 Modulus of Elasticity

As shown in , the modulus of elasticity of both the steel (ES) and concrete (EC) can affect the thermal behavior or the bridge. These parameters directly impact the restrained displacement of the structure. If these parameters are larger than the design value, the restrained displacement reduces, causing the structure to measure a larger unrestrained displacement. Conversely, if these parameters are smaller than designed, the unrestrained displacement of the structure will be smaller.

8.2.1.2.2 Coefficient of Thermal Expansion

As shown in , the coefficient of thermal expansion of both the steel (CTES) and the concrete (CTEC) can also influence the thermal behavior of the structure. These parameters affect the total displacement of the structure. If these parameters are larger than

designed, the bridge will experience more total displacement and, thus, more measured unrestrained displacement.

8.2.2 Development of Sample Space

8.2.2.1 Prior Probability Distributions

8.2.2.1.1 Boundary/Continuity Parameters

The parameters pertaining to the bridge boundary and continuity conditions had a large degree of uncertainty regarding their true value due to decades of use and exposure. Therefore, these parameters were uniformly distributed between a fully mobile condition (where the structure expands/contracts freely) to a fully fixed condition (where the structure is hindered from expansion/contraction). Each connectivity parameter was independently analyzed to determine the bounds which constitute free or fixed conditions. These bounds are shown in Table 10.

Table 10: Prior Probability Distributions of Boundary/Continuity Parameters

Model Parameter	Prior Probability Distribution		
	Type	Bounds	
		(kN/m)	(kip/ft)
P7D	Uniform	$14.6 * [10 - 10^7]$	$[10 - 10^7]$
P7B	Uniform	$14.6 * [10 - 10^7]$	$[10 - 10^7]$
PHT	Uniform	$14.6 * [10^2 - 10^6]$	$[10^2 - 10^6]$
PHB	Uniform	$14.6 * [10^2 - 10^6]$	$[10^2 - 10^6]$
P5D	Uniform	$14.6 * [1 - 10^7]$	$[1 - 10^7]$
P5B	Uniform	$14.6 * [1 - 10^7]$	$[1 - 10^7]$
P6B	Uniform	$14.6 * [1 - 10^7]$	$[1 - 10^7]$

8.2.2.1.2 Material Property Parameters

Steel and concrete properties are strictly regulated within the industry. Significantly more information is known about the specifics of the material properties and less uncertainty exists. However, slight variations in these parameters can affect the thermal behavior of the bridge. As a result, the material properties were normally distributed by means of a multiplier of the property value used for design. The multiplier was chosen to have a mean of 1.00 and a standard deviation of 0.04 and a variance of 0.20 as shown in Table 11.

Table 11: Prior Probability Distributions of Material Property Parameters

Model Parameter	Prior Probability Distribution		
	Type	Design Value	Multiplier
ES	Normal	200,000 MPa (29,000 ksi)	Mean = 1.00, Var. = 0.20
EC	Normal	24,900 MPa (3,610 ksi)	Mean = 1.00, Var. = 0.20
CTES	Normal	11.7 e-6 /°C (6.5e-6 /°F)	Mean = 1.00, Var. = 0.20
CTEC	Normal	10.0 e-6 /°C (5.6 e-6 /°F)	Mean = 1.00, Var. = 0.20

The sample space was developed by randomly sampling within each of the model parameter distributions using LHS simulations as discussed in Section 5. The initial sample size was chosen as 100,000 models due to previous literature and engineering judgement. Furthermore, the sample space contained 100,000 unique combinations of the model parameters. In order to show some of the detail, the sample space of the first 2,000 samples is shown in Figure 93 below. The histograms along the diagonal confirm that the parameters were sampled correctly: uniform distributions for the boundary/continuity parameters and normal distributions for the material properties.

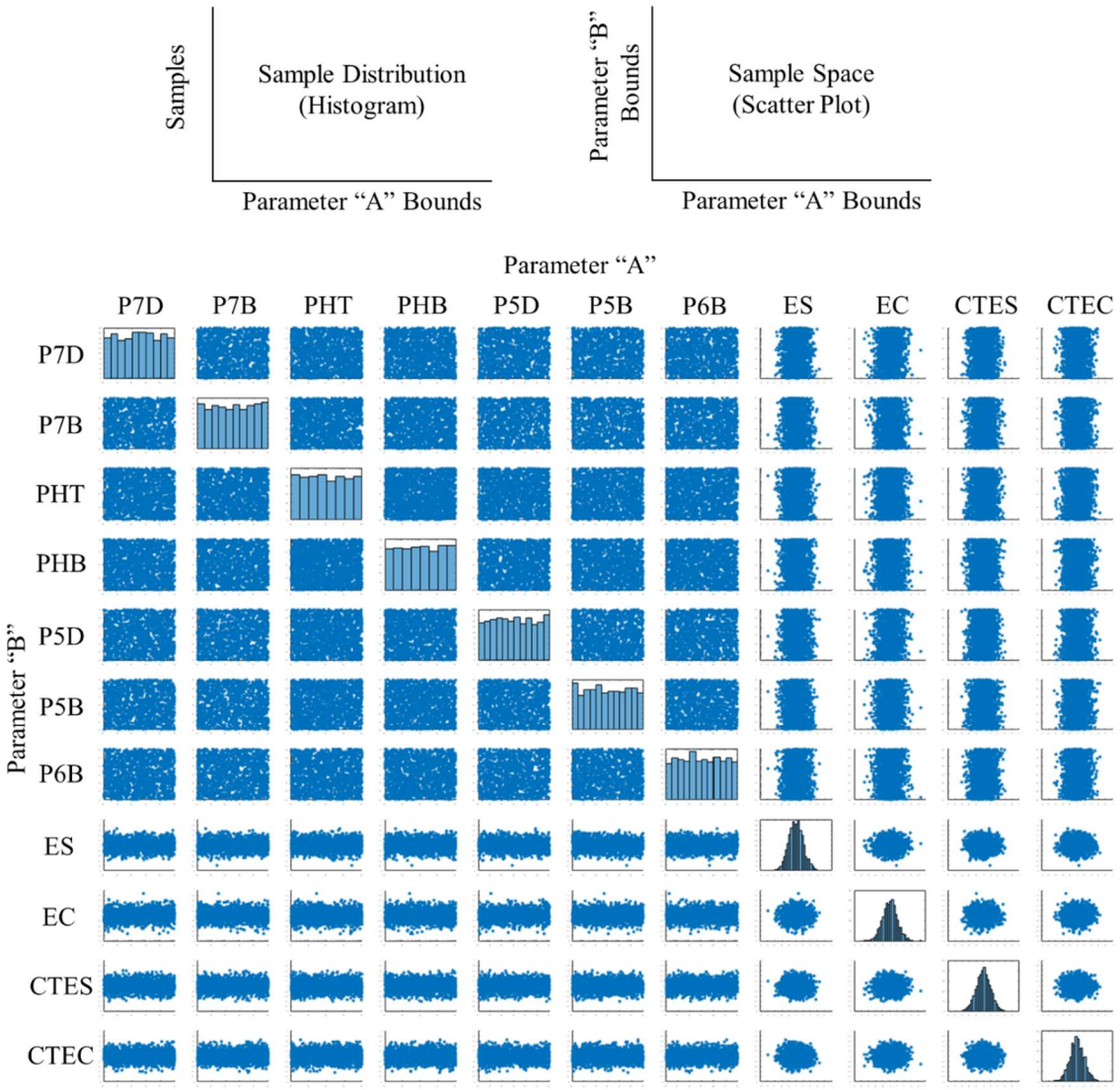

Figure 93: Sample Space for first 2,000 of 100,000 Total Samples

8.2.3 Structural Models via Finite Element Analysis

Once the sample size was determined and the sample space developed, a structural model was created within Strand7 with each parameter combination of the sample space for a total of 100,000 samples.

8.3 Single Model Analysis using Bayes Theorem

8.3.1 Calibrated Model

In order to identify the calibrated model, the first task was to ensure that response distribution included the value of the measured response. All of the measured responses were within the distribution for their respective responses. The next task was to proceed to calibration with the measured responses using Bayes Theorem. Once Bayes Theorem was completed on the data, the posterior probabilities of each of the samples were analyzed. The model with the largest posterior probability was identified and used as the calibrated model.

8.3.2 Parameter Identification

The boundary/continuity model parameters associated with the calibrated model are shown in Figure 94-Figure 97 and quantified in Table 12 below. Most of the boundary/continuity parameters experienced partial restraint to some degree. Pier 7 Deck was the only parameter that was essentially a free condition, whereas Pier 6 was nearly a fully fixed condition.

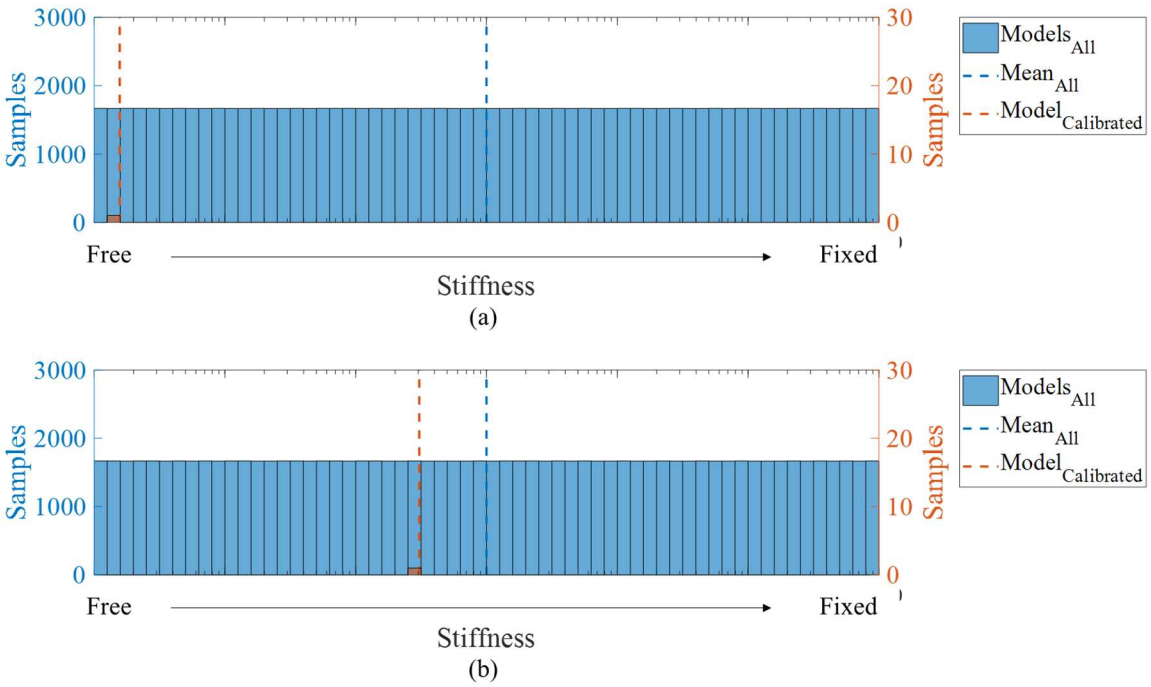

Figure 94: Calibrated Model Parameters of Pier 7: a) Deck and b) Bearing

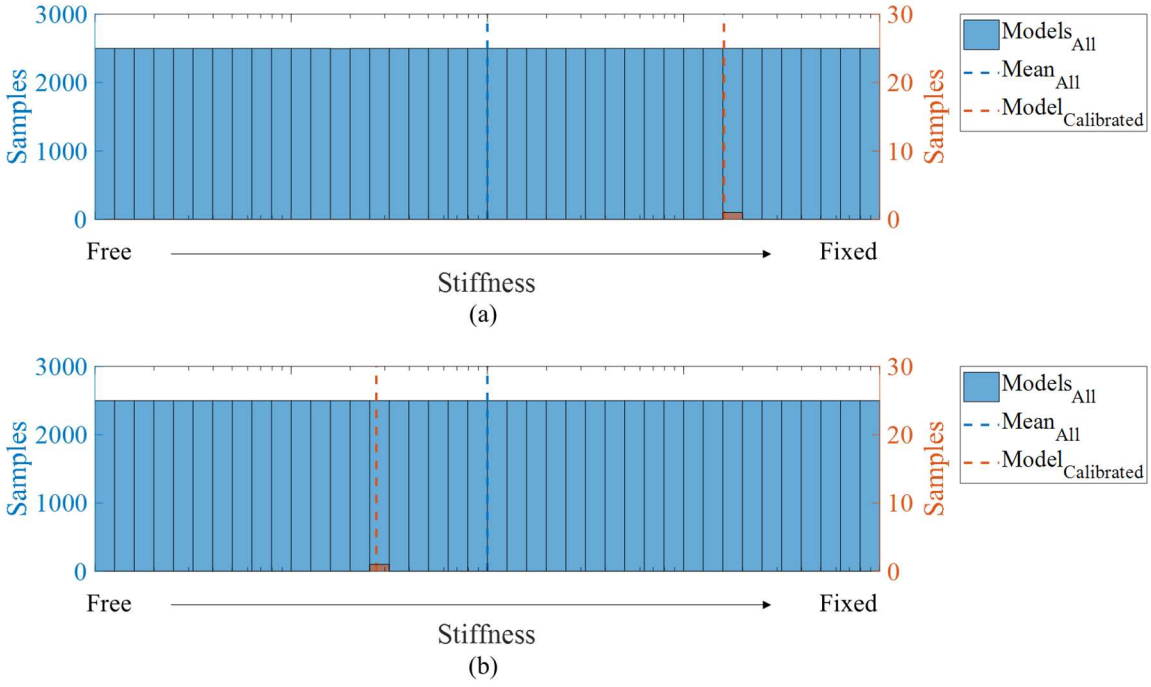

Figure 95: Calibrated Model Parameters of Pin and Hanger: a) Top and b) Bottom

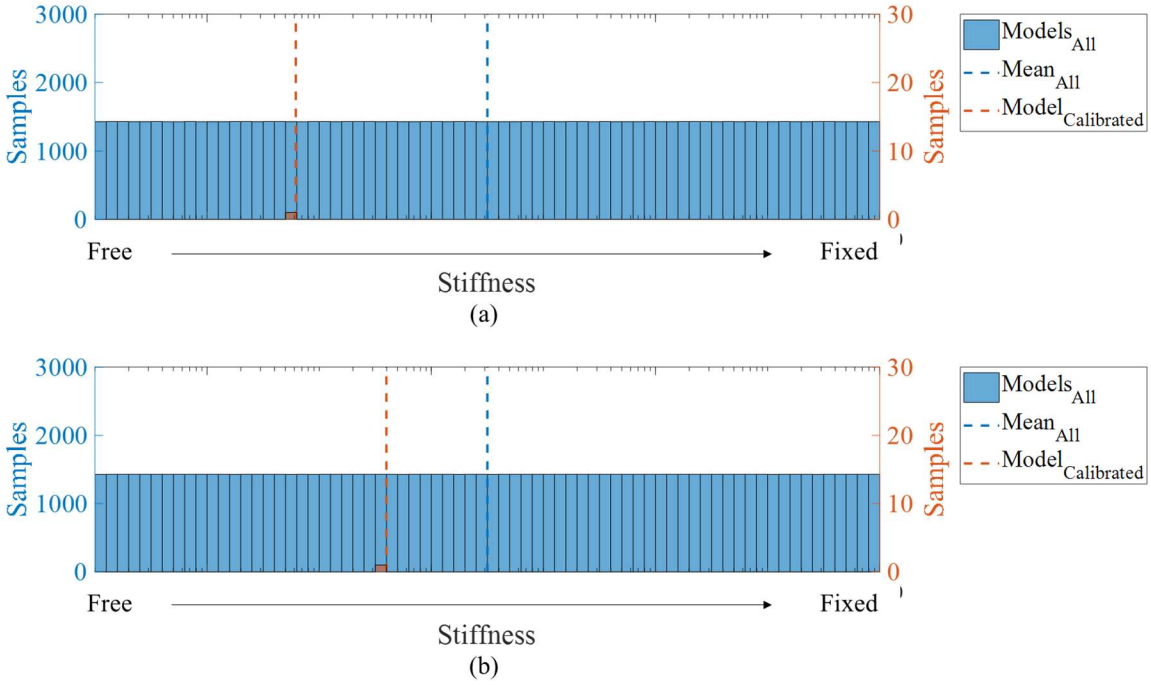

Figure 96: Calibrated Model Parameters of Pier 5: a) Deck and b) Bearing

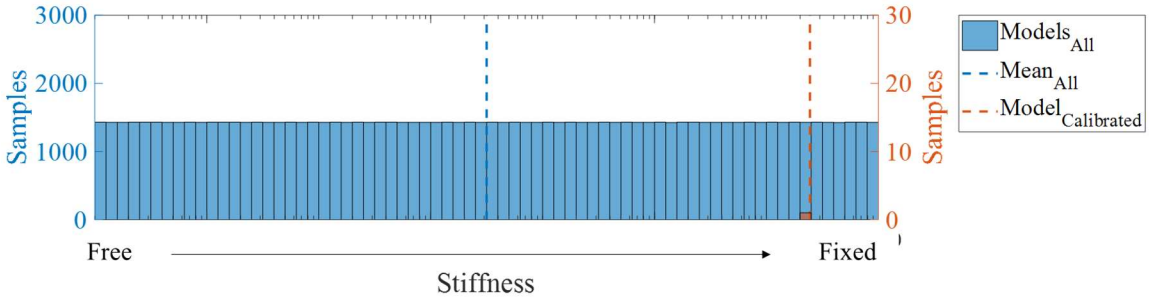

Figure 97: Calibrated Model Parameter of Pier 6

The material property parameters associated with the calibrated model are shown in Figure 98 and Figure 99. The modulus of elasticity multipliers for the steel and concrete

were identified as 1.18 and 1.13, respectively. The coefficient of thermal expansion multipliers were identified as 0.99 for the steel and 1.19 for the concrete.

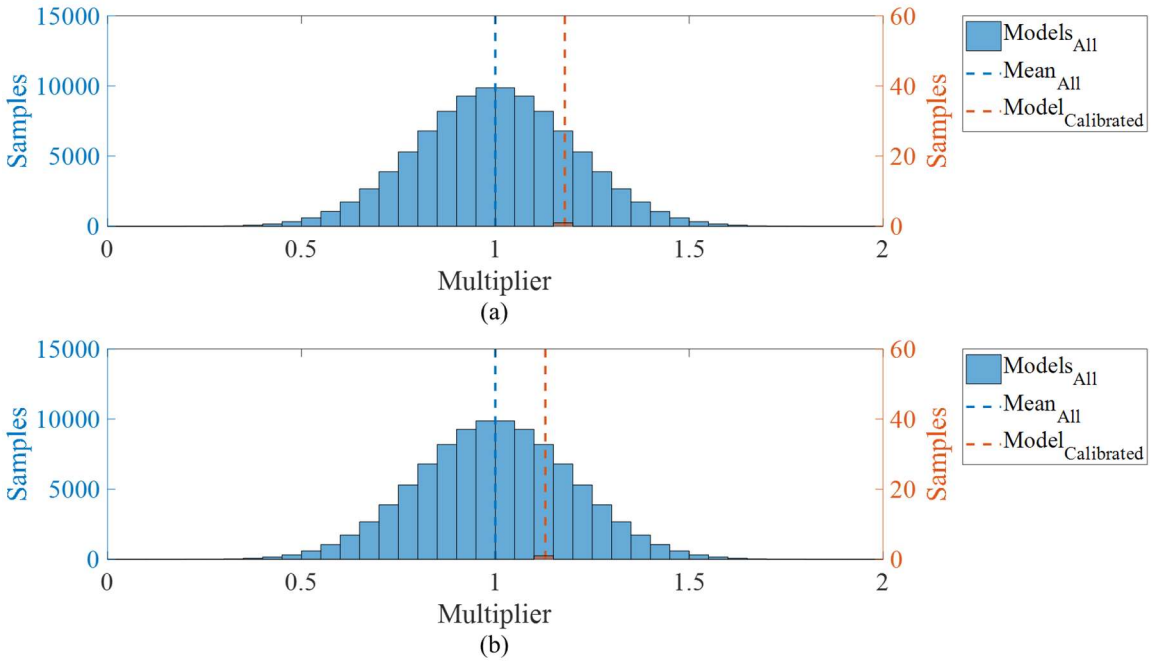

Figure 98: Calibrated Model Parameters of Modulus of Elasticity: a) Steel and b) Concrete

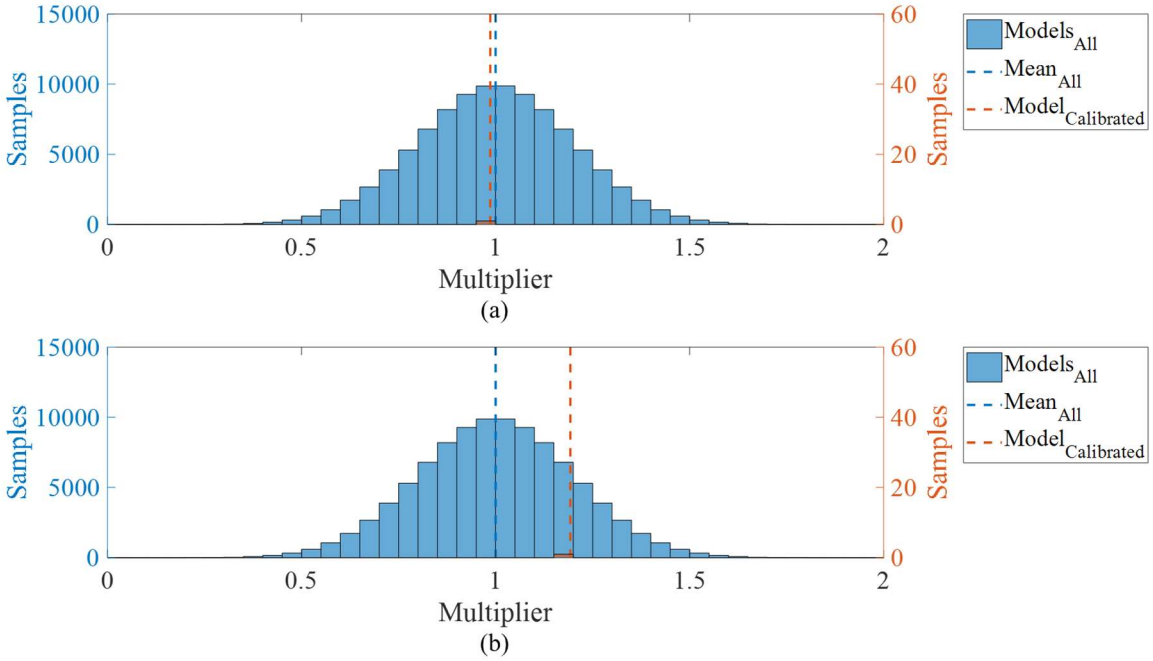

Figure 99: Calibrated Model Parameters of Coefficient of Thermal Expansion: a) Steel and b) Concrete

Table 12: Calibrated Model Parameters

Parameter	Calibrated	
	Stiffness kN/m (10^x kip/ft)	Multiplier
P5D	9.02e5 (4.79)	-
P5B	5.80e6 (5.60)	-
P6B	3.57e10 (9.39)	-
P7D	2.29e5 (4.20)	-
P7B	4.47e7 (6.49)	-
PHT	2.34e9 (8.21)	-
PHB	3.96e7 (6.43)	-
ES	-	1.18
EC	-	1.13
CTES	-	0.99
CTEC	-	1.19

8.3.3 Predictive Responses

The predictive responses are analyzed by comparing the responses from the calibrated model to the measured responses. The displacement responses associated with the calibrated model are shown in Figure 100 and Figure 101 and quantified in Table 13. The measurement with the largest percent difference was the displacement at the deck level of Pier 7 with a percent difference of 14%. Otherwise, the evaluation method calibrated within a percent difference of 5% for the remaining three measurements.

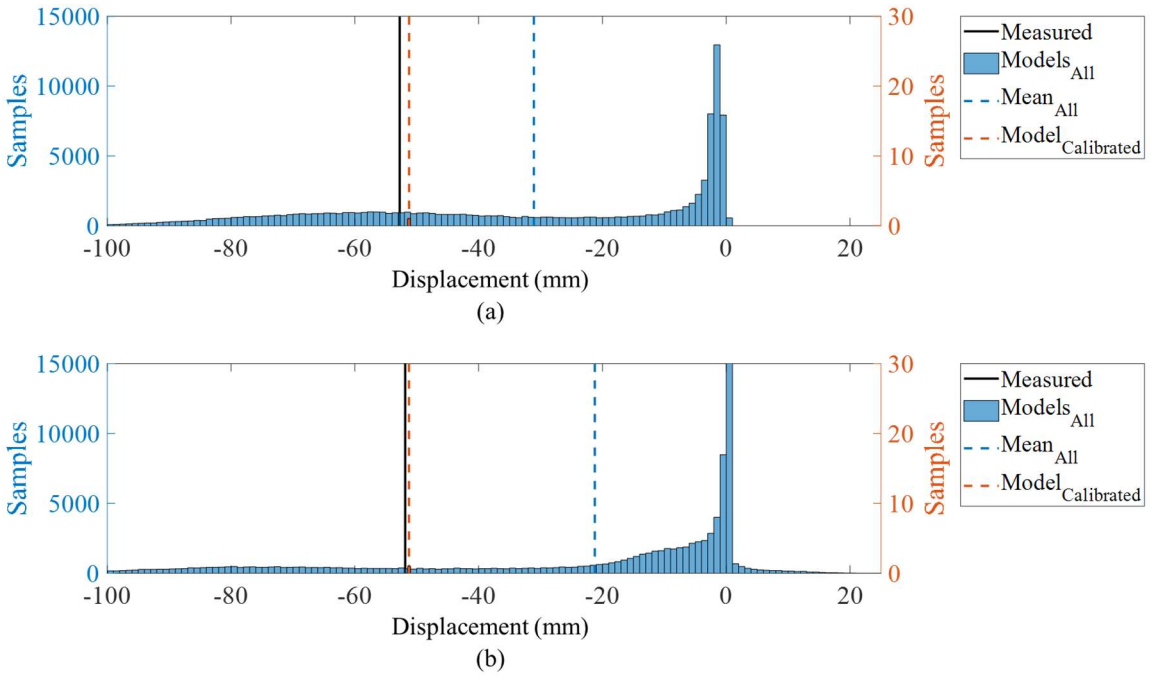

Figure 100: Calibrated Model Displacement Response of Pier 5: a) Top and b) Bottom

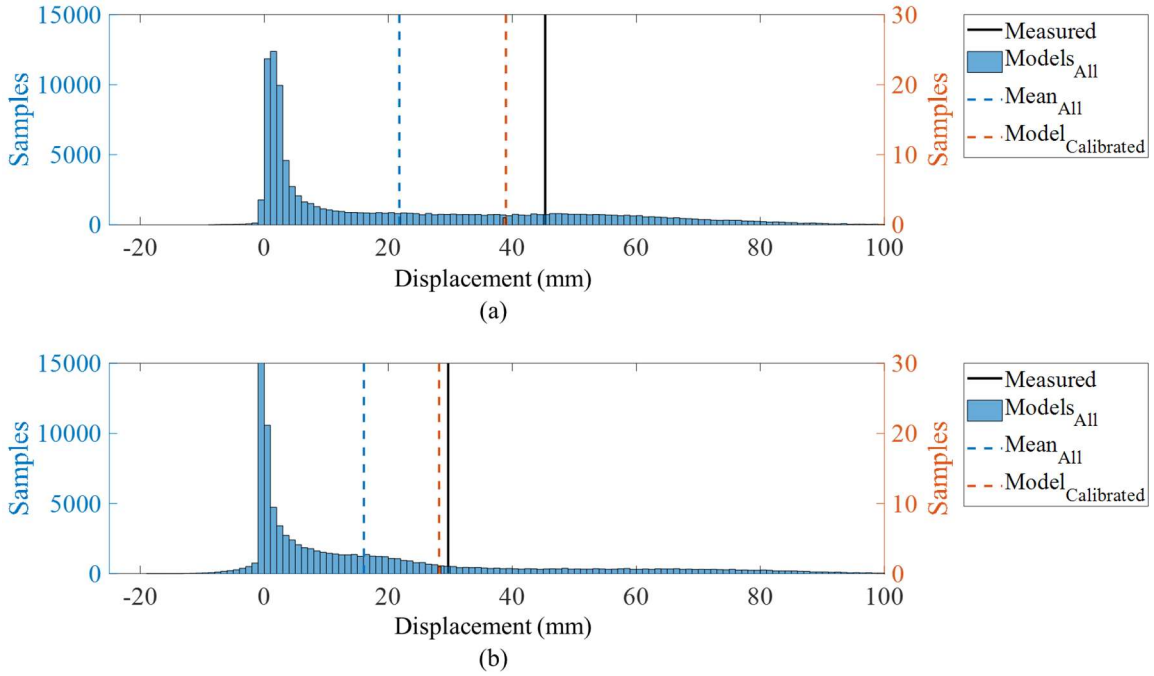

Figure 101: Calibrated Model Displacement Response of Pier 7: a) Top and b) Bottom

Table 13: Calibrated Model Response

Gage	Measured	Calibrated	% Diff.
Pier 5 Deck	52.8 mm (2.1 in.)	51.2 mm (2.0 in.)	3%
Pier 5 Bearing	51.9 mm (2.0 in.)	51.3 mm (2.0 in.)	1%
Pier 7 Deck	45.3 mm (1.8 in.)	39.0 mm (1.5 in.)	14%
Pier 7 Bearing	29.7 mm (1.2 in.)	28.2 mm (1.1 in.)	5%

8.4 Multiple Model Analysis using Bayes Theorem

8.4.1 Candidate Models

The calibration process using Bayes Theorem described in Section 5 was also used to identify the candidate models. Once Bayes Theorem was completed on the data, the posterior probabilities of each of the samples were analyzed. The candidate models were identified as the samples with the highest probabilities that comprised 95% of the total posterior probability. For the Hurricane Bridge, the number of samples required to meet or exceed 95% total probability was 122 models. Furthermore, the 122 models that were most probable were used as the candidate models.

8.4.2 Predictive Responses

The candidate models were used to analyze the responses of the bridge. Figure 102 and Figure 103 show the displacement response distributions from all of the structural models as well as from just the candidate models. The values of the measured displacements are also shown.

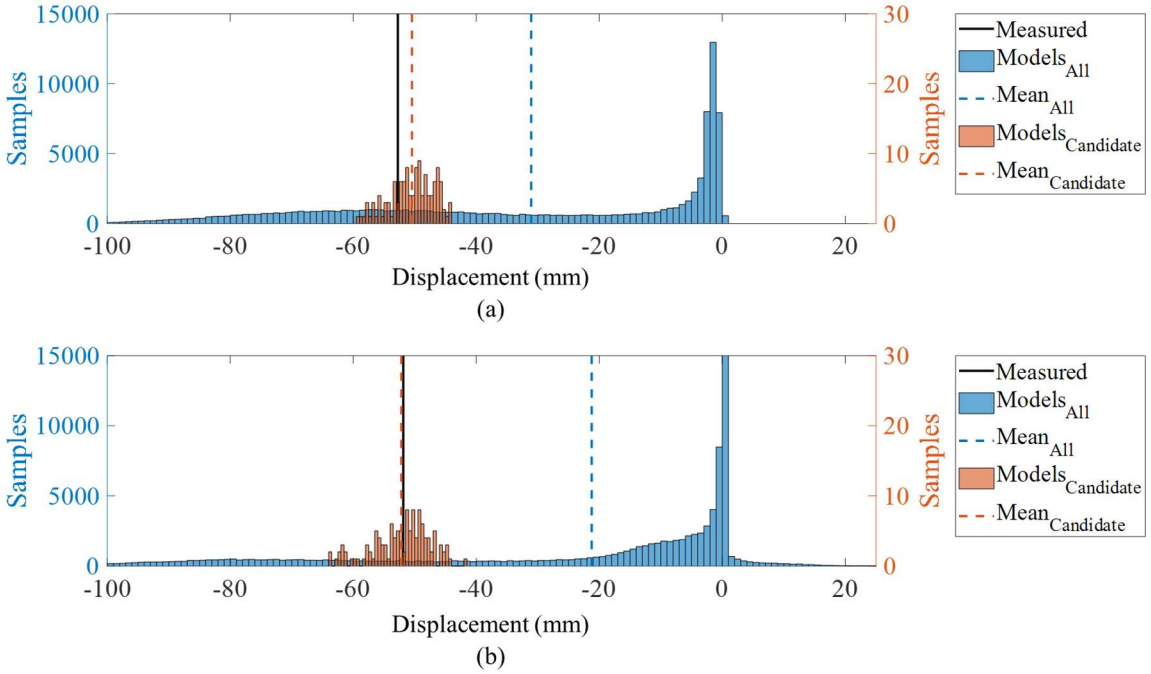

Figure 102: Model Displacement Response of Pier 5: a) Top and b) Bottom

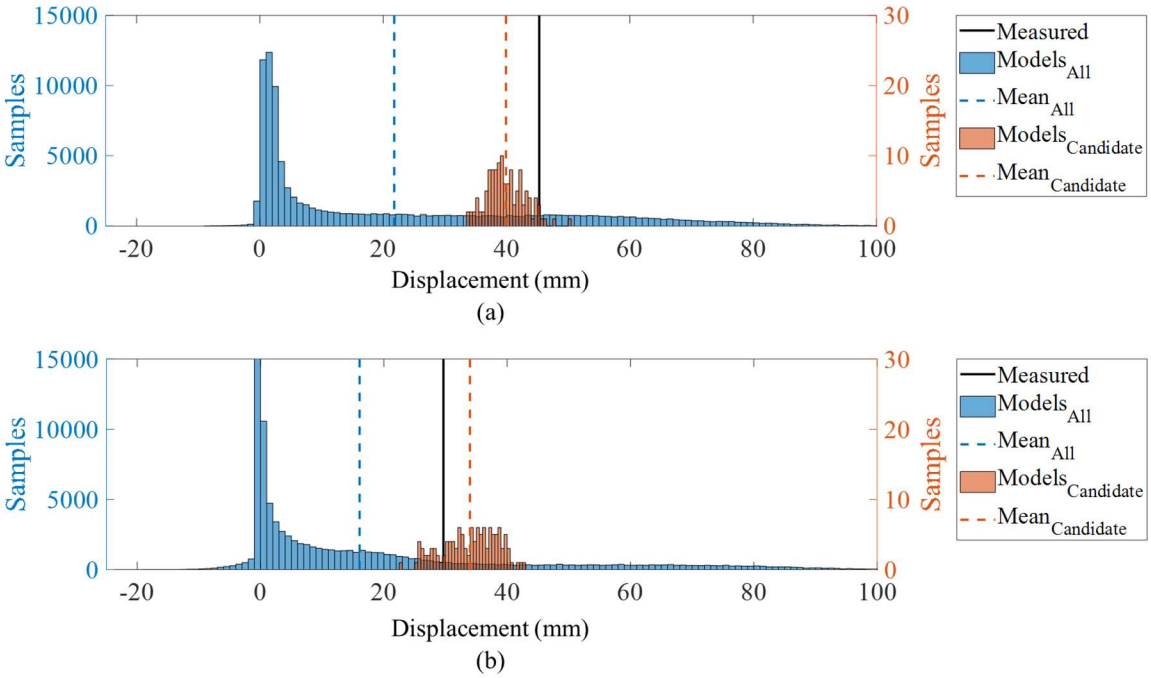

Figure 103: Model Displacement Response of Pier 7: a) Top and b) Bottom

The response distributions are given numerically in Table 14. Through the calibration process, the response distributions from the structural models were significantly reduced to the response distributions of the candidate models. The variance of each parameter distribution reduced between 81% and 88%. As expected, the candidate model distributions were also more accurate to the measured responses. The gages with the most percent differences were located at Pier 7 with percent differences of 11% and 14% for deck and bearing levels, respectively. The gages at Pier 5 experienced a mean percent difference of less than 5%.

Table 14: Candidate Model Response Distributions

Gage	Measured	Prior Distribution		Posterior Distribution		Uncert. Red.	Mean % Diff.
		Mean	Var.	Mean	Var.		
Pier 5 Deck	52.8 mm (2.1 in.)	31.1 mm (1.2 in.)	29.4 mm (1.2 in.)	50.5 mm (2.0 in.)	3.6 mm (0.1 in.)	88%	4%
Pier 5 Bearing	51.9 mm (2.0 in.)	21.2 mm (0.8 in.)	30.2 mm (1.2 in.)	52.2 mm (2.1 in.)	4.7 mm (0.2 in.)	84%	1%
Pier 7 Deck	45.3 mm (1.8 in.)	21.8 mm (0.9 in.)	24.6 mm (1.0 in.)	39.9 mm (1.6 in.)	3.1 mm (0.1 in.)	87%	11%
Pier 7 Bearing	29.7 mm (1.2 in.)	16.1 mm (0.6 in.)	23.4 mm (0.9 in.)	34.0 mm (1.3 in.)	4.4 mm (0.2 in.)	81%	14%

8.4.3 Refined Parameters

The candidate models were also used to refine the parameters of the models and hence provide insight regarding the boundary conditions of the structure. Figure 104-Figure 109 show the model parameter distributions from all of the structural models as well as the parameter distributions from just the candidate models.

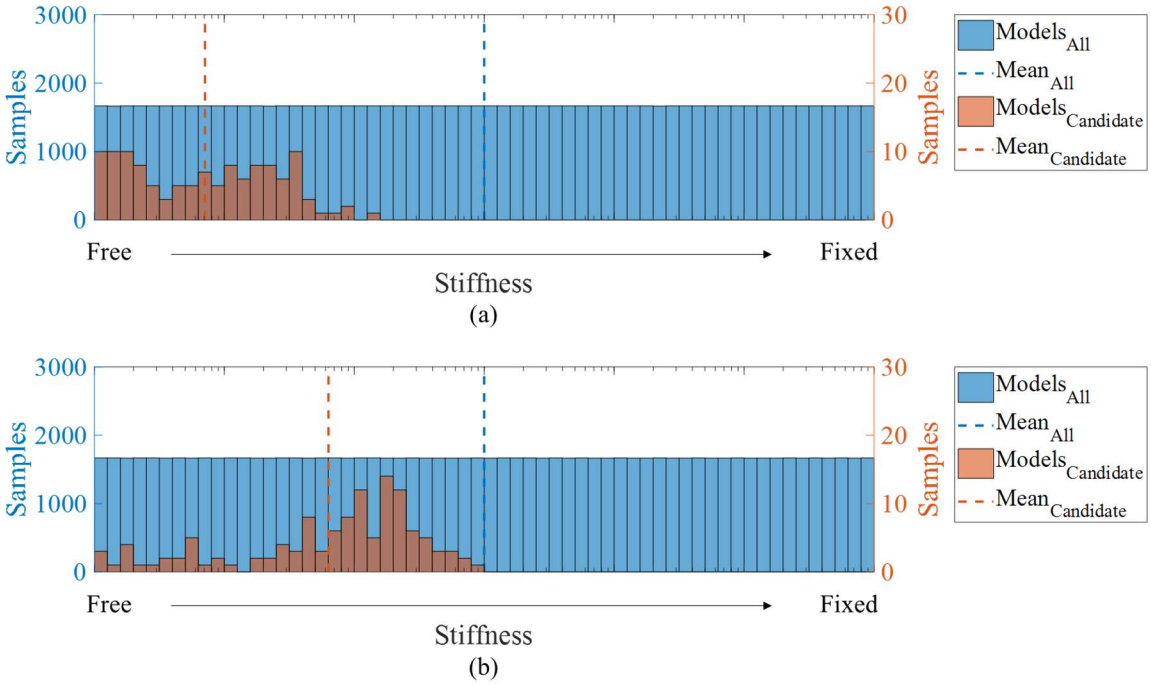

Figure 104: Refined Model Parameters of Pier 7: a) Deck and b) Bearing

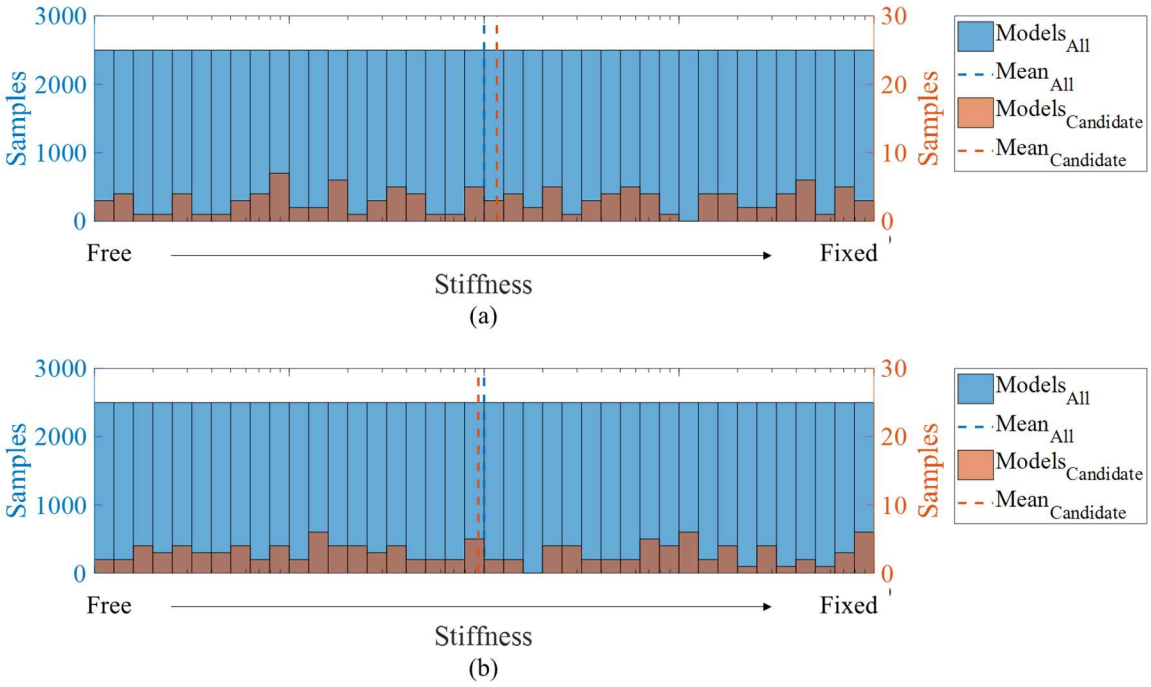

Figure 105: Refined Model Parameters of Pin and Hanger: a) Top and b) Bottom

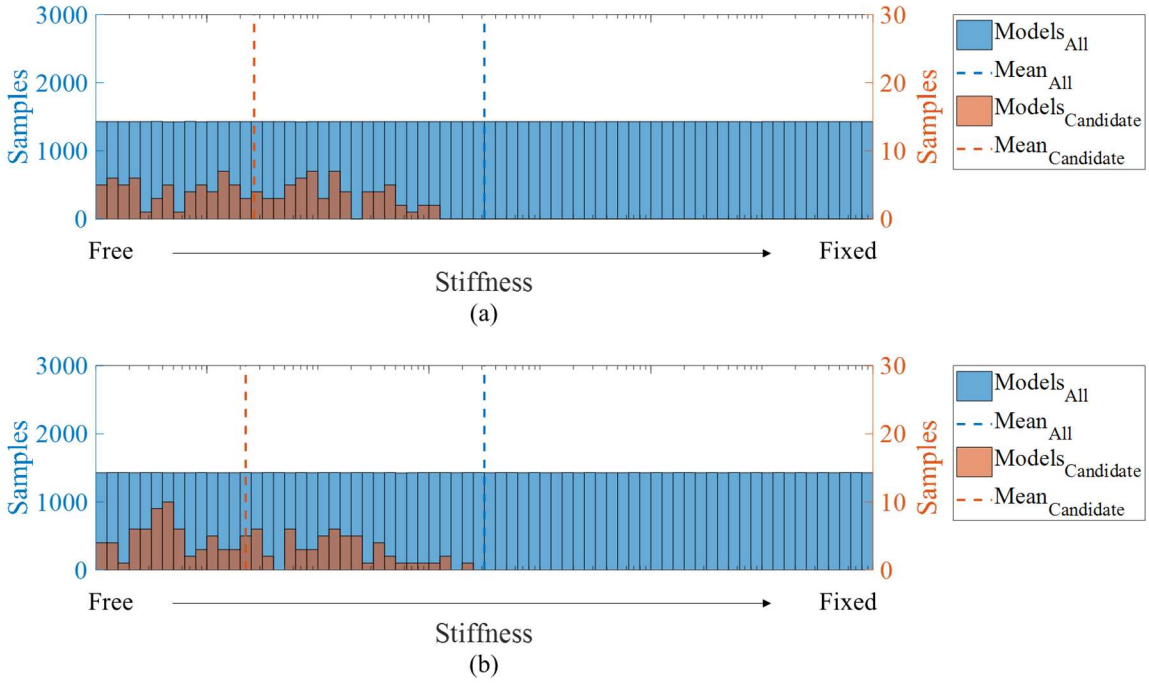

Figure 106: Refined Model Parameters of Pier 5: a) Deck and b) Bearing

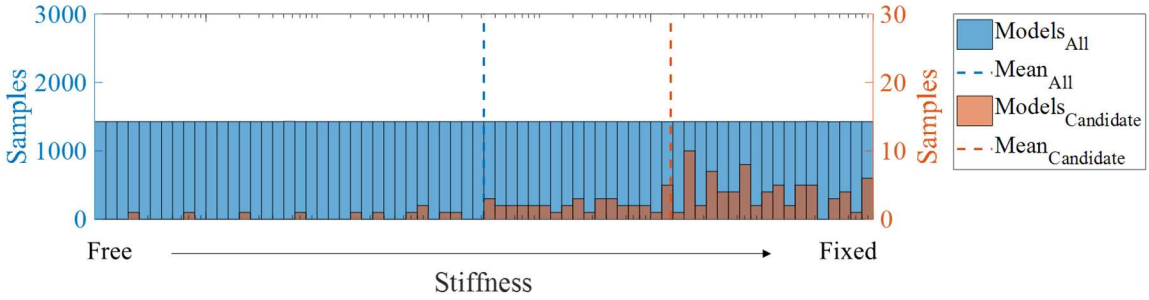

Figure 107: Refined Model Parameter of Pier 6

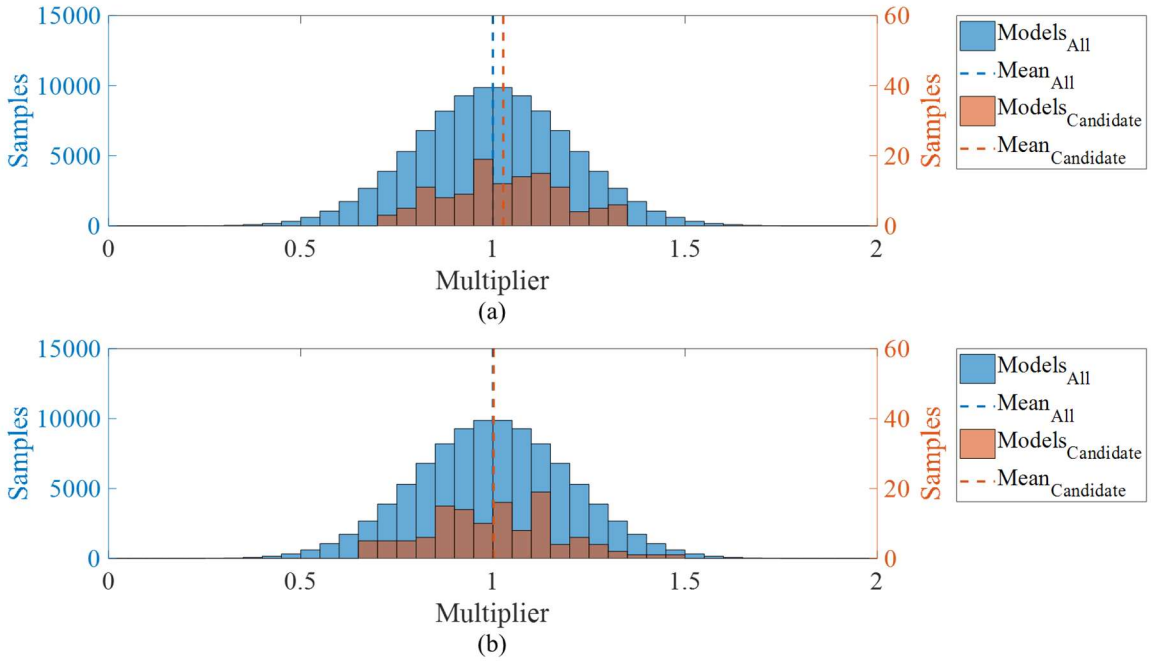

Figure 108: Refined Model Parameters of Modulus of Elasticity: a) Steel and b) Concrete

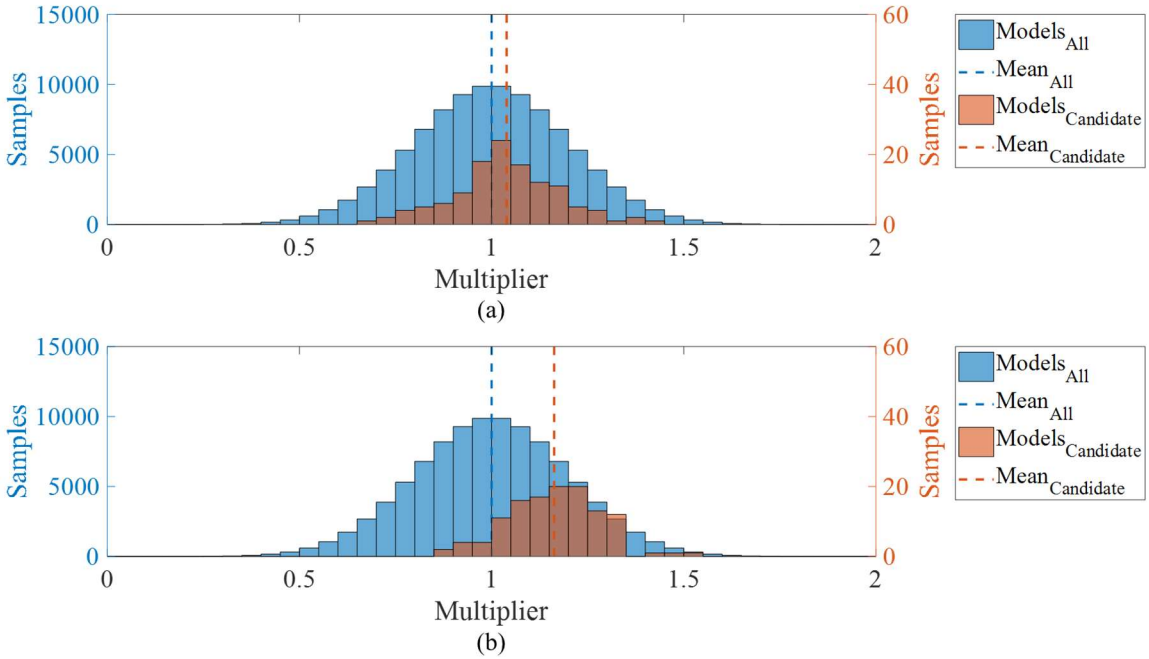

Figure 109: Refined Model Parameters of Coefficient of Thermal Expansion: a) Steel and b) Concrete

The parameter distributions are given numerically in Table 15 below. The model parameters pertaining to the pin and hanger did not experience a large reduction of uncertainty. The variance of the distributions reduced less than 1% from all of the models to the candidate models. However, the remaining boundary/continuity parameters experienced uncertainty reductions between 34% and 68%. The uncertainty of the material property parameters was also reduced between 16% and 39% as shown in Table 16.

Table 15: Boundary/Continuity Model Parameter Distributions

Parameter	Prior Distribution				Posterior Distribution				Uncert. Red.
	(kN/m)		10^x (kip/ft)		(kN/m)		10^x (kip/ft)		
	Mean	Var.	Mean	Var.	Mean	Var.	Mean	Var.	
P5D	4.61e7	1.53e4	6.50	2.02	3.89e5	103	4.43	0.85	58%
P5B	4.61e7	1.53e4	6.50	2.02	3.26e5	103	4.35	0.85	58%
P6B	4.61e7	1.53e4	6.50	2.02	2.21e9	310	8.18	1.33	34%
P7D	1.46e8	787	7.00	1.73	1.04e6	52	4.85	0.56	68%
P7B	1.46e8	787	7.00	1.73	9.25e6	77	5.80	0.72	58%
PHT	1.46e8	208	7.00	1.15	1.70e8	204	7.07	1.14	<1%
PHB	1.46e8	208	7.00	1.15	1.36e8	212	6.97	1.16	<1%

Table 16: Material Property Model Parameter Distributions

Parameter	Prior Distribution		Posterior Distribution		Uncertainty Reduction
	Mean	Var.	Mean	Var.	
ES	1.00	0.20	1.03	0.15	24%
EC	1.00	0.20	1.00	0.17	16%
CTES	1.00	0.20	1.04	0.14	31%
CTEC	1.00	0.20	1.16	0.12	39%

8.4.4 Additional Investigation: Identification and Validation of Unmeasured Predicted Responses

An additional investigation was performed to determine how well a measurement could be identified if it was not directly measured. For this investigation, four analyses were performed, each with one of the four gages excluded from the calibration. In each analysis, three displacement measurements were used for calibration of the structural models. The remaining measurement was then used to validate whether the evaluation method could predict the value of the excluded measurement. The results from each analysis are provided in Table 17– Table 20 below.

Table 17: Response Distributions with Pier 7 Deck excluded from Calibration

Gage	Measured	Prior Distribution		Posterior Distribution		Uncert. Red.	Mean % Diff.
		Mean	Var.	Mean	Var.		
Pier 5 Deck	52.8 mm (2.1 in.)	31.1 mm (1.2 in.)	29.4 mm (1.2 in.)	50.7 mm (2.0 in.)	3.5 mm (0.1 in.)	88%	4%
Pier 5 Bearing	51.9 mm (2.0 in.)	21.2 mm (0.8 in.)	30.2 mm (1.2 in.)	52.1 mm (2.0 in.)	3.8 mm (0.1 in.)	87%	<1%
Pier 7 Deck	45.3 mm (1.8 in.)	21.8 mm (0.9 in.)	24.6 mm (1.0 in.)	31.2 mm (1.2 in.)	4.7 mm (0.2 in.)	81%	31%
Pier 7 Bearing	29.7 mm (1.2 in.)	16.1 mm (0.6 in.)	23.4 mm (0.9 in.)	29.0 mm (1.1 in.)	2.4 mm (0.1 in.)	90%	2%

Table 18: Response Distributions with Pier 7 Bearing excluded from Calibration

Gage	Measured	Prior Distribution		Posterior Distribution		Uncert. Red.	Mean % Diff.
		Mean	Var.	Mean	Var.		
Pier 5 Deck	52.8 mm (2.1 in.)	31.1 mm (1.2 in.)	29.4 mm (1.2 in.)	49.7 mm (2.0 in.)	2.6 mm (0.1 in.)	91%	6%
Pier 5 Bearing	51.9 mm (2.0 in.)	21.2 mm (0.8 in.)	30.2 mm (1.2 in.)	51.0 mm (2.0 in.)	3.1 mm (0.1 in.)	90%	2%
Pier 7 Deck	45.3 mm (1.8 in.)	21.8 mm (0.9 in.)	24.6 mm (1.0 in.)	43.3 mm (1.7 in.)	3.4 mm (0.1 in.)	86%	5%
Pier 7 Bearing	29.7 mm (1.2 in.)	16.1 mm (0.6 in.)	23.4 mm (0.9 in.)	41.0 mm (1.6 in.)	6.6 mm (0.3 in.)	72%	38%

Table 19: Response Distributions with Pier 5 Deck excluded from Calibration

Gage	Measured	Prior Distribution		Posterior Distribution		Uncert. Red.	Mean % Diff.
		Mean	Var.	Mean	Var.		
Pier 5 Deck	52.8 mm (2.1 in.)	31.1 mm (1.2 in.)	29.4 mm (1.2 in.)	49.7 mm (2.0 in.)	4.9 mm (0.2 in.)	83%	6%
Pier 5 Bearing	51.9 mm (2.0 in.)	21.2 mm (0.8 in.)	30.2 mm (1.2 in.)	51.7 mm (2.0 in.)	5.3 mm (0.1 in.)	82%	<1%
Pier 7 Deck	45.3 mm (1.8 in.)	21.8 mm (0.9 in.)	24.6 mm (1.0 in.)	40.2 mm (1.6 in.)	3.3 mm (0.1 in.)	86%	11%
Pier 7 Bearing	29.7 mm (1.2 in.)	16.1 mm (0.6 in.)	23.4 mm (0.9 in.)	33.7 mm (1.3 in.)	4.0 mm (0.2 in.)	83%	13%

Table 20: Response Distributions with Pier 5 Bearing excluded from Calibration

Gage	Measured	Prior Distribution		Posterior Distribution		Uncert. Red.	Mean % Diff.
		Mean	Var.	Mean	Var.		
Pier 5 Deck	52.8 mm (2.1 in.)	31.1 mm (1.2 in.)	29.4 mm (1.2 in.)	50.0 mm (2.0 in.)	4.6 mm (0.2 in.)	85%	5%
Pier 5 Bearing	51.9 mm (2.0 in.)	21.2 mm (0.8 in.)	30.2 mm (1.2 in.)	44.3 mm (1.7 in.)	18.1 mm (0.7 in.)	40%	14%
Pier 7 Deck	45.3 mm (1.8 in.)	21.8 mm (0.9 in.)	24.6 mm (1.0 in.)	40.4 mm (1.6 in.)	2.9 mm (0.1 in.)	88%	11%
Pier 7 Bearing	29.7 mm (1.2 in.)	16.1 mm (0.6 in.)	23.4 mm (0.9 in.)	32.3 mm (1.3 in.)	4.1 mm (0.2 in.)	82%	9%

With the exception of the Pier 5 Bearing scenario (40% uncertainty reduction), the evaluation method still significantly reduced the uncertainty of the missing measurement, ranging between 72% and 83%. Also, with the exception of the Pier 5 Deck scenario (6% mean percent difference), the missing measurement experiences the largest percent difference and smallest uncertainty reduction in comparison to the other gages within each scenario. This is somewhat expected as the missing measurement is not used for the calibration.

8.5 Conclusions

The thermal behavior of the Hurricane Bridge was shrouded with uncertainty after years of use and a massive rehabilitation. TD St-Id was performed to identify and reduce

uncertainty regarding the bridge conditions and the overall health of the structure. The thermal behavior as a result of daily thermal temperature changes was used to identify the boundary/continuity conditions and material properties of the structure. Through this study, several conclusions can be made regarding the data analysis of thermal behavior. This structure experienced seasonal temperature gradients due to direct solar radiation from the sun. Since the bridge was oriented nearly parallel with the sun path during certain times of the year, the bridge was subjected to transverse gradients seasonally. The bridge experienced vertical gradients throughout the entire monitoring period. The bridge experienced highly nonlinear strain behavior throughout the structure as the strains drifted throughout the monitoring period. This nonlinearity was postulated as the presence of local behavior rather than global behavior of the structure. Unfortunately, the nonlinearity of the strains could not be addressed within the evaluation method and the analysis was performed using displacement measurements alone. The structure exhibited daily bi-linear displacement behavior consisting of times when the bridge was at steady-state with the ambient air around it and when the bridge and air temperatures were not consistent (during and directly after sunrise and sunset). The long term behavior showed that the effects of direct sunlight did not significantly skew the results of the thermal behavior of the full dataset, thus the data from the entire monitoring period was used for analysis. Although not fully linear, the displacement data could accurately be represented by a smeared linear relationship with high correlation values.

The nonlinearity of the strain measurements illuminated a significant limitation of the TD St-Id evaluation method. However, the displacement measurements were able to be used for analysis as their behavior characterized linear, global responses. Through the

utilization of single and multiple modeling approaches of TD St-Id, the uncertainty of multiple bridge conditions was reduced. The SM St-Id analysis identified boundary/continuity conditions as well as material properties that produced simulated model responses similar to the measured responses. The percent differences of the calibration were as low as 1% and no greater than 14%. However, the SM St-Id produced relatively large modulus of elasticity values. After further investigation, many models were found to have a posterior probability close in value to that of the single calibrated model. Therefore, in this case, the MM St-Id was necessary to confidently identify the model parameters. The MM St-Id provided a more comprehensive understanding of the bridge conditions of the structure. The accuracy of calibration was similar to the SM approach with percent differences again ranging from 1% to 14%. The boundary conditions at Piers 5-7 displayed partial stiffness to an extent, and the uncertainty of each condition was reduced between 34% and 68%. The boundary conditions of the pin and hanger could not be identified or reduced as the uncertainty reduction of these conditions was less than 1%. The material properties also were identified. The steel properties were found to be in close proximity to their design values. The concrete properties deviated slightly as the coefficient of thermal expansion was found to be 1.16 times the design value. This behavior was postulated as the result of the reinforcement in the concrete contributing to this behavior. The MM approach was found to be a more accurate representation of the thermal behavior. The material properties of the SM approach seemed high compared to the MM approach. After deliberation using engineering judgement, this study concluded that the MM approach better characterized the thermal behavior of the bridge.

Overall, the TD St-Id evaluation method provided insight to the thermal behavior of the Hurricane Bridge and alleviated some of the uncertainty regarding its structural performance and health. The TD St-Id evaluation method proved to be a viable option for assessing a bridge structure using thermal behavior. This study added to the body of knowledge of thermal behavior of structures as well as increased confidence in using this method as a means of structural evaluation.

9. PHASE III: SYNTHESIS OF TEMPERATURE-DRIVEN BRIDGE STUDIES

Both bridge studies from Phases I and II are compiled into a synthesis of other temperature-driven studies (TS) in Phase III. In an attempt to provide the most realistic guidance possible, the TD studies analyzed for this research are restricted to bridges that are exposed to in-situ environmental conditions at the time of monitoring. Nineteen of these projects (identified in Table 21) are included in the synthesis and described below. These projects comprise a broad spectrum of approaches, parameters, and objectives utilized for TD evaluation. The purpose of the synthesis is to dissect each study and identify intellectual contributions/value provided by each thermal evaluation. For example, these contributions are in the form of measured parameters, type of bridge, data analysis method, and model calibration technique to name a few.

Table 21: Temperature-Driven Bridge Studies

TS#	Bridge Name	TS#	Bridge Name
1	Route 61 Bridge	11	Cleddau Bridge
2	Hurricane Bridge	12	Zhanjiang Bay Bridge
3	Tacony-Palmyra Bridge	13	Jiangyin Yangtze River Bridge
4	Streicker Bridge	14	Jiubao Bridge
5	Ricciolo Vedeggio Viaduct	15	Shanghai Yangtze River Bridge
6	Dashengguan Yangtze River Bridge	16	Tsing Ma Bridge
7	Hernando Desoto Bridge	17	Tamar Bridge
8	I-35W St. Anthony Falls Bridge	18	Humber Bridge
9	Commodore Barry Bridge	19	Sutong Bridge
10	Steel Multigirder Bridge		

9.1 Temperature-Driven Value

The most significant aspect of structural monitoring is that the data acquired can be transformed into valuable information. The following section identifies what each TD study contributes to the body of knowledge of thermal bridge evaluation and attempts to address the following questions:

1) Does the data from a TD test translate into valuable information?

2) If valuable, what type of information is contributed to the body of knowledge?

3) What successes or failures did the author experience throughout the project?

4) What guidance can be deduced from these successes/failures?

9.2 Investigation of Bridge Studies

9.2.1 TS#1: Route 61 Bridge

The TS of the Route 61 Bridge is published in Murphy and Yarnold (2018) and explained in detail in Section 7. The TD value of this study pertained to the determination of the thermal signature of a damaged structure using strain and displacement measurements. This study also provided information regarding integral abutment behavior. Adverse effects from direct sunlight were a concern and resulted in nonlinear behavior of some measurements, especially the strain measurements of the exterior girders. The nonlinearity was accounted for using a smeared linear relationship between the measurements and temperature and by utilizing night-only (from midnight to 4:00 a.m.) data. By using both single and multiple model evaluation processes, the identification and uncertainty of the boundary conditions were determined. This study provided an explanation as well as a recommendation for rehabilitation to mitigate further damage to the structure. While relative displacements did provide some valuable information regarding the thermal movement of the bridge and abutments, the project could have benefitted from absolute displacement measurements like those available with global positioning systems (GPS). The relative displacement measurements could not distinguish between the movement of the bridge and the movement of the abutment due to expanding approaches. However, absolute displacement measurements could have provided the ability to decouple the bridge and abutment movement in order to have a more comprehensive understanding of the thermal behavior.

9.2.2 TS#2: Hurricane Bridge

The TS of the Hurricane Bridge is published in Murphy and Yarnold (2017, 2019-pending). This bridge study is also explained in detail in Section 8. The TD value of this study pertained to the determination of a thermal signature of a complex structure with many moving mechanisms. This structure is also provided insight regarding the thermal behavior of a structure that has undergone a massive rehabilitation. This study investigated the thermal behavior of the bridge using strain and displacement measurements. The strain measurements proved extremely difficult to analyze as they appear to drift throughout the monitoring period and are severely nonlinear. The strain measurements likely did not represent global behavior but local behavior at various locations along the bridge. Originally designed to characterize global behavior, the robustness of the monitoring system could not adequately address the local behavior of the strains, rendering them useless for calibration purposes. Instead, only the displacement measurements were used for the thermal evaluation of the bridge. The displacements behaved in a bi-linear relationship with temperature. Direct sunlight was not a significant issue for this project as the sun path was generally parallel to the bridge and most gages were shielded by the deck; therefore, the displacements of the entire monitoring period were used for the thermal analysis. Through single and multiple model analyses, the identification and uncertainty of boundary/continuity conditions as well as material properties were determined. A potential improvement of this study would have been the addition of measurements pertaining to the deck behavior. Deck behavior would have been beneficial to see the influence the deck has compared to the overall bridge thermal behavior especially regarding thermal gradients present on the bridge.

9.2.3 TS#3: Tacony-Palmyra Bridge

Figure 110: Tacony-Palmyra Bridge (Reprinted from Yarnold et al. 2012b)

The TS of the Tacony-Palmyra Bridge (Figure 110) is published in Yarnold et al. (2012a; b) and Yarnold and Moon (2015). This study utilized strains and displacement measurements to define the thermal behavior of the bridge. The monitoring system was able to adequately capture intrinsic forces throughout the load path of the structure. Significant forces were present as a result of temperature load response of movement mechanisms. The behavior between the thermal strains and displacements was found to have a bi-linear relationship. This study also identified linear and stick-slip nonlinear behavior. This study

used an objective function for model calibration in order to identify boundary/continuity conditions. Furthermore, the thermal evaluation was used as a preventative measure to assess bearing performance, expansion joint performance, deck or substructure cracking, member/connection overstress and linearity of the structure. This TD study was used in conjunction with vibration tests to provide a more comprehensive understanding of the structural behavior.

9.2.4 TS#4: Streicker Bridge

Figure 111: Streicker Bridge (Courtesy of Google Maps)

The TS of the Streicker Bridge (Figure 111) is published in Abdel-Jaber and Glisic (2016), Reilly et al. (2016, 2017), and Sigurdardottir and Glisic (2013). This TD study was the only strictly pedestrian traffic bridge study within the synthesis. The bridge is a deck-stiffened arch constructed primarily of concrete. The monitoring system was implemented during construction and utilized strain and displacement measurements. The importance of redundancy within a monitoring system was highlighted as some measurements provided

nonsensical results or were damaged during installation. Appropriate selection of gages was also addressed as two types of gages were compared. The comparison of gages determined that long-gauge FBG sensors outperformed distributed sensors in this case. The study also thoroughly investigated thermal gradients of the structure. Thermal gradients were found to be more prevalent during certain times of the year (summer and spring). In order to mitigate adverse effects from the gradients, periods of minimal thermal gradient (when the temperature distributions are uniform and at steady-state) were identified and used for evaluation of the structure. Since the structure was primarily concrete, night-only data could not be used for analysis as the structure was still dissipating heat during that time. Sectioning the data into small time periods allowed for better determination of thermal relationships. The measured data indicated slightly nonlinear behavior that could be defined using a smeared linear relationship. The monitoring system was robust and detected early-age cracking of the concrete deck from thermal gradients and shrinkage. Creep and shrinkage effects significantly altered thermal evaluations because they introduce mechanical strain. This study showed that creep and shrinkage affect the determination of material properties such as the coefficient of thermal expansion. The study found that the CTE of a concrete structure can be difficult to assess as it is constantly changing, especially in early stages of its lifetime. The CTE determination of the reinforced concrete of the bridge did not coincide with the CTE value of just concrete. The steel reinforcement contributed to the behavior of the concrete deck and caused the CTE to be for the structure rather than the material. The study also concluded that thermal effects from substructure needed to be accounted for as they too expanded/contracted and introduced loads on the bridge.

9.2.5 TS#5: Ricciolo Vedeggio Viaduct

Figure 112: Ricciolo Vedeggio Viaduct (Reprinted from Glisic et al. 2008)

The TS of the Ricciolo Vedeggio Viaduct (Figure 112) is published in Glisic et al. (2008) and Inaudi (2009). The TS of this bridge included a monitoring system that was installed during construction of the bridge. This study proved that the structural behavior was different during construction than it was after the bridge is operational. Construction caused unusual structural behaviors that were identified by the relationship between the temperature and the displacement. A statistical evaluation of the structural behavior was performed using Moving Principal Component Analysis (MPCA). This study concluded that horizontal bending occurred due to thermal variations but only between -0.4 mm and +0.1 mm.

9.2.6 TS#6: Dashengguan Yangtze River Bridge

Figure 113: Dashengguan Yangtze River Bridge (Reprinted from Ding et al. 2015)

The TS of the Dashengguan Yangtze Bridge (Figure 113) is published in Ding et al. (2015, 2017) and Wang et al. (2015, 2016). This TD study was the only rail traffic bridge included within the synthesis. Thermal strains were used to assess the performance of the bridge. The strain response of the train live load was significantly greater than temperature effects and had to be filtered out to complete the thermal evaluation. Direct solar radiation was also identified and filtered from the data. Thermal strain behavior was difficult to comprehend from the data due to the indeterminance of the structure. This study postulated that structural members transferred loads to and from adjacent members of the bridge, leading to the measurement of local strain behavior rather than global. Strain influence lines of structural members under train loads were significantly influenced by temperature variations. The static strain and temperature relationship were smeared as linear with a great correlation of 0.92 or more. High-order polynomials were needed to represent the

temperature-induced strain influence lines. Thermal behavior according to the influence lines changed with respect to the traffic loading. However, temperature loads had little effect on the dynamic load factors.

9.2.7 TS#7: Hernando Desoto Bridge

Figure 114: Hernando Desoto Bridge (Courtesy of Google Maps)

The TS of the Hernando Desoto Bridge (Figure 114) is published in Alexander (2017) and Yarnold et al. (2017). This study utilized the thermal behavior of the structure to analyze the bearing mechanisms of the bridge. The bridge displacement measurements in response to thermal loads clearly show a daily bi-linear relationship. Evening-only data was used to characterize the thermal behavior over the long-term while mitigating data from thermal gradients. The long-term displacement-temperature data could be defined by a smeared linear relationship. This study also investigated whether the structure exhibited symmetric thermal behavior. The data concluded that the bridge behavior was not symmetric. Thermal expansion of one of the two spans was accommodated by movement

of the bearings, whereas the expansion of the other span was accommodated by flexure/rotation of the pier.

9.2.8 TS#8: I-35W St. Anthony Falls Bridge

Figure 115: I-35W St. Anthony Falls Bridge (Courtesy of Google Maps)

The TS of the I-35W St. Anthony Falls Bridge (Figure 115) is published in Hedegaard et al. (2012, 2013, 2017a; b) and Inaudi (2009). The monitoring system of this study was implemented during construction. This study investigated thermal gradients along the bridge and illuminated the need for robust monitoring systems in order to analyze the behavior of thermal gradient effects. Generally, nonlinear thermal gradients existed through the depth of the webs, but thermal gradients through the width of the webs were considered negligible. This study also proved that thermal gradients not only experience seasonal trends but daily as well. Maximum positive gradients occurred in the afternoon between 2:00 p.m. and 4:00 p.m., while maximum negative gradients occur between 5:00 a.m. and 8:00 a.m.

Seasonally, gradient effects of the bridge surpassed AASHTO LRFD magnitudes in the summers.

9.2.9 TS#9: Commodore Barry Bridge

Figure 116: Commodore Barry Bridge (Courtesy of Google Maps)

The TS of the Commodore Barry Bridge (Figure 116) is published in Catbas and Aktan (2002). This study showed the importance of having a robust enough monitoring system and sufficient monitoring period to capture behavioral anomalies of the bridge. Thermal strains mimicked the pattern of temperature changes. Long-term measurements of a significant number of structural members were required in order to use TD analysis for the purpose of identifying damage or deterioration. In this study, the order of magnitude of the thermal effects surpassed the magnitude of the live load effects. Thermal pulses or shocks in which the temperature changed drastically in a short period of time (several hours) changed the movement and intrinsic strains in sections of the bridge. This study proved that thermal responses of a bridge vary over the long-term life of the structure and may not be symmetric.

9.2.10 TS#10: Steel Multi-girder (Unnamed) Bridge

The TS of the unnamed steel multi-girder bridge is published in Warren and Dubbs (2017). Tilt, strain, and displacement measurements were used to characterize the thermal behavior of the bridge. Tilt meters were used to measure the movement of the top of the piers but exhibited an insufficient signal-to-noise ratio which excluded them from use in the analysis. The bridge displayed nonlinear temperature-strain behavior indicating the influence of other factors such as local behavior. The thermal displacements experienced a smeared linear relationship with temperature change. The three-dimensional relationship between strain, displacement, and temperature was planar, indicating that the local strains were temperature-induced. Boundary conditions of movement mechanisms (bearings) were determined for the structure. Local and global thermal behavior was beneficial for comprehending and assessing the performance of the bridge. Absolute displacement measurements would have been beneficial for this project. The relative displacement measurements between the bridge and the substructure could not distinguish which component was moving. Decoupling this behavior could provide a more comprehensive understanding of the thermal behavior of the structure.

9.2.11 TS#11: Cleddau Bridge

Figure 117: Cleddau Bridge (Reprinted from Kromanis and Kripakaran 2014)

The TS of the Cleddau Bridge (Figure 117) is published in Kromanis et al. (2016) and Kromanis and Kripakaran (2014). This study utilized displacements to define the thermal behavior. Thermal displacements closely mimicked temperature patterns and showed seasonal trends. Generally, temperature loads produced a higher response at expansion joints than vehicle loads with the exception of a heavy vehicle. This study identified boundary conditions associated with the roller bearings and determined the why the bearings experienced deterioration. The high sample frequency of the monitoring system showed that bearing behavior was not smooth but incremental as friction greatly affected the movement. An investigation of the force required to release a locked bearing was also conducted. This study also thoroughly investigated thermal gradients. The thermal

gradients experienced on this bridge were significantly different than the thermal gradients specified in design standards. Temperature gradients were present not only longitudinally along the bridge but transversely and vertically throughout the depth as well. In an attempt to address the thermal gradients, temperature time histories were used as input to each of the nodes of the structural model. The study determined that thermal effects were causing plan bending of the bridge, affecting the roller bearings' ability to function properly.

9.2.12 TS#12: Zhanjiang Bay Bridge

Figure 118: Zhanjiang Bay Bridge (Courtesy of Google Maps)

The TS of the Zhanjiang Bay Bridge (Figure 118) is published in Cao et al. (2011). This study primarily analyzed the thermal gradients of the bridge. Gradient effects were found to be larger than design specifications. Large bridge components like the towers were affected by thermal effects as well, not just the components such as the deck. This study discovered that parts of the structure preserved heat causing the structure to have a different temperature than the ambient air around it. The time at which the structure was closest to

ambient temperature occurred between midnight and early morning hours. Temperature lag between the concrete and steel components of the structure was determined as 5-6 hours. No temperature lag was found between stay cables and the concrete towers. This study analyzed the displacement of the towers in the direction of the bridge as well as the vertical displacement of the girders. Finally, a finite element model was developed to accurately depict the bridge's thermal behavior.

9.2.13 TS#13: Jiangyin Yangtze River Bridge

Figure 119: Jiangyin Yangtze River Bridge (Courtesy of Google Maps)

The TS of the Jiangyin Yangtze River Bridge (Figure 119) is published in Xia et al. (2017). This study identified damage using measured temperature and temperature-induced strain data. This study used ensemble empirical mode decomposition (EEMD) to separate vehicle strains from temperature-induced strains and then detected stiffness reduction in single or multiple locations. Also, the TD study used thermal behavior to assess the health of the bridge before and after a ship collision. Damage from the collision was identified and

analyzed. However, other damage such as corrosion could not be detected with the method described in this study.

9.2.14 TS#14: Jiubao Bridge

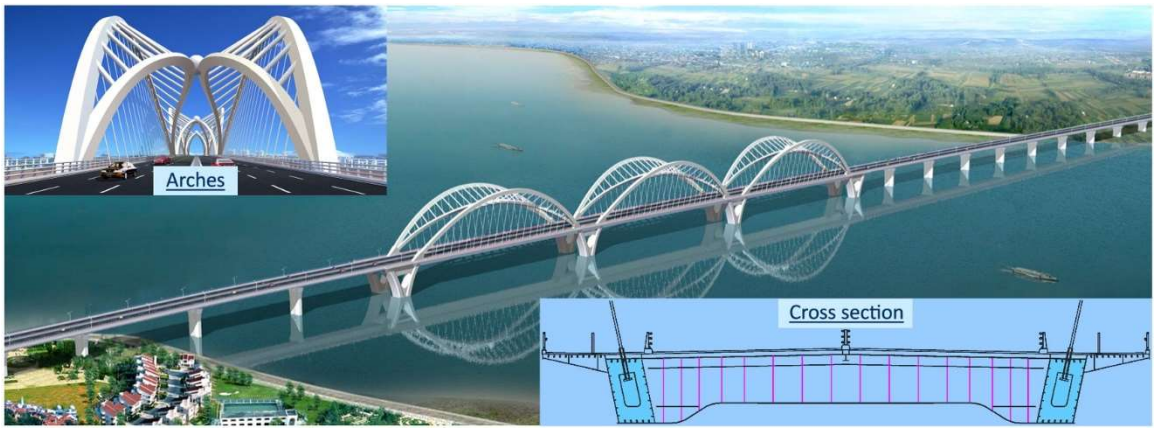

Figure 120: Jiubao Bridge (Reprinted from Zhou et al. 2017)

The TS of the Jiubao Bridge (Figure 120) is published in Zhou et al. (2018, 2017). The monitoring system on the bridge was installed during construction. This thermal study was not extensive however still provided valuable information regarding thermal behavior. The temperature measurements discussed in this study were affected by direct solar radiation during the day and had to be addressed appropriately. The displacement data measured in this study was nonlinear but could be represented by a smeared linear relationship.

9.2.15 TS#15: Shanghai Yangtze River Bridge

The TS of the Shanghai Yangtze River Bridge is published in Zhou and Sun (2018). This study investigated the temperature field of the bridge and discovered that thermal gradients existed vertically but not longitudinally or transversely. Rather than long-term

monitoring over the course of a year, thermal responses were only analyzed for two months (the hottest and the coldest of the year). These periods served as an envelope of the thermal behavior. The longitudinal displacement of the bridge exhibited consistent linear behavior with respect to temperature in each of the two months. Vertical deflection at the center of the bridge did not represent a linear relationship at all times of the year. Winter months did not produce a large correlation between the vertical deflection and the girder temperature. Longitudinal displacement was a simple linear relationship because it dealt with one bridge component, the composite deck and girder system. The vertical displacement depended on more than just one component as both the expansion of the cable and the deck and girder system contributed to the thermal displacement. These two behaviors could not be separately distinguished in this study. Finally, this study identified which temperature variables affected the thermal behavior of the structure.

9.2.16 TS#16: Tsing Ma Bridge

Figure 121: Tsing Ma Bridge (Courtesy of Google Maps)

The TS of the Tsing Ma Bridge (Figure 121) is published in Tong et al. (2002). Thermal gradients were analyzed as part of this study. Transverse gradients were found to

be negligible but vertical gradients were significant enough to warrant consideration in the thermal analysis. Extreme temperature distributions required long-term monitoring. This study concluded that the temperature distribution of steel bridges is most influenced by ambient air within shaded areas and direct sunlight. Also, closed steel sections were subjected to more temperature gradient effects than open steel sections.

9.2.17 TS#17: Tamar Bridge

Figure 122: Tamar Bridge (Reprinted from Jesus et al. 2018)

The TS of the Tamar Bridge (Figure 122) is published in Brown (2007), Brownjohn et al. (2015), Jesus et al. (2018), Koo et al. (2010), and Westgate et al. (2015). The effects of solar radiation were thoroughly investigated on this bridge. An estimation of cloud coverage was conducted to determine the solar radiation applied to the structure. Absorption

and convection of the bridge components proved to be the most influential parameters defining the thermal behavior of the bridge. Expansion of the deck, truss, and cable exhibited a linear relationship with temperature but varied when the solar intensity was increased. One tower experienced nonlinear behavior while the other experienced mostly linear behavior. Also, the thermal behavior of the tower was proven as seasonal. Average vehicle loading affected the thermal data and had to be addressed appropriately. This study utilized Markov Chain Monte Carlo (MCMC) simulations and Bayes Theorem calibration for the thermal analysis. Additionally, multiple parameters were identified in this study using Metropolis-Hastings (MH) and Monte Carlo (MC) techniques. Finally, a finite element model was developed as a baseline.

9.2.18 TS#18: Humber Bridge

Figure 123: Humber Bridge (Courtesy of Google Maps)

The TS of the Humber Bridge (Figure 123) is published in Brownjohn et al. (2015). This study utilized thermal displacement data to analyze bearing behavior. Temperature was confirmed to be the biggest factor of deformations of long-span bridges. Vertical movement and expansion of the main span were investigated. The thermal responses followed daily temperature trends and were linear. In this study, wind effects were substantial and surpassed the magnitude of vehicle effects; however, temperature was still the primary load on this long-span bridge. Responses from temperature were the slowest of all the loading scenarios. The monitoring system was found to be most beneficial for determining potential rehabilitation of the deck surface or the bearings.

9.2.19 TS#19: Sutong Bridge

The TS of the Sutong Bridge is published in Guo et al. (2015). This study was not extensive but did provide some valuable information regarding thermal behavior. The thermal response time history closely resembled the temperature time history. The temperature and thermal displacement relationship was found to be nonlinear due to a time lag, but the relationship could be represented by a smeared linear relationship. This study also concluded that the thermal response data was better represented using a 1-hr time lag which produced a linear relationship. Using this time lag, the finite element model of the bridge was able to simulate the measured responses with good correlation.

10. PHASE IV: TEMPERATURE-DRIVEN FRAMEWORK AND GUIDANCE

Once a study has been proven to contribute valuable information about TD evaluations, each research study is analyzed according to its structure details, monitoring criteria, and data/analysis information. The purpose of analyzing these logistics is to understand the specific methods of how each research study within the synthesis arrived at its conclusions. These contributions are combined and organized to provide insight to the overall scope of how and why TD evaluations are being conducted. An example of the TD framework using only parameters from the Route 61 Project (TS #1) and the Hurricane Bridge Project (TS #2) is shown in Figure 124. This framework matured with the addition of parameters from the remaining TD studies of the synthesis and is discussed throughout this section. Through investigation of each of these studies, guidance regarding thermal evaluations was gathered and compiled as the topics shown in Table 22. Each topic is discussed further below.

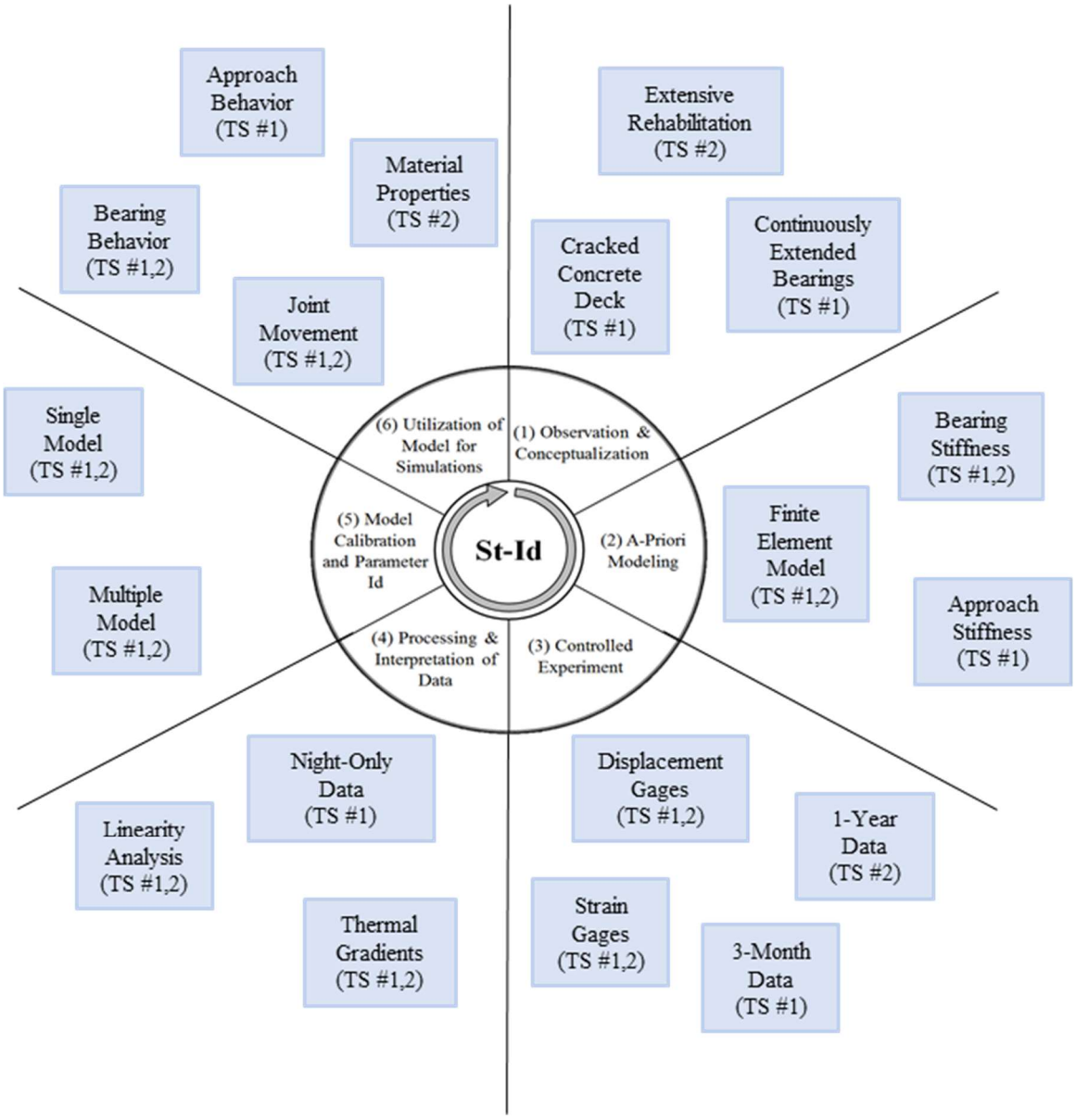

Figure 124: Example of TD Framework using Parameters from only TS #1 and TS#2

Table 22: Guidance for TD Evaluations

Area of Interest	Guidance Topics
Structure Details	• Motivation • Construction implementation/monitoring • Sensitivity to various loads • Bridge/traffic type dependence • Identification/uncertainty of boundary and continuity conditions • Bearing movement • Bridge component effects • Thermal gradients • Bi-linear thermal relationship • Identification/uncertainty of material properties
Monitoring Criteria	• Robustness of monitoring system • Redundancy of monitoring system • Versatility of monitoring system • Local/global thermal behavior • Gage selection
Data and Analysis	• Linearity of thermal response • Model calibration • Sampling technique • Parameter selection • Seasonal trends in thermal behavior • Time lag of thermal response • Finite element model • Solar radiation effects • Thermal pulses/shocks

10.1 Structure Details

- Motivation: Most TD studies are generally separated by two classifications for motivation: older and damaged or new and preventative. Many bridges that have undergone a thermal evaluation have been for the purpose of identifying the sources of damage on the structure. Recently, monitoring systems have also been installed on new bridges during construction and have conducted thermal evaluations as a preventative measure to identify changes in behavior before damage occurs.

Generally, these studies have been conducted on large, complex structures with robust monitoring systems. Preventative thermal studies are becoming more prevalent and should contribute substantial knowledge regarding the thermal behavior of bridges in the years to come. Also, monitoring structures throughout construction has proven beneficial. Bridges can experience highly vulnerabilities during construction as the structural behavior during this time is often different than the structural behavior after the bridge is operational.

10.1.1 Bridge Geometry

- Sensitivity to various loads: Loading other than temperature such as wind and vehicle loads should be carefully considered and accounted for appropriately. Multiple bridge studies in the synthesis show that the temperature loads produce responses of similar or greater magnitude to live loads, especially with large structures. Generally, these loads are identified and filtered out of the data prior to conducting the thermal analysis. To achieve this, techniques such as EEMD have been used to distinguish behavior from vehicle traffic and temperature effects so that only thermal behavior is used for analysis.
- Bridge/traffic type dependence: TD studies are not strictly limited to a certain types of bridge or traffic. Performance evaluation through thermal testing has seen success with various types of bridges and live loads. Longer bridges have shown a greater thermal response than shorter bridges, making the distinction between thermal effects and effects from other loads more defined. Thermal evaluations of smaller structures are also possible; however, distinguishing the thermal behavior from other loads may be more difficult.

- Identification/uncertainty of boundary/continuity conditions: TD studies have shown significant success in identifying boundary and continuity conditions of bridges. These conditions provide information regarding bearing performance, expansion joint performance, composite nature between deck and girder/truss systems, out-of-plane bending, and identification/extent of damage in some instances.
- Bearing movement: Bearing movement is highly influenced by friction and rarely occurs in a smooth manner. Studies with high sample rates have shown this behavior is due to incremental stick-slip behavior. If global bridge behavior is desired, a low sampling rate may be sufficient for thermal monitoring and analysis purposes. However, if the focus of the study pertains more to the behavior of the bearing itself rather than the bridge behavior at the bearing, a more thorough understanding of the bearing behavior may be achieved using a high sampling rate.
- Bridge component effects: Bridges with large structural components like the towers of a suspension bridge or cable-stayed bridge or tall piers of a substructure may be subjected to temperature effects as well. Also, bridge cables have the potential of being affected by temperature changes. Thermal influences from these components must be accounted for when analyzing the behavior of the bridge as a whole. The thermal behavior of each component should be decoupled if possible.
- Thermal gradients: Many studies investigate thermal gradients within a bridge. These gradients have been shown to exist longitudinally along the length of the bridge, transversely along the width, and vertically along the depth. Solar radiation and shade are major contributors to thermal gradients. Also, thermal gradients are often present due to the use of steel and concrete as the construction materials of a

bridge. The difference in material properties generally allows steel to heat/cool at a faster rate than concrete producing differential temperatures throughout the structure and thus temperature gradients. As shown in several TD studies, thermal gradients also have the potential to be more than what is specified in design standards.

10.1.2 Bridge Composition

- Bi-Linear Thermal Relationship: Several of the studies confirm a bi-linear relationship between temperature and bridge responses. Each linear behavior can be attributed to periods of time when the structure is at steady-state conditions with the surrounding ambient air and when the structure is not the same temperature as the ambient air. The latter generally occurs when the bridge experiences an appreciable temperature change in a relatively short period of time such as during a sunrise or a sunset. The bi-linear behavior is especially noticeable with structures that contain concrete. Concrete does not disperse heat quickly and thus requires longer periods of time to reach ambient temperature.
- Identification/uncertainty of material properties: TD studies can reduce uncertainty of material properties. Thermal properties of concrete change over time due to curing and creep/shrinkage. Therefore, long-monitoring is necessary if concrete properties are the primary focus of the TD investigation. The thermal properties of a concrete structure are likely not consistent with the thermal properties of pure concrete and must be adjusted accordingly. The steel reinforcement likely affects thermal properties of the structure such as the coefficient of thermal expansion.

10.2 Monitoring Criteria

- Robustness of monitoring system: A robust monitoring system with a significant number of sensors is necessary to accurately establish a temperature field of a bridge. This can be investigated by a single cross-section or by the bridge as a whole. Also, if local behavior is desired, a robust monitoring system may be required to accurately characterize the thermal behavior of the bridge.
- Redundancy of monitoring system: Monitoring systems for thermal evaluations are generally operational for long periods of time. As such, gages can be damaged or otherwise ineffective over time. Redundancy allows for the continued use of the monitoring system even if some gages are lost throughout the monitoring period. Also, redundancy can help identify axial and/or bending behavior.
- Versatility of monitoring system: TD studies can potentially be integrated to/from vibration or static testing studies. Some studies have conducted short-term dynamic tests and then continued monitoring for long periods of time in order to identify the thermal behavior of the bridge.
- Local/global behavior: When designing the monitoring system, consideration of local and global behavior must be given. Local behavior may not be adequately characterized by a system designed for global behavior and often requires a robust monitoring system. Displacement has shown to be an excellent measurement of global behavior, but strains have proven more subject to local behavior.
- Gage Selection: Many types of gages exist to measure thermal responses such as displacement, strain, and tilt. Sensing technology is also important as vibrating-wire or fiber optic technology may be beneficial in certain circumstances over others (Zuk

1965). Some studies utilize GPS or LPS displacement gages when absolute displacement is desired over relative displacement. Although absolute displacement is generally used for long-span bridges, short- and medium-span bridges can also benefit from these measurements. Absolute displacements have the potential to decouple thermal behavior of the superstructure and substructure of a bridge providing a more comprehensive understanding of the bridge behavior.

10.3 Data and Analysis

- Linearity: Nonlinear behavior is common among bridges experiencing damage and has proven difficult to analyze. If possible, nonlinear behavior is represented by a smeared linear relationship that represents the thermal data at uniform, steady-state conditions. The nonlinear behavior can also be represented by a polynomial relationship. Nonlinear behavior of bridge conditions such as bearing stiffness, for example, can be modeled if adequate information regarding the behavior is available and can be characterized accurately. Nonlinear data can be sectioned into smaller time periods to analyze the behavior. Three-dimensional relationships between strain, displacement, and temperature have been used to understand strain nonlinearity. Most of the early-life bridges do not have this problem as they generally act linearly as designed. Some evaluation methods such as the TD St-Id method presented in Section 5 are ineffective at analyzing nonlinear behavior.
- Model calibration: Strains and displacements are rarely both used to calibrate a model. Often strains exhibit too much local behavior for analysis of global behavior of the bridge. Objective functions and maximum likelihood estimation within Bayes Theorem are valid methods for calibrating a model with measured results.

- Sampling technique: Markov Chain Monte Carlo (MCMC) is highly beneficial selection parameter combinations of structural models. This is a self-informed technique that helps minimize the number of models necessary for a structural analysis. Other sampling techniques such as the generic Monte Carlo (MC), Metropolis-Hastings (MH) or deterministic approaches can also be used for developing the sample spaces for thermal analyses.
- Parameter selection: The complexity of the thermal analysis may be minimized by carefully considering parameters and making assumptions where valid. Sensitivity studies are beneficial for determining which parameters should be utilized for various conditions under thermal loading. Also, sensitivity studies can provide insight to the adequate range of values for the parameters. Proper selection of parameters can reduce time and greatly increase efficiency of the analysis within evaluation methods.
- Seasonal trends: Temperature effects have been found to trend seasonally. Seasonal drifts of measurements may be present making assumptions and predictions for future years difficult. Long-term monitoring provides the most complete characterization of thermal behavior. However, if long-term monitoring is available, several thermal evaluation studies use the hottest and coldest months within a year to establish an envelope of the thermal behavior of a bridge.
- Time lag: Thermal responses mimic the pattern of temperature change but have been shown to have a time lag compared to the temperature. For several TD studies, this time lag was approximately one hour. However, the exact time lag varies on a bridge by bridge basis. Bridge structures containing concrete generally experience a greater

time lag than steel structures. Concrete absorbs/dissipates heat slower than steel, and thus reacts to the thermal load at a slower pace as well.

- Finite element model: Finite element models are not required for all thermal evaluations. However, if a finite element model is used for analysis, the accuracy of the model is of utmost importance. Finite element software such as Strand7, ABAQUS, and ANSYS have all been used for thermal evaluations.
- Solar radiation effects: Investigation of the sun path proved beneficial for analyzing direct sunlight effects and out of plane bending. Solar radiation and its effects can be characterized and accounted for appropriately by estimating cloud coverage and analyzing extreme temperature measurements of gages. These effects can be more prevalent in particular months of the year such as during the spring or summer. Night-only data (roughly between the hours of midnight and 4:00 a.m.) can be used to mitigate adverse effects from direct solar radiation and represents the thermal behavior at steady-state.
- Thermal pulses/shocks: Large temperature changes within short periods of time can change the force distribution and movement of bridge. These may cause the bridge responses to act in an unsymmetrical manner.

Table 23: TS Framework: Project Details

Temperature Driven Study #	1	2	3	4	5	6	7	8	9	10	11	12	13	14	15	16	17	18	19
Bridge Age																			
<25 years				■	■	■		■				■	■	■	■	■			■
25-50 years	■						■		■	■	■							■	
50-75 years		■															■		
75-100 years			■																
Primary Traffic Load																			
Pedestrian				■															
Truck	■	■	■		■		■	■	■	■	■	■	■	■	■	■	■	■	■
Rail						■													
Bridge Type																			
Cable-Stayed															■				■
Arch			■	■		■	■							■					
Suspension																■	■	■	
Girder	■				■			■		■	■	■	■						
Truss		■							■										

Table 23 Continued

Temperature Driven Study #	1	2	3	4	5	6	7	8	9	10	11	12	13	14	15	16	17	18	19
Bridge Material																			
Steel	■	■	■	■		■	■		■	■	■	■	■	■		■	■	■	■
Concrete					■			■				■			■				
Total Bridge Length																			
<50 meters																			
50-200 meters	■			■	■														
200-500 meters						■		■											
500-1000 meters		■								■	■						■		
>1000 meters			■				■		■			■	■	■	■	■		■	■
Monitored Thermal Length																			
Short <30 meters										■									
Medium 30-100 meters	■			■	■														
Long >100 meters		■	■			■	■	■	■		■	■	■	■	■	■	■	■	■
Monitoring Duration																			
< 3 Months	■											■		■					
3 Months – 1 Year				■		■	■			■									
> 1 Year		■	■		■			■	■		■		■		■	■	■	■	■

Table 23 Continued

Temperature Driven Study #	1	2	3	4	5	6	7	8	9	10	11	12	13	14	15	16	17	18	19
Monitoring System Install																			
During Construction				■	■			■				■		■	■	■			■
After Construction	■	■	■			■	■		■	■	■		■				■	■	
Sensing Technology																			
Vibrating-Wire	■	■	■				■	■		■									
Fiber Optic (FBG)				■	■	■		■					■	■	■				■
Electrical Resistance			■					■						■			■		
Draw Wire											■								■
Electromagnetic (Cable)												■							
GPS or LPS															■			■	■
Electronic Distance Measuring																	■		
Laser							■											■	
Thermal Response Measured																			
Strain (Surface)	■	■	■			■		■	■	■		■	■	■			■		■
Strain (Embedded)				■	■			■						■					
Displacement	■	■	■				■	■		■	■	■		■	■		■		■
Rotation/Tilt			■		■		■			■								■	■

Table 23 Continued

Temperature Driven Study #	1	2	3	4	5	6	7	8	9	10	11	12	13	14	15	16	17	18	19
Analysis Method																			
Direct Data Analysis	■	■	■	■	■	■	■	■	■	■	■	■	■	■	■	■	■	■	■
Model Calibration	■	■	■					■			■			■	■		■		■
TD Value																			
Thermal Gradients	■			■				■			■	■		■	■	■	■		
Boundary/Continuity Conditions	■	■	■				■			■	■								
Material Properties		■		■								■							
Linearity	■	■	■	■		■	■	■		■				■	■		■	■	■
Damage Detection				■									■					■	
Intrinsic Forces			■								■								
Construction Behavior				■	■									■					
Influence Lines/Strain Behavior						■			■										
Non-thermal Loading									■		■		■				■	■	

The ability to evaluate a bridge is dependent on many factors primarily including the assessment metric used, the climate, the bridge itself, the monitoring system, and the duration of monitoring. Using the guide provided in Figure 125, consideration of these factors could highly benefit any individual using thermal behavior to conduct structural performance evaluations.

- Assessment metric: Is the assessment metric influenced by thermal behavior? The assessment metric is the structural behavior that is being used to evaluate the bridge such as condition of the bearings, structural mode shape, load rating, etc. Thermal evaluations are beneficial for assessing boundary/continuity conditions through investigation of movement mechanisms. However, TD evaluations have seen little success using assessment metrics such as mode shapes, load ratings, and distribution factors. If these are the assessment metrics available for a project, an alternative evaluation technique such static load or vibration testing may be more appropriate rather than temperature testing.
- Climate: Is there a sufficient magnitude of thermal load (temperature change) throughout the monitoring period to measure changes in thermal response? An absolute requirement of thermal evaluations is that the structure must experience an appreciable change in temperature to produce the thermal response. Therefore, thermal evaluations may not be ideal for locations where the ambient temperature remains fairly constant at all times.
- Bridge: Is the bridge itself sensitive enough to thermal stimulation? This primarily pertains to the size of the structure. If the thermal length of a structure is so small that the thermal response is the same order of magnitude as the resolution of the

sensors measuring the behavior, the thermal behavior may not be accurately characterized. Preliminary calculations can be conducted to estimate the thermal response of the structure before beginning an evaluation of the bridge.

- Monitoring System: Can only the thermal behavior of the bridge be identified? The monitoring system needs to have the capability of clearly distinguishing the thermal behavior of the bridge from the behaviors of other loads and/or local versus global behavior. Preliminary calculations of thermal load effects versus vehicle/wind load effects can be conducted to estimate magnitudes of each loading type prior to evaluation. Also, consideration of the load path of the structure may determine whether global behavior alone can be measured and/or identify the potential areas for local behavior.
- Monitoring Duration: Is the thermal behavior fully characterized within the monitoring period? Bridges have shown different behavior during times of steady-state temperature changes and during periods of thermal shock. Comprehension of the thermal behavior during both times can be beneficial. Long-term monitoring is ideal to encompass the seasonal variations of the structural behavior. However, if a long-term monitoring duration cannot be arranged, a short-term duration with the potential of encompassing both types of behavior should be targeted.

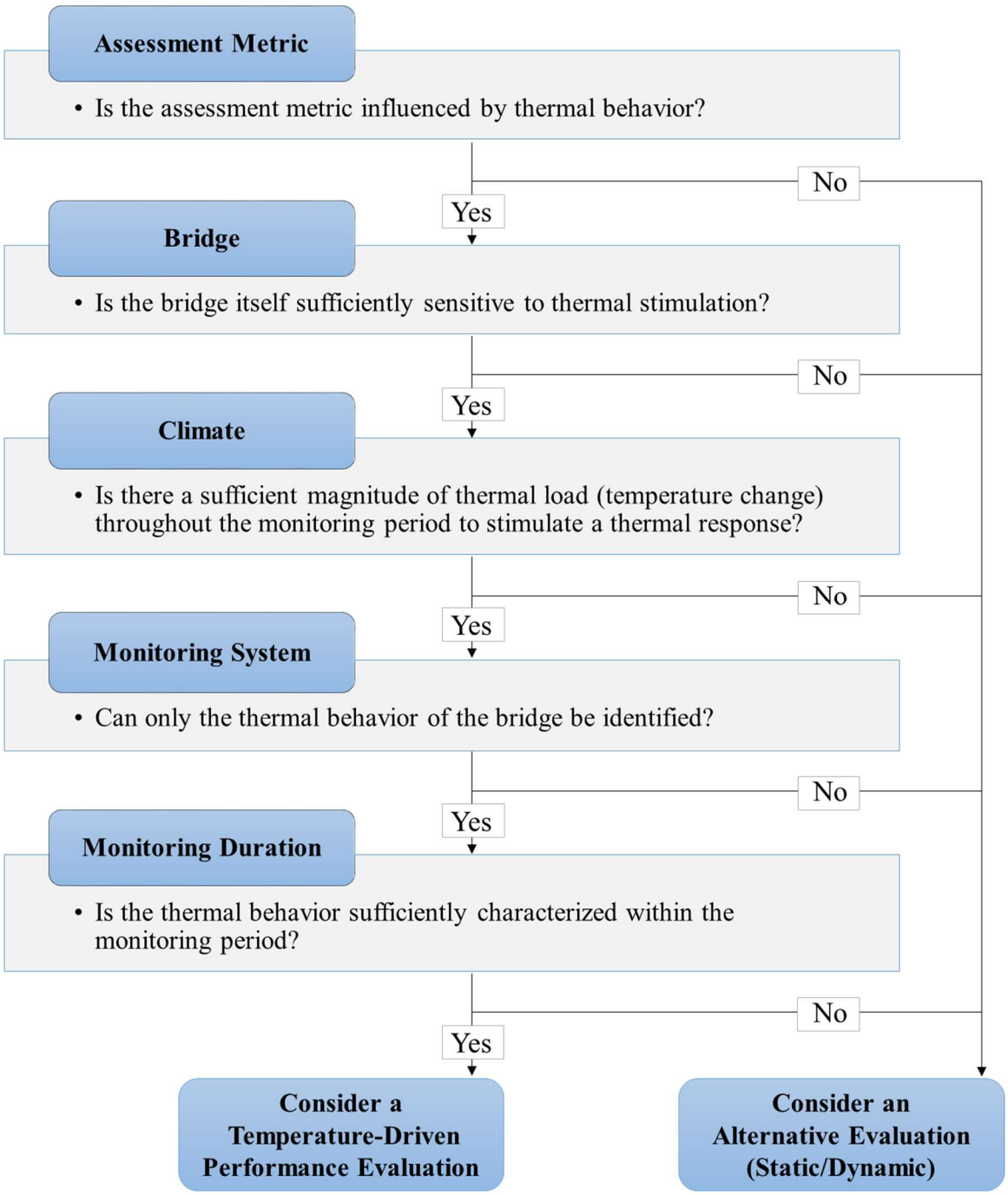

Figure 125: Temperature-Driven Performance Evaluation Guidance

11. CONCLUSIONS

Through the evaluation of two bridge structures, the temperature-driven structural identification (TD St-Id) method was proven as a valuable resource for bridge owners, engineers, and researchers to better assess bridge behavior. The TD St-Id method was able to successfully reduce uncertainty regarding bridge parameters such as boundary/continuity conditions as well as material properties. However, a limitation of this method was found to be its incapability of addressing nonlinear behavior of measured responses due to complex thermal gradients and unique bridge mechanisms. This is a significant limitation for certain structure in that it requires a high resolution of measurement locations to adequately characterize the system behavior.

Valuable insight to the overall thermal behavior of bridges was gained through both bridges included in this research. For a relatively simple structure such as the Route 61 Bridge, strain measurements along the girders and displacement measurements at the expansive end of the structure sufficiently defined the thermal behavior of the bridge and could be used for evaluation purposes. For a complex structure such as the Hurricane Bridge, the thermal behavior of strains and displacements characterized the thermal behavior of the structure; however, the nonlinearity of the strains was too complex to provide adequate characterization of the thermal behavior necessary to evaluate the structure with the given method. The bridge experienced localized structural behavior and produced nonlinear strains, which was a major limitation of the TD St-Id method. As a result, the characterization of the thermal behavior for evaluation purposes relied solely on displacement measurements. The global measurements from both bridges confirmed a bi-

linear relationship between the thermal response and the temperature. The primary linear relationship is due to steel and concrete reacting during near steady-state temperature conditions. Both studies postulated that the secondary linear relationship is due to the concrete's thermal conductivity. As concrete disperses heat slower than steel, the secondary linear relationship occurs during times of drastic temperature changes such as sunrise or sunset. Both studies provided valuable information regarding the effects of solar radiation and thermal gradients. The Route 61 Bridge experienced significant adverse effects from thermal gradients and thus had to be evaluated using night-only data. Investigation of the thermal gradients of the Hurricane Bridge showed that thermal gradients did not significantly alter the overall global thermal behavior, and thus the data from the entire monitoring period was used.

Experimental methods utilizing thermal behavior were further evaluated through a synthesis study. Nineteen studies were reviewed on various bridge structures and all provided intellectual value regarding thermal behavior and/or TD structural evaluations. The synthesis identified many ways of conducting TD evaluations. The project logistics and intellectual merit from each TD study were dissected and then reassembled into a framework in order to provide guidance for future TD evaluations. The TD guidance developed during this research pertained to structure details, monitoring criteria, and data and analysis procedures. Finally, this research provided advice regarding whether to conduct a TD evaluation by considering the assessment metric used for structural performance evaluation, the details of the bridge itself, the climate of the bridge's surrounding environment, the monitoring system's ability to distinguish the thermal behavior from other loads, and the monitoring duration required to sufficiently characterize the structure's thermal behavior.

12. RECOMMENDATIONS FOR FUTURE WORK

This research stands to benefit many individuals within the civil engineering profession. Structural engineers and bridge owners can use the guidelines to better develop TD monitoring systems based on project-specific parameters. Also, the synthesis allows for easy access to additional information regarding a variety of thermal evaluations. This research also stands to benefit researchers, both academic professionals and students alike. Future research endeavors can utilize the guidelines to further the knowledge of the thermal behavior of bridges and the execution of TD evaluations. The presented studies illuminate immediate opportunities for improvement and advancement. Some of these research opportunities are direct continuations of the presented research while others are more innovative ideas that involve conducting thermal evaluations with artificial intelligence. These potential areas of research are further detailed below.

12.1 Continuation of Presented TD Evaluation Method

12.1.1 Nonlinear behavior due to thermal gradients

One of the major limitations of the presented research is addressing nonlinear behavior due to the effects of thermal gradients. In an attempt to better represent thermal gradients within these evaluations, the next progressive step is to include many various thermal gradient scenarios in the pool of structural models used for calibration. Essentially, this means that the temperature field of the bridge becomes a model parameter. However, the temperature field parameter is deterministic rather than probabilistic. The thermal gradients can include those in the vertical, transverse, and longitudinal directions or combinations thereof as shown in Figure 126 below.

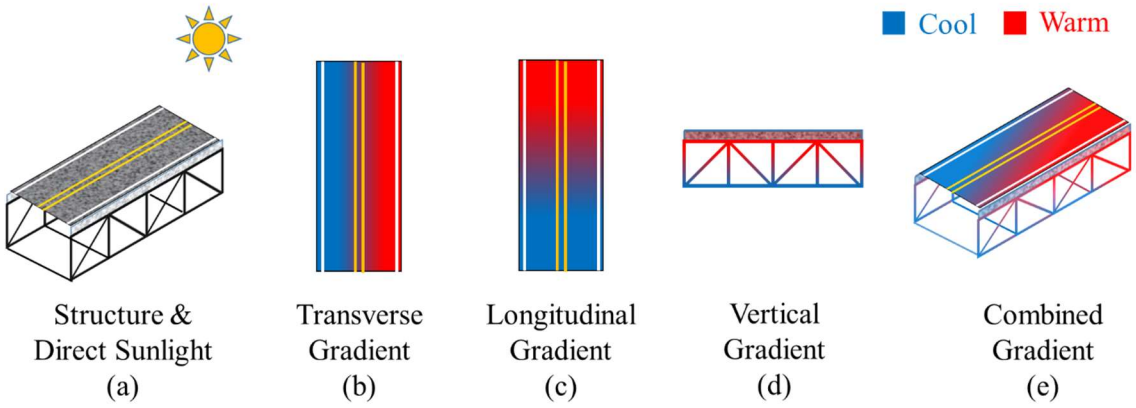

Figure 126: Thermal Gradients: a) Structure, b) Transverse Gradient, c) Longitudinal Gradient, d) Vertical Gradient, and e) Combined Gradient

The thermal gradients can also be varied in extent in accordance with environmental and/or weather conditions that the bridge likely experiences such as rain/snow accumulation on the deck, cloud coverage, shade from surrounding structures, and water temperature beneath the bridge to name a few. The extent is defined by gradient distribution profiles like the three shown in Figure 127(a-c). These gradient profiles can be easily transformed into a variety of gradients with different magnitudes by altering the maximum temperature values of T_1 and T_2. Since thermal behavior is linear with respect to temperature change, a significant number of structural models to be added to the pool without having to perform a structural analysis for every gradient combination separately. This greatly reduces the time required to obtain a large number of structural models and increases the efficiency of this method. Each of these gradients are analyzed independently or combined if desired.

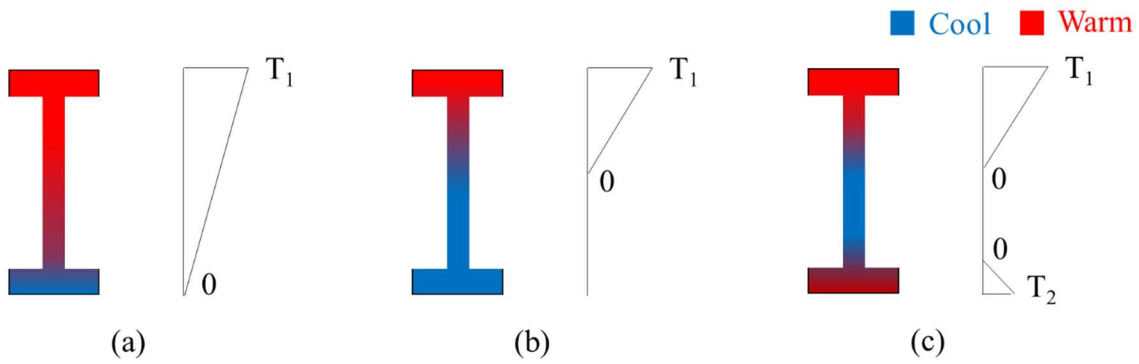

Figure 127: Thermal Gradient Distributions: a) Single Gradient through Entire Cross-section, b) Single Gradient through Portion of the Cross-section, and c) Double Gradient through Portion of Cross-section

Once the structural analyses of the gradients are complete, these structural models are then used to evaluate the structure at different points in time. The boundary conditions determined for each time are then tracked and compared to investigate whether certain parameters change over time or if they exhibit consistent behavior. For instance, Figure 128 shows how this might be completed for a structure. Three time points (A, B, and C) are identified in the temperature time history. For each of these times, an St-Id thermal evaluation is completed using five pools of structural models. The pool T_A includes the structural models developed using a uniform temperature distribution with the measured temperature at time A. The pools G_L, G_T, G_V, and G_C each include the structural models for the thermal gradients in the longitudinal, transverse, vertical, and combined directions, respectively. Then, all five pools of structural models are used within the TD St-Id analysis. The structural models undergo calibration via Bayes Theorem with the measured responses at Time A, and the model parameters are analyzed as discussed previously in Section 3. This process is completed for other times throughout the time history, in this case for Time B and

C. Note that the structural models from the gradient distributions are consistent and do not change from one time point to another. Finally, the model parameters from the evaluations at each time point are analyzed to determine if the model parameter changes over time or if it remains consistent throughout the monitoring duration. For the fictitious data shown, the model parameter experiences a change in behavior at Time B. While more of a time-step progression approach, this method could prove beneficial in identifying seasonal behavior. This technique would also likely provide more benefit with structures that are experiencing highly nonlinear behavior due to damage.

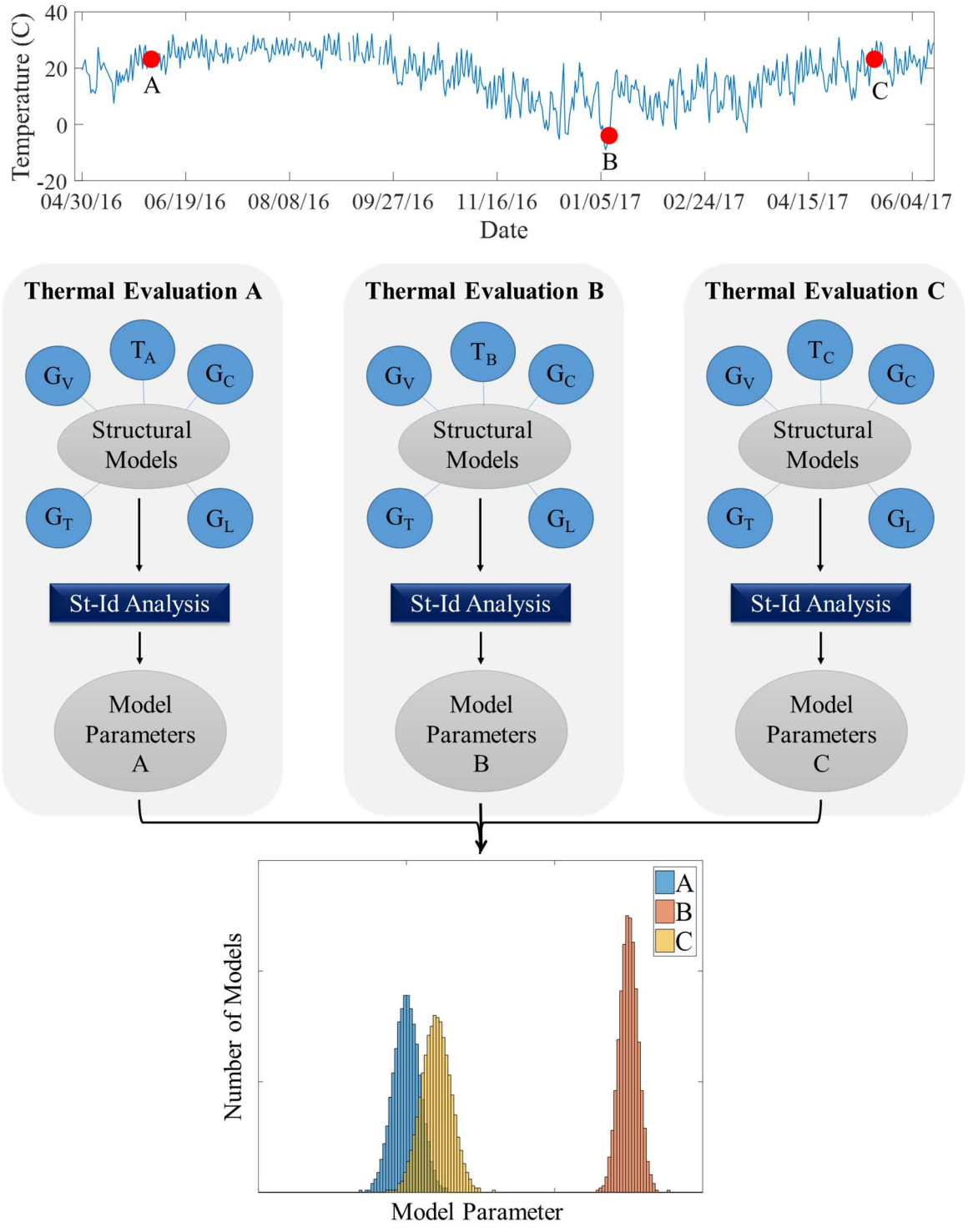

Figure 128: Process for Model Parameter Comparisons using Structural Models with Thermal Gradients

12.1.2 Damage Identification

Expansion of the pool of structural models may also provide the ability to identify damage. Much like the thermal gradients above, pools of structural models are developed for various damage scenarios as shown in Figure 129 and included during calibration. An additional task of this method is that the models from each damage scenario are also assigned with a damage index (DI), identifying which damage scenario the model is associated with.

Figure 129: Damage Scenarios and Indices

The “No Damage” scenario is performed as using boundary conditions and measured responses as discussed earlier in Section 3. Then, the model is altered to represent some form of damage. By varying the boundary condition parameters just like the “no damage” scenario, the damaged model is then used to develop a pool of structural models. This process is repeated for various damage scenarios so that the pool of structural models encompasses a vast array of damaged models. Once all of the structural models have been developed, an St-Id analysis is performed. Figure 130 shows the distribution of a model parameter and damage indices from the candidate models of a fictitious set of data. While the model parameter distribution shown in Figure 130(a) can be determined using the presented study, Figure 130(b) displays the distribution of damage indices and provides insight to the damage conditions of the structure. In this instance, the majority of the candidate models were associated with a damage index of 4, indicating that the measured responses closely resembled many of the models with girder damage. This insight could identify that damage exists as well as assist engineers with the locating the damage.

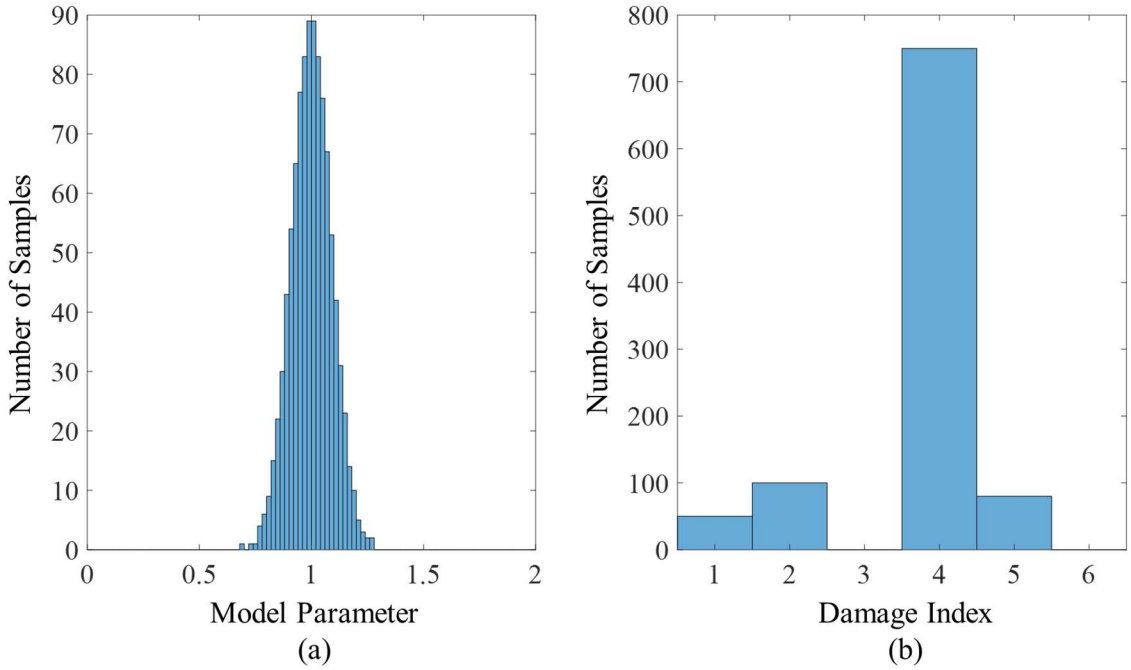

Figure 130: Candidate Model Data: a Model Parameter and b) Damage Index

.

12.2 Thermal Evaluation through Artificial Neural Networks

In recent years, artificial intelligence has developed an ever-growing presence in structural engineering. Just one of the many tools within artificial intelligence, the use of artificial neural networks (ANNs) has seen much success with various structural engineering applications. ANNs are mathematical models that can characterize relationships between sets of data using pattern recognition and machine learning. Rather than the need to perform many finite element analyses of various scenarios, ANNS can infer information about the structural behavior of a bridge based on measured data alone or in conjunction with a smaller subset of structural models. For the purpose of structural evaluations, one of the benefits of

ANNs is their ability to address the often imprecise measurements from a physical structure. Additionally, ANNs have the ability to accurately characterize complex nonlinear behavior.

In the last two decades, ANNs have been utilized for the purpose of structural evaluations; however, most of these studies address dynamic behavior and testing. Mehrjoo and Khaji 2008 utilized mode shapes to assess the damage of truss bridge joints using a back-propagation based neural network. Li et al. 2010 investigated the dependence of dynamic properties on environmental conditions such as temperature and wind. Ni et al. 2009 investigated how well neural networks can generalize the correlation between frequency and temperature of a bridge. ANNs can be used to determine the importance of bridge attributes with respect to the structural behavior (Mangalathu et al. 2018). Another benefit of this method is that ANNs can consider errors in finite element models and still conduct a damage detection analysis (Lee et al. 2005). ANNs also have the ability to utilize static measurements to identify boundary conditions (Park et al. 2017).

12.2.1 Thermal signature of measured responses using temperature field

The use of artificial neural networks (ANNs) allows for the relationship between the temperature field experienced on the bridge and the resulting thermal responses to be investigated. To explore this relationship, an ANN must be trained with sufficient amounts of data from the structure. For the purpose of this research, the training data includes both the temperature field of the bridge (input) as well as the measured responses (target) as shown in Figure 131 below.

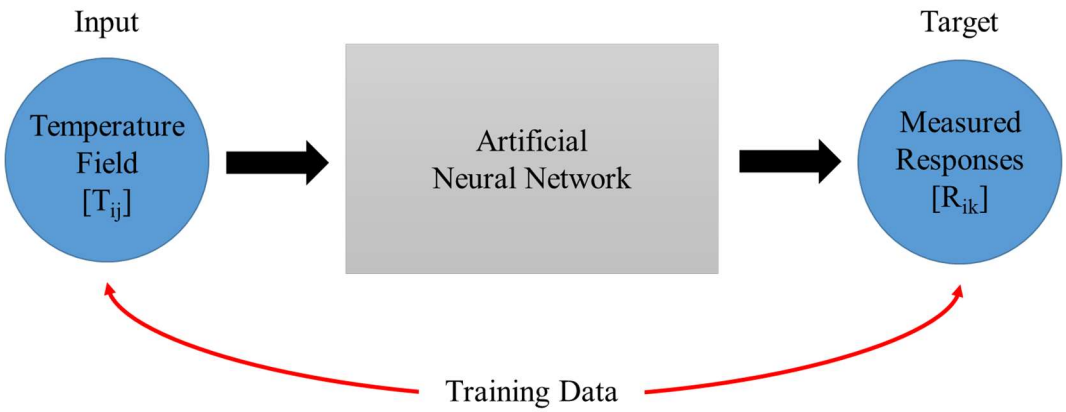

Figure 131: Artificial Neural Network Concept for Thermal Evaluation

The ANN can be defined by Equation 22, where *i* is the time point of measurement, *j* is input number, *k* is the target number, *T* is a matrix of the temperature field, *R* is a matrix of the measured responses, and *w* is a matrix of the weights that characterize the relationship between the inputs and targets. The ANN trains the data and determines the values of the weights. Once the weights are determined, the relationships between the input and the targets are defined and thus measured responses can be determined for various temperature fields.

$$\boldsymbol{R_{ik} = f(w_{ijk}\ T_{ij})} \tag{22}$$

For example, if ANNs were applied to the Route 61 Bridge project described in Section 7, the training data would be collected from the bridge according to Figure 132 below. For this project, each of the eight gages recorded temperature as well as a thermal response. These measurements comprise the T and R matrices.

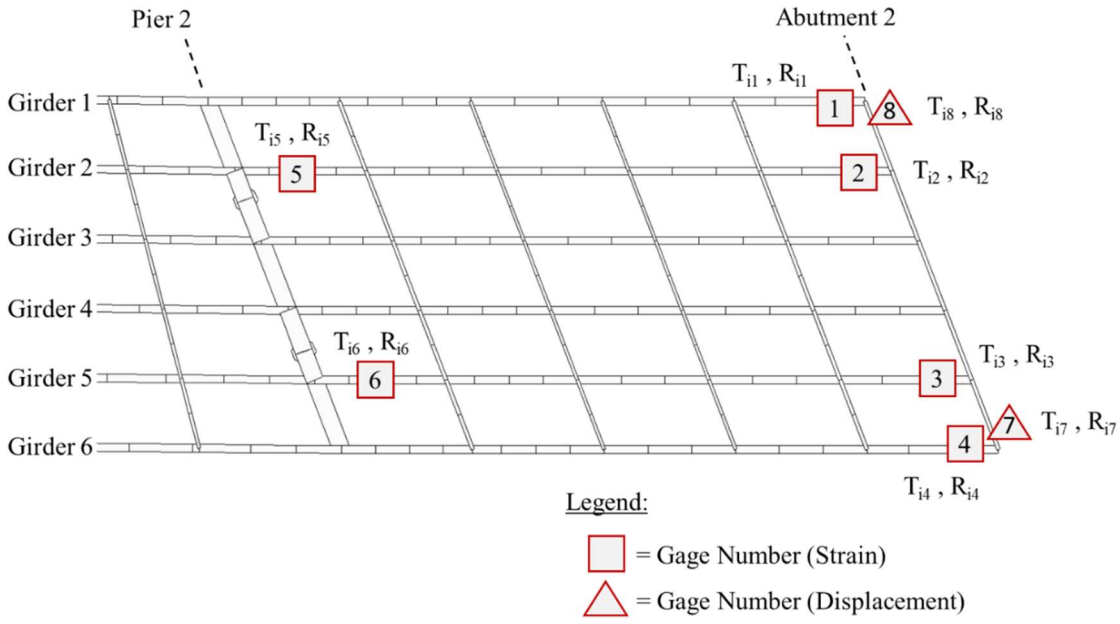

Figure 132: Temperature Field and Measured Responses for the Route 61 Bridge

ANNs allow for the investigation of one response at a time or multiple by use of perceptrons. For the Route 61 Bridge project, a single perceptron is shown in Figure 133(a). The single perception analyzes the influence of the temperature field on one single response. The weight associated with each temperature within the temperature field is determined by feedforward propagation. Similarly, investigation of more than one response is completed using a multiclass perceptron. The multiclass perceptron for the Route 61 Bridge would look similar to Figure 133(b) where each of the eight responses are related to each of the temperatures in the temperature field by their respective weights.

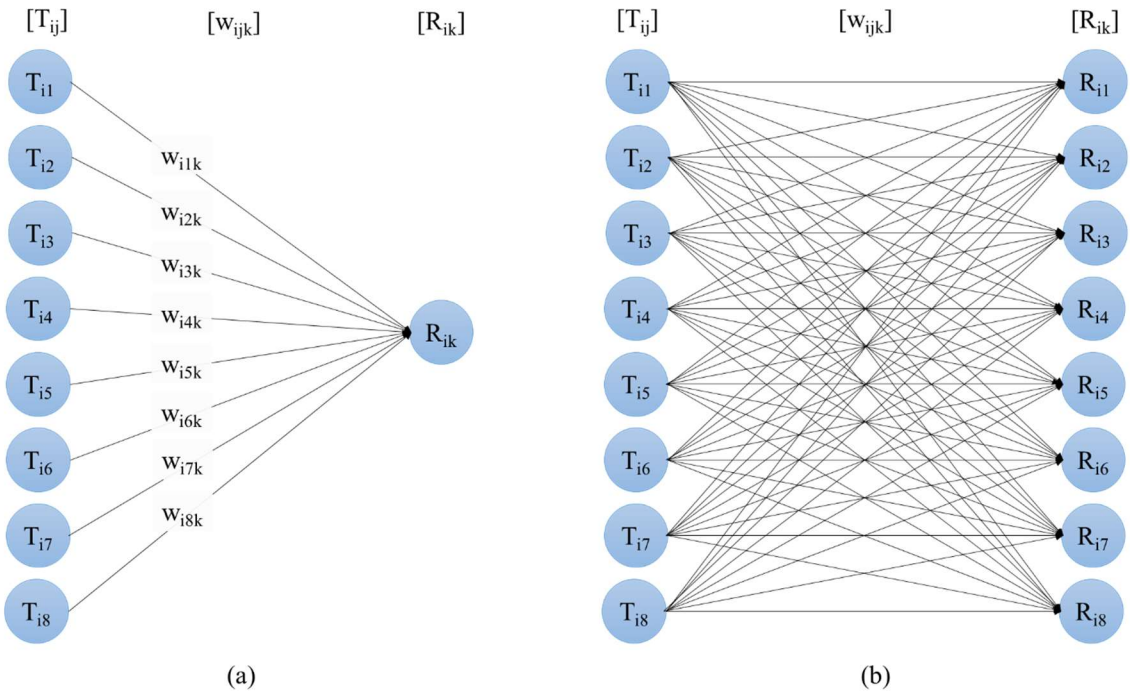

Figure 133: Perceptrons of the ANN: a) Single and b) Multiclass

As previously stated, the overarching purpose of the ANN is to determine the relationships between the input and the targets by identifying the weights. Once the weights have been determined, the relationship can be used to predict the responses for untrained temperature fields similar to what is shown in Figure 134 below. This method could be extremely beneficial for new bridges that begin monitoring early in their design lives when the structural behavior is as designed. Furthermore, the training data will be comprised of data that represents the "as designed" behavior. This can be useful to track the health of the bridge and identify when the structure begins to behave differently than the trained data. If the measured data begins to deviate from the predicted data, a more comprehensive investigation of the behavior can be conducted.

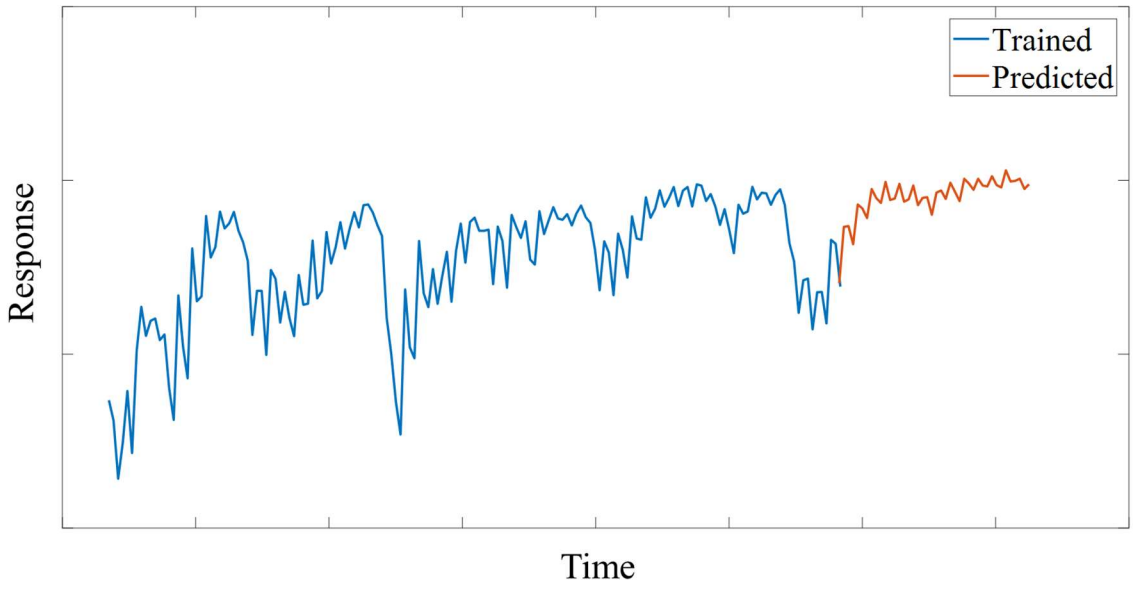

Figure 134: Response Prediction using Trained Data

12.2.2 Damage Identification using ANNs of Simulated Damage Scenarios

One of the major drawbacks of the thermal evaluation method presented in Section 3 is the time expended for the calibration of so many structural models. For the purpose of damge detection, the time increases even more as pools of structural models from various damage scenarios are required. One potential alternative to identifying damage within a thermal evaluation is through the use of ANNs. For this method, calibration is omitted alltogether, and the temperatures of the temperature field are considered the model parameters rather than the boundary conditions. A model is created using "as designed" conditions and then subjected to various temperature fields. The thermal responses resulting from each temperature field are recorded. An ANN is trained on the temperature field and response data, and the relationship is determined. The ANN is then used to show the

response of various temperature fields. Then, this process is repeated but for multiple damage scenarios of the model. If boundary conditions such as whether a bearing is seized is desired, these conditions can simply be imposed in a damage scenario. Finally, the measured responses are compared to the behavior shown by each of the ANNs. Figure 135 below shows a theoretical and simple application of this technique. As shown, the measured response data closely resembles the "No Damage" scenario for a long period of time. Suddenly, damage occurs and the measured behavior now resembles the thermal signature of the "Damage" scenario. The use of multiple damage scenarios could identify what type of damage and when the damage occurs. The benefit of this method is that once the ANNs are sufficiently trained with the simulated damage data, the ANNs do not need to be retrained and thus the damage identification process becomes very simple, user-friendly, time efficient, and easily applicable option for thermal evaluations.

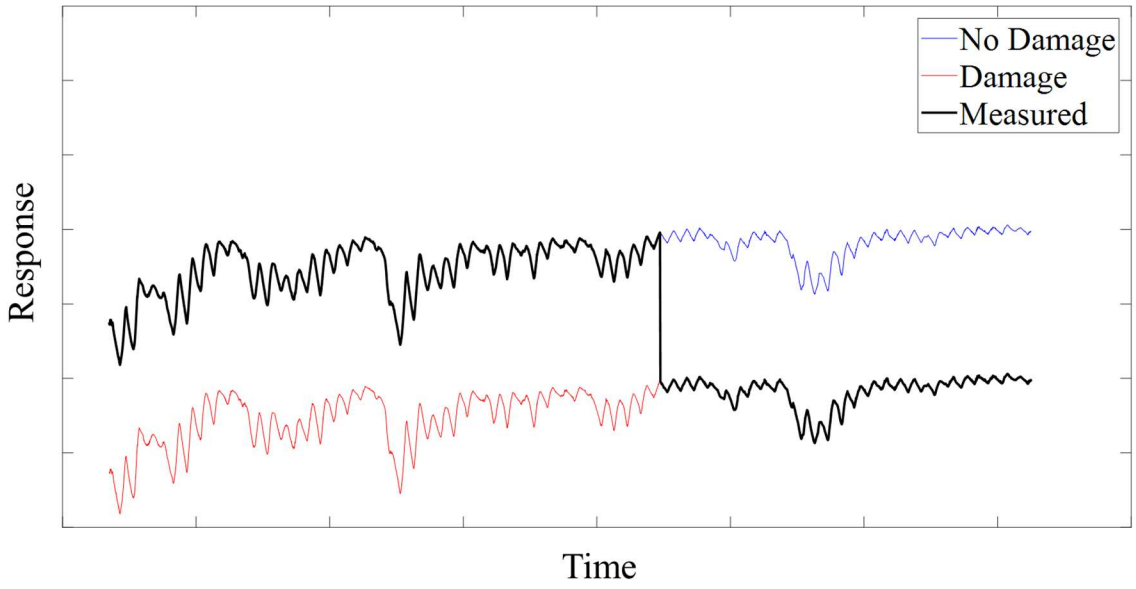

Figure 135: Damage Identification using ANNs of Simulated Data

13. SUMMARY

Bridges serve as integral components of infrastructure all around the world. Their direct impact to society is substantial, and their reliability is paramount. As such, confidence in the integrity of these structures is important not only for individuals who utilize these structures but also for the bridge owners and engineers who operate and maintain them. In order to develop a comprehensive understanding of the structural behavior of a bridge, evaluations are conducted to assess the structure's performance and health. By utilizing input-output relationships between loads and responses, structural performance evaluations provide an opportunity to assess unique bridge behavior such as complex mechanisms or deterioration.

The research presented herein investigated a novel, temperature-driven evaluation of bridge performance wherein thermal behavior in response to environmental temperature changes was used to assess the structure. Within this research, two bridges were evaluated using a probabilistic approach of single and multiple model updating within the temperature-driven structural identification process. This technique utilized Latin Hypercube Sampling as well as Bayesian calibration to assess the bridge conditions of the structures and evaluate the bridge's structural performance. Then, these studies were compiled into a synthesis of temperature-driven evaluations from nineteen bridge studies to develop a comprehensive framework of project logistics and provide guidance for using thermal behavior for performance evaluations. The intellectual value from each study illuminated various motivations, methods, successes, and challenges of temperature-driven evaluations. Guidance regarding structure details, monitoring criteria, as well as data and analysis was

provided to assist bridge owners, engineers, and researchers who utilize this temperature-driven technique to conduct evaluations. Based on the research presented herein, temperature-driven performance evaluations provided extensive insight not only to the thermal behavior of the bridge but the overall structural health as well.

REFERENCES

AASHTO. (1944). *Standard Specification for Highway Bridges*. American Association of State Highway and Transportation Officials, Washington, D.C.

AASHTO. (1977). *Standard Specification for Highway Bridges*. American Association of State Highway and Transportation Officials, Washington, D.C.

Abdel-Ghaffar, A., and Scalan, R. (1985). "Ambient Vibration Studies of Golden Gate." *Journal of Engineering Mechanics*, 111(4), 463–482.

Abdel-Jaber, H., and Glisic, B. (2016). "Systematic method for the validation of long- term temperature measurements." *Smart Materials and Structures*, IOP Publishing, 25(12), 1–12.

Aktan, a. E., Farhey, D. N., Helmicki, A. J., Brown, D. L., Hunt, V. J., Lee, K.-L., and Levi, A. (1997). "Structural Identification for Condition Assessment: Experimental Arts." *Journal of Structural Engineering*, 123(12), 1674–1684.

Aktan, A., and Moon, F. (2005). "Structural identification of constructed systems." *ASCE-SEI performace of structures track technical committee*.

Alampalli, S., and Ettouney, M. (2008). "Role of structural health monitoring in bridge security." *Bridge Structures*, 4(3–4), 143–154.

Alampalli, S., Ettouney, M. M., and Agrawal, A. K. (2005). "Structural health monitoring for bridge maintenance." *Bridge Structures*, 1(3), 345–354.

Alampalli, S., and Kunin, J. (2003). "Load testing of an FRP bridge deck on a truss bridge." *Applied Composite Materials*, 10(2), 85–102.

Alexander, J. (2017). "Structural Health Monitoring of the Hernando Desoto Bridge

(Master's Thesis)." Tennessee Technological University.

ARTBA. (2016). "2016 Structurally Deficient Bridges." *American Road & Transportation Builders Association*, <www.artba.org/economics/2016-u-s-deficient-bridges> (Oct. 18, 2016).

ASCE. (2017). "ASCE's 2017 Infrastructure Report Card." *American Society of Civil Engineers*, <www.infrastructurereportcard.org/cat-item/bridges> (Apr. 20, 2017).

Bacinskas, D., Kamaitis, Z., Jatulis, D., and Kilikevicius, A. (2013). "Load testing and model updating of a single span composite steel-concrete railway bridge." *Procedia Engineering*, Elsevier B.V., 57, 127–135.

Bakht, B., and Jaeger, L. G. (1990). "Bridge Testing-A Surprise Every Time." *Journal of Structural Engineering*, 116(5), 1370–1383.

Barr, P. J., Eberhard, M. O., and Stanton, J. F. (2001). "Live-load distribution factors in prestressed concrete girder bridges." *Journal of Bridge Engineering*, 6(5), 298–306.

Beck, B. J. L., and Katafygiotis, L. S. (1998). "Updating Models and their Uncertainties. I: Bayesian Statistical Framework." *Journal of Engineering Mechanics*, 124(April), 455–461.

Bell, E. S., Lefebvre, P. J., Sanayei, M., Brenner, B., Sipple, J. D., and Peddle, J. (2013). "Objective Load Rating of a Steel-Girder Bridge Using Structural Modeling and Health Monitoring." *Journal of Structural Engineering*, 139(October), 1771–1779.

Bolton, R., Sikorsky, C., Park, S., Choi, S., and Stubbs, N. (2005). "Modal Property Changes of a Seismically Damaged Concrete Bridge." *Journal of Bridge Engineering*, 10(4), 415–428.

Bolton, R., Stubbs, N., Park, S., Choi, S., and Sikorsky, C. (2001). "Documentation of

changes in modal properties of a concrete box-girder bridge due to environmental and internal conditions." *Computer-Aided Civil and Infrastructure Engineering*, 16(1), 42–57.

Breña, S. F., Jeffrey, A. E., and Civjan, S. a. (2013). "Evaluation of a Noncomposite Steel Girder Bridge through Live-Load Field Testing." *Journal of Bridge Engineering*, 18(7), 690–699.

Brown, A. J. (2007). "The tamar bridge." *Proceedings of Bridge Engineering 2 Conference 2007*, University of Bath, Bath, UK, 1–10.

Brownjohn, J. M. W., Koo, K., Scullion, A., and List, D. (2015). "Operational deformations in long-span bridges." *Structure and Infrastructure Engineering*, Taylor & Francis, 11(4), 556–574.

Brownjohn, J. M. W., De Stefano, A., Xu, Y.-L., Wenzel, H., and Aktan, A. E. (2011). "Vibration-based monitoring of civil infrastructure: challenges and successes." *Journal of Civil Structural Health Monitoring*, 1(3–4), 79–95.

Cao, Y., Yim, J., Zhao, Y., and Wang, M. L. (2010). "Temperature effects on cable stayed bridge using health monitoring system: a case study." *Structural Health Monitoring*, 10(5), 523–537.

Catbas, F. N., and Aktan, A. E. (2002). "Condition and Damage Assessment: Issues and Some Promising Indices." *Journal of Structural Engineering*, 128(8), 1026–1036.

Catbas, F. N., Ciloglu, S. K., Hasancebi, O., Grimmelsman, K., and Aktan, A. E. (2007). "Limitations in Structural Identification of Large." *Journal of Structural Engineering*, 133(8), 1051–1066.

Catbas, F. N., Kijewski-Correa, T., and Aktan, A. (2013). *Structural Identification of*

Constructed Systems. American Society of Civil Engineers, Reston, Virginia.

Chajes, M. J., and Shenton, H. W. (2006). "Using diagnostic load tests for accurate load rating of typical bridges." *Bridge Structures*, 2(1), 13–23.

Chong, K. P., Carino, N. J., and Washer, G. (2003). "Health monitoring of civil infrastructures." *Smart Materials and Structures*, 12, 483–493.

Coppolino, R. N., and Rubin, S. N. (1980). "Detectability Of Structural Failures In Offshore Platforms By Ambient Vibration Monitoring." *12th Annual Offshore Technology Conference*, Houston, Texas.

Ding, Y.-L., Wang, G.-X., Sun, P., Wu, L.-Y., and Yue, Q. (2015). "Long-Term Structural Health Monitoring System for a High-Speed Railway Bridge Structure." *The Scientific World Journal*, 2015, 1–17.

Ding, Y.-L., Zhao, H.-W., and Li, A.-Q. (2017). "Temperature Effects on Strain Influence Lines and Dynamic Load Factors in a Steel-Truss Arch Railway Bridge Using Adaptive FIR Filtering." *Journal of Performance of Constructed Facilities*, 31(4), 1–11.

Dubbs, N., and Moon, F. (2015). "Comparison and Implementation of Multiple Model Structural Identification Methods." *Journal of Structural Engineering*, 141(11), 1–13.

Eom, J., and Nowak, A. (2001). "Live load distribution for steel girder bridges." *Journal of Bridge Engineering*, 6(6), 489–497.

Fang, I.-K., Chen, C.-R., and Chang, I.-S. (2004). "Field Static Load Test on Kao-Ping-Hsi Cable-Stayed Bridge." *Journal of Bridge Engineering*, 9(6), 531–540.

Farrar, C. R., Duffy, T. A., Cornwell, P. J., and Doebling, S. W. (1999). "Excitation methods for bridge structures." *IMAC-XVII, Applied Modal Analysis: Reducing Time*

to Market, Kissimmee, Florida.

Farrar, C. R., and Worden, K. (2007). "An introduction to structural health monitoring." *Philosophical Transactions of the Royal Society A: Mathematical, Physical and Engineering Sciences*, 365, 303–315.

FHWA. (2001). *FHWA Rep. Nos. FHWA-RD-01-020 and FHWA-RD-01-021: Reliability of visual inspection*.

Figueiredo, E., Moldovan, I., and Marques, M. B. (2013). *Condition assessment of bridges: Past, present, and future. A complementary approach*. Universidade Catolica Editora.

Glisic, B., Posenato, D., Inaudi, D., and Figini, A. (2008). "Structural health monitoring method for curved concrete bridge box girders." *Proceedings of SPIE Smart Structures and Materials + Nondestructive Evaluation and Health Monitoring*, San Diego, California, 1–9.

Goulet, J.-A., Kripakaran, P., and Smith, I. F. C. (2010). "Multimodel Structural Performance Monitoring." *Journal of Structural Engineering*, 136(October), 1309–1318.

Del Grosso, A., and Lanata, F. (2014). "A long-term static monitoring experiment on R.C. beams: Damage identification under environmental effect." *Structure and Infrastructure Engineering*, Taylor & Francis, 10(7), 911–920.

Del Grosso, A. E. (2013). "The role of SHM in infrastructure management." *Structural Health Monitoring*, 2554–2561.

Guo, T., Liu, J., Zhang, Y., and Pan, S. (2015). "Displacement Monitoring and Analysis of Expansion Joints of Long-Span Steel Bridges with Viscous Dampers." *Journal of*

Bridge Engineering, 20(9), 1–11.

Hedegaard, B. D., French, C. E. W., and Shield, C. K. (2013a). "Investigation of Thermal Gradient Effects in the I-35W St. Anthony Falls Bridge." *Journal of Bridge Engineering*, 18(9), 890–900.

Hedegaard, B. D., French, C. E. W., and Shield, C. K. (2017a). "Time-Dependent Monitoring and Modeling of I-35W St. Anthony Falls Bridge. I: Analysis of Monitoring Data." *Journal of Bridge Engineering*, 22(7), 1–11.

Hedegaard, B. D., French, C. E. W., and Shield, C. K. (2017b). "Time-Dependent Monitoring and Modeling of I-35WAnthony, St Bridge, Falls Modeling, I I Finite-element." *Journal of Bridge Engineering*, 22(7), 1–15.

Hedegaard, B. D., French, C. E. W., Shield, C. K., Stolarski, H. K., and Jilk, B. J. (2013b). "Instrumentation and Modeling of I35W St. Anthony Falls Bridge." *Journal of Bridge Engineering*, 18(June), 476–485.

Inaudi, D. (2009). "Structural health monitoring of bridges: general issues and applications." *Structural Health Monitoring of Civil Infrastructure Systems*, V. Karbhari and F. Ansari, eds., Woodhead Publishing Limited, 339–370.

James, E. D. (2016). "Development of a rapid field evaluation method for steel girder bridges (Master's Thesis)." Tennessee Technological University.

James, E., and Yarnold, M. (2017). "Rapid Evaluation of a Steel Girder Bridge : Case Study." *Journal of Bridge Engineering*, 22(12), 1–9.

Jesus, A., Brommer, P., Westgate, R., Koo, K., Brownjohn, J., and Laory, I. (2018). "Bayesian structural identification of a long suspension bridge considering temperature and traffic load effects." *Structural Health Monitoring*, 1–14.

Jesus, A., Brommer, P., Zhu, Y., and Laory, I. (2017). "Comprehensive Bayesian structural identification using temperature variation." *Engineering Structures*, Elsevier Ltd, 141, 75–82.

Jesus, A., Zhu, Y., and Laory, I. (2016). "Comprehensive Bayesian structural identification using temperature expansion of a scale aluminium bridge." *Proceedings of 8th European Workshop on Structural Health Monitoring*, Bilbao, Spain, 1–9.

Karbhari, V. M., and Lee, L. S.-W. (2009). "Vibration-based damage detection techniques for structural health monitoring of civil infrastructure systems." *Structural Health Monitoring of Civil Infrastructure Systems*, V. M. Karbhari and F. Ansari, eds., Woodhead Publishing Limited, 177–212.

Kim, B. H., Stubbs, N., and Park, T. (2005). "A new method to extract modal parameters using output-only responses." *Journal of Sound and Vibration*, 282(1–2), 215–230.

Kim, J., and Stubbs, N. (1995). "Damage Detection in Offshore Jacket Structures from Limited Modal Information." *International Journal of Offshore and Polar Engineering*, 5(1), 58–66.

Koo, K. Y., List, D. I., and Cole, R. (2010). "Structural health monitoring of the Tamar Suspension." *Structural Control and Health Monitoring*, 20(4), 609–625.

Kromanis, R., and Kripakaran, P. (2014). "Predicting thermal response of bridges using regression models derived from measurement histories." *Computers and Structures*, Elsevier Ltd, 136, 64–77.

Kromanis, R., and Kripakaran, P. (2016). "SHM of bridges: Characterizing thermal response and detecting anomaly events using a temperature-based measuremnet interpretation approach." *Journal of Civil Structural Health Monitoring*, 6(2), 237–

254.

Kromanis, R., Kripakaran, P., and Harvey, B. (2016). “Long-term structural health monitoring of the Cleddau bridge: Evaluation of quasi-static temperature effects on bearing movements.” *Structure and Infrastructure Engineering*, Taylor & Francis, 12(10), 1342–1355.

Kulprapha, N., and Warnitchai, P. (2012). “Structural health monitoring of continuous prestressed concrete bridges using ambient thermal responses.” *Engineering Structures*, Elsevier Ltd, 40, 20–38.

Laory, I., Westgate, R., and Brownjohn, J. (2013). “Temperature variations as load cases for structural identification.” *Proceeding of the 6th International Conference on Structural Health Monitoring of Intelligent Infrastructure (SHMII)*, (EPFL-CONF-191303), Hong-Kong, China.

Lee, J. J., Lee, J. W., Yi, J. H., Yun, C. B., and Jung, H. Y. (2005). “Neural networks-based damage detection for bridges considering errors in baseline finite element models.” *Journal of Sound and Vibration*, 280, 555–578.

Li, H., Li, S., Ou, J., and Li, H. (2010). “Modal identification of bridges under varying environmental conditions : Temperature and wind effects.” *Structural Control and Health Monitoring*, 17, 495–512.

Liu, S., and Yao, J. T. (1978). “Structural identification concept.” *Journal of the Structural Division*, 104(12), 1845–1858.

Mangalathu, S., Heo, G., and Jeon, J. (2018). “Arti fi cial neural network based multi-dimensional fragility development of skewed concrete bridge classes.” *Engineering Structures*, Elsevier, 162, 166–176.

Masri, S. F., Sheng, L.-H., Caffrey, J. P., Nigbor, R. L., Wahbeh, M., and Abdel-Ghaffar, A. M. (2004). "Application of a Web-enabled real-time structural health monitoring system for civil infrastructure systems." *Smart Materials and Structures*, 13(6), 1269–1283.

Mazurek, D. F., and Dewolf, J. T. (1990). "Experimental study of bridge monitoring technique." *Journal of Structural Engineering*, 116(9), 2532–2549.

Mehrjoo, M., and Khaji, N. (2008). "Damage detection of truss bridge joints using Artificial Neural Networks." *Expert Systems with Applications*, 35, 1122–1131.

Moon, F. (2008). "CAREER: Structural Identification to Support Infrastructure Decision-Making." N. S. Foundation, ed., Washington, D.C.

Murphy, B., and Yarnold, M. (2017). "Temperature-driven assessment of a cantilever truss bridge." *Proceedings of Structures Congress 2017*, Denver, Colorado, 461–473.

Murphy, B., and Yarnold, M. (2018). "Temperature-driven structural identification of a steel girder bridge with an integral abutment." *Engineering Structures*, Elsevier, 155, 209–221.

Murphy, B., and Yarnold, M. (2019). "Temperature-Driven Structural Performance Evaluation of the Hurricane Bridge via Multiple Model Approach." *9th International Conference on Structural Health Monitoring of Intelligent Infrastructure (ISHMII)*, Saint Louis, Missouri.

Nakamura, S., and Sakamoto, Y. (2000). "Forced and Ambient Vibration Tests and Vibration Monitoring of Hakucho Suspension Bridge." *Transportation Research Record: Journal of the Transportation Research Board*, 1696(1), 57–63.

Ni, Y. Q., Zhou, H. F., and Ko, J. M. (2009). "Generalization Capability of Neural

Network Models for Temperature-Frequency Correlation Using Monitoring Data." *Journal of Structural Engineering*, 135(October), 1290–1300.

Park, S., Kim, Y. B., and Stubbs, N. (2002). "Nondestructive damage detection in large structures via vibration monitoring." *Electronic Journal of Structural Engineering*, 2, 59–75.

Park, Y., Kim, S., Kim, N., and Lee, J. (2017). "Finite element model updating considering boundary conditions using neural networks." *Engineering Structures*, Elsevier Ltd, 150, 511–519.

Peeters, B., and De Roeck, G. (2001). "One-year monitoring of the Z24-bridge: Environmental effects versus damage events." *Earthquake Engineering and Structural Dynamics*, 30, 149–171.

Ravindran, S., Kripakaran, P., and Smith, I. F. C. (2007). "Evaluating Reliability of Multiple-Model System Identification." *14th International Workshop on Intelligent Computing in Engineering (EG-ICE)*, Maribor, Slovenia, 1–15.

Reilly, J., Abdel-Jaber, H., Yarnold, M., and Glisic, B. (2016). "Identification of steady-state uniform temperature distributions to facilitate a temperature driven method of Structural Health Monitoring." *Proceedings of SPIE Smart Structures and Materials + Nondestructive Evaluation and Health Monitoring*, Las Vegas, Nevada, 1–7.

Reilly, J., Abdel-Jaber, H., Yarnold, M., and Glisic, B. (2017). "Evaluating the coefficient of thermal expansion using time periods of minimal thermal gradient for a temperature driven structural health monitoring." *Proceedings of SPIE Smart Structures and Materials + Nondestructive Evaluation and Health Monitoring*, Portland, Oregon, 1–7.

De Roeck, G. (2003). “The state-of-the-art of damage detection by vibration monitoring: The SIMCES experience.” *Journal of Structural Control*, 10, 127–134.

Rytter, A. (1993). “Vibration based inspection of civil engineering structures (Doctoral Dissertation).” Aalborg Universiy, Denmark.

Sigurdardottir, D. H., and Glisic, B. (2013). “Neutral axis as damage sensitive feature.” *Smart Materials and Structures*, 22(7), 1–18.

Sikorsky, C. S., Stubbs, N., Bolton, R., Choi, S., Karbhari, V. M., and Seible, F. (2001). “Measuring bridge performance using a structural health monitoring system.” *Proc. SPIE 4330, Smart Structures and Materials 2001: Smart Systems for Bridges, Structures, and Highways*, Newport Beach, California, 179–190.

Smith, I. F. C., and Saitta, S. (2008). “Improving Knowledge of Structural System Behavior through Multiple Models.” *Journal of Structural Engineering*, 134(4), 553–561.

Sohn, H. (2007). “Effects of environmental and operational variability on structural health monitoring.” *Philosophical Transactions of the Royal Society A: Mathematical, Physical and Engineering Sciences*, 365, 539–560.

Tong, M., Tham, L. G., Asce, M., and Au, F. T. K. (2002). “Extreme Thermal Loading on Steel Bridges in Tropical Region.” *Journal of Bridge Engineering*, 7(6), 357–366.

Wang, G.-X., Ding, Y.-L., Song, Y.-S., Wu, L.-Y., Yue, Q., and Mao, G.-H. (2016). “Detection and Location of the Degraded Bearings Based on Monitoring the Longitudinal Expansion Performance of the Main Girder of the Dashengguan Yangtze Bridge.” *Journal of Performance of Constructed Facilities*, 30(4), 1–10.

Wang, G. X., Ding, Y. L., Sun, P., Wu, L. L., and Yue, Q. (2015). “Assessing static

performance of the dashengguan yangtze bridge by monitoring the correlation between temperature field and its static strains." *Mathematical Problems in Engineering*, 2015, 1–12.

Warren, M. E., and Dubbs, N. C. (2017). "Periodic Temperature-Based Bearing Assessment of a Steel Multi-Girder Bridge." *Transportation Research Record: Journal of the Transportation Research Board*, (2642), 26–34.

Westgate, R., Koo, K., and Brownjohn, J. (2014). "Effect of Solar Radiation on Suspension Bridge Performance." *Journal of Bridge Engineering*, 20(5), 1–12.

Xia, Q., Cheng, Y., Zhang, J., and Zhu, F. (2017). "In-Service Condition Assessment of a Long-Span Suspension Bridge Using Temperature-Induced Strain Data." *Journal of Bridge Engineering*, 22(3), 1–11.

Yarnold, M., Alexander, J., and Huff, T. (2017). "Structural Health Monitoring of the Hernando Desoto Bridge." *34th Annual International Bridge Conference (IBC)*, National Harbor, Maryland, USA.

Yarnold, M., Moon, F., Dubbs, N., and Aktan, A. (2012a). "Evaluation of a long-span steel tied arch bridge using temperature-based structural identification." *Bridge Maintenance, Safety, Management, Resilience and Sustainability - Proceedings of the Sixth International Conference on Bridge Maintenance, Safety and Management*, 2397–2403.

Yarnold, M. T., and Moon, F. L. (2015). "Temperature-based structural health monitoring baseline for long-span bridges." *Engineering Structures*, Elsevier Ltd, 86, 157–167.

Yarnold, M. T., Moon, F. L., and Aktan, A. E. (2015). "Temperature-based structural identification of long-span bridges." *Journal of Structural Engineering*, 141(11), 1–

10.

Yarnold, M. T., Moon, F. L., Aktan, A. E., and Glisic, B. (2012b). "Structural Monitoring of the Tacony-Palmyra Bridge using Video and Sensor Integration for Enhanced Data Interpretation." *Bridge Maintenance, Safety, Management, Resilience and Sustainability - Proceedings of the Sixth International Conference on Bridge Maintenance, Safety and Management*, Stresa, Lake Maggiore, Italy, 2168–2172.

Yarnold, M. T., and Wilson, G. S. (2015). "Forensic Investigatin of the Route 61 Bridge." *Proceedings of Structures Congress 2015*, American Society of Civil Engineers, Portland, Oregon, 309–321.

Yuen, K., Au, S., and Beck, J. (2004). "Two-stage structural health monitoring approach for phase I benchmark studies." *Journal of Engineering Mechanics*, 130(January), 16–33.

Zhou, G. D., Yi, T. H., and Chen, B. (2017). "Innovative Design of a Health Monitoring System and Its Implementation in a Complicated Long-Span Arch Bridge." *Journal of Aerospace Engineering*, 30(2), 1–17.

Zhou, G., Yi, T., Chen, B., and Chen, X. (2018). "Modeling Deformation Induced by Thermal Loading Using Long-Term Bridge Monitoring Data." *Journal of Performance of Constructed Facilities*, 32(3), 1–9.

Zhou, Y., and Sun, L. (2018). "Insights into temperature effects on structural deformation of a cable- stayed bridge based on structural health monitoring." *Structural Health Monitoring*, 1–14.

Zhu, Y., Jesus, A., and Laory, I. (2016). "Predicting Thermal Response for Structural Health Monitoring Using Blind Source Separation Method." *Proceedings of 8th*

European Workshop On Structural Health Monitoring (EWSHM 2016), Bilbao, Spain.

Zuk, W. (1965). "Thermal Behavior of Composite Bridges - Insulated and Uninsulated." *Highway Research Record*, 231–253.

APPENDIX A

ADDITIONAL FIGURES OF SECTION 7

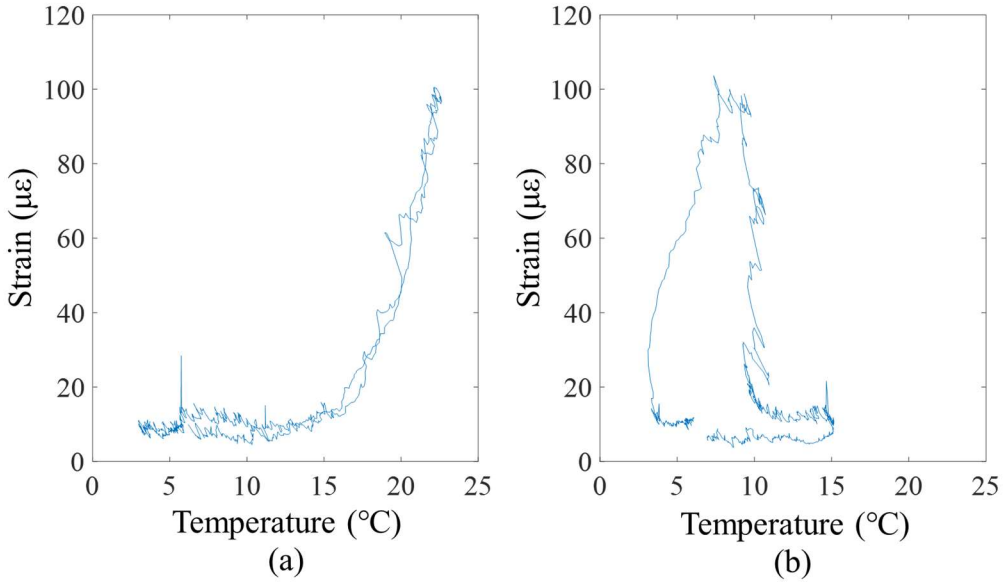

Figure 136: Measured Strain Response of Bottom Flange of Exterior Girders at Abutment 2 on March 30, 2014: a) Girder 1 and b) Girder 6

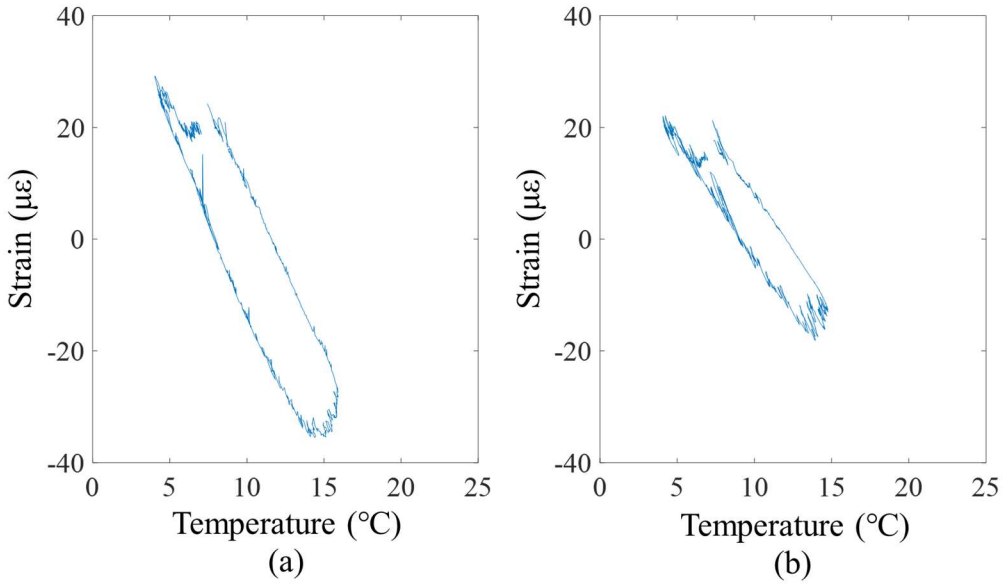

Figure 137: Measured Strain Response of Web of Interior Girders at Abutment 2 on March 30, 2014: a) Girder 2 and b) Girder 5

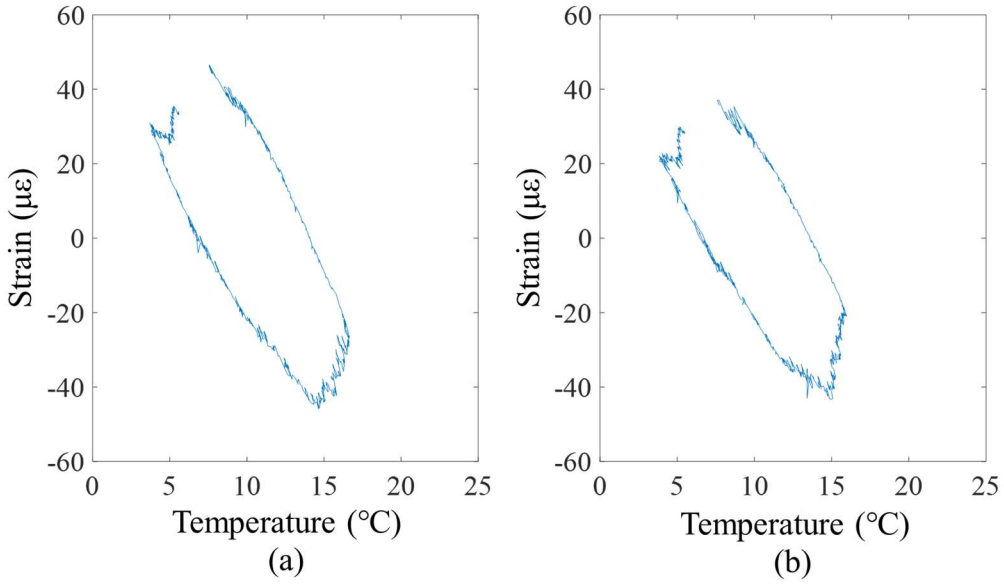

Figure 138: Measured Strain Response of Web of Interior Girders at Pier 2 on March 30, 2014: a) Girder 2 and b) Girder 5

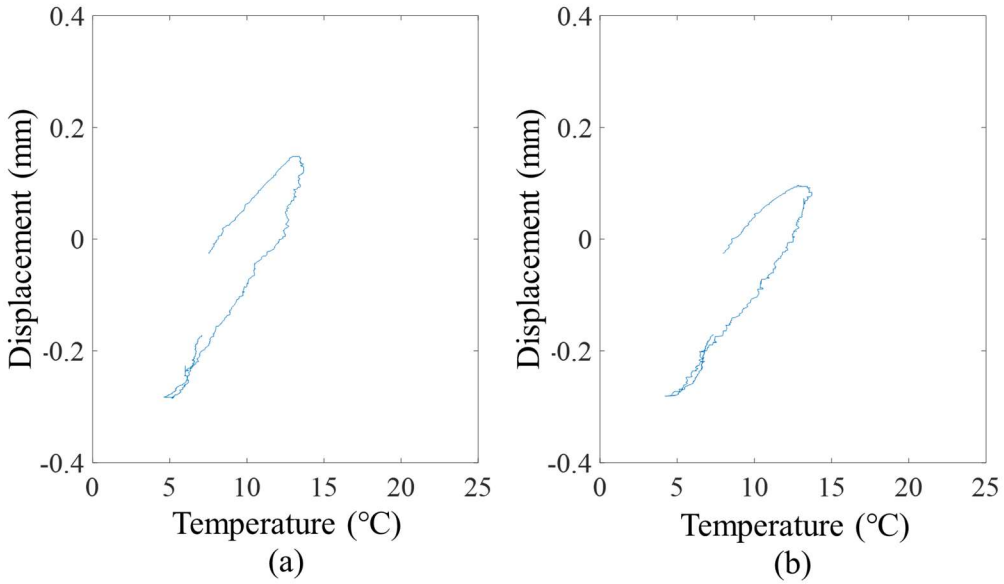

Figure 139: Measured Displacement Response of Interior Girders at Abutment 2 on March 30, 2014: a) Girder 2 and b) Girder 5

APPENDIX B

ADDITIONAL FIGURES OF SECTION 8

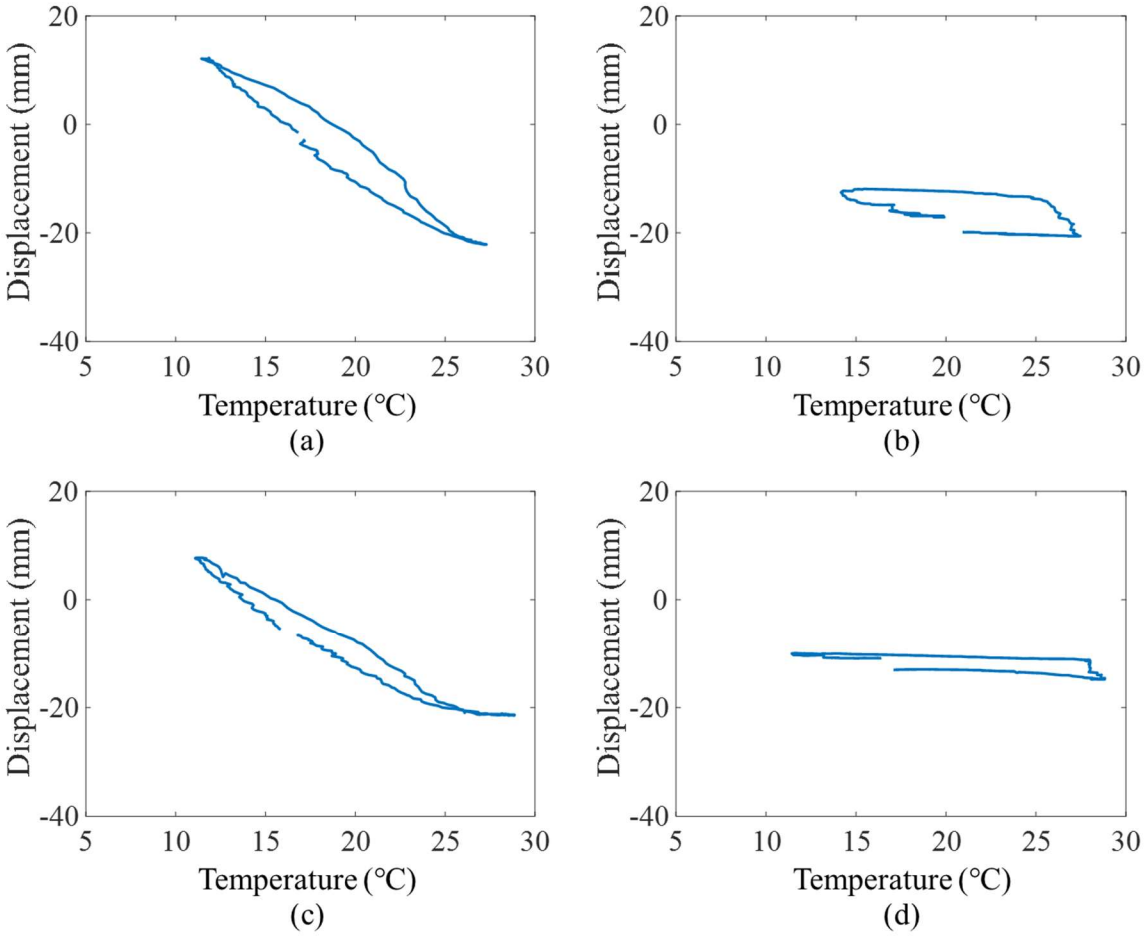

Figure 140: Measured Displacement Response on April 7, 2017: a) Pier 5 Deck Level, b) Pier 7 Deck Level, c) Pier 5 Bearing Level, and d) Pier 7 Bearing Level